



Universitetet  
i Stavanger

**FACULTY OF SCIENCE AND TECHNOLOGY**

# **MASTER'S THESIS**

Study program/specialist: Master of Science  
in Marine and Offshore Technology

Spring semester 2019

Open/~~confidential~~

Author: Nicolai Bull Eriksson

*Nicolai Bull Eriksson*  
.....

(signature of author)

Program coordinator:

Prof. Muk Chen Ong, UiS

Supervisor(s):

Prof. Muk Chen Ong, UiS

Prof. Yihan Xing, UiS

Christian Knudsen, CTO, IK-Norway

Title of Semester Project:

Design, Testing and Analysis of a New Pipeline Recovery Tool

Credits: 30

Keywords:

Wedge lock, Bearing steel balls, Contact stresses,  
Spherical indentation, Designing test rigs,  
DNVGL, ASME, DIN, Finite element analysis,

Number of pages: 94

+ supplemental material/other: 185

Stavanger 14.06.2019

date/year

# Preface

This thesis has been written as a final project of my two-year Master of Science education in Marine and Offshore Technology at the University of Stavanger. This thesis is executed in the last semester of the master's thesis degree program. The knowledge gained throughout this study program becomes very useful during this thesis. Moreover, new challenges have been met through the specific thesis topics and new knowledge are achieved.

I would very much like to thank my supervising professor Muk Chen Ong at the Department of Mechanical and Structural Engineering and Material Science for his help and guidance. I would also thank my co-supervisor professor at the Department of Mechanical and Structural Engineering and Material Science, Yihan Xing for supporting and sharing his knowledge about simulation and topics applicable to this thesis. I also want to give special thanks to IK-Norway's CTO Christian Knutsen, for sharing his experienced knowledge about how to approach the thesis topics, critical thinking and empirical testing.

I would also like to thank all other IK-Norway personnel which has helped me during this thesis.

Stavanger, 14.06.2019

A handwritten signature in black ink that reads "Nicolai Bull Eriksson". The signature is written in a cursive, flowing style.

Nicolai Bull Eriksson

# Table of Content

Table of Content .....	ii
1. Introduction.....	1
1.1. Background and Motivation.....	1
1.2. Previous work .....	2
1.3. Scope of work .....	2
1.4. Structure of report .....	4
2. Current and previously made PRT's.....	5
2.1. Ballgrab.....	5
2.2. PII-Technomarine PRT .....	7
2.3. Industrikonkonsult PRT .....	7
2.4. MORGRIP .....	9
2.5. IK-Norway Pipeline Recovery Tool .....	11
2.6. Industrikonsult IPLT .....	13
3. Theoretical background.....	14
3.1. Introduction.....	14
3.2. Contact Stresses .....	14
3.2.1. Fundamental Assumptions .....	15
3.2.2. Key equation used considered contact stresses.....	16
3.3. Hertzian contact stresses .....	20
3.3.1. Unimodal Contact .....	20
3.3.2. Contact between two spherical bodies .....	21
3.4. The relationship between depth and contact radius in a spherical indentation .....	22
3.5. Brinell Hardness.....	23
3.6. Meyer's Law .....	24
3.7. Comparison of Brinell and Meyer hardness.....	27
3.8. The deformation of metals by spherical indenters: ideal plastic metals .....	28
3.8.1. Initial plastic deformation .....	28
3.8.2. When the plastic deformation occurs.....	29
3.8.3. Complete or full plastic deformation .....	30
3.8.4. Pressure-load characteristics .....	32
3.8.5. Range of validity of Meyer's law.....	33
3.8.6. Deformation of the indenter.....	35
3.8.7. Effect of surface roughness.....	35
3.8.8. Piling-up and sinking-in.....	36
3.9. Castable elastomers: Polyurethane.....	37

3.10.	Finite Element Analysis .....	39
4.	Chapter 4: PRT System description .....	42
4.1.	Design of a ROV compatible PRT.....	43
5.	Test description .....	44
5.1.	Introduction.....	44
5.2.	Test with a cone alloyed with 34CrNiMo6.....	44
5.3.	Test with a cone alloyed with Calmax Uddeholm .....	47
6.	Material description of the interacting parts .....	51
6.1.	Bearing steel balls .....	51
6.2.	The 4-inch pipeline DIN 2448 .....	51
6.3.	Annealed Calmax Uddeholm Cone.....	51
6.3.1.	Calmax Uddeholm .....	51
6.3.2.	Hardening Process.....	52
7.	ANSYS Modelling.....	55
7.1.	Elastic-Plastic mesh refinement study .....	58
7.2.	Sensitivity Study on Elastic-Plastic .....	60
7.3.	Linear-Elastic mesh refinement study.....	63
8.	Calculations, empirical results and FEA results .....	66
8.1.	Analytical Calculations .....	66
8.2.	Empirical results: .....	73
8.3.	ANSYS Results.....	80
9.	Discussion .....	86
10.	Conclusion and Recommendations for Future Work.....	90
10.1.	Conclusion .....	90
10.2.	Recommendations for Future Work.....	91
	References.....	92
	Appendices.....	i

# Abstract

Pipeline Recovery Tools (PRT's) are used in decommissioning and recovery of subsea pipelines. The PRT often use a mechanical system to insert and lock itself onto the subsea pipeline. This thesis examines a unique connection system that uses steel balls casted within polyurethane. The steel balls provide a wedge-lock mechanism that is locked onto the subsea pipeline; and then the subsea pipeline can be retrieved. The locking process creates an indentation on the steel pipeline. The sealing ability of polyurethane will ensure that the water will not pass through the PRT. However, there were not carried out any tests containing polyurethane in this study. The present study investigates how the steel balls interact with the different components in the wedge-lock mechanism. The areas of interest within the investigated PRT, are the contact surfaces between the bearing steel ball and the pipeline, the cone and the set-pipe. The key parameters evaluated in the present study are the angle of the wedge ( $\alpha$ ), different material properties, the friction coefficient, the indentation from bearing steel balls and the force exerted on the bearing steel balls.

A comprehensive investigation based on analytical, numerical and experimental approaches were performed in this thesis. First, analytical calculation methods of contact stresses in both linear-elastic and elastic-plastic areas, Brinell and Meyers hardness and spherical fully plastic and elastic indentation, were applied and investigated. Second, experimental tests using two test-rigs were performed to obtain the empirical data. The first test rig was designed to obtain the load carrying capacity of the PRT and the resulting indentation at the pipeline. The second test rig was designed to test the sealing properties. The test rigs are designed according to ASME and DIN standards of a 4-inch pipe. Furthermore, six cones alloyed with Calmax were manufactured. These cones have angles of 3, 4, 5, 6, 8 and 10 degrees. The cones alloyed with Calmax, that were empirically tested, had angles of 3, 4 and 10 degrees. In addition, one 34CrNiMo6 alloyed cone with an angle of 5 degrees was machined and tested. Third, finite element model in ANSYS with detailed contact modelling was built to perform sensitivity studies on friction coefficients and material properties. The model built in ANSYS, had a cone-angle of 3 degrees. Last, the results from the empirical tests, analytical calculations and finite element analyses were compared in term of spherical indentations, stresses, reaction forces and friction coefficients in both linear-elastic and fully plastic areas.

The deformation occurring on the cone, steel balls and/or pipeline wall was found to depend strongly on the material properties, the friction coefficients, the sizing and the reaction forces between the interacting surfaces. Moreover, if the PRT is not aligned perpendicular to the pipeline, the steel balls will experience an uneven reaction force around the diameter of the pipeline. This leads to an uneven deformation pattern that may affect the lifetime of the PRT main body. The knowledge of the friction coefficient is crucial when predicting the indentation depth in the pipeline. The result from finite element analysis shows that a low friction coefficient will cause in less indentation. Lubrication of the steel balls is one suggestion to maintain a low friction coefficient. Yield stress is also a parameter that strongly affects the indentation. To keep the plastic deformation at a minimum on the cone and at a maximum on the pipeline, the cone must be around 2.5 times the hardness of the steel balls and the steel balls must be around 2.5 times the hardness of the pipeline.

The tests show promising results in terms of the PRT's lifting capacity. However, the reaction forces acting between the steel balls, the cone and the pipeline are very high with small cone-angles, which will often result in spherical deformations on the cone. An increase in cone-angle will reduce the mean pressure between the cone and the steel balls with a fixed magnitude of force acting on the steel balls, which will decrease the indentation depth. Moreover, this results in if self-locking and onset of plastic deformation are present between the steel balls and pipeline, the angle should be as large as possible.

The results from this thesis contributes to a better understanding of the innovative wedge lock mechanisms used in the studied PRT. The findings can also be applied to other PRT applications that uses a ball and taper wedge-lock mechanism.

# List of Figures

Figure 1:1 : Scope of the thesis .....	3
Figure 2:1: Ballgrab PRT [51] .....	5
Figure 2:2: Cross-section view of PII-Technomarine PRT [3] .....	7
Figure 2:3: Detailed technical drawing from Industriekonsult of their PRT [6] .....	8
Figure 2:4: MORGRIP connection quarter section view [27] .....	9
Figure 2:5: Detailed view of MORGRIP connector [27] .....	9
Figure 2:6: IK 14-inch PRT [10] .....	11
Figure 2:7: Overview of Industriekonsult IPLT 48” to 84” [12] .....	13
Figure 3:1: Two curved surfaces with different radii pressed against each other with a force P [16].	14
Figure 3:2: Analysis of contact stresses [16] .....	15
Figure 3:3: Geometry of contact surface [16] .....	16
Figure 3:4: Distance $Z_0$ at which $\tau_{\text{max}}$ occurs [16]. .....	18
Figure 3:5: Stress and deflection coefficients for two bodies in contact at a point for any value of B/A [16]. .....	19
Figure 3:6: Stress and deflection coefficients for two bodies in contact at a point for any value of B/A [16]. .....	19
Figure 3:7: Illustrates the deformation from a spherical indenter onto a flat surface in elastic area [20] .....	21
Figure 3:8: illustrates the contact zone between two circular bodies and the elastic deformation [20].	22
Figure 3:9: A spherical cap marked with blue colour, for which the area changes with the variable h [24]. .....	22
Figure 3:10: (a) geometrically similar indentations produced by spherical indenters of different diameters. (b) mean pressure is calculated between a spherical indenter, and it is assumed that there is no friction at the interface [29]. .....	23
Figure 3:11: Plot of the load W against the indentation diameter d from the indentation of a spherical indenter onto a flat metal surface [29]. .....	25
Figure 3:12: Illustrates the Brinell hardness number and Meyer hardness number for Annealed and Work-hardened copper as the load increases and indentation for a spherical indenter with a diameter of 10mm increases [29]. .....	27
Figure 3:13: Illustration of a hard sphere that makes an indentation into a flat surface [29]. .....	28
Figure 3:14: Pressure distribution of a circle contact from a spherical surface deformed elastically against a flat surface [29]. .....	29
Figure 3:15: Elastic deformation of a flat surface by a sphere and shear stress distribution [29]. .....	29
Figure 3:16: The indentation from a spherical indenter on a flat surface [29]. .....	30
Figure 3:17: Illustrates the slip-line obtained for a spherical indenter on an ideally plastic metal [29].	31
Figure 3:18: pressure distribution over the indentation from a spherical indenter in an ideally plastic material of constant yield stress [29]. .....	31
Figure 3:19: Theoretical pressure-load characteristics of an ideally plastic metal deformed by a spherical indenter [29]. .....	32
Figure 3:20: Experimental pressure-load characteristic of indentation formed in work-hardened mild steel by a hard-spherical indenter. The broken line is the theoretical result for elastic deformation [29]. .....	33
Figure 3:21: Indentation of work-hardened mild steel plotted against the load, with a yield stress of 755 MPa [29]. .....	34
Figure 3:22: Deformation of asperities: (a) hemispherical asperity deformed by a flat surface. (b) flat surface deformed by a hemisphere. The deformation process is similar in both cases [29]. .....	35
Figure 3:23: Profile of the deformation from a cylinder-shaped indenter, placed parallel to the grooves: (a) light load, (b) heavier load, (c) very heavy load [29]. .....	36

Figure 3:24: (a) the flow around a indenter from a highly worked-hardened metal produces “piling-up”. (b) For annealed metals the metal flow at a small distance from the indenter is illustrated and called “sinking in” [29].	37
Figure 3:25: Stress-strain diagram for tensile specimen [16]	39
Figure 3:26: Stress-strain models (a) Elastic-perfectly plastic curve, (b) Bilinear curve and (c) Multilinear curve.	40
Figure 3:27: Element types: (a) triangle node (b) quadrilateral node (c) triangle node (d) quadrilateral node [38]	40
Figure 4:1: Design of a ROV compatible PRT	42
Figure 5:1: Shows an overview of where the main parts are located and where the force (F) and reaction force acts ( $R_r$ ). A detailed view of the cone angle is also illustrated to the left.	45
Figure 5:2: Detailed view over the main interacting parts and reaction force from the bearing steel ball when exerted a force from the set-pipe.	46
Figure 5:3: Overview of hardness in the different parts, where 1 is the hardest.	46
Figure 5:4: Shows an overview of where the main parts are located and where the force (F). A detailed view of the cone angle is also illustrated to the left.	49
Figure 5:5: Detailed view over the main interacting parts and reaction force from the bearing steel ball when exerted a force from the set-pipe.	49
Figure 5:6: Overview of hardness in the different parts, where 1 is the hardest.	50
Figure 6:1: Overview of the measured areas on the cone	53
Figure 6:2: Six cones are presented with angles 3,4,5,6,8 and 10, with the following order starting from the left.	54
Figure 7:1 : Overview of the mesh elements in ANSYS. Contact size element is 0,2 mm.	55
Figure 7:2: Overview of the location of Reaction force and Displacement of the bearing steel ball	56
Figure 7:3: Elastic-plastic ANSYS model equivalent stress development in bearing steel ball	56
Figure 7:4: Overview of where the steel ball slides and sticks to the contact surfaces.	57
Figure 7:5: Reaction force vs Contact size element in elastic-plastic simulation	58
Figure 7:6: Indentation in pipeline wall vs Contact size element in elastic-plastic simulation	59
Figure 7:7: Maximum equivalent stress vs Contact size element in elastic-plastic simulation	59
Figure 7:8: Yield stress vs Indentation in pipeline in elastic-plastic area.	60
Figure 7:9: Yield stress vs Reaction force in pipeline in elastic-plastic area.	61
Figure 7:10: Yield stress vs Maximum equivalent stress in pipeline in elastic-plastic area.	61
Figure 7:11: Tangent Modulus vs Indentation in pipeline in pipeline in elastic-plastic area.	62
Figure 7:12: Tangent Modulus vs Reaction force in pipeline in elastic-plastic area.	62
Figure 7:13: Tangent Modulus vs Maximum equivalent stress in elastic-plastic area.	63
Figure 7:14: Reaction force vs Contac sizing element in a Linear-elastic model.	64
Figure 7:15: Indentation in pipeline vs Contac sizing element in a Linear-elastic model	64
Figure 7:16: Maximum Equivalent stress vs Contac sizing element in a Linear-elastic model	65
Figure 8:1: Indentation depth vs average stress with a reaction coefficient of 7,17 and a set-pressure of 5 MPa.	68
Figure 8:2: Brinell hardness number in terms of force applied on the steel balls and indentation diameter into the pipeline.	70
Figure 8:3: Reaction forces from the bearing steel ball	72
Figure 8:4: Cylinder pressure when testing 34CrNiMo6 alloyed cone.	74
Figure 8:5: Deformation on the 34CrNiMo6 alloyed cone and inside of the pipe wall.	75
Figure 8:6 : Indentation depth vs Set-Pressure from empirical testing	77
Figure 8:7: Picture of spherical deformation on the pipeline wall with Set-Pressure of 15,30 and 50 bar when used a cone of 3-degree angle alloyed with Calmax.	77
Figure 8:8: Picture of spherical deformation on the pipeline wall with Set-Pressure of 7,5 , 10 and 12,5 bar when used a cone of 4-degree angle alloyed with Calmax.	78

Figure 8:9: Picture of spherical deformation on the pipeline wall with Set-Pressure of 17,5 and 25 bar when used a cone of 4-degree angle alloyed with Calmax. ....	78
Figure 8:10: Picture of spherical deformation on the pipeline wall with Set-Pressure of 25 and 35 bar when used a cone of 10-degree angle alloyed with Calmax. ....	79
Figure 8:11 Reaction force vs friction coefficient results from ANSYS simulation of an Elastic-Plastic model .....	80
Figure 8:12: Indentation in pipeline vs friction coefficient results from ANSYS simulation of an Elastic-Plastic model.....	81
Figure 8:13: Maximum Equivalent stress vs friction coefficient results from ANSYS simulation of an Elastic-Plastic model.....	81
Figure 8:14: Pipeline indentation in ANSYS with a displacement of 0,5 mm and friction coefficient of 0,2. ....	82
Figure 8:15: Pipeline indentation in ANSYS with a displacement of 1 mm and friction coefficient of 0,2. ....	82
Figure 8:16: Pipeline indentation in ANSYS with a displacement of 2 mm and friction coefficient of 0,2. ....	83
Figure 8:17: Pipeline indentation in ANSYS with a displacement of 3 mm and friction coefficient of 0,2. ....	83
Figure 8:18: Reaction force vs friction coefficient results from ANSYS simulation of a Linear-Elastic model .....	84
Figure 8:19: Indentation in pipeline vs friction coefficient results from ANSYS simulation of a Linear-Elastic model.....	84
Figure 8:20: Maximum equivalent stress vs friction coefficient results from ANSYS simulation of a Linear-Elastic model.....	85
Figure 9:1: Strain-Stress variation of the same material .....	89



# List of Tables

Table 1:1: Features of previously made PRT.....	2
Table 2:1: Advantages and disadvantages of Ballgrab PRT.....	6
Table 2:2 : Table of Ballgrab PRT size correlated with lifting capacity [52].....	6
Table 2:3: Advantages and disadvantages of PII-Technomarine PRT .....	7
Table 2:4: Advantages and disadvantages of Industrikonsult PRT.....	8
Table 2:5: Technical specification from a 16-inch PRT [6] .....	8
Table 2:6: Advantages and disadvantages of MORGRIP.....	10
Table 2:7: Technical data for different parts in PRT [10].....	12
Table 2:8: Advantages and disadvantages of IK-Norway PRT .....	12
Table 3:1:(a) Shown the observed data of the development of plastic deformation as the load increases in a work-hardened mild steel with a 10 mm diameter steel ball. (b) The ratio between W and WL and $P_m/P_N$ . [29] .....	24
Table 3:2: Shows at what load plastic deformation and fully plastic deformation occurs for different materials [29]. .....	34
Table 3:3: Shows when the plastic deformation occurs with respect to type of material and the radii of curvature of the asperities [29].....	35
Table 3:4: Properties of two curatives [30].....	38
Table 3:5 : Different phase of the elastomer in terms of temperature [30].....	38
Table 5:1: Description and approximate hardness number of the main interaction parts.....	46
Table 5:2: Description and approximate hardness number of the main interaction parts.....	48
Table 5:3: Description and approximate hardness number of the main interaction parts.....	50
Table 6:1: Tensile and Yield stress for Calmax [44] .....	52
Table 6:2: Measurements before the hardening process .....	53
Table 6:3: Measurements after the hardening process.....	53
Table 6:4: Percentage change in the selected measurements: X,Y,Z,H and $\Theta$ .....	54
Table 7:1: Non-linear material properties for S355 steels [39].....	57
Table 7:2: Number of elements and Nodes with different contact size element in an Elastic-plastic model .....	59
Table 7:3: Number of elements and Nodes with different contact size element in a Linear-Elastic model .....	65
Table 8:1: Static reaction force from bearing steel ball on pipeline and cone illustrated in Figure A-3 .....	66
Table 8:2: Friction coefficient and reaction force from bearing steel ball with an angle of 3 degrees. 66	66
Table 8:3: Cylinder set-pressure and reaction force from the bearing steel balls .....	67
Table 8:4: Approximated indentation depth into the pipeline .....	68
Table 8:5: Huber-Mises and Tresca criterion for when plastic deformation starts to occur with a spherical indenter with various yield stresses .....	69
Table 8:6: When fully plastic deformation occurs with various Yield stresses. ....	69
Table 8:7 : Loads for when plastic deformation occurs with a spherical indenter with a radius of 5mm with various yield stresses. ....	70
Table 8:8: Contact stress constants. ....	71
Table 8:9: Analytical calculated stresses between each bearing steel ball and cone with an angle of 3 degrees .....	71
Table 8:10: Analytical calculated stresses between each bearing steel ball and pipeline with a cone angle of 3 degrees .....	72
Table 8:11: Contact area and deflection that occurs between the 3-degree cone and bearing steel ball .....	73

Table 8:12 : Set-Force on steel balls, pipeline distance travelled and applied load on pipeline with a 34CrNiMo6 alloyed cone.....	73
Table 8:13: 34CrNiMo6 alloyed cone test results with an angle of 5 degrees.....	74
Table 8:14: Empirical testing results with 3,4- and 10-degree cone-angle alloyed with Calmax.....	76
Table 9:1: Friction coefficient, Displacement and stresses obtained from ANSYS results.....	88

# Abbreviations

PRT	Pipeline Recovery Tool
DNV	Det Norske Veritas
ROV	Remotely Operated Vehicle
OD	Outer Diameter
ID	Inner Diameter
IPLT	internal pile lifting tool
HV	Hardness Vickers
HB	Hardness Brinell
HRC	Hardness Rockwell C
PUR	Polyurethane
B.H.N	Brinell Hardness Number
DIN	Deutsches Institut für Normung
ASME	American Society of Mechanical Engineers
CTO	Chief Technology Officer
FEA	Finite Element Analysis
UiS	Universitetet I Stavanger
PPG	Poly-Propylene Glycol
PTMEG	Polytetramethylene Ether Glycol
TDI	Toluene diisocyanate
MDI	Methylene diphenyl diisocyanate
FDA	Food & Drug Administration
PPDI	Para-phenylene diisocyanate
CHDI	Eyclohexane diisocyanate
vs	versus
“	Inch

# Nomenclature

Symbol	Description	Unit
P, F	total force exerted by body 1 on body 2 and otherwise	N
$P_m$	Mean pressure	MPa
W	Load	Kg
p	Pressure	MPa
$R_f$	Wedge lock reaction force	N
E	Youngs Modulus	MPa
Y	Yield stress	MPa
$\theta$	Angle between the cone and pipeline inner walls	°
$\alpha$	Angle between planes of principle curvatures	°
A, B	Roots of a quadratic equation	mm <sup>-1</sup>
a	Semimajor axis	mm
b	Semiminor axis	mm
R, r	Radius	mm
D	Diameter	mm
$\nu_1, \nu_2, \sigma_1, \sigma_2$	Poisson ratio for two bodies	(-)
$R_1, R'_1, R_2, R'_2$	Principle radii	Mm
$Z_s$	Distance from contact surface to max shear stress	mm
$\sigma_{max}$	Maximum stress	MPa
$\tau_{max}$	Maximum shear stress	MPa
$\tau_{(oct(max))}$	Maximum orthogonal shear stress	MPa
$\delta$	Deflection between two bodies	mm
$\sigma_{xx}, \sigma_{yy}, \sigma_{zz}$	Principle stresses	MPa
e	Deformation radius	mm
V	Volume	mm <sup>3</sup>
$P_0$	Pressure centre of spherical indenter	MPa
$W_L$	Plastic deformation load of a spherical indenter	Kg
n	Number of bearing steel balls	(-)
$E_T$	Tangent modulus	MPa
$\sigma_{yield}, \sigma_{yield2}, \sigma_{ult}, \sigma_{prop}$	Yield stress (strain-stress curve parameter)	MPa
$\epsilon_{p\_y1}, \epsilon_{p\_y2}, \epsilon_{p\_ult}, \epsilon_t, \epsilon_e, \epsilon_p$	Strain-stress curve parameter	(-)

# 1. Introduction

The retrieval of a subsea pipeline from the seabed can occur for various reasons such as decommissioning and repair. Furthermore, a pipeline recovery tool is used to retrieve the pipeline. According to Soheil Manouchehri [1], during the next years, the decommissioning market for offshore and subsea pipeline is going to significantly grow. The reason for that is that many producing fields will reach the end of their lives. There has been a large production in subsea pipelines since 2003 according to DNV's report [2]. These pipelines will eventually be decommissioned, and this will potentially lead to increased market demand for PRT's in the near future. There are many different solutions to retrieve a pipeline as presented in Chapter 2. However, the technology presented in this study, is to the author's knowledge not published. Which might be because of competition or that there is no good research on it. The key drivers for developing a PRT are cost, weight, functionality, capacity and size, which was considered when the PRT presented in Chapter 4 was designed.

This study investigates on a new concept to retrieve pipelines, which can compete with development, production and maintenance costs in the well-established industry. It is focused on using applicable theory, empirical testing and finite element analysis to optimize the design and development of the recovery tool. Through simulations in ANSYS and empirical testing it is possible to investigate which of the parameters that affects the spherical deformations and lifting capacity of the recovery tool.

## 1.1. Background and Motivation

The new concept studied in this thesis has its origin from IK-Norway's plug technology. IK-Norway's plug technology uses steel balls casted into polyurethane as a part of a wedge lock and sealing mechanism or as a PUR extrude preventer in plugs. This led to further interest to apply this technology in a PRT. The use of steel balls in a wedge-lock mechanism is well known and are used in various ways: bike gears, lock cable ties, truck brakes and PRT's. With the results from the plug technology and the fact that steel balls are widely used in wedge-locking, it was believed that combining polyurethane and bearing steel balls in a PRT would allow it to retrieve subsea pipelines while sealing it at the same time.

As a final PRT product, the operation will follow the following steps:

- The tool is first inserted at the end of the subsea pipeline using an ROV.
- A load applied using hydraulic pressure on the set-pipe to push the packer containing the bearing steel balls (Ref. Figure 4:1).
- As a result, the packer and the bearing steel ball will move along the cone surface and will press against inside of the pipeline wall. The steel ball will be mechanically locked between the pipeline and cone, the polyurethane will seal off the area between the PRT and pipeline.
- By sealing off the area between the PRT and the pipeline, gives the possibility to remove the water inside the pipeline by using a pig.
- The PRT is then retrieved with the wireline that is connected at the end of the PRT.
- As a result, the reaction forces between the PRT and pipeline wall will increase, and it will lock itself even more onto the subsea pipeline. This cause a self-locking mechanism.

This thesis investigates how the main components affect each other in the wedge lock mechanism. Furthermore, the thesis studies how the wedge lock mechanism with bearing steel balls affects the interacted parts. Moreover, how the indentation and reaction forces respond to changes in material properties and design parameters are also investigated. The test-rig is modelled in the finite element analysis tool, ANSYS in order to study the phenomena in great details.

## 1.2. Previous work

BSW Limited (founded in 1983 and renamed to First Subsea), is one of the first companies to use a ball and taper mechanism in a pipeline recovery tool. They invented the Ballgrab tool in 1983, which was also at a time when subsea development was growing. Ballgrab has been in the market for a long time and has a wide range of dimensional use and lifting capacity. This tool is further explained in Chapter (2.1). Another company which uses steel balls as it's gripping mechanism is Hydratight. They invented the recovery tool MORGRIP which is further explained in Chapter (2.4). Other recovery tools which uses slips comes from Industrikonsult, which is now named IK-Norway (Ref. Chapter 2.6), PII-Technomarine (Ref. Chapter 2.2) and Industrikonsult (Ref. Chapter 2.3). Another tool from IK-Norway which uses a pin through the pipeline to recover it, is explained in (Ref. Chapter 2.5). A quick overview of the features of the different recovery tools is presented in Table 1:1. Each recovery tool is awarded a score from 1-6, where 6 is the best score.

Name	Cost	Operation time	Size/weight	Capacity	Reliability/Safe to use	ROV compatible	DNV approved	Total Score
Ballgrab	2	5	3	5	5	Yes	Yes	20
PII-Technomarine PRT	2	5	3	4	5	Yes	Yes	19
Industrikonsult PRT	3	4	3	4	5	Yes	Yes	19
MORGRIP	3	4	2	5	5	No	Yes	19
IK-Norway PRT	4	3	4	5	4	Yes	Yes	20
Industrikonsult IPRT	3	4	2	6	5	Yes	Yes	20

Table 1:1: Features of previously made PRT

## 1.3. Scope of work

The goal for this thesis is to study the grabbing mechanism of a new pickup-tool for subsea pipelines. As previously mentioned, this new concept can retrieve and seal off the pipeline. The ability to seal off the pipeline allows the water inside the pipeline to be removed using a pig. This greatly reduces subsea operational costs.

As shown in Figure 1:1, the design of the PRT can be divided into three main sections. This thesis will focus on studying the mechanical wedge lock mechanism with bearing steel balls in detail. The items studied include the effect of geometrical change and material properties on the design, reliability and load capacity of the PRT. The thesis uses extensive empirical testing and finite element analysis for this purpose.

First, two test-rigs were designed and fabricated to model the wedge-lock mechanism of the PRT. The purpose of the first test-rig (Ref. Figure 5:1) is to characterize the mechanical wedge-lock mechanism of the bearing steel balls. The purpose of the second test rig (Ref. Figure 5:4) is to allow tests on the wedge-lock properties from the steel balls and the sealing properties of the PUR to be performed. Most of the fabrication of the test-rigs were performed by the author. Further details of the test-rigs can be found in Chapter 5.

After, a computational model was developed in ANSYS to perform a series of sensitivity studies on a wide range of design parameters. The parameters studied were:

- The cone angles ( $\alpha$ ) (Ref. Figure 5:1)
- Yield stress for the interacted parts
- Hardness of the interacted parts
- Friction coefficient
- Displacement vs reaction force with various friction coefficients
- Reaction force vs indentation with various friction coefficients
- Maximum equivalent stress that occurs between the bearing steel ball and its contact zones with various friction coefficients

More details of the parameters above can be found in Chapter 5 and Chapter 7.

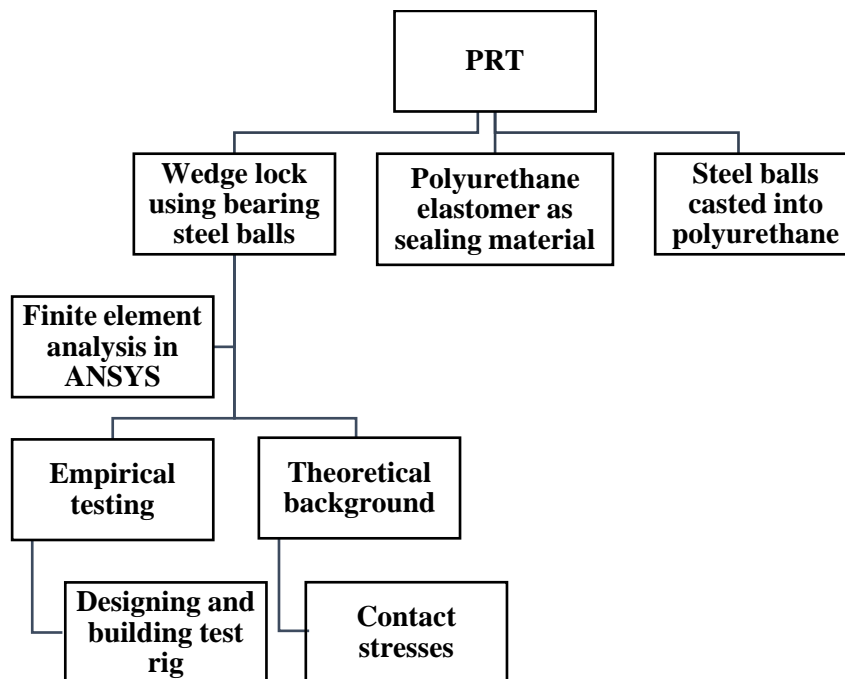


Figure 1:1 : Scope of the thesis

To the author's knowledge, there is no published work on the detailed experimental and computational analysis of the wedge-lock mechanism in a PRT.

## 1.4. Structure of report

This thesis is arranged in the following manner:

- Chapter 2: Current and previously made PRT's
- Chapter 3: Theoretical background on previous PRT's, spherical indentation in linear-elastic and elastic-plastic area, contact stresses, introduction to polyurethane and finite element analysis.
- Chapter 4: System description and design of a ROV compatible PRT
- Chapter 5: Test-rig description with cone alloyed with 34CrNiMo6 and cone alloyed with Calmax from Uddeholm.
- Chapter 6: Material description of the interaction parts: Cone, Pipeline and bearing steel balls.
- Chapter 7: Validation, sensitivity study and a presentation of the ANSYS model.
- Chapter 8: Presentation of the analytical calculation, empirical and FEA results.
- Chapter 9: Discussion of the results and reflection of how that's affecting the final PRT product.
- Chapter 10: Conclusion of this study and recommendations for future work.



## 2. Current and previously made PRT's

### 2.1. Ballgrab

This is a mechanical PRT, which uses the ball and taper technology to grab the inside of the pipeline wall. The metal balls are activated mechanically, using applied horizontal loading. Due to an incline, the balls are being pushed into the inside of the pipeline wall, which causes the PRT to lock on to the pipeline. The loading causes the balls to make dents into the pipeline. The depth of the dent depends on several parameters which includes material properties, incline angle and weight of the pipeline. The Ballgrab has a self-locking mechanical system. This type of system is often called fail-safe lifting system. After the tool has been hydraulically set, the initial reaction force between the steel balls and the pipeline are added to the lifting force, which makes the principle of self-locking. Figure 2:1 presents the Ballgrab technology PRT with the PIG receiver, elastomer packers and steel balls highlighted. The elastomer packers provide self-sealing capability to the PRT.

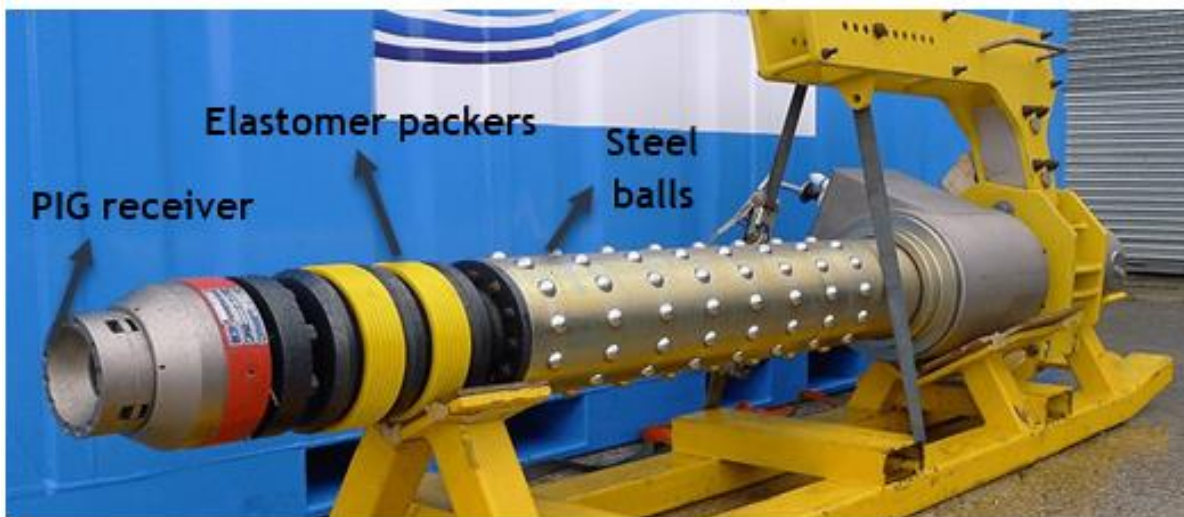


Figure 2:1: Ballgrab PRT [51]

The tool is guided into the end of the pipeline and once it has been activated, it cannot be removed before the tension on the PRT is zero. When the tool is retrieved, it can be reused. Ballgrab is available in both male and female versions. It also has a seal section, which can be used to de-watering the pipe if necessary [3]. The typical size of the Ballgrab is 2-48 inch in OD of the tool. Furthermore, advantages and disadvantages are listed in Table 2:1. Table 2:2 contains the lifting capacity and dimensions for a Ballgrab recovery tool.

Advantages	Disadvantages
Fast to install and attach to the pipeline	It is a big and heavy PRT relative to the pipe. The tool size depends on the weight and ID of the pipe.
Easy to operate	The seal property does not work properly in air.
De-watering of the pipeline can be done with Ballgrab	
The tool is ROV compatible and can be controlled from a vessel, without the impact from the vessel motion.	
The tool is DNV approved, which means that is it an approved equipment from a third part company.	

Table 2:1: Advantages and disadvantages of Ballgrab PRT

Size (")	WLL (T)	Proof Load (T)	Working Range (mm)	Max Working Range (mm)	Mandrel Length (mm)	Actuation
30	300	386	680	735,6	1000	Hydraulic
24	278	260	563	585,5	2528	Hydraulic
20	90	198	450	486,2	796	Paddle
18	1000	1220	390	439,7	2880	Hydraulic
16	200	264	352	378	1026	Paddle
14	145	196,9	337	369,9	1983	Hydraulic
12	120	166,4	282	306,7	1472	Hydraulic
10	327	419	215	256,7	2643	Hydraulic
8	48	96	172	199,5	2344	Paddle
6	230	300	134	171,4	1235	Paddle
5	42,5	299,89	117	128	1799	Paddle
4	37,7	46	94,6	106,8	599	Spring
3,5	39	68	79	90	869	Spring
2,5	15	46	62	66,5	748	Spring

Table 2:2 : Table of Ballgrab PRT size correlated with lifting capacity [52]

## 2.2. PII-Technomarine PRT

This PRT grabs from inside the pipe walls, by using driving taper slips. The slips grab approximately 0.1 mm into the walls of the pipeline. Hydraulic pressure is used to activate the slips. The hydraulic pressure applied on the slips can come from an ROV or from the topside. This system also has a sealing property [3]. Figure 2:2 shows a detailed cross-section view and the connection points of PII-Technomarine PRT.

Advantages	Disadvantages
The tool is ROV compatible and can be controlled from a vessel, without the impact from the vessel motion.	This tool is quite expensive to develop and produce.
De-watering of the pipeline can be done with PII- Technomarine PRT.	Hydraulic force is required for tensioning and setting the packers.
The tool is DNV approved, which means that is it an approved equipment from a third part company.	

Table 2:3: Advantages and disadvantages of PII-Technomarine PRT

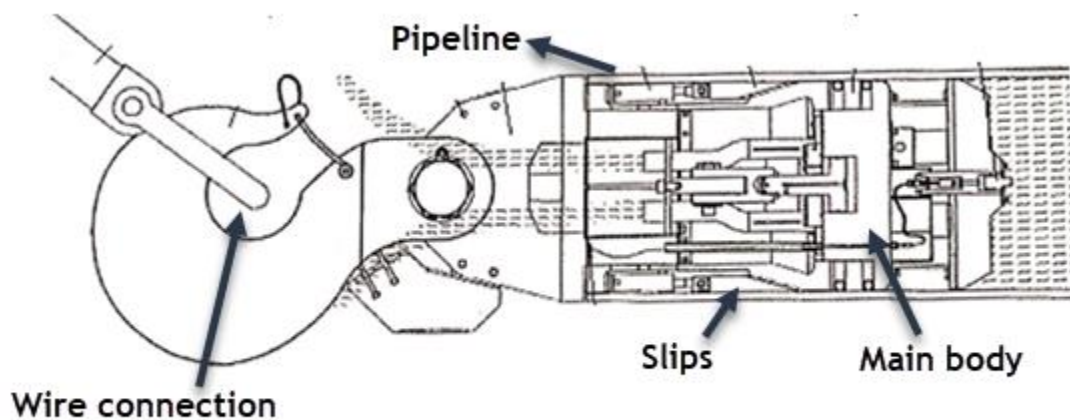


Figure 2:2: Cross-section view of PII-Technomarine PRT [3]

## 2.3. Industrikonkonsult PRT

Industrikonkonsult's pipeline recovery tool grabs inside of the pipeline wall using slips. The tool is inserted at one end of the pipeline. Once it is in position, a hydraulic load is applied to the slips. The slips will then slide on the incline and grip the inside of the pipeline walls [6]. Figure 2:3 shows a detailed illustration of Industrikonkonsult's PRT, which contains the locations and explanations of the different components in the PRT. The lifting capacities are presented in Table 2:5.

Advantages	Disadvantages
The tool is ROV compatible and can be controlled from a vessel, without the impact from the vessel motion.	The weight of this PRT is quite high. This makes it more demanding to handle.
Redundancy on hydraulic circuits, which means that it is often required multiple pressure sources.	Hydraulic force is required for pre-tensioning, which may result in the need for a big umbilical when performing the lifting operation with this recovery tool.
The tool is DNV approved, which means that is it an approved equipment from a third part company.	

Table 2:4: Advantages and disadvantages of Industrikonsult PRT

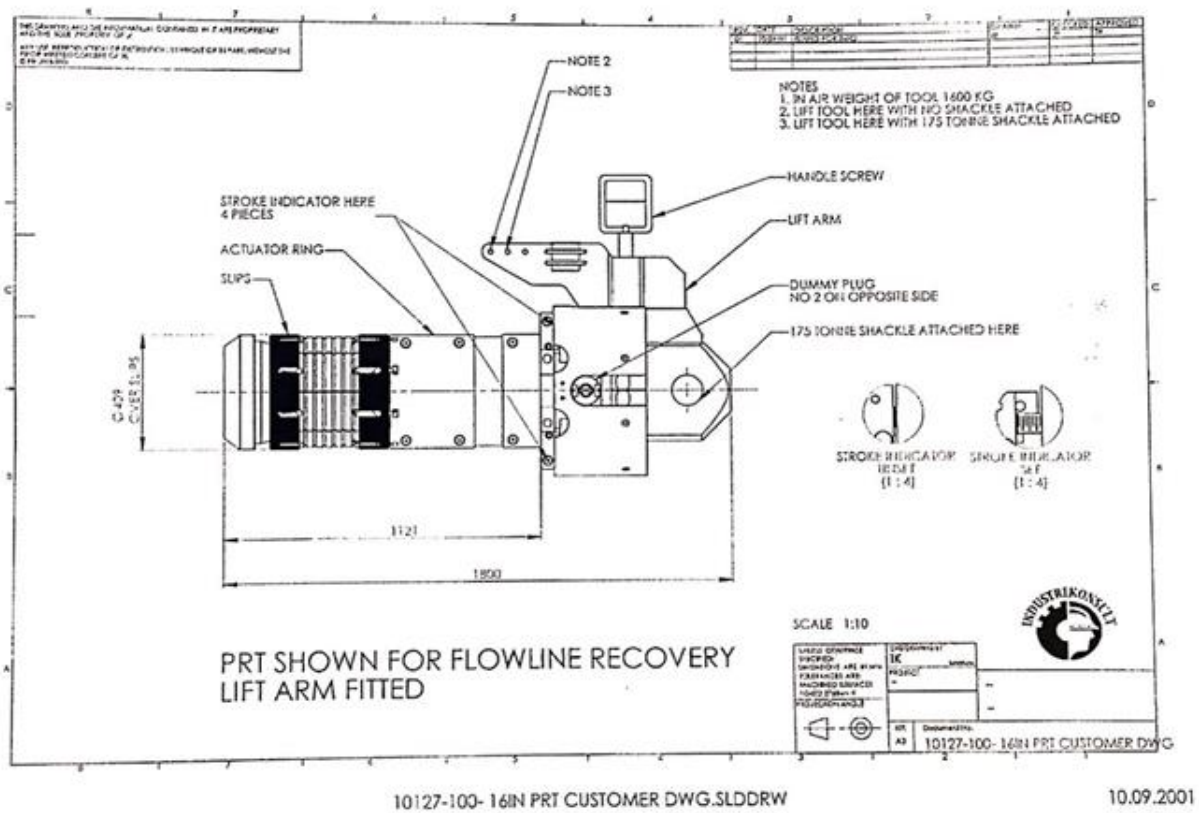


Figure 2:3: Detailed technical drawing from Industrikonsult of their PRT [6]

Description	Magnitude
Design load:	130 tons
Proof Test Load	180 tons
Bending moment at max operation tension:	67 KNm at 130 tons axial tension
Maximum bending moment:	118 KNm at 0 axial tension

Table 2:5: Technical specification from a 16-inch PRT [6]

## 2.4. MORGRIP

MORGRIP is a mechanical grip tool that is applied around the pipeline. It uses metal balls to grab the outside of the pipeline walls. This tool is usually used as a connector between pipelines and not as a recovery tool for pipelines. However, it has been used as a PRT in 2001 [3]. Figure 2:4 illustrates a quarter section of an MORGRIP. The location of the metal balls is shown in Figure 2:4. A detailed view with explanations and locations of the different components in the PRT are illustrated in Figure 2:5.

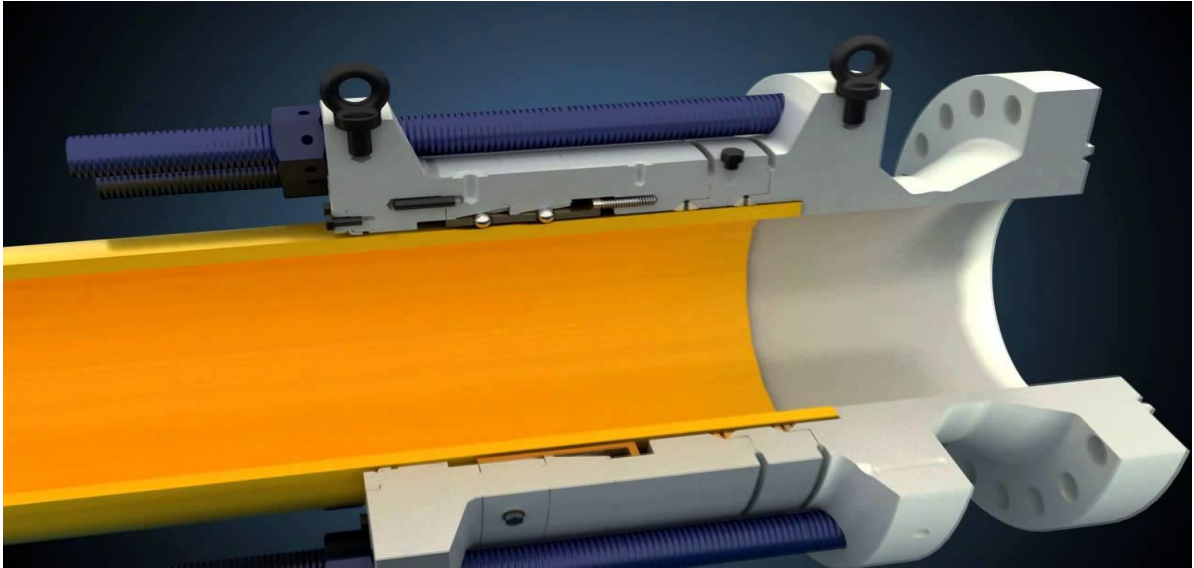


Figure 2:4: MORGRIP connection quarter section view [27]

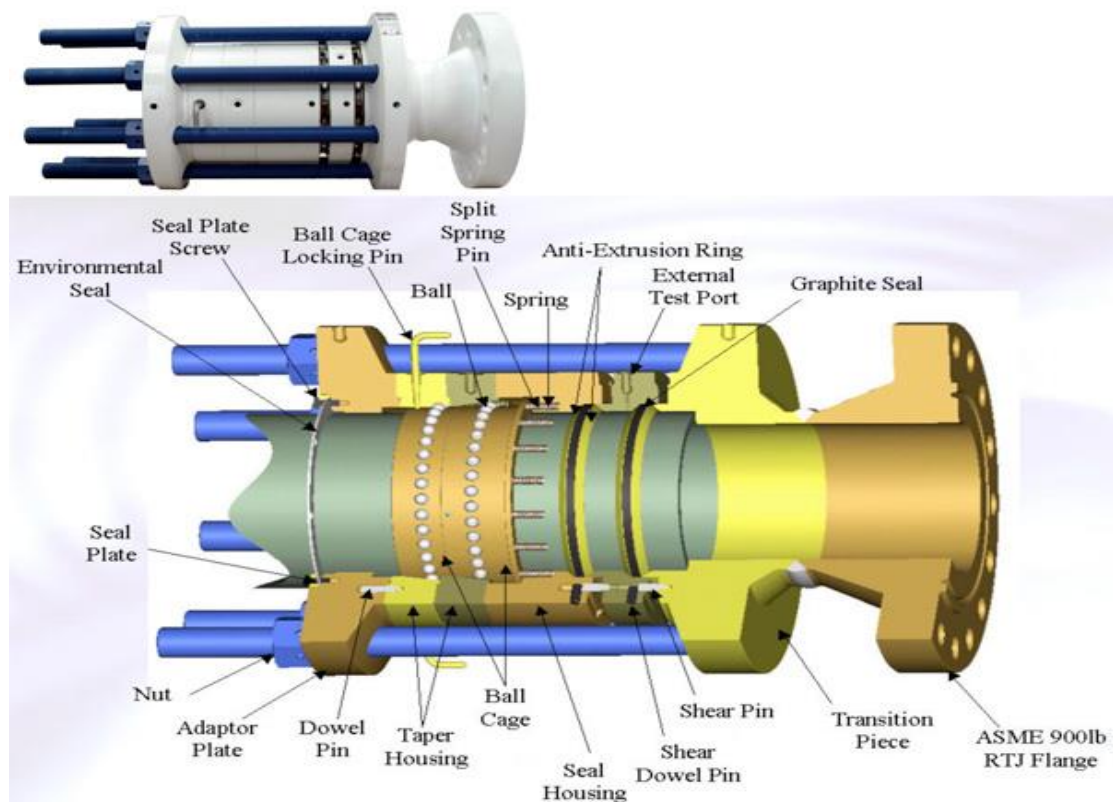


Figure 2:5: Detailed view of MORGRIP connector [27]

The steel balls are activated by using a spring force. The studbolts are turned and this pushes the metal flanges together. This in turn transfers the force onto the balls. The pipeline walls have the lowest yield stress and hardness, therefore; the metal balls will make dents into the pipeline. Moreover, the applied wedge-locking force makes enough reaction force to withstand a large amount of tensile force on the pipeline. The tool seals at the end of each side using compressed O-rings as shown in Figure 2:5. These tools are often used when the internal diameter of the pipe is too small for an internal PRT to enter. Deep-water pipelines are exposed to higher hydrostatic pressure and requires an increase in wall thickness. This causes the pipeline to increase in weight and can cause the space inside the pipeline to decrease. The technology for Ballgrab and MORGRIP is in principle the same, just inverted. The advantages and disadvantages are presented in Table 2:6.

<b>Advantages</b>	<b>Disadvantages</b>
Easy to confirm the sealing properties in the field	It is a big and heavy PRT relative to the pipe. The tool size depends on the weight and ID of the pipe.
Easy to pre-tension	Relatively expensive tool.
The tool is DNV approved, which means that is it an approved equipment from a third part company.	Gripping outside the pipeline, which will destroy any coating.
	Not ROV compatible

Table 2:6: Advantages and disadvantages of MORGRIP

## 2.5. IK-Norway Pipeline Recovery Tool

This is a mechanical PRT, which have no sealing opportunities. Figure 2:6 illustrates and enumerates the different components in the PRT. The tool is placed around the pipe with help of an ROV. Furthermore, the tool drills a hole in the pipeline, and then insert the pins (4.4 and 4.3). After the pins have been locked in its functional position, the lifting lug (4.2) are connected topside and the pipeline can be dragged back up to the surface [10]. Table 2:7 presents the lifting capacity of the different parts in the PRT.

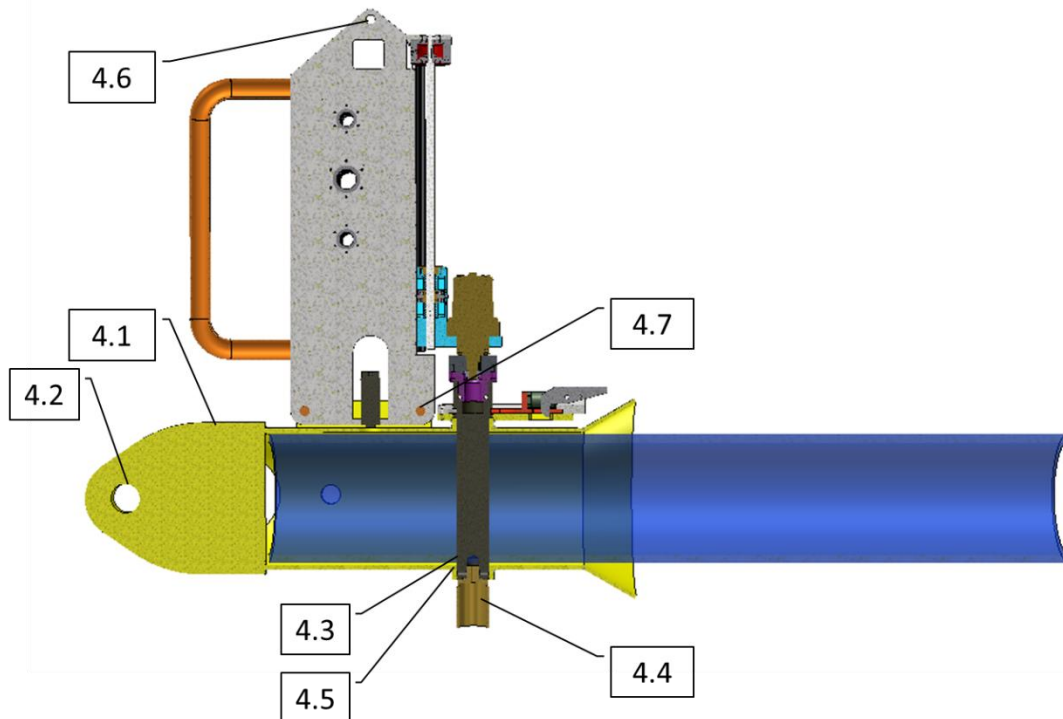


Figure 2:6: IK 14-inch PRT [10]

Section	Calculations	Utilization* wrt. dynamic load	Capacity	Safety factor* wrt. utilization
<b>4.1</b>	<b>Pad Eye Plate/14" Pipe Schedule 100</b>			
	Stress in weld	72.0%	-	1.4
<b>4.2</b>	<b>75 Tonne Lifting Lug</b>			
	Tear-out stress	24%	319 Tons	4,1
	Contact stress	50%	150.4 Tons	2
	Cheek plate welds	50%	148 Tons	2
<b>4.3</b>	<b>Lifting pin/ 1</b>			
	Contact stress	18%	414 Tons	5,6
<b>4.4</b>	<b>Lifting Pin</b>			
	Shear force check	23%	330 Tons	4,3

	Moment check	63%	8.9 Tons*m	1.6
	Combined shear and moment check	81.7%	-	1.2
<b>4.5</b>	<b>Lifting Pin/14” pipe schedule 100</b>			
	Contact stress	8%	924 Tons	12,5
<b>4.6</b>	<b>1,5 tons lifting lug in drill rig</b>			
	Tear-out stress	19%	7.8 Tons	5,3
	Contact stress	7%	22.9 Tons	14
	Cheek plate welds	19%	8 Tons	5,3
<b>4.7</b>	<b>Lock Pin Capacity (0,28ton load)</b>			
	Shear stress	9%	3.2 Tons	11

Table 2:7: Technical data for different parts in PRT [10]

<b>Advantages</b>	<b>Disadvantages</b>
The tool is DNV and NORSOK approved, which means that it is an approved equipment from a third part company.	The lifting capacity and the PRT itself are sensitive to external forces
Easy to use	There is a limitation to how thick the wall thickness can be.
Simple mechanical solution	
High lifting capacity	
It is relatively small tool, which makes it easier to handle during operations.	

Table 2:8: Advantages and disadvantages of IK-Norway PRT



## 2.6. Industrikonsult IPLT

This PRT is often used for large ID pipelines. This tool uses slips to grab the inside of the pipeline. The drive plate has a slight incline. When a force is applied to the slips, a normal force gets applied to the wall of the pipeline. Moreover, it causes the wedge lock force increase, and the pipeline will deform slightly in this process. Figure 2:7 illustrates and points out the different components in the PRT [11].

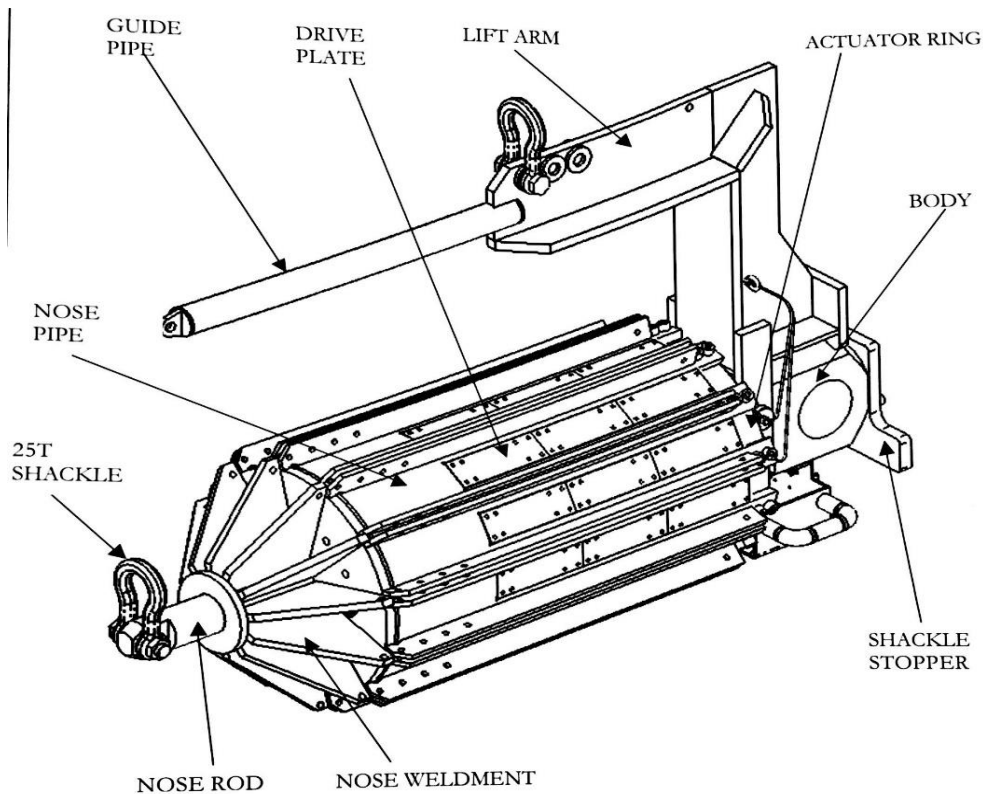


Figure 2:7: Overview of Industrikonsult IPLT 48" to 84" [12]

Some of the features in this recovery tool are [12]:

1. 500 tons SWL, DNV certified.
2. Hydraulically set slips that are fail-safe once self-locking. The IPLT cannot be released if it's under tension.
3. Hydraulic Power Unit, HPU, with hose reel on separate skids.
4. Hot stab for ROV backup.
5. Internal gripping on the pipeline wall at least 170 mm from the pile end.
6. The tool has been designed to suit a 1000T WLL shackle to allow heavier loads to be lifted in the future.
7. Lifting arm fitted to IPLT for horizontal installation can be removed after the tool is set.
8. The lift arm also has a guide pipe where a rope/tugger wire can be connected and used to guide the IPLT into the pile.

## 3. Theoretical background

### 3.1. Introduction

The dominating physical problem in the wedge-lock mechanism is the contact stress problem. This chapter will introduce and discuss the theoretical background behind the contact stress problem.

Properties of PUR which are used in the PRT are also presented in this chapter. Lastly, an introduction of finite element analysis and material models are presented in this chapter.

### 3.2. Contact Stresses

Pressure from one solid to another over a limited contact area causes contact stresses. Of a structure/body most of the failures happens “far” away from where the applied load and contact area occurs, due to high stresses and strains [16]. Some engineering examples where there is significant stress at the contact are between a locomotive wheel and the railroad rail and between a roller or ball and its race in a bearing. Moreover, these examples are often not in a static position, and are often exposed to cyclical loading. This would result in fatigue and development of cracks over time. Moreover, contact stresses often lead to fatigue cracks and may therefore reduce the actual loading capacity of the body. Due to the fatigue crack area it is also reason to believe that the significant stress also lay near the contact stresses [16].

Figure 3:1 shows two different bodies with different radii that are in contact with each other, with an applied force  $P$ . Initially the contact area of these two structures are infinitely small.

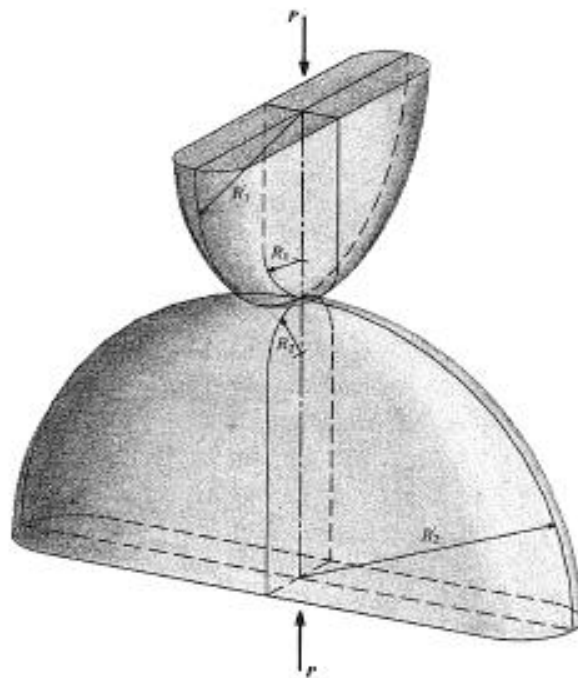


Figure 3:1: Two curved surfaces with different radii pressed against each other with a force  $P$  [16].

Figure 3:2 shows that the lines  $V_1$  and  $V_2$  forms an angle  $\alpha$ , which lies in the plane section containing the radii  $R_1$  and  $R_2$  illustrated in Figure 3:2 (a). The load  $P$  lies at the axis that goes through the centre of the curvatures and contact surface, illustrated in Figure 3:2 (a) and (e). It is assumed that the two

bodies cannot slide respectively to each other, hence there is no friction force acting of the bodies. The acting load  $P$  cause the two bodies to elastically deform which will make the contact area shown in Figure 3:2 (e). The challenge is to determine the relationship between the applied load  $P$ , the maximum compressive stress on the small area and the principal stresses in any of the bodies. The principal stresses are shown in Figure 3:2 (c).

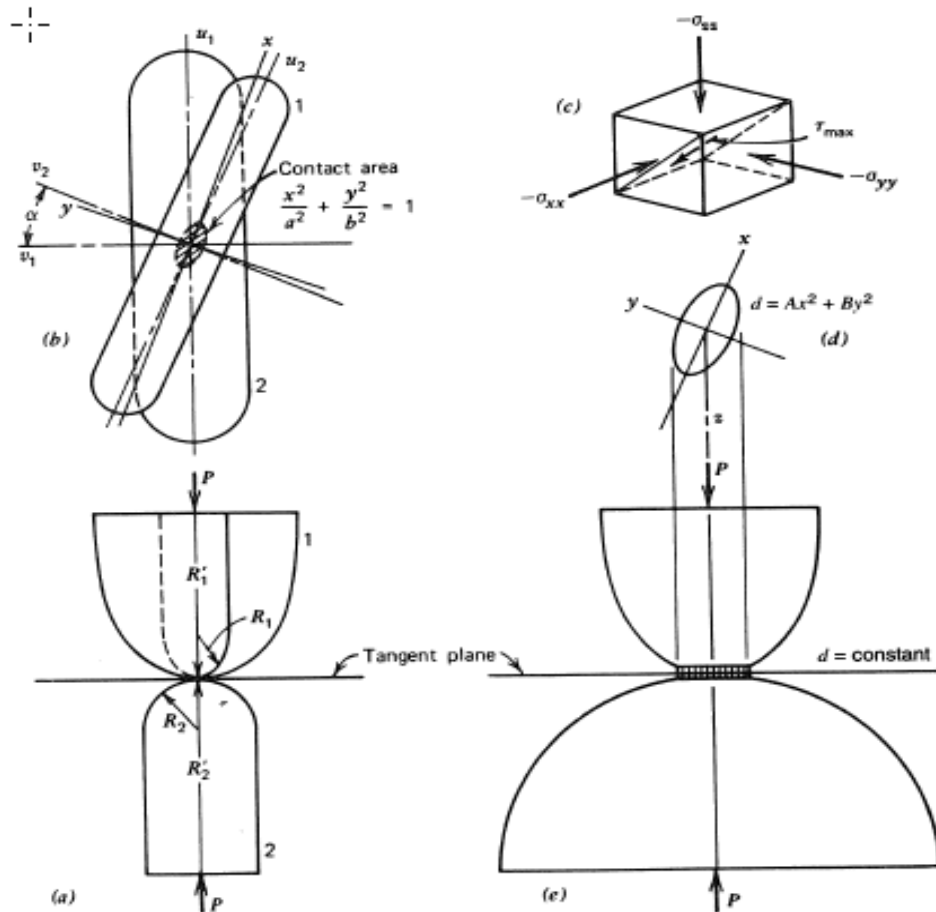


Figure 3:2: Analysis of contact stresses [16]

### 3.2.1. Fundamental Assumptions

The solution for contact stresses are based on the following two assumptions:

- (a) **Properties of Materials.** “The material of each body is homogeneous isotropic, and elastic in accordance with Hooke’s law, but the two bodies are not necessarily made of the same material” [16].
- (b) **Shape of Surfaces near Point of Contact, Before Loading.** There is a common tangent plane to the surfaces at the point of contact, when two bodies are in contact at a point. When solving the contact stress, an expression for the distance between two points near the point of contact is required; This equation is expressed with the two distances  $z_1$  and  $z_2$ , which gives an approximate of total distance for any given two surfaces used [16]:

$$d = Ax^2 + Bx^2 = z_1 + z_2 \quad (3.1)$$

Where A and B are positive constants that depends on the radii and curvature of the two bodies. X and y are the coordinates with respect to the point of contact and lies in the tangent plane shown in Figure 3:2. Figure 3:3 illustrates an example on which points the distance  $z_1$  and  $z_2$  are calculated from.

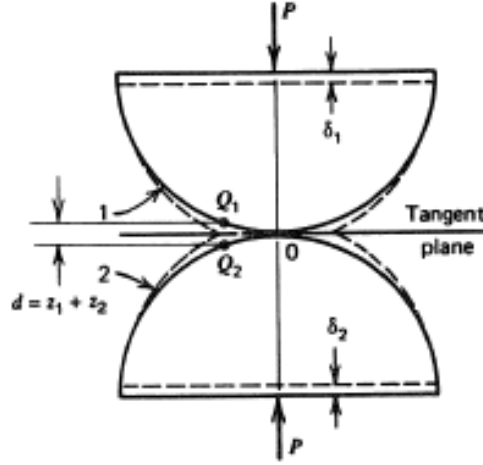


Figure 3:3: Geometry of contact surface [16]

### 3.2.2. Key equation used considered contact stresses

A and B are the roots of a quadratic equation. The equations for A and B are:

$$B = \frac{1}{4} \left( \frac{1}{R_1} + \frac{1}{R_2} + \frac{1}{R'_1} + \frac{1}{R'_2} \right) + \frac{1}{4} \sqrt{\left[ \left( \frac{1}{R_1} - \frac{1}{R'_1} \right) + \left( \frac{1}{R_2} - \frac{1}{R'_2} \right) \right]^2 - 4 \left( \frac{1}{R_1} - \frac{1}{R'_1} \right) \left( \frac{1}{R_2} - \frac{1}{R'_2} \right) \sin^2 \alpha} \quad (3.2)$$

$$A = \frac{1}{4} \left( \frac{1}{R_1} + \frac{1}{R_2} + \frac{1}{R'_1} + \frac{1}{R'_2} \right) - \frac{1}{4} \sqrt{\left[ \left( \frac{1}{R_1} - \frac{1}{R'_1} \right) + \left( \frac{1}{R_2} - \frac{1}{R'_2} \right) \right]^2 - 4 \left( \frac{1}{R_1} - \frac{1}{R'_1} \right) \left( \frac{1}{R_2} - \frac{1}{R'_2} \right) \sin^2 \alpha} \quad (3.3)$$

$$\Delta = \frac{1}{A+B} \left( \frac{1-\nu_1^2}{E_1} + \frac{1-\nu_2^2}{E_2} \right) \quad (\text{mm}^3/\text{N}) \quad (3.4)$$

$$\sigma_{max} = -c_\sigma \left( \frac{b}{\Delta} \right) \quad (\text{N/mm}^2) \quad (3.5)$$

$$\tau_{max} = c_\tau \left( \frac{b}{\Delta} \right) \quad (\text{N/mm}^2) \quad (3.6)$$

$$\tau_{(\text{oct(max)})} = c_G \left( \frac{b}{\Delta} \right) \quad (\text{N/mm}^2) \quad (3.7)$$

$$\delta = c_\delta \frac{P}{\pi} \left( \frac{A+B}{\frac{b}{\Delta}} \right) \quad (\text{mm}) \quad (3.8)$$

$$b = c_b \sqrt[3]{P\Delta} \quad (\text{mm}) \quad (3.9)$$

$$z_s = c_{z_s} b \quad (\text{mm}) \quad (3.10)$$

Where:

P=total force exerted by body 1 on body 2 and otherwise

$E_1, E_2$  = Tensile or compressive modulus, called Young's modulus for body 1 and 2.

$\nu_1, \nu_2$  = Poisson ratio for body 1 and 2.

a = semimajor axis of ellipse of contact.

b = semiminor axis of ellipse of contact.

$K=b/a=\cos(\theta)$ ;  $k \leq 1$

$k'=\sqrt{1-k^2}=\sin(\theta)$

$R_1, R'_1$  = Principle radii values relative to the point of contact of body 1. The plane section in which  $R_1, R'_1$  lies in, are perpendicular to each other. See Figure 3:1 for illustration. If the centre of curvature lies inside (body surface is convex) the radius is positive. If the centre of curvature lies outside (body surface is concave) the radius is negative.

$R_2, R'_2$  = The same as  $R_1, R'_1$ , but has principle radii values relative to the point of contact of body 2.

$z_s$  = distance from contact surface to which the maximum shear stress and maximum orthogonal shear stress occurs in either body.

$\sigma_{max}$  = maximum stress

$\tau_{max}$  = maximum shear stress

$\tau_{(\text{oct}(max))}$  = maximum orthogonal shear stress

$\delta$  = deflection between two bodies as they approach each other. This is also shown in Figure 3:3 as it is the sum of  $\delta_1$  and  $\delta_2$ .

At  $k=0$  and  $z/b=0$  gives the maximum principle stresses occur at the contact surface. This gives the formulas:

$$\begin{aligned} \sigma_{xx} &= -\frac{b}{\Delta} \quad (\text{N/mm}^2) \\ \sigma_{yy} &= -2\nu\left(\frac{b}{\Delta}\right) \quad (\text{N/mm}^2) \\ \sigma_{zz} &= -\frac{b}{\Delta} \quad (\text{N/mm}^2) \end{aligned} \quad (3.11)$$

Maximum shear and orthogonal stress are found used equation (3.12) and (3.13), when  $k=0$  and  $z_s/b = 0.7861$ .

$$\tau_{max} = 0.3 \left(\frac{b}{\Delta}\right) \quad (\text{N/mm}^2) \quad (3.12)$$

$$\tau_{\text{oct(max)}} = 0.27 \left( \frac{b}{\Delta} \right) \quad (\text{N/mm}^2) \quad (3.13)$$

Figure 3:4, Figure 3:5 and Figure 3:6 are used to compute contact stresses and provide stress coefficients in static loading.

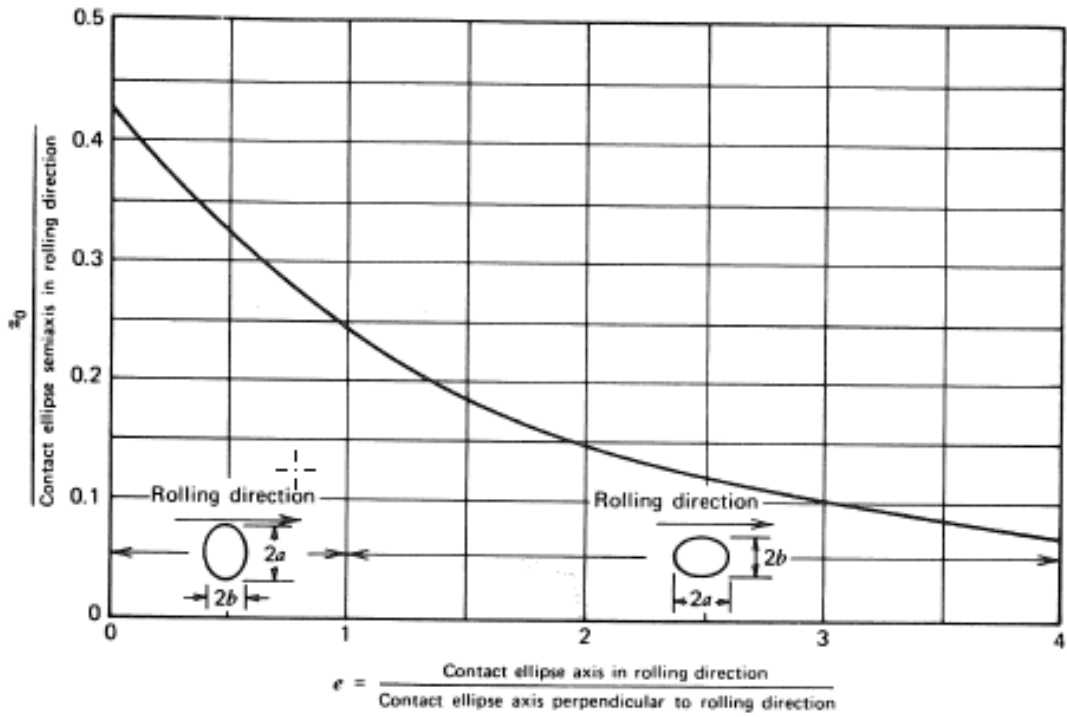


Figure 3:4: Distance  $Z_0$  at which  $\tau_{\text{oct(max)}}$  occurs [16].

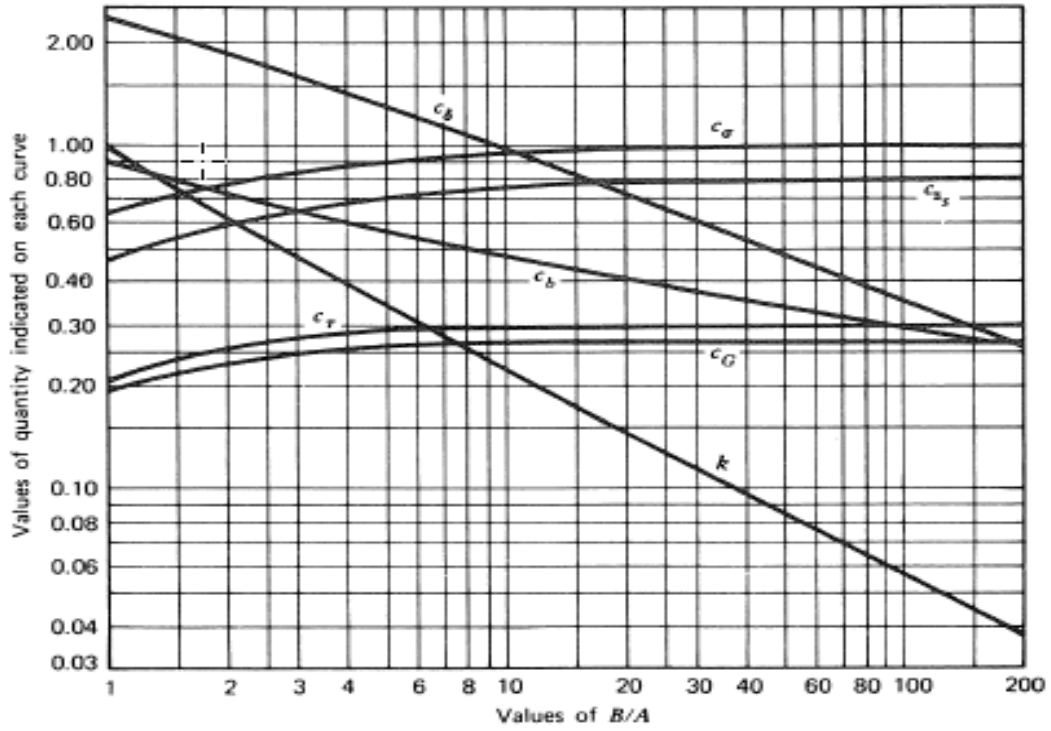


Figure 3:5: Stress and deflection coefficients for two bodies in contact at a point for any value of  $B/A$  [16].

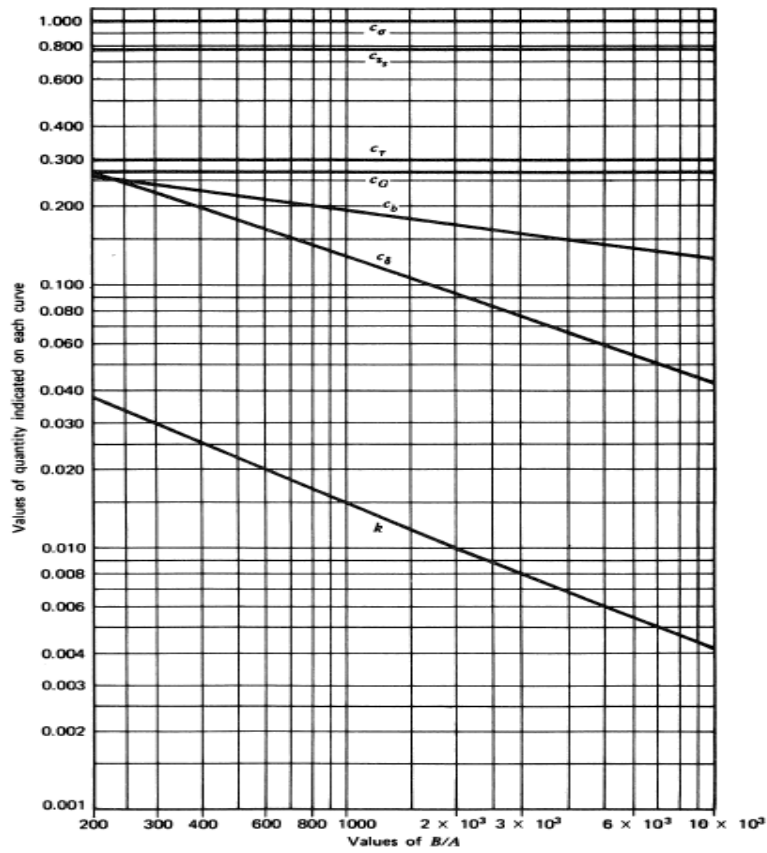


Figure 3:6: Stress and deflection coefficients for two bodies in contact at a point for any value of  $B/A$  [16].

### 3.3. Hertzian contact stresses

When two bodies with a curvature at different radii are in contact, the contact area will be a point or a line. The deformation caused by an applied load between the two bodies can result in plastic or elastic deformation, depends on the magnitude of the stress located on the area looked at. The first analysis was presented by Heinrich Hertz in 1881 and is based on the following assumptions [23]:

- i. The surfaces of the bodies are continuous, smooth, nonconforming and frictionless.
- ii. Contact area is very small compared to the size of the bodies and the strains associated with the deformations are small.
- iii. Both bodies can be considered to behave as an elastic half-space in the area near the contact zone.
- iv. The gap between two points at two undeformed surfaces are the same as formula (3.1) explained in Chapter 3.2.1.

#### 3.3.1. Unimodal Contact

Based on Hertz findings and according to elastic mechanics, the deformation due to applied load on a hard steel ball is given through the following equations [20]:

$$a = \left( \frac{3WR}{4E'} \right)^{\frac{1}{3}} \quad (\text{mm}) \quad (3.14)$$

$$\frac{1}{E'} = \frac{1-\nu_1^2}{E_1} + \frac{1-\nu_2^2}{E_2} \quad (\text{mm}^2/\text{N}) \quad (3.15)$$

$$\delta = \left( \frac{9W^2}{16RE'^2} \right)^{\frac{1}{3}} \quad (\text{mm}) \quad (3.16)$$

$$e^2 = 2R\delta - \delta^2 \quad (\text{mm}) \quad (3.17)$$

Where:

W = applied force on spherical shaped body (N).

R = radius of body (mm).

a = radius of the spherical indenter in elastic area (mm).

e = reel radii of the spherical indenter if the flat specimen reaches fully plastic deformation (mm).

$\delta$  = Deflection of the spherical indenter (mm).

Figure 3:7 illustrates the elastic deformation that occurs from a spherical indenter onto a flat surface.



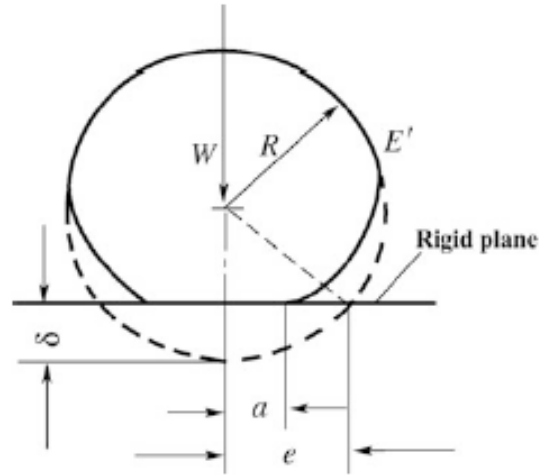


Figure 3:7: Illustrates the deformation from a spherical indenter onto a flat surface in elastic area [20]

### 3.3.2. Contact between two spherical bodies

Figure 3:8 illustrates two circular bodies compressed into each other in the elastic area with an applied force  $W$  and the contact area with the radius  $a$ .

Equations where  $p$  is stress and  $a$  is contact radius are expressed as [20]:

$$p = \frac{3W}{2\pi a^2} \left(1 - \frac{x^2}{a^2} - \frac{z^2}{a^2}\right)^{\frac{1}{2}} \quad (\text{N/mm}^2) \quad (3.18)$$

$$a = \left(\frac{3WR}{8E'}\right)^{\frac{1}{3}} \quad (\text{mm}) \quad (3.19)$$

If the two circular bodies have different radii, the following contact radius are expressed as:

$$R = \frac{R_1 R_2}{R_1 + R_2} \quad (\text{mm}) \quad (3.20)$$

$$a = \left(\frac{3WR}{4E'}\right)^{\frac{1}{3}} \quad (\text{mm}) \quad (3.21)$$

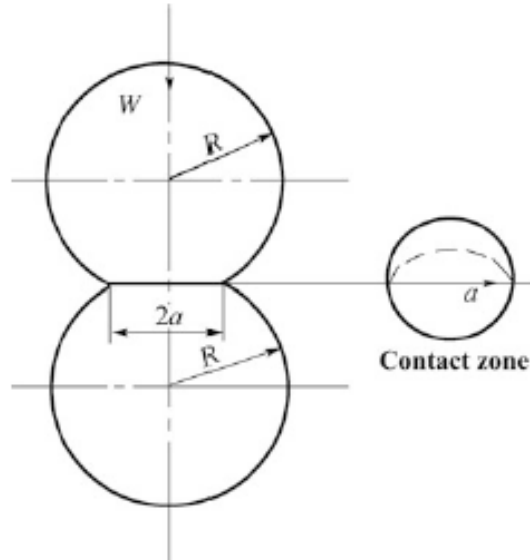


Figure 3:8:illustrates the contact zone between two circular bodies and the elastic deformation [20].

### 3.4. The relationship between depth and contact radius in a spherical indentation

It is important to know the correlation between dent depth and the curved contact surface area. Figure 3:9 visualize the area of a sphere with a variable h.

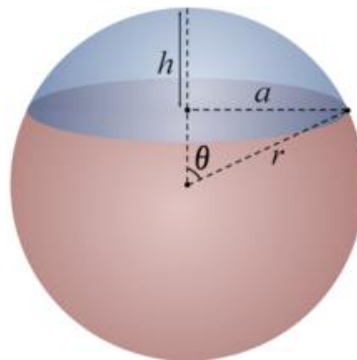


Figure 3:9: A spherical cap marked with blue colour, for which the area changes with the variable h [24]

A spherical cap is the region which lies above or below a defined plane as shown in Figure 3:9. A hemisphere is the same as if the spherical cap plane lies in the centre of the sphere. The volume and area equations for a sphere are defined as [24]:

$$A = 2\pi r h \quad (\text{mm}^2) \quad (3.22)$$

$$V = \frac{\pi h^2}{3} (3r - h) \quad (\text{mm}^3) \quad (3.23)$$

### 3.5. Brinell Hardness

The Brinell hardness test was invented by Brinell in 1900 and is a spherical indenter being pressed under fixed normal load on to a smooth surface of a specimen that's being examined. After equilibrium has been reached in around 15s to 30s, the load is removed, and the indenter is retreated to its initial position. This leaves a permanent indentation. The Brinell hardness number is being expressed through the following formula [29]:

$$B.H.N. = \frac{2 \cdot W}{\pi D^2 \left[ 1 - \sqrt{1 - \left(\frac{d}{D}\right)^2} \right]} \tag{3.24}$$

However, in most of the cases the Brinell hardness number is not constant for a given metal but depends on the load and the size of the spherical steel ball. The physical principles suggest that it is expected with geometrically similar indentations, no matter the actual size of indentation, the hardness number should be constant. This is found to be true. If a steel ball with a diameter  $D_1$  produces an indentation of diameter  $d_1$ , the hardness number will be the same as if it is used a steel ball with diameter  $D_2$ , which makes an indentation with a diameter  $d_2$ , provided that the indentations are geometrically similar and that the angle of indentation  $\phi$  as shown in Figure 3:10(a).

This will happen when  $d_1/D_1 = d_2/D_2$ . However, Brinell hardness number is not a satisfactory physical concept, since the ratio for the load over the curved area of the indentation does not give the mean pressure  $P$  over the surface of the indentation. If there is no friction between the indenter and the indentation surface, the pressure is normal to the surface of the indentation. Furthermore, consider the forces acting over a region with radius  $x$  and width  $ds$  shown in Figure 3:10(b). The area of this region is lying on a curved surface of the indentation, where  $A = 2\pi x ds$  and the force acting is expressed as  $P2\pi x ds$ . If taking the sum over the whole surface area, the resultant horizontal force is zero. The vertical force which is the same as the normal load  $W$  is expressed with the following equation [29]:

$$W = \int_0^a P2\pi x dx = P\pi a^2 \tag{3.25}$$

Where  $a$  is the radius of the indenter.

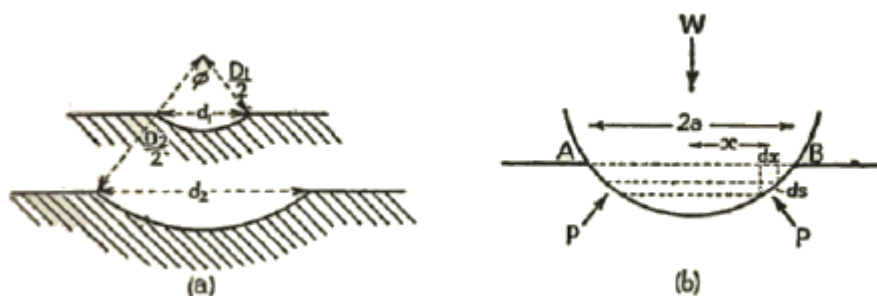


Figure 3:10:(a) geometrically similar indentations produced by spherical indenters of different diameters. (b) mean pressure is calculated between a spherical indenter, and it is assumed that there is no friction at the interface [29].

The harder the indenter is, the higher Brinell number it reads out with the same amount of load at the same material test specimen. This applies only for hardness measurements over 525 Brinell. This happens even though the hardness is much larger than the test material [29].

With the assumption of that the metal specimen has been fully work-hardened, the mean pressure  $P_m$  and load  $W$  characteristics is essentially the same as the work-hardened mild steel in Figure 3:20. Figure

3:20 illustrates the growth of the plastic region and the increase in yield pressure  $P_m$  in terms of load. This is also given in Table 3:1(a), while in Table 3:1 (b) the same results have been given in terms of  $W/W_L$ , where  $W_L$  is the load necessary to start plastic deformation into the specimen, the yield pressure is expressed as the ratio  $P_m/P_N$ , where  $P_N$  is the pressure at full plasticity and is also approximately equal to (B.H.N. observed)/(True B.H.N) [29].

(a)		(b)	
Load $W$ (kg.)	$P_m$ (kg./sq.mm.)	Ratio $\frac{W}{W_L}$	Ratio $\frac{P_m}{P_N}$
( $W_L$ ) 2	84	1	1 : 2.55
5	105	2.5	1 : 2.05
10	120	5	1 : 1.8
20	142	10	1 : 1.5
40	160	20	1 : 1.35
80	180	40	1 : 1.2
125	186	62	1 : 1.17
250	200	125	1 : 1.08
500	210	250	1 : 1.03
700	216	350	1 : 1
2,000	220	1,000	1 : 1

Table 3:1:(a) Shown the observed data of the development of plastic deformation as the load increases in a work-hardened mild steel with a 10 mm diameter steel ball. (b) The ratio between  $W$  and  $W_L$  and  $P_m/P_N$ . [29]

This also confirms that a reliable hardness measurement occurs at when the load exceeds 100 to 200 times the load required to form a plastic deformation.

### 3.6. Meyer's Law

The relation between the size of the indenter and the load for spherical indenter can be expressed by several empirical relations. Meyer's law, states that for a ball with a fixed diameter, fixed load  $W$  and a diameter  $d$  from the indentation gives the following relationship [29]:

$$W = kd^n \quad (3.26)$$

Where  $k$  and  $n$  are constants for the material which is tested. Usually the value  $n$  lies between 2 and 2.5. It is found that for fully annealed metals the value  $n$  lies close to 2.5 and for fully work-hardened metals is lies close to 2. This is shown in Figure 3:11 with different hardened methods with different metals in correlation with the load  $W$  and indentation  $d$  of a spherical indenter with the diameter of 2 mm and plotted with logarithmic ordinates. In Figure 3:11 the slopes are equal to the value of the Meyer index  $n$ , which gives that the load  $W$  is numerically equal to the value  $k$  when the indentation  $d$  is 1. This method of analysing indentation is known as the Meyer analysis. Moreover, when indenters with different diameter size are used,  $k$  and  $n$  change in value. There is also a correlation between the diameter size  $D_1, D_2, D_3, \dots$ , and indentation diameter  $d_1, d_2, d_3, \dots$ , which results in the following equation [29]:

$$W = k_1 * d_1^{n_1} = k_2 * d_2^{n_2} = k_3 * d_3^{n_3} \dots \quad (3.27)$$

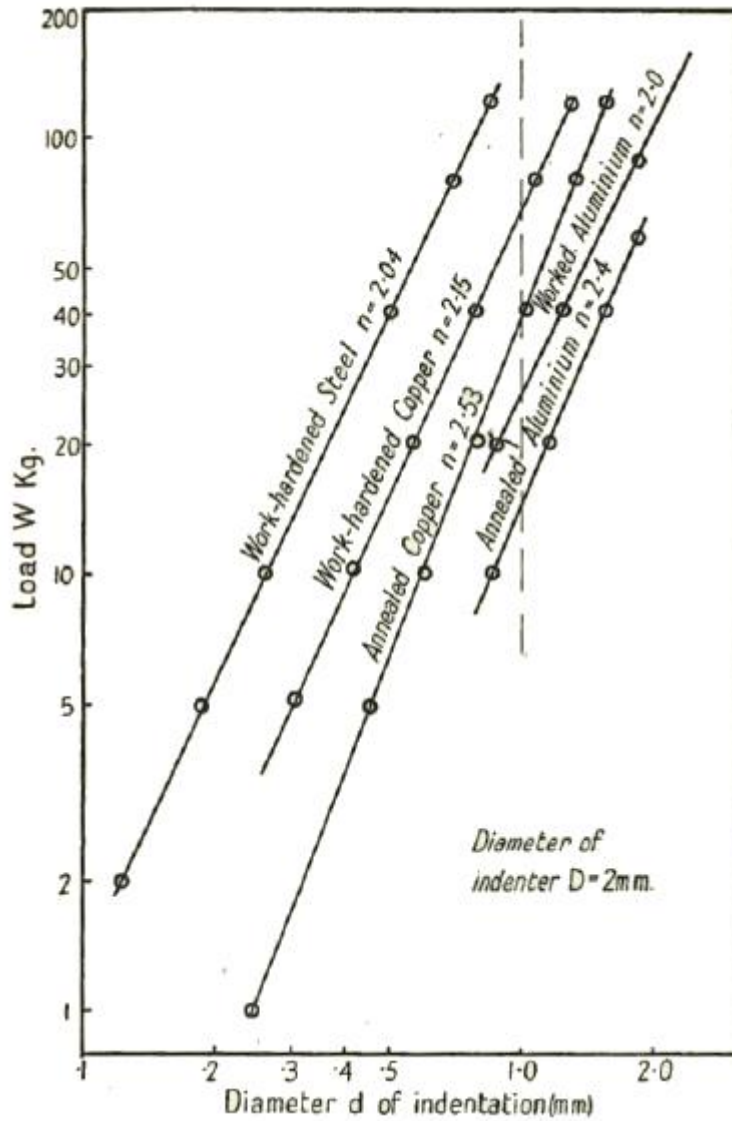


Figure 3:11: Plot of the load W against the indentation diameter d from the indentation of a spherical indenter onto a flat metal surface [29].

It was also found through empirical testing that the index n was almost independent of D. However, k decreased with an increasing of D which gives the following equation [29]:

$$A = k_1 D_1^{n-2} = k_2 D_2^{n-2} = k_3 D_3^{n-2} \dots \quad (3.28)$$

Where A is a constant. This gives the equation [29]:

$$W = \frac{A*d_1^n}{D_1^{n-2}} = \frac{A*d_2^n}{D_2^{n-2}} = \frac{A*d_3^n}{D_3^{n-2}} = \dots \quad (3.29)$$

Which can be rewritten as [29]:

$$\frac{W}{d^2} = A * \left(\frac{d}{D}\right)^{n-2} \quad (3.30)$$

Geometrically, the ratio between indentation diameter and the diameter of the indenter ( $d/D$ ) must be a constant. This ratio is proportional to the Meyer hardness. Moreover, the Brinell hardness is simply a geometrical factor depending on ( $d/D$ ), times the Meyer hardness. From equation (3.29), with the geometrically similar indentations gives out the same Brinell and Meyer hardness number. Furthermore, from equation (3.29) gives [29]:

$$\frac{W}{D^2} = A * \left(\frac{d}{D}\right)^n \quad (3.31)$$

Again, the geometrically similarities gives out that the ratio  $d/D$  and  $W/d^2$  must be constants. This means that with a spherical ball with a diameter of 10mm and a load of 3000 kg gives the similar indentation as with a spherical ball with a diameter of 1 mm and a load with 30 kg. In these two cases, the hardness number is the same. This result is often used in empirical hardness tests. Furthermore, the most general relation from this principle is [29]:

$$\frac{W}{d^2} = \psi * \left(\frac{d}{D}\right) \quad (3.32)$$

Where  $\psi$  is a suitable function for the given case. This gives that equation (3.30) is a special case of (3.32) and equation (3.29) is a special case of the principle of geometric similarity rather than an explanation itself. Moreover, (3.31) depends on the Meyer relation. As the Meyer relation is not exact which results in the similarities between the 10 mm indenter diameter and 3000 kg load and 1mm diameter and 30 kg is not exact. However, for all practical purposes, the differences are small enough to be ignored. The Meyer hardness is described as the following equation [29]:

$$\text{Meyer hardness} = \frac{4W}{\pi d^2} \quad (3.33)$$

### 3.7. Comparison of Brinell and Meyer hardness

Comparison between Brinell and Meyer hardness in annealed and work-hardened copper are shown in Figure 3:12. It is seen that with highly work hardened copper, the Meyer hardness number is almost the same and independent of the loading, which means that the mean pressure resisting indentation is almost constant and the Meyer index  $n$  has a value of 2. Moreover, for the same metal, the Brinell hardness number is nearly constant, but fall with the increasing in loading because of the increase of size in the curved area from the indenter. This result is giving the impression that Brinell hardness number may be lower with higher loads than with smaller loads. The change in hardness number in relation with the load is shown in Figure 3:12 for annealed and work-hardened copper. From the results presented in Figure 3:12, Meyers hardness is shown to be the most reliable measure of hardness [29].

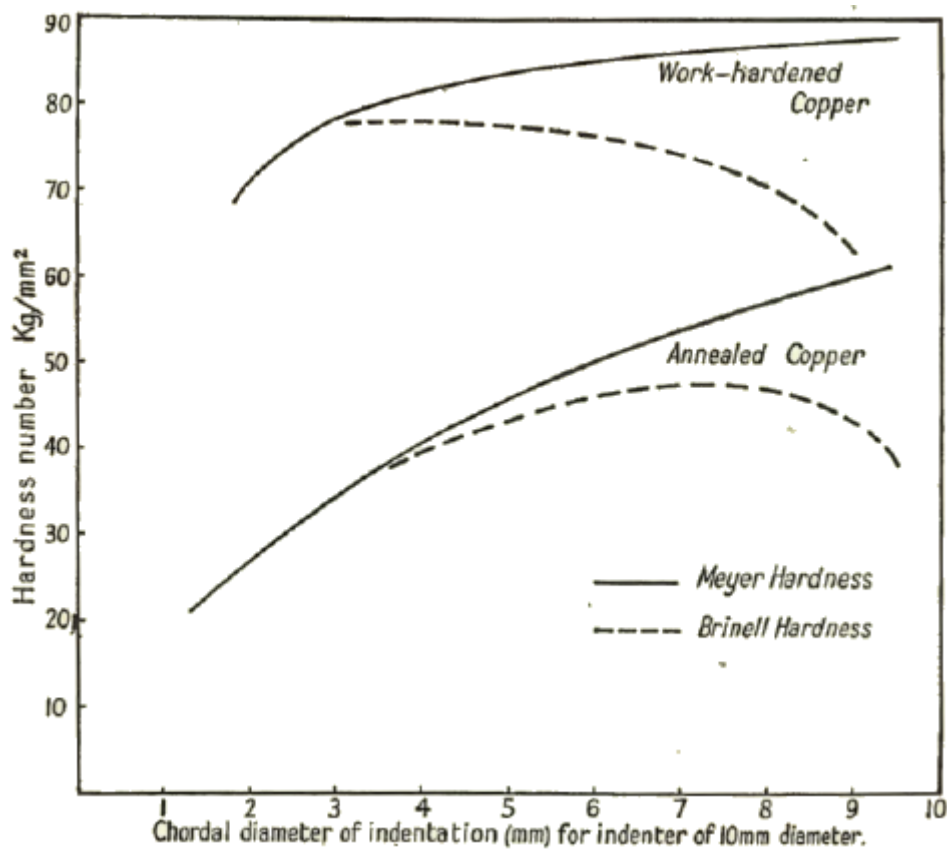


Figure 3:12: Illustrates the Brinell hardness number and Meyer hardness number for Annealed and Work-hardened copper as the load increases and indentation for a spherical indenter with a diameter of 10mm increases [29]

## 3.8. The deformation of metals by spherical indenters: ideal plastic metals

### 3.8.1. Initial plastic deformation

Figure 3:13 illustrates the deformation of an ideal plastic metal with the yield stress  $Y$  and the indenter shaped as a sphere with radius  $r$ . The friction between the indenter and the contact surface is assumed to be negligibly small. When a load is applied the indenter and the surface will both be elastically and plastically deformed, depending on the material properties and the magnitude of the force. If the force acts in the elastic area, Hertzian theory is applicable as explained in Chapter 3.3. The radius  $a$  as shown in Figure 3:13, follows the equation in Chapter 3.3.1, where  $\sigma_1$  and  $\sigma_2$  is the Poisson ratio of the indenter and the surface, and  $E_1$  and  $E_2$  are the corresponding Young modulus. If the pressure is in the elastic area, the radius will be proportional to  $W^{(1/3)}$  [29].

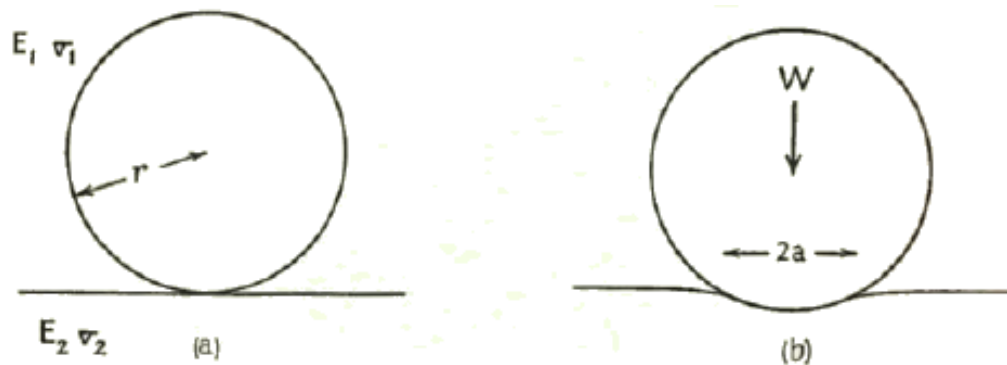


Figure 3:13: Illustration of a hard sphere that makes an indentation into a flat surface [29].

Even though the projected area  $A$  and the mean pressure  $P_m$  of the indentation is proportional to  $W^{1/3}$ . The normal stress across the circle is not uniform, but at any point with a distance  $x$  from the centre of the indentation has the value  $P = P_0 * \left(1 - \frac{x^2}{a^2}\right)^{1/3}$ , where  $P_0$  is the pressure at centre of Figure 3:14. which follows that  $P_0 = \frac{3}{2}P_m$ . Figure 3:14 illustrates the pressure distribution over a circle contact when a flat surface is deformed elastically by a hard metal with a shape of a sphere [29].



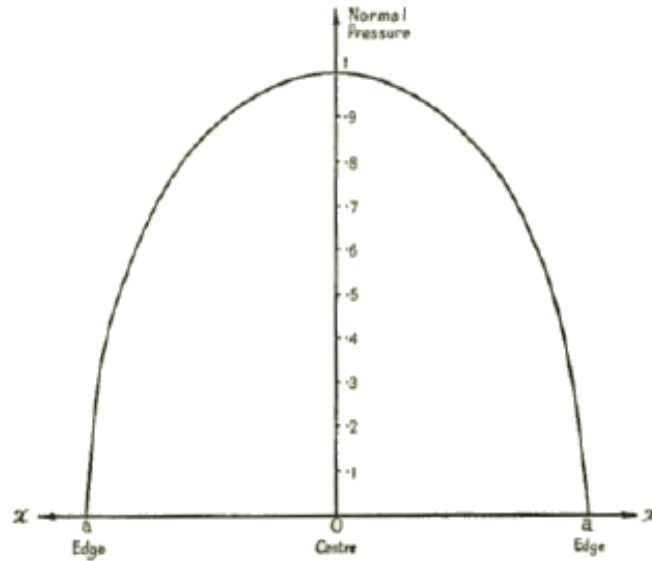


Figure 3:14: Pressure distribution of a circle contact from a spherical surface deformed elastically against a flat surface [29].

### 3.8.2. When the plastic deformation occurs

With the application of Tresca or the Huber-Mises criterion to calculate the stresses, it is found that plastic deformation happens below the actual contact point. This is also stated in the Chapter 3.2. Figure 3:15 illustrates the maximum shear stress lines below the contact point and the locations where they occur. Maximum shear stress occurs straight below the centre of contact and has a value of  $0.47 \cdot P_m$ . Furthermore, plastic deformation occurs when the shear stress is  $0.5 \cdot Y$ , when  $P_m \approx \frac{1}{2} \cdot Y$ , where  $Y$  is the yield stress of the deformed material [29].

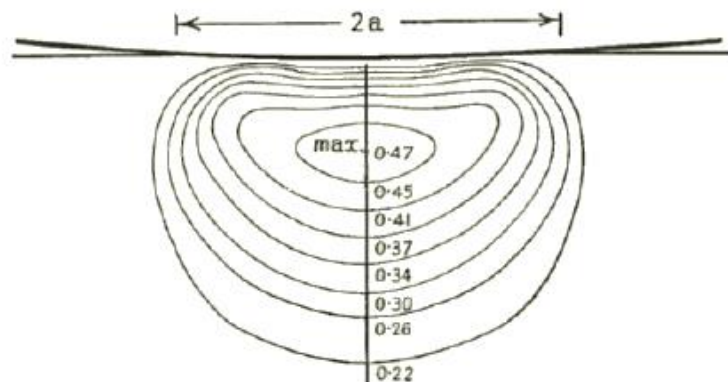


Figure 3:15: Elastic deformation of a flat surface by a sphere and shear stress distribution [29].

The calculated shear stress in the metal has been plotted, and it is seen that the maximum shear stress occurs at about  $0.5 \cdot a$  below the contact surface. The magnitude of the shear stress at this point depends slightly on the Poisson ratio, however this value is 0.3 for most of the materials. This means the shear stress is about  $0.47 \cdot P_m$ , where  $P_m$  is the mean pressure over the contact area. Moreover, at this point the two radial stresses are equal, the Tresca and Huber-Mises criterion suggests that the plastic flow will occur when the shear stress is equal to  $0.5 \cdot Y$ ,  $0.47 \cdot P_m = 0.5 \cdot Y$ . This means that the plastic deformation starts when [29].

$$P_m \approx 1.1 * Y \quad (3.34)$$

This implies that if the mean pressure is below  $1.1 * Y$ , it will be in the elastic area and will go back to its original shape. As soon as the mean pressure reaches the value of  $1.1Y$ , plastic deformation will start to occur. As discussed above maximum pressure occurs below the contact surface, which means that some deformation will start at point z shown in Figure 3:16, as the rest of the material will be deformed elastically. Figure 3:16(a) illustrates the location of where the plastic deformation first occurs in region Z when  $P_m \approx 1.1 * Y$ . Furthermore, Figure 3:16(b) shows the deformation at the later stage with higher loads when the whole material around the spherical indenter flows plastically. When removing the load, the residual deformation will be very small [29].

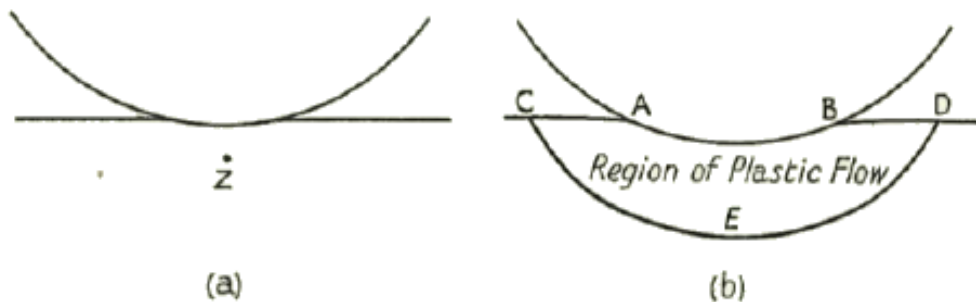


Figure 3:16: The indentation from a spherical indenter on a flat surface [29].

### 3.8.3. Complete or full plastic deformation

As the load of the indenter starts to increase the area around that is plastically deformed starts to increase and the mean pressure rises until the whole material around the indenter is plastically deformed as shown in Figure 3:16 (b). It is difficult to state when plastic flow occurs, the simplest way to state this is to say it is reached when the yield pressure varies little with further increase in indentation size. Defining the fully plastic stage theoretically is also difficult and it is assumed that the stage of fully plasticity has been reached when the whole slip-line field covers the region around the indenter as shown in Figure 3:16 (b). Even with this assumption, the theoretical analysis for fully plastic stage cannot be carried out properly since the axially symmetrical problem in plasticity presents certain difficulties which is impossible to overcome [29].

However, with the use of Harr-Karman criterion of plasticity (Ishlinsky 1944), it is possible to determine analytically the pressure between a spherical indenter and the indentation under fully plastic condition. However, it must be kept in mind that this criterion is based on physical assumptions, which is strictly not valid, but the errors that does occur does not appear to be severe and the result could be a very good approximation.

As shown in Figure 3:17, slip-line pattern is obtained and the pressure distribution is shown in Figure 3:18. This analysis is based on Haar-Karman criterion of plasticity which does not take the displacement of the deformed material into account. The dotted line is a representation of the elastic plastic boundary, corresponding to CED in Figure 3:16(b). With a circular flat indentation, it is seen that the pressure over the surface area is not uniform and is higher in the centre than at the edges. Moreover, the mean pressure that is divided over the projected area has a value of around  $2.66 * Y$ . It is also found that the mean pressure does not markedly depend on the size of the indentation. However, the mean pressure varies with the indentation depth and it is analysed that it is greater with a flat circular punch than for a spherical indenter submerged to an appreciable depth. Trough experiments it is suggested that mean pressure  $P_m$  should increase somewhat with the depth of the indentation, rather than decrease [29].

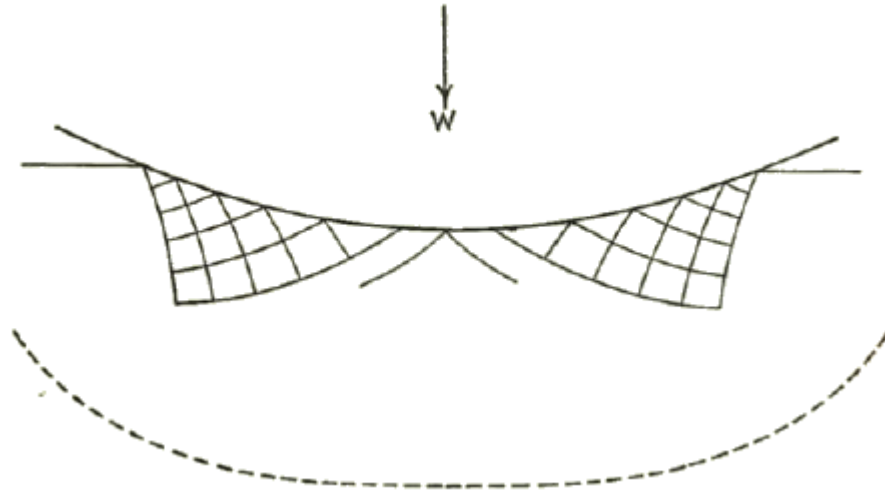


Figure 3:17: Illustrates the slip-line obtained for a spherical indenter on a ideally plastic metal [29].

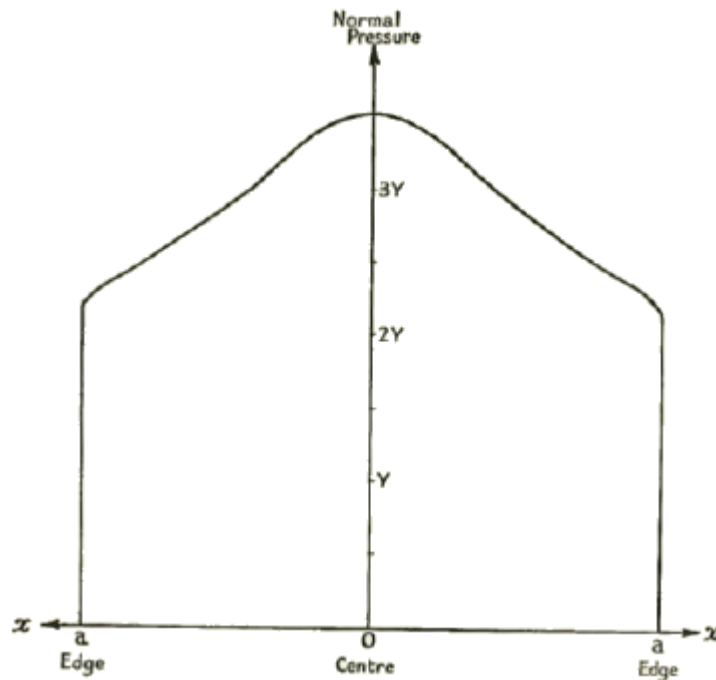


Figure 3:18: pressure distribution over the indentation from a spherical indenter in an ideally plastic material of constant yield stress [29].

This effect does not have a markable impact on the average pressure, Ishlinsky's calculation suggest that for a flat punch give a value of  $P_m=2.84*Y$ , which is only a few percent different from the calculated spherical indenter. From this analysis and experiments is seems like  $P_m=2.66*Y$  to  $2.84*Y$ . However, there is some friction between the indenter and the flat surface that's being indented which will lead to some increase in  $P_m$  [29].

### 3.8.4. Pressure-load characteristics

The expected pressure-load characteristics of a spherical indenter penetrating an ideal plastic body will follow the curve shown in Figure 3:19. The line represented from the points OA is the initial elastic deformation curve, where mean pressure is proportional to  $W^{1/3}$  (Hertzian). The point L represent where the plastic deformation starts to occur when  $P_m=1.1*Y$ . The dotted line from points LM represent transitional region as the plastic flow increases and the line between the points MN represent fully plasticity where  $P_m$  is around  $3*Y$ .

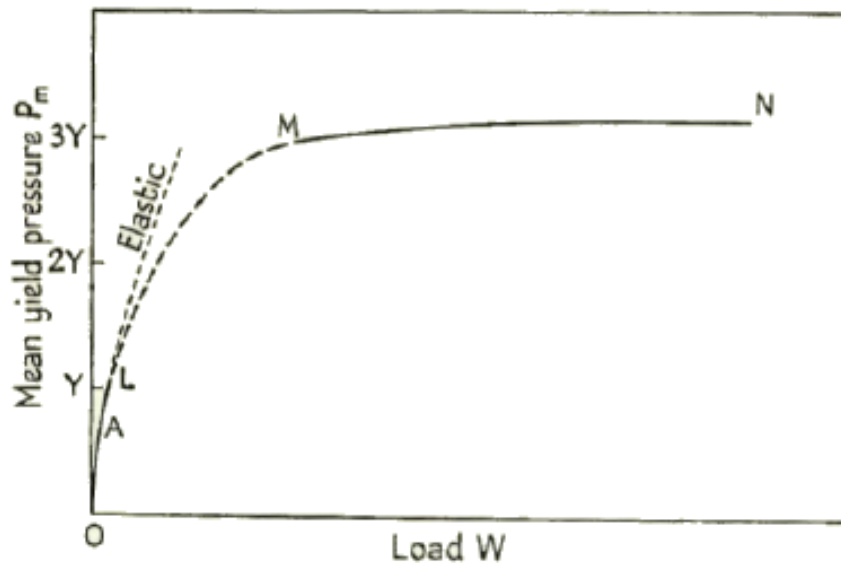


Figure 3:19: Theoretical pressure-load characteristics of an ideally plastic metal deformed by a spherical indenter [29].

This graph can be confirmed by most simply making a large Brinell indentation into a metal specimen, which has been hardened. This is done to prevent further work hardening when performing the Brinell test and obtain a constant yield stress  $Y$  through the specimen.

Some results found from Tabor in 1948, shows that the value  $P_m$  increases slightly with the depth of the indentation, assumed because of the displaced material. This observation appears to have some variance compared to the theoretical conclusion discussed in Chapter 3.8.3, but the effect is so small that full plastic deformation occurs at the following equation [29]:

$$P_m = c * Y \quad (3.35)$$

Where  $c$  is nearly a constant with a value of approximately 3.

The results give that for fully hardened materials,  $P_m$  is independent of the load pressure and the size of the indentation.

### 3.8.5. Range of validity of Meyer's law

The plot in Figure 3:20, shows the result of mean pressure  $P_m$  against load  $W$  for highly worked mild steel with a yield stress of 755 MPa, where the dotted line referring to the calculated elastic deformation. It is seen that this curve has all the characteristics of the theoretical calculated curve illustrated in Figure 3:19. As discussed previously, the plastic deformation is illustrated even more strikingly in Figure 3:21, where load  $W$  is plotted against the indentation diameter  $d$ . In Figure 3:21, the line OL corresponds to the elastic region of the straight line of slope 3, which is calculated from the elastic equation described in Chapter 3.3.1, where L is the point where plastic deformation occur, LM is the transition area and MN is the range where fully plastic deformation occur (slope 2). Across the line MN is the area which Meyers's law is valid for highly worked steel. Moreover, the Meyer index  $n$  has a value of 2 and is constant. As a load decreases the value of Meyer's index gradually increases until the deformation becomes completely elastic and reaches a value of around 3 [29].

It is not difficult to estimate for where the load is applicable to Meyer's law in Figure 3:21. From the elastic region, the load for when plastic deformation occurs  $W_L$  can be calculated with the following equation [29]:

$$W_L = 13.1 * P^3 * r^2 * \left(\frac{1}{E_1} + \frac{1}{E_2}\right)^2 \quad (3.36)$$

Where  $r$  is the radius of the indenter,  $E$  is the Youngs modulus and  $P = 1.1*Y$  is the stress when the plastic deformation starts to occur, given from equation (3.14).

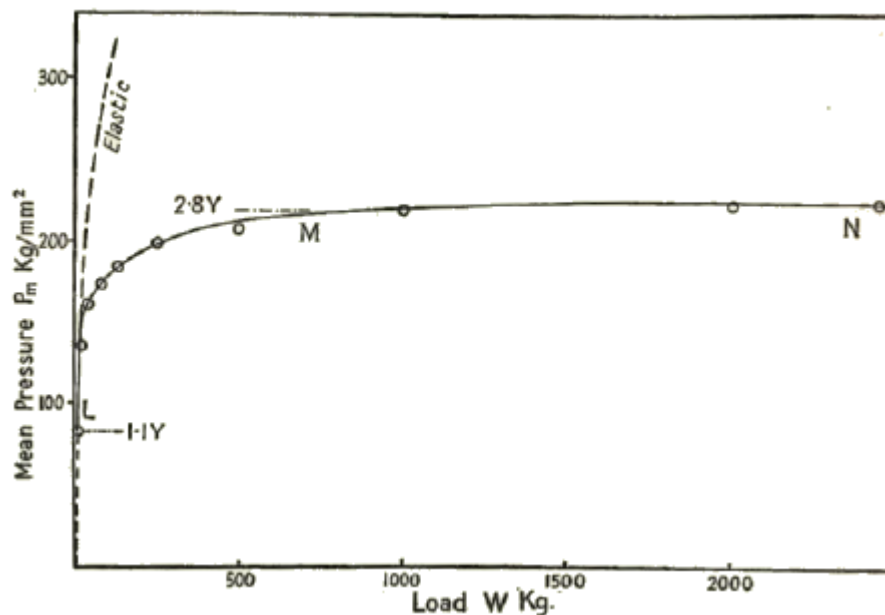


Figure 3:20: Experimental pressure-load characteristic of indentation formed in work-hardened mild steel by a hard-spherical indenter. The broken line is the theoretical result for elastic deformation [29].

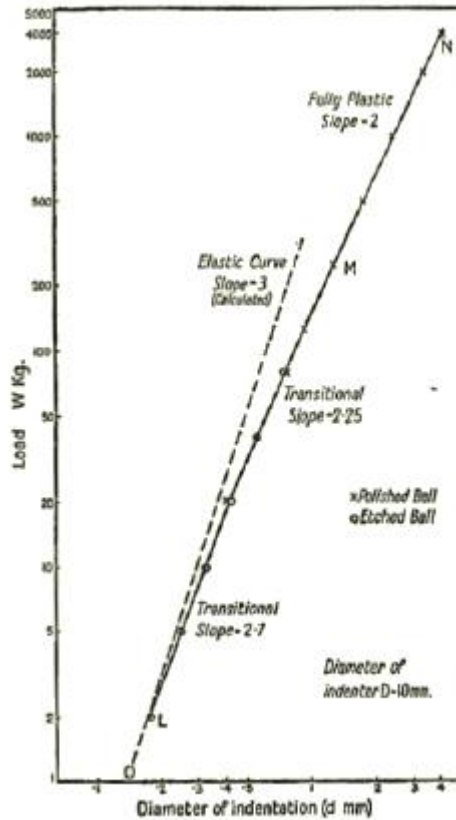


Figure 3:21: Indentation of work-hardened mild steel plotted against the load, with a yield stress of 755 MPa [29].

Table 3:2 shows when the different materials starts to plastically deform in terms of both average stress and Meyer's law. The diameter of the indenter which is used to get the results illustrated in Table 3:2 is 10 mm. Due to Meyer's law for very hard steels it is valid for loads above 5200 kg to get an indentation diameter of greater than 3 mm. Similar to very soft materials, the plastic deformations starts at around 2 g and reaches fully plastic flow at around 300 g [29].

<i>Metal (Work-hardened)</i>	<i>Y (kg./mm.<sup>2</sup>)</i>	<i>E<sub>2</sub> (dynes/cm.<sup>2</sup>)</i>	<i>W<sub>L</sub> to give P<sub>m</sub> = 1.1Y (g.)</i>	<i>Approximate load for Meyer's law to be valid (kg.)</i>
Tellurium-lead	2.1	1.6 × 10 <sup>11</sup>	2	0.3
Copper	31	12 × 10 <sup>11</sup>	230	35
Mild steel	65	20 × 10 <sup>11</sup>	1,200	180
Alloy steel	130	20 × 10 <sup>11</sup>	9,800	1,500
Very hard steel	200	20 × 10 <sup>11</sup>	35,000	5,200

Table 3:2: Shows at what load plastic deformation and fully plastic deformation occurs for different materials [29].

### 3.8.6. Deformation of the indenter

For soft surface materials the indenter itself is most likely to be deformed elastically, but for harder metals a permanent deformation may occur. Let say that the metal has a yield pressure at full plasticity of  $B$  corresponding to a yield stress  $Y$ , where  $B \approx 2.8 * Y$ . The same with the indenter, has a yield pressure of  $B_i$  corresponding to a yield stress  $Y_i$ , where  $B_i \approx 2.8 * Y_i$ . The first approximation is that the yield pressure or Meyers hardness, is the same as Brinell hardness value. Furthermore, as the load on the indenter starts to increase, plastic deformation starts to occur into the test metal at a mean pressure of  $1.1 * Y$ . Moreover, if  $Y_i > Y$ , there will be no plastic deformation in the indenter. To be sure that there is no plastic deformation occurring on the indenter, the following criteria must be fulfilled:  $2.8 * Y < 1.1 * Y_i$  or  $Y_i > 2.5 * Y$  or  $B_i > 2.5 * B$ . It is therefore set as rule that the indenter should always be 2.5 times the hardness of the test specimen, to avoid permanently deformation onto the indenter [29].

### 3.8.7. Effect of surface roughness

The surface roughness also has an influence on the indentation. The deformation of one asperity by a harder surface and a hemisphere deforming a flat surface is shown in Figure 3:22. For simplicity it is assumed that the surface roughness has a spherical shape and that the indenter has a much larger radius compared to the surface roughness.



Figure 3:22: Deformation of asperities: (a) hemispherical asperity deformed by a flat surface. (b) flat surface deformed by a hemisphere. The deformation process is similar in both cases [29].

However, the deformation of each asperity may be considered as the process of pressing a hard flat surface upon a softer spherical surface Figure 3:22(a). This is essentially the same that's occurring between a hard-spherical indenter pressing into a flat softer surface Figure 3:22(b). It is therefore possible to use equation (3.36) to calculate the necessary load to plastically deform the asperities of a specified radii of curvature. Typically results from various metals are given in Table 3:3, and it shows that for surfaces with small radii of curvature ( $r$ ), plastic deformation starts at very little load.

Metal	Approximate Brinell hardness (kg./sq. mm.)	Yield stress, $Y$ (kg./sq. mm.)	Load at which onset of plastic deformation occurs ( $P_m = 1.1 Y$ ) (g.)			
			$r = 10^{-4}$ cm.	$r = 10^{-2}$ cm.	$r = 0.5$ cm.	$r = 1$ cm.
Tellurium-lead	6	2.1	$8 \times 10^{-8}$	$8 \times 10^{-4}$	2	8
Soft copper	55	20	$2.5 \times 10^{-6}$	0.025	62	250
Work-hardened copper	90	31	$9.0 \times 10^{-6}$	0.09	230	910
Work-hardened mild steel	190	65	$4.7 \times 10^{-5}$	0.47	1,200	4,700
Alloy steel	350	130	$3.8 \times 10^{-4}$	3.8	9,500	38,000

Table 3:3: Shows when the plastic deformation occurs with respect to type of material and the radii of curvature of the asperities [29].

In general, the yield pressure of the asperities will be higher, mainly because of further work-hardening of the asperities which can occur even if the specimen has already been work hardened. Moreover, this will also be assisted by the friction between the asperities and the indenter. The yield pressure calculated from the macroscopic indentation will provide a reliable measure of the hardness, although the asperities has been work-hardened. Therefore, the hardness of the material will not be determined by the surface finish of the test specimen. The same for irregularities in the surface of the indenter, it will not affect the macroscopic deformation [29].

The effect from the asperities is shown from experiments done by Moore (1948). Moreover, it was more convenient to use a smooth cylinder instead of a spherical ball. Furthermore, the cylinder was pressed into the surface of a work-hardened copper. There were cut series of small grooves into the test specimen, and the cylinder was pressed parallel to the small grooves with various lodes. Figure 3:23 illustrates the plastic deformation after different loading from the cylinder. For light loads only the tip of the asperities experience plastic deformation. At high loads, the bulk material experience plastic deformation. However, the topography remains its irregularities and is clearly visible at the bottom of the indentation. The area that the tip is supporting the load is around one-half of the area that has been indented, this means that the yield pressure of the asperities is around double the yield pressure of the bulk material. This effect will be even more marked with annealed metals [29].

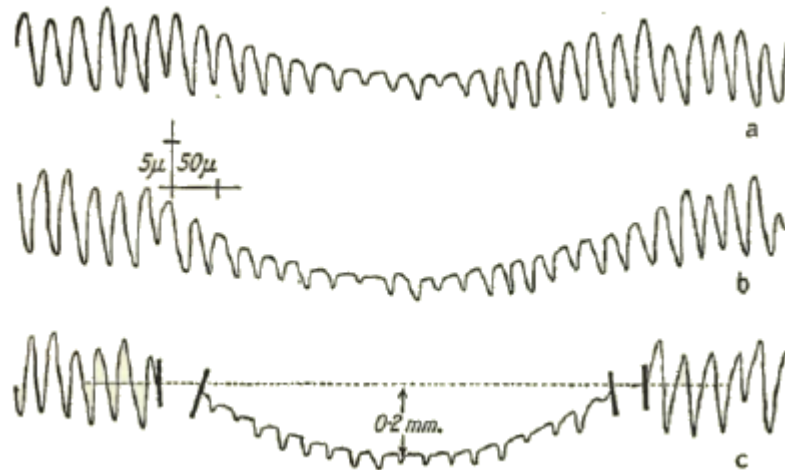


Figure 3:23: Profile of the deformation from a cylinder-shaped indenter, placed parallel to the grooves: (a) light load, (b) heavier load, (c) very heavy load [29].

### 3.8.8. Piling-up and sinking-in

When a surface is being plastically deformed it will either “pile up” or “sinking down”. This is illustrated in Figure 3:24. The metal that is being displaced by the indenter will flow between ac or bd, so that the material is being raised up above the general level as illustrated in Figure 3:24. Indentation into an ideal plastic material that of highly worked metal will have the most piling up around the edges of the indenter, marked with a and b in Figure 3:24. However, if the material is annealed, the behaviour is different. The early displacement of metal in the plastic region produces much work-hardening and it becomes easier to displace the metal laying around the work-hardened area, which lay deeper below the indentation. This effect is illustrated in Figure 3:24(b). Consequently, when this area has yielded, it also work-hardens, and further displacement occurs at a greater depth. The result is that the metal around the indenter is left at a lower point than the surface further away from the indenter. This is the characteristics of “sinking in” observed with annealed metals [29].



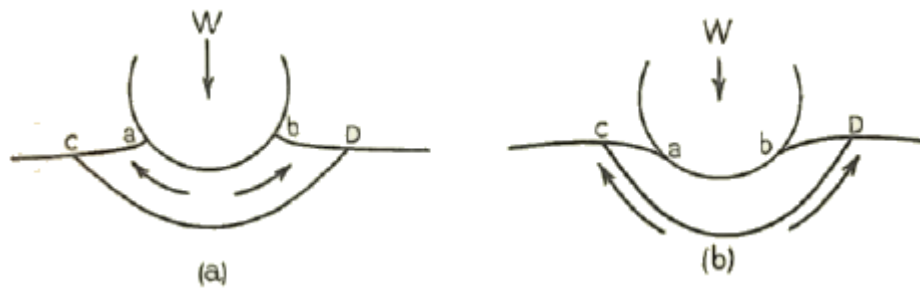


Figure 3:24: (a) the flow around an indenter from a highly worked-hardened metal produces “piling-up”. (b) For annealed metals the metal flow at a small distance from the indenter is illustrated and called “sinking in” [29].

### 3.9. Castable elastomers: Polyurethane

Polyurethane are a group of organic polymers that derive their name from the presence of the urethane bond in their structure, which is a reaction between polyol (curative) and isocyanate (prepolymer). This type of elastomer was developed in the 1930s. Nylon is closely related to polyurethane [30].

Polyurethane has a very good green strength and grab properties. Which makes them ideal when components are joined together without the use of clamps or jigs [30].

Polyurethane is used as a sealer in both solid form and gap filling foams. One of the major uses on polyurethane is to provide moisture barriers in buildings. As a waterproof barrier it is used in between concrete and floor surface. Moreover, polyurethane sealants used as a waterproof barrier has the following properties [30]:

- Adequate hydrolytic stability to last the lifetime of the structure
- Adequate elasticity to withstand normal movement in the concrete
- Fill out small gap
- Form a continuous layer with no holes
- Enough thixotropy to allow vertical coating

Castable polyurethane elastomers is one of the biggest segments of the polyurethane industry. The casting process consists of a few steps [30]:

- Dispense two or five “dry” ingredients at the required temperature
- Mix completely
- Cast into pre-heated mold
- Cure fully
- Demold
- Trim excess flash

Even the polyurethane itself can be used as a mold.

#### Properties of polyurethane

The most important factor that influence the final properties are [30]:

- Type of backbone used
- Length of the backbone
- Type of isocyanate
- Ratio of reactants
- Type and concentration of curative (chain extender)
- Final processing conditions

**Type of backbone:** PTMEG (C4) and PPG (C3). C4 has better mechanical properties than C3. Polyesters produced through oil-resistant polyurethane has lower hydrolysis resistance compared to polyurethane made from polyether's. Two new types of polyesters have much better resistance against hydrolysis and are called polycaprolactone and polycarbonate based, but they are expensive. The best one is basic polyester polyurethanes [30].

**Backbone length:** It is the frequency of the hard segment presented in the polyurethanes. This will define the hardness in the elastomer. Longer backbone the more flexible it will be. However, some short backbone length with a degree of coordinate cross linking will produce a material with high hardness and good compression set.

**Type of isocyanate:** TDI-based polyurethane produces the best material properties, when not taking food handling into account. If the use of this elastomer is going to be in touch with food, it is better to use MDI-based polyurethane to get FDA approval. To get a wider usable temperature range, the use of cyanates like PPDI and CHDI are applied [30].

**Ratio of reactants:** Both the production ratio and the curing ratio of the prepolymer production will affect the final properties of polyurethane. The effect of varying the mixing ratios of the chain extender affects the final properties. Hardness remains relatively constant between 85% - 100% of the theoretical curative addition. A curative is a type of polyol. Compression set need a lower level of curative 85-95% [30].

Properties like abrasion resistance, resilience and heat build-up are normally best at low curative. Tensile strength needs a curative level of just below 90-95%. Tear strength, flex and elongation require the curative to be at or above theoretical level.

Two different curatives are presented in Table 3:4 and their unique properties.

	MOCA	Ethacure 300
Nicked tear strength	Higher	Lower
Unnicked tear strength	Lower	Higher
Compression set	Lower (better)	Higher(worse)
Tensile strength	Lower	Higher
Production	Solid at ambient	Liquid at ambient
OH&S	Potential carcinogen	Not listed as such

Table 3:4: Properties of two curatives [30]

All polyurethane needs the complete cure to develop the desired properties. If the product stands for a week in air temperature, the full properties will be developed. If the polyurethane is annealed in approximately 18 hours in 130 °C, properties such as tear, tensile and toughness will improve. Very hard PUR such as 80 shore D and above, needs extra heat treatment.

Table 3:5 shows how the temperature effects the state of the polyurethane.

Below -80 °C	The material is a hard solid and in a glassy state.
-80 to +20 °C	The hard segments of the urethane begins to rotate and move.
20 to 130 °C	The material is usable.
130 to 180 °C	The polyurethane starts to soften severely.
Above 180 °C	The polyurethane starts to break down irreversibly.

Table 3:5 : Different phase of the elastomer in terms of temperature [30]

Every range of temperature and its state can be changed, depending on the backbone, isocyanate and curative [30].

### 3.10. Finite Element Analysis

Finite element analysis is a numerical method used to solve physical field problems for example stress, temperature distribution and displacement. Integrals or differential equations are used to describe the field problem. The field or a structure is discretized into smaller parts which are called finite elements. Each finite element has a limited spatial variation, which can be modelled by simpler equations. This gives out an approximated solution to the field problem, since the real variation in the field is often more complicated [35].

#### Material Models

In finite element method, different material models are used to describe the response from various stresses and loading conditions. Various material models have different stress-strain relationships. Description of a selection of material models are presented below:

#### Linear-elastic material model

The most used material model in solid mechanics is the linear-elastic model. The linear-elastic model assumes to have a linear behaviour of the material, where stress is proportional to strain, commonly known as Hooke’s law,  $\sigma = E\varepsilon$ . Material which is subjected to small stress or strains has an elastic behaviour and when released, the material goes back to its original form and position. The model in Figure 3:25, has the assumption that the stress is proportional to strain and the elastic linear part is represented with the line that connects point O and A [16, 36 ].

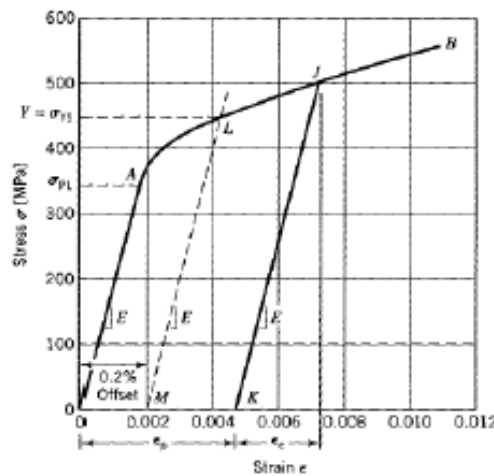


Figure 3:25: Stress-strain diagram for tensile specimen [16]

#### Rate independent plastic material model

When a specimen is loaded beyond its elastic limit, the material has gone into plastic area, which cause a permanent deformation. Moreover, load that exceeds the elastic limit has a total strain equal to the sum of the elastic and plastic strain component  $\varepsilon_t = \varepsilon_e + \varepsilon_p$ . When the load is released, the elastic strain is recovered, but the plastic strain remains and is the permanent displacement. The point J in Figure 3:25 illustrates where plastic deformation occurs, when unloading occurs, the permanent strain follows the line JK which corresponds to elastic strain  $\varepsilon_e$ . Plastic strain,  $\varepsilon_p$  remains as the permanent deformation in the material [16].

The theoretical material done in FEA, the stress-strain curves are shown in Figure 3:26 as bilinear, multilinear or elastic-perfectly plastic. However, the simplest form of bilinear stress-strain curve is elastic-perfectly plastic stress-strain model. Moreover, this material follows a linear stress-strain curve,

until yield point has been reached and with no hardening behaviour, it will continue to elongate without increasing the load [37]. This is an idealized model which can be used when strains are small [16]. In the model, the tangent modulus sets the angle of the initial plastic region. In the elastic-perfectly plastic model, the tangent modulus,  $E_T=0$ .

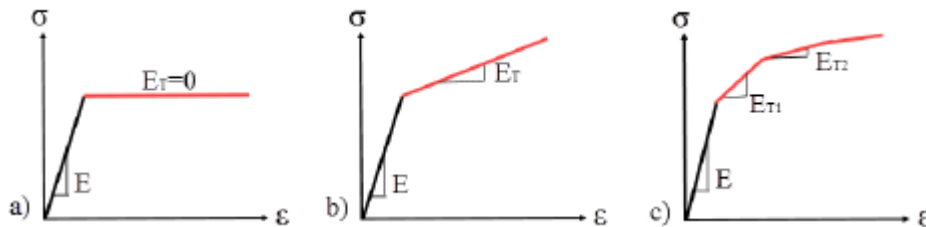


Figure 3:26: Stress-strain models (a) Elastic-perfectly plastic curve, (b) Bilinear curve and (c) Multilinear curve

Strain hardening is the material’s ability to resist further strain when the load exceeds the yield stress. As the material deforms, the elastic proportion of the curve and yield stress increases until the ultimate stress limit has been reached. In FEA a bilinear or a multilinear stress-strain curve can be used to describe stress hardening. Furthermore, the tangent modulus in the plastic region is constant for bilinear curves, while for multilinear curve, the tangent modulus shifts for each segment in the plastic region as shown in Figure 3:26 [16, 36, 37].

## 2-D plane elements and meshing

In FEA, meshing is the process of discretizing the model into a finite number of elements. The mesh grid is a system of algebraic equations which are used to numerically solve the structural case. Naturally, the mesh quality and element geometry are important to get out accurate and stable results. In Figure 3:27, there are some examples of element geometry used for 2-D problems. These elements can represent both planar and axisymmetric solids. Moreover, elements with no mid nodes are linear, which means that linear interpolation gives out the approximated values between the nodes. If the element includes mid nodes, they become quadratic and quadratic interpolation is used to approximate the values. Furthermore, the elements which has mid nodes also allows the elements sides to form quadratic curves and will therefore give a good geometric fit to curved structure boundaries [35, 36].

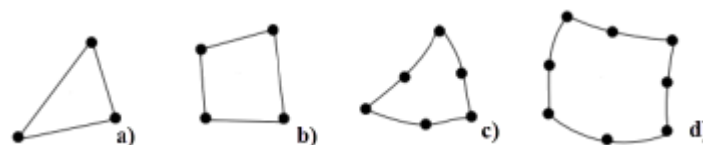


Figure 3:27: Element types: (a) triangle node (b) quadrilateral node (c) triangle node (d) quadrilateral node [38]

Geometry models for FEA often needs to be simplified compared to real scale drawings of the structure. If the structure has a lot of parts or special geometries, it is often necessary to leave out or simplify details because they interfere with having a good element mesh [39].

The effect these simplifications may have, should be evaluated. Typical simplifications are listed below:

- Cut-outs or local reinforcements are not included
- Eccentricities are not included for beam elements or in thickness transitions in shell models
- Not include weld metals

- Use contact surfaces instead of using the weld in the model to connect two parts.

## **Section of element type**

The element type is strongly dependent of the problem or case. Items that should be considered are:

- Solid or shell elements
- Elements based on constant, linear or higher-order shape functions
- Reduced, full or hybrid integration formulations
- Number of through thickness integration points(shell)
- Volumetric locking, membrane locking and transverse shear locking
- Hourglass control/artificial strain energy (for reduced integration elements)
- Drilling rotation stiffness/artificial strain energy (for shell elements)
- Warping stiffness (shell elements)

Usually higher-order elements are preferred for accurate stress estimation. Moreover, elements with simpler shape functions like constant or linear will require more elements to give the same stress accuracy as with higher-order elements. In the area of interest, constant stress elements like linear tetrahedron is not recommended [40]. For large displacement, simpler element formulations give a more robust numerical model and analysis than higher-order elements. Some elements are used as transition elements to make the generation of the element easier but are known to perform poorly. Usually 3-noded plates/shells and 4-noded tetrahedrons are often used as transition elements and should be avoided in the area of interest [39].

## **Mesh density**

The element mesh should be good enough to capture the relevant failure modes. Two recommendation are listed below:

- For ductility evaluations, preferably several elements should be present in the yield zone in order to have good strain estimates
- For stability evaluations, adequate number of elements and degrees of freedom to capture relevant buckling modes, typically minimum 3 to 6 elements dependent upon element type per expected half wave should be used

In areas of interest, the element aspect ratio should be according to requirements for the selected element formulation. Furthermore, areas in or nearby large deformation should have an aspect ratio close to unity. Distribution of load and load type has an impact on the mesh density. The nodes at where the load is applied needs to be correctly located [39].

## **Mesh refinement study**

Usually it is necessary to run mesh sensitivity studies in order to verify that the results from the analysis are sufficiently accurate. It is also performed to make sure that the element mesh is representing all the relevant failure modes in a sufficient and effective way. In general, the mesh refinement studies are completed by checking that the convergence of the results are obtained, which is showing that the results are stable when rerunning the analysis with decreased element size. Geometric sharp corners will have infinite small area and will therefore never converge [39].

## 4. Chapter 4: PRT System description

This chapter discusses and gives an overview of the final PRT product, along with some of the challenges that involves the development of the PRT. Furthermore, the PRT presented in Figure 4:1 is designed to operate a 12-inch pipe because this dimension is often used in subsea industry.

Part List	
Item	Title
1	Main Body PRT
2	Set-Force Body
3	PUR-Pipeline Packer
4	PUR-sealing packer with bearing steel balls
5	ROV-Handle
6	Two-Way Cylinder
7	Studbolt
8	Bearing Steel Ball

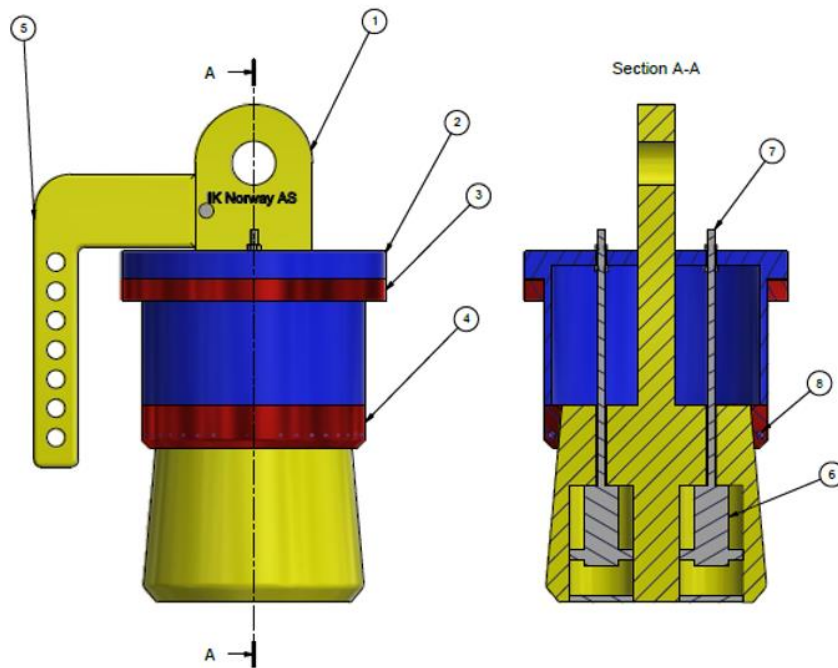


Figure 4:1: Design of a ROV compatible PRT

## 4.1. Design of a ROV compatible PRT

The designed PRT shown in Figure 4:1, is designed to retrieve a 12-inch pipeline. It has been designed with respect to ANSI-B 36 pipeline standard. The capacity for this tool has not been determined yet. When comparing the dimensions to other PRT's, it is remarkably smaller in size. Maintenance work appears to not be a financial issue because of its simple shape and easy access to parts. There are two cylinders that are operating the "Set-Force Body" and adjusts the amount of pre-set force in the bearing steel balls casted into polyurethane. "PUR-Pipeline Packer" attached to the "Set-Force Body" gives the PRT some elasticity and take some of the impact-force when inserted into the pipeline. On the main body, there is a connection point to the wire that is attached topside, which is used to pull the tool out of the water. The tool is also ROV compatible and this allows pipeline retrievals at deeper water depths that does not allow the use of divers.

One of the challenges with this tool is the infinitely small contact area between the steel balls and the internal pipeline walls. This causes high stresses around the contact area. Moreover, deformation from the spherical steel ball has a multiaxial direction along an angle. This results in that the background literature is a simplified case of the real physical phenomena. Furthermore, the indentation pattern is best described through the empirical results and results in ANSYS.

# 5. Test description

## 5.1. Introduction

Two test-rigs were designed and fabricated to model the wedge-lock mechanism of the RPT. The purpose of the first test-rig (Ref. Figure 5:1) is to characterize the mechanical wedge lock mechanism of the bearing steel balls. The purpose of the second test rig (Ref. Figure 5:4) is to allow tests on the wedge lock properties from the steel balls and the sealing properties of the PUR to be performed. The test-rigs was designed according to DIN and ASME standards on 4-inch pipelines. Most of the machining of the parts of the test rigs were performed by the author.

A perfectly circular ball has an infinite small contact point and it becomes very hard to predict the stresses and deformations that occurs on the steel balls, cone and the pipeline. The ideal way to obtain valid results is to build a test rig.

The procedures used to obtain the empirical data are presented in Appendix D and Appendix E. The procedures were design to run the tests to just before any permanent deformation occurs at the cone. This is to allow the reuse of the cone as it is an expensive component. The collected data is going to indicate how the different parameters are influencing each other and give an indication of the PRT lifting capacity.

The output data collected from the test-rigs are listed below:

- Angle ( $\alpha$ ) to achieve self-locking and optimum capacity (ref. Figure 5:1).
- Amount of steel balls.
- How metal properties in the interacted parts affects the indentation.
- Pre-set force vs onset of pipeline deformation.
- Pre-set force vs sealing properties of PUR.
- Indication of maximum capacity of the PRT.

## 5.2. Test with a cone alloyed with 34CrNiMo6

The objective for this test-rig, is to measure the deformation that occurs on the pipeline and the cone. This is to obtain an indication on the capacity of the PRT. The data that is collected from this test rig are presented in Chapter 8.2. The cone-angle ( $\alpha$ ) that is used in this test-rig is 5 degrees, which is shown in Figure 5:1.

The test-rig shown in Figure 5:1 is operated in the following steps:

- First, assembly and place every part in its right position.
- Second, apply pressure into the cylinder. This will cause the set-pipe to push on the steel balls, which will cause reaction forces illustrated in Figure 5:2.
- Third, as a result from the reaction forces, the spherical steel balls will cause indentations onto the pipeline. This makes a wedge lock position for the steel balls, which makes a great mechanical locking-force ( $R_f$ ).
- Forth, apply a load on the top of the pipeline as illustrated in Figure 5:1, to measure the total capacity.
- Last, disassembly the test-rig and gather the results.



The procedure followed is presented in Appendix D. The technical drawings of each component are presented in Appendix B.

One test with the 34CrNiMo6 alloyed cone was performed. The initial set-force pressure on the steel balls was around 40 bars. Furthermore, the test rig was then placed in a press, which applied a force of 10 000 kg onto the pipeline. See Appendix G for pictures of the test-rig. Since the spherical indentation on the cone was much bigger than first expected, this test was only completed one time as this damaged the cone and therefore the cone cannot be reused.

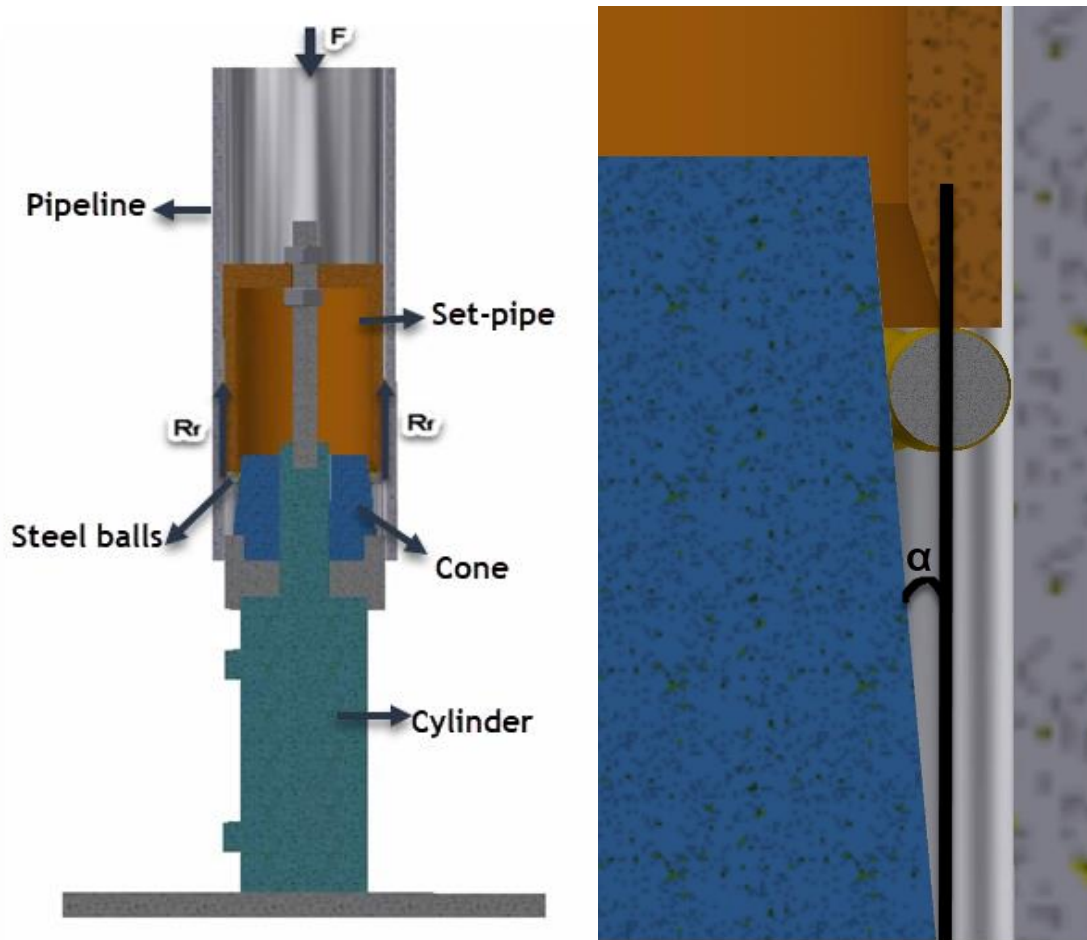


Figure 5:1: Shows an overview of where the main parts are located and where the force (F) and reaction force acts ( $R_r$ ). A detailed view of the cone angle is also illustrated to the left.

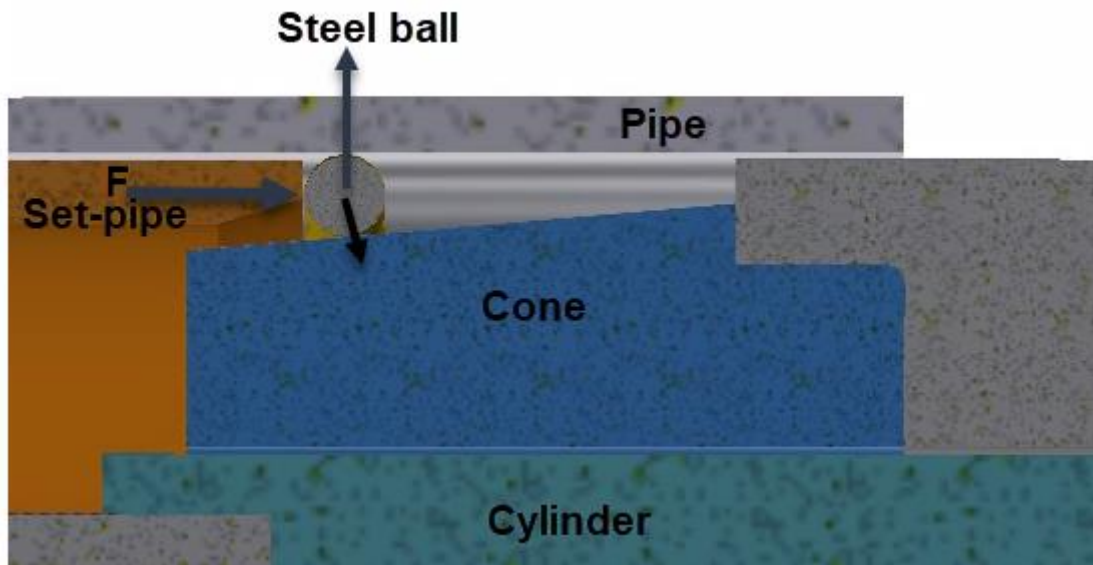


Figure 5:2: Detailed view over the main interacting parts and reaction force from the bearing steel ball when exerted a force from the set-pipe.

Figure 5:3 represents the relative hardness of each component where 1 is assigned to the component with the highest hardness and 3,4 and 5 are assigned to the components with the lowest hardness. To minimize the deformation occurring on the cone (2), this should be the hardest component, but due to industry standards and cost, the steel balls were made the hardest. The pipeline is the softest material and is therefore the first part to be plastically deformed. The approximate hardness numbers and descriptions of the interacting parts are presented in Table 5:1.

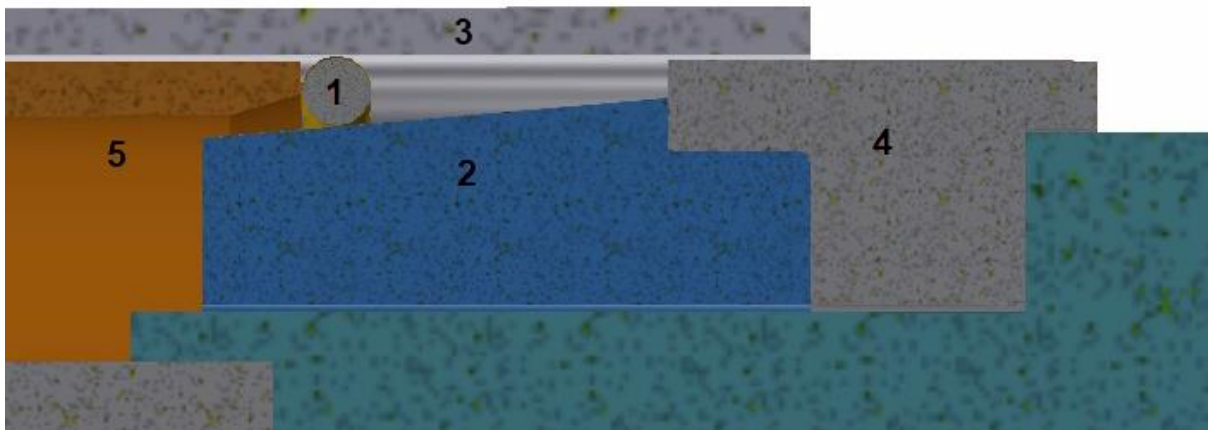


Figure 5:3: Overview of hardness in the different parts, where 1 is the hardest

Description	Part	Hardness (HV)
Steel ball	1	At least 740 HV10
Cone part 2	2	≈340
Pipe	3	≈150
Cone part 1	4	≈150
Set-pipe	5	≈150

Table 5:1: Description and approximate hardness number of the main interaction parts

### **5.3. Test with a cone alloyed with Calmax Uddeholm**

The second test-rig as mentioned previously in Chapter 5.1 was used in this test. The second test-rig has the ability to test the sealing abilities of the PUR. O-rings were installed in the test-rig as illustrated in Figure 5:5 to allow the test-rig to seal of the volume between the O-ring and the PUR packer, so that the area can be pressurized with water. This results in the ability to test the sealing property of the steel balls casted in PUR. The O-ring groove illustrated in Figure 5:5 was made according to Simrit catalogue [42]. This means that this test-rig can test (i) the grab and seal ability of the PUR packer containing steel balls (ii) the mechanical wedge lock mechanism of the bearing steel balls.

In addition, some parts in this test-rig differ to the one (the first test-rig) described in Chapter 5.2. These are:

- Six cones with a different material alloy and dimensions
- New pipeline with bigger dimensions
- The set-pipe was turned to another dimensions.
- The cone part 1 shown in Figure 5:4 was also turned to different dimensions

The six cones were made with the following angles: 3,4,5,6,8 and 10 degrees. The purpose of testing multiple cone-angles are to obtain which angle is the optimum angle in the PRT, in terms of deformation and lifting capacity. The material descriptions for the most important parts are described in Chapter 6. The cones were alloyed with Calmax which has a much higher hardness number than the previously tested cone. This is to decrease the cone deformations. Technical drawings are given in Appendix C.

In additions the cones were tested to verify their self-locking abilities. This means to apply a force on the top of the pipeline as shown in Figure 5:1 and checking if the pipeline was slipping against the steel balls. The load that was applied went from the weight of the pipeline, which was approximately 6 kg to approximately 85 kg.

### **Bearing steel balls not casted in polyurethane**

The objective to this test-rig is equal to the one described in Chapter 5.2 and the setup is the same as illustrated in Figure 5:4 except for the PUR is not present. However, in this study, no capacity tests were performed, i.e., applying a force  $F$  on top of the pipeline to evaluate the maximum load capacity of the wedge-lock mechanism as described in Chapter 5.2.

The tests described in this section were performed to measure the onset of pipeline deformation from the spherical steel balls and the corresponding set-pipe force. The variation of the deformation pattern with respect to different cone angles and set-pipe forces was also evaluated. The procedure that was used to evaluate the spherical indentation follows Part 2 in Appendix D. The initial set-force/cylinder pressures were logged using ESI software and all pressure loggings are presented in Appendix F.

The onset of fully plastic deformation in pipeline from the steel balls were measured for the cone angles of 3,4 and 10 degrees. The results are given in Table 8:14.

This test rig also follows the same setup as illustrated in Figure 5:3 in Chapter 5.2. As mentioned in Chapter 5.2, the cone (2) should be the hardest, but due to fabrication costs, the steel balls were made the hardest. However, the cones were hardened and is close to the hardness of the bearing balls. The pipeline is the softest material and is therefore the first part to experience plastic deformation. The approximate hardness numbers and description of the interacting parts are presented in Table 5:2.

Description	Part	Hardness
Steel ball	1	At least 740 HV10
Cone part 2	2	55-58 HRC see Table 6:3
Pipe	3	125-150 HV
Cone part 1	4	≈150 HV
Set-pipe	5	≈150 HV

Table 5:2: Description and approximate hardness number of the main interaction parts

## Bearing steel balls casted in polyurethane

The objective for this test setup is to evaluate:

- How the polyurethane interacts with the steel balls.
- Pre-set force required to seal and grab the pipeline.
- The stresses occurring between the steel balls casted in PUR and the pipeline and the cone (Ref. Figure 5:5).
- Indentation pattern from the steel balls.
- Total lifting capacity.

The technical drawing of the packer is shown in Appendix C and pictures is presented in Appendix H. The procedure for the test-rig is shown in Appendix E.

Figure 5:4 illustrates an overview of the test-rig setup and a detailed view of the angle between the cone and the pipeline. Furthermore, a quarter section view of the test rig is shown in Figure 5:5, which also shows the reaction forces from the set-pipe.

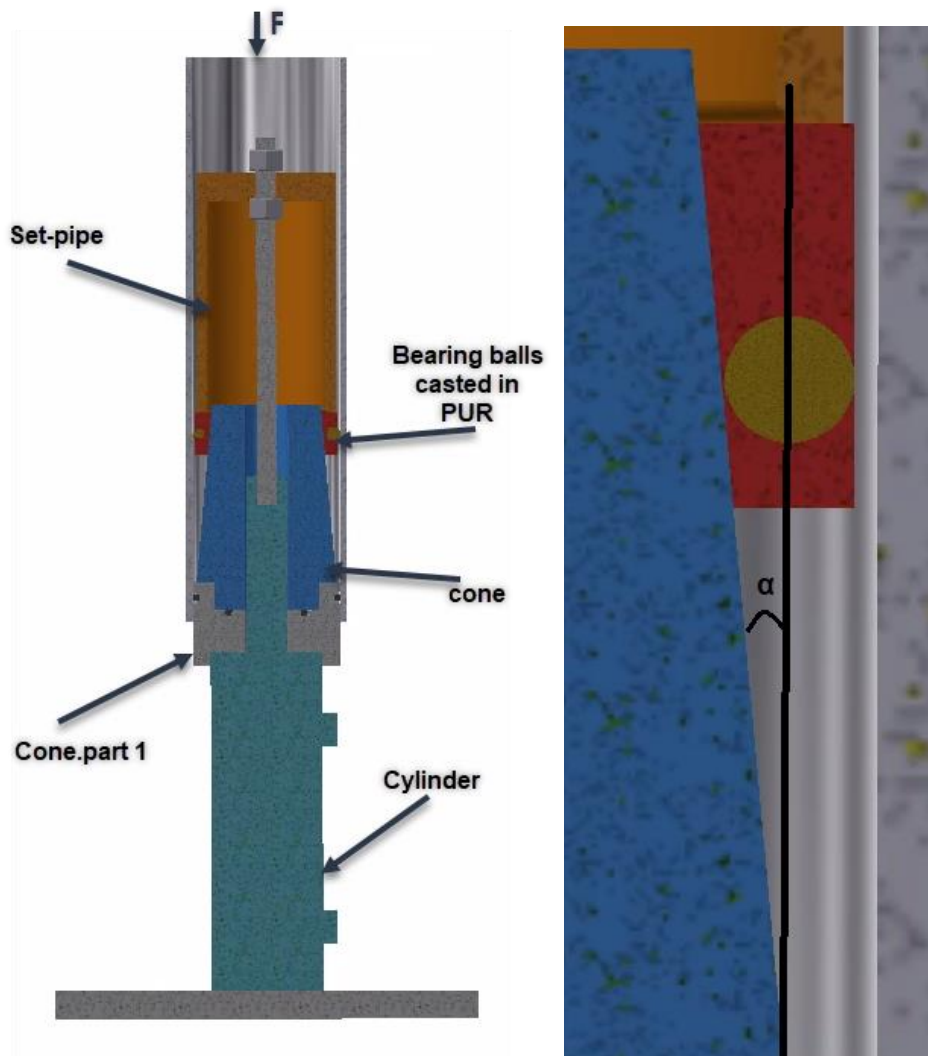


Figure 5:4: Shows an overview of where the main parts are located and where the force (F). A detailed view of the cone angle is also illustrated to the left.

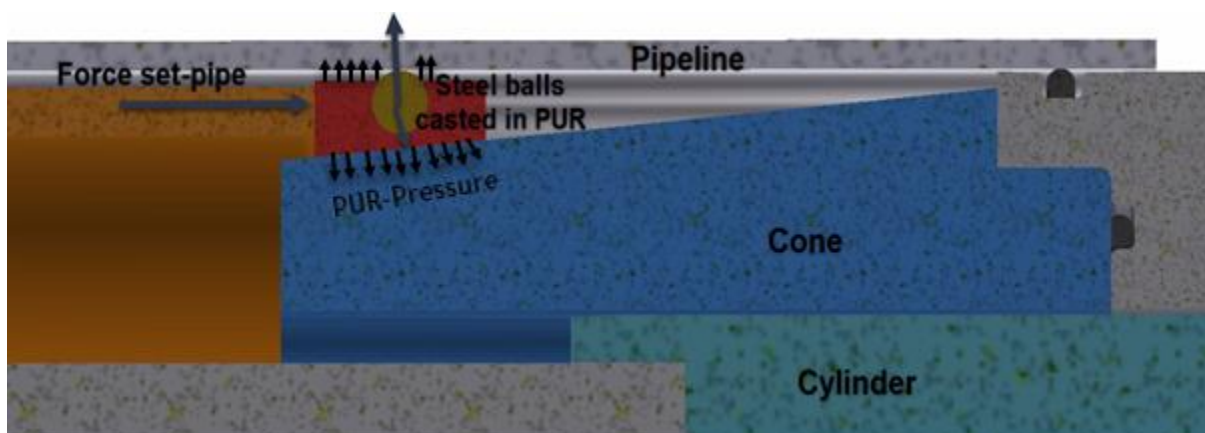


Figure 5:5: Detailed view over the main interacting parts and reaction force from the bearing steel ball when exerted a force from the set-pipe

Figure 5:6 represents hardness numbering where 1 is the hardest and 3,4 and 5 is the softest of the metals. As previously mentioned, normally, the cone (2) should be the hardest, but due to fabrication costs, the steel balls were made the hardest. However, the hardness cone is made just below the hardness of the bearing balls. The pipeline is the softest material and is therefore the first part to experience plastic deformation. The test will be performed with the packer having shore hardness values of 90 A and 70 A. Moreover, the hardness of each interacted part is presented in Table 5:3.

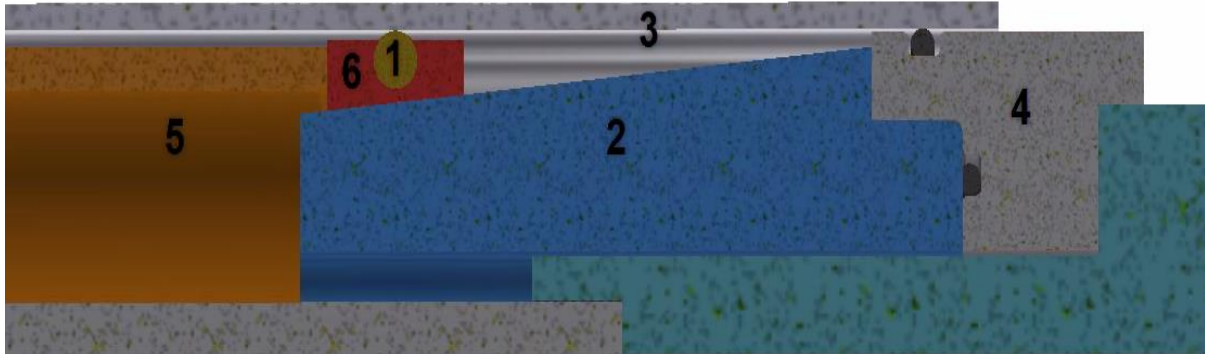


Figure 5:6: Overview of hardness in the different parts, where 1 is the hardest

Description	Part	Hardness
Steel ball	1	At least 740 HV10
Cone part 2	2	55-58 HRC Table 6:3
Pipe	3	≈125-150 HV
Cone part 1	4	≈150 HV
Set-pipe	5	≈150 HV
PUR	6	Shore 90 A and 70 A

Table 5:3: Description and approximate hardness number of the main interaction parts

Due to production cost it was only made one mold for the PUR packer. The packer is made to fit a cone with an angle of 6 degree. However, this packer is going to be inserted on all the 6 cones and test the seal ability. There were produced 4 packers, two with shore 90 A hardness and two with shore 70 A hardness shown in Appendix H. Part 2 in Appendix E is performed to evaluate the sealing ability of the packer.

## **6. Material description of the interacting parts**

### **6.1. Bearing steel balls**

The steel balls used, are usually used in bearings and has a diameter of 10 mm. In a bearing, the steel balls are exposed to high contact stresses. That makes high hardness a desired property in the steel balls. Moreover, the steel balls are made in accordance with the standard DIN 17 230 and have a hardness of at least 740 HV10, which is between 57 and 58 HRC [43].

### **6.2. The 4-inch pipeline DIN 2448**

The pipeline is a steel tube with a tensile strength of 450 MPa and a yield strength of 388 MPa at the measured section. However, requirements for the tensile strength varies from 415 MPa to 500 MPa. Yield strength also had a minimum requirement of 245 MPa. Nevertheless, this makes the steel pipe the weakest component in contact with the steel balls. The material certificate is presented in Appendix I.

### **6.3. Annealed Calmax Uddeholm Cone**

#### **6.3.1. Calmax Uddeholm**

Today most of the presswork tools are made from tool steels such as O1, A2, D2, D3 or D6. These steels often satisfy the requirements in wear resistance and hardness in most applications. However, the poor toughness, flame and induction hardenability and weldability often results in productivity and high maintenance cost due to unexpected failure of the tool. The aim for using the Calmax steel is to secure the lowest tooling cost per part produced [44].

Uddeholm Calmax is a material better suited to modern requirement and manufacturing methods. Calmax also offers a high degree of safety and maximum performance [44].

In general, Calmax have the following properties [44]:

- High toughness
- Great wear resistance
- Great through hardening properties
- Great dimensional stability in hardening
- Great polishability
- Great weldability
- Great flame and induction hardenability

This material has an excellent combination of toughness and wear resistance, which makes it suitable with the following applications [44]:

- General blanking and forming
- Heavy duty blanking and forming
- Deep drawing
- Coining
- Cold extrusion dies with complicated geometry
- Rolls
- Shear blades

- Prototype tooling

The compressive strength after the hardening process is presented in Table 6:1.

Hardness HRC	Rcm N/mm <sup>2</sup>	Rc0,2 N/mm <sup>2</sup>
54	2100	1800
56	2300	1900
58	2500	2000
60	2700	2100

Table 6:1: Tensile and Yield stress for Calmax [44]

### 6.3.2. Hardening Process

Kverneland Group AS carried out the hardening process. This company has long experience with materials and their properties, as they make a lot of tools to the farming industry. The hardening process was done according to the standard procedure for Calmax [44].

The heat procedure for hardening the 6 cones are described below:

- Preheating temperature: 700 °C
- Austenitizing temperature: 960 °C, hold at this temperature for 30 minutes.
- Quench medium: 180 °C salt + 0.5vol% water
- Tempering temperature 1: 200 °C
- Tempering temperature 2: 220 °C

The reason for preheating the parts is to make sure that the whole part goes into austenite area at the same time. At 960 °C the components are in the austenite area. After quenching for 30 minutes, the components should have gone from austenite to martensite structure. However, there are some retained austenite. The purpose of the tempering process is to improve the toughness of the parts by making the microstructure go approach to equilibrium, which makes it less brittle. The retained austenite will transform into bainite or perlite, depending on the temperature. However, due to this alloy, it will most likely transform into bainitic ferrite and cementite [45, 46].

The initial measurements are represented in Table 6:2. One of the unwanted side effects from the hardening process, was that the volume increase. Table 6:3 presents the measurements after the hardening process. Table 6:4 illustrates the change after the annealing process. The results show that the volume change is very low. Figure 6:1 illustrates where the different measures were measured. Moreover, Figure 6:2 shows the different cones after the annealing process. The hardness for the different cones is presented in Table 6:3 after the annealing process. Prior to the hardening tests, the test surface was ground with grid paper 80 and 220.



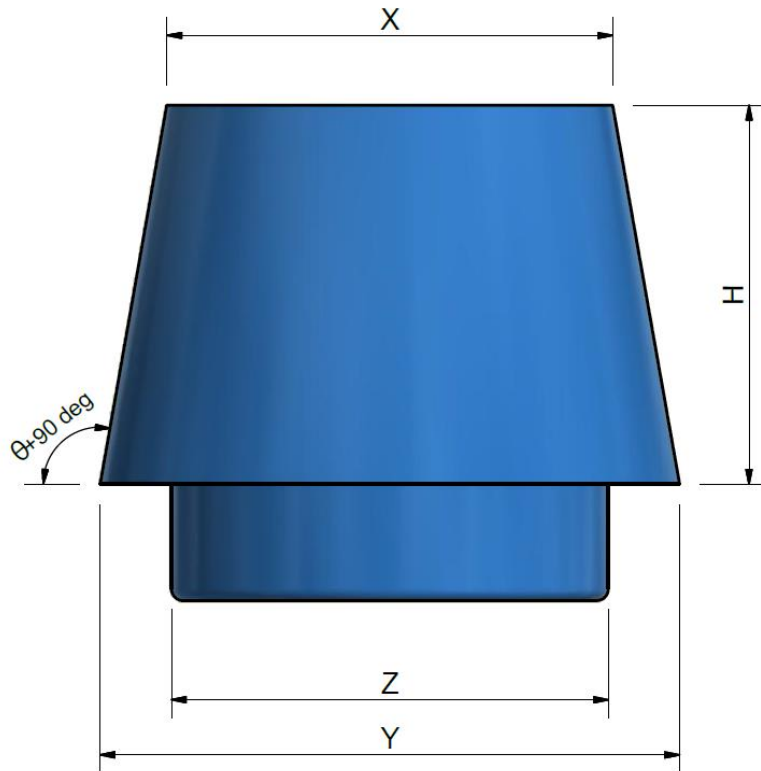


Figure 6:1: Overview of the measured areas on the cone

Part nr	X (mm)	Y (mm)	Z (mm)	H (mm)	Θ (deg)	Hardness (HB)
1	78,71	99,86	75,11	201,36	3	200
2	77,3	99,52	75,16	157,75	4,03	200
3	76,98	99,41	75	127,72	5,018	200
4	75,6	99,36	74,98	113,75	5,96	200
5	74,02	99,05	75	90,5	7,87	200
6	74,53	97,94	75	66,79	9,94	200

Table 6:2: Measurements before the hardening process

Part nr	X (mm)	Y (mm)	Z (mm)	H (mm)	Θ (deg)	Hardness (HRC)
1	79,09	99,88	75,08	201,36	2,955	55
2	78,29	99,48	75,01	157,75	3,84	55
3	77,87	99,41	74,89	127,72	4,82	56
4	76,69	99,375	74,96	113,75	5,694	55
5	75,08	99,03	74,86	90,5	7,54	58
6	75,62	97,9	74,83	66,79	9,73	57

Table 6:3: Measurements after the hardening process

Part nr	$\Delta X$ (%)	$\Delta Y$ (%)	$\Delta Z$ (%)	$\Delta H$ (%)	$\Delta \Theta$ (%)
1	0,482785	0,02	-0,04	0	-1,50
2	1,280724	-0,04	-0,20	0	-4,71
3	1,156144	0,00	-0,15	0	-3,95
4	1,441799	0,02	-0,03	0	-4,46
5	1,432045	-0,02	-0,19	0	-4,19
6	1,462498	-0,04	-0,23	0	-2,11

Table 6:4: Percentage change in the selected measurements: X,Y,Z,H and  $\Theta$

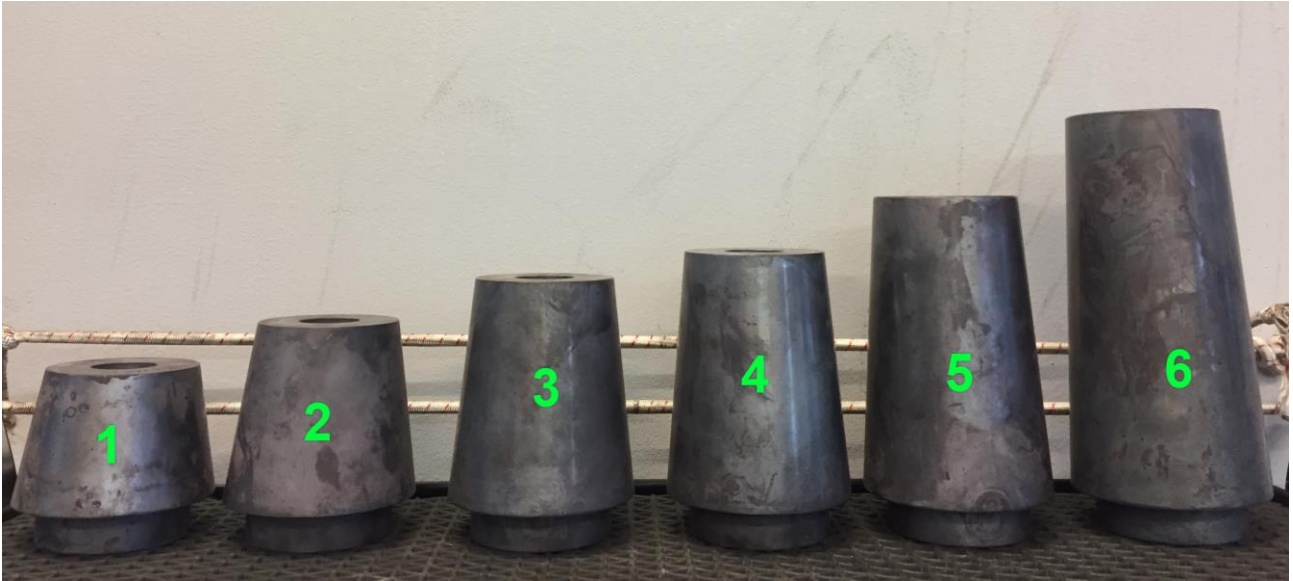


Figure 6:2: Six cones are presented with angles 3,4,5,6,8 and 10, with the following order starting from the left.

## 7. ANSYS Modelling

The overall purpose of performing this analysis, is to model the physical representation of the test-rig computationally. The objective is to verify the model setup, the indentation diameter and indentation depth. This was done by comparing against the empirical data. Furthermore, the reaction force and stresses are compared with analytical calculation.

In this study, there were only performed simulations with a cone-angle of 3 degrees.

The original model was made in Inventor and was then converted into a STEP-file to make it compatible with ANSYS. Originally the model was very big, and the number of nodes and elements made the simulation very time-consuming. Since the model is perfectly axisymmetric, it was possible to model a single ball section in the model. Furthermore, this made the analysis less time-consuming and more accurate. An overview of the model is presented in picture Figure 7:1.

The output data from the ANSYS simulation are reaction force, Indentation in pipeline, friction coefficient and maximum equivalent stress. The reaction force is applied as a horizontal vector from the set-pipe as illustrated in Figure 7:2. Friction is applied in the contact area between the steel ball and set-pipe, pipeline and cone. Furthermore, the friction coefficient is assumed to have the same magnitude between all the contact areas. The maximum equivalent stress is located between the bearing steel ball and the contact surface.

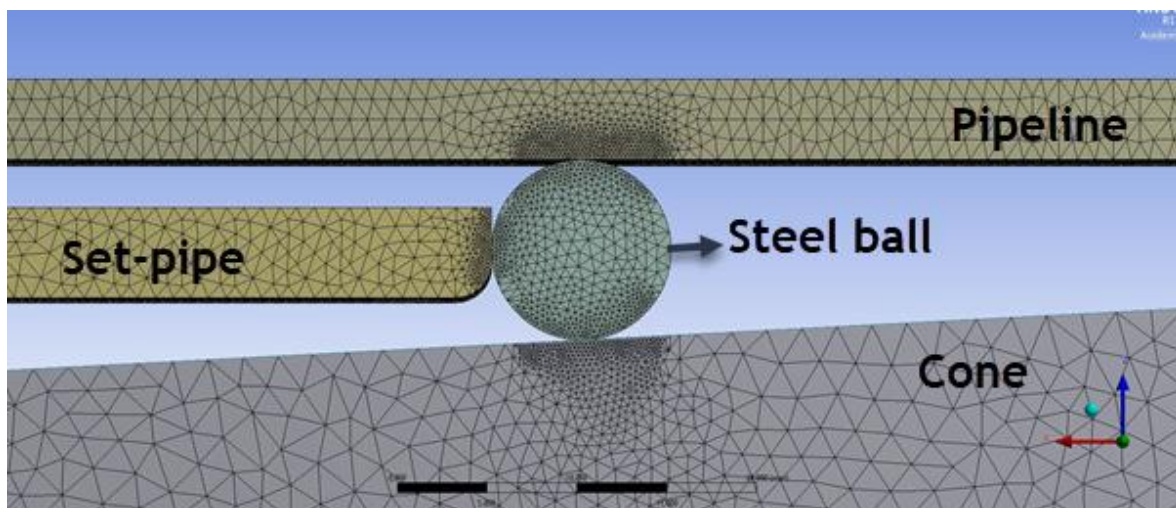


Figure 7:1 : Overview of the mesh elements in ANSYS. Contact size element is 0,2 mm.

In order to make the ANSYS simulation compute in a more efficient way, the displacement of the bearing steel ball was varying, instead of applying a force to the set-pipe. There were performed simulations with various displacement in both linear-elastic and elastic-plastic models. In both cases it is evaluated how displacement and friction affects reaction force, indentation in pipeline and equivalent stress. Figure 7:2 gives an overview of where the reaction force and displacement occur. The development and occurrence of equivalent stress are illustrated in Figure 7:3. The pressure that occurs between the steel ball and the pipeline causes indentation to occur in the pipeline walls. Figure 7:4 illustrates how the steel ball slides and sticks in the model.

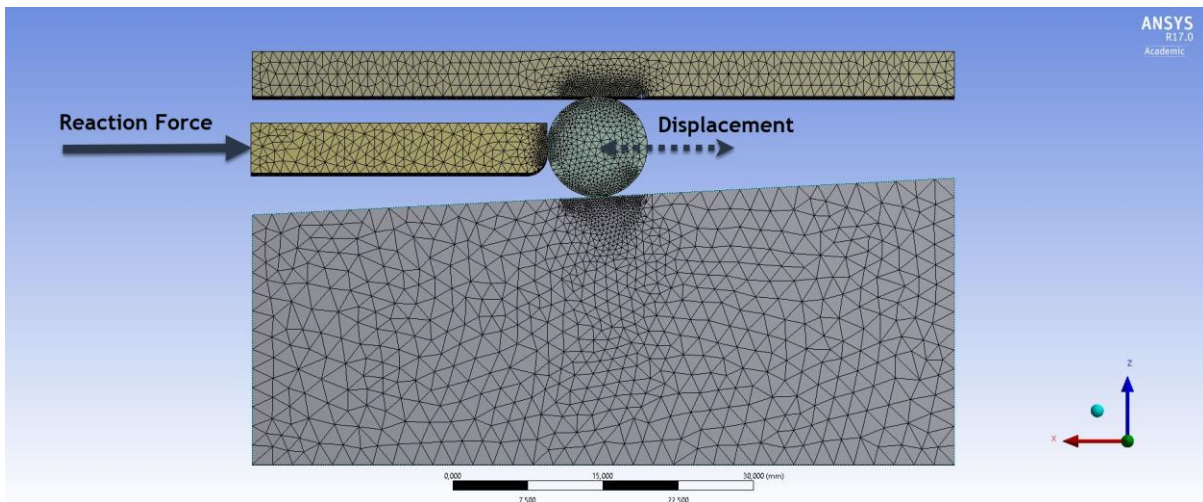


Figure 7:2: Overview of the location of Reaction force and Displacement of the bearing steel ball

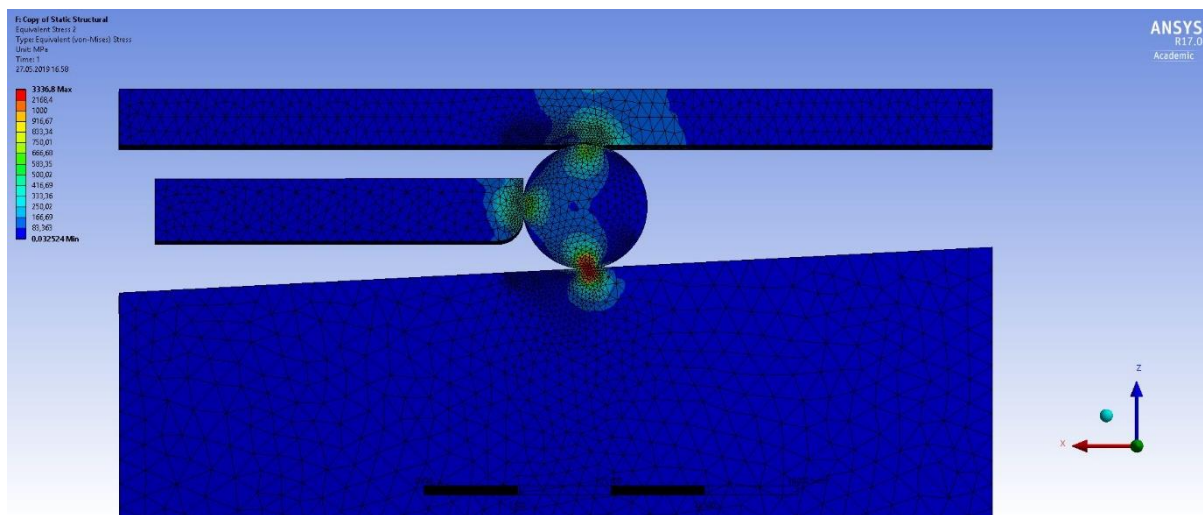


Figure 7:3: Elastic-plastic ANSYS model equivalent stress development in bearing steel ball

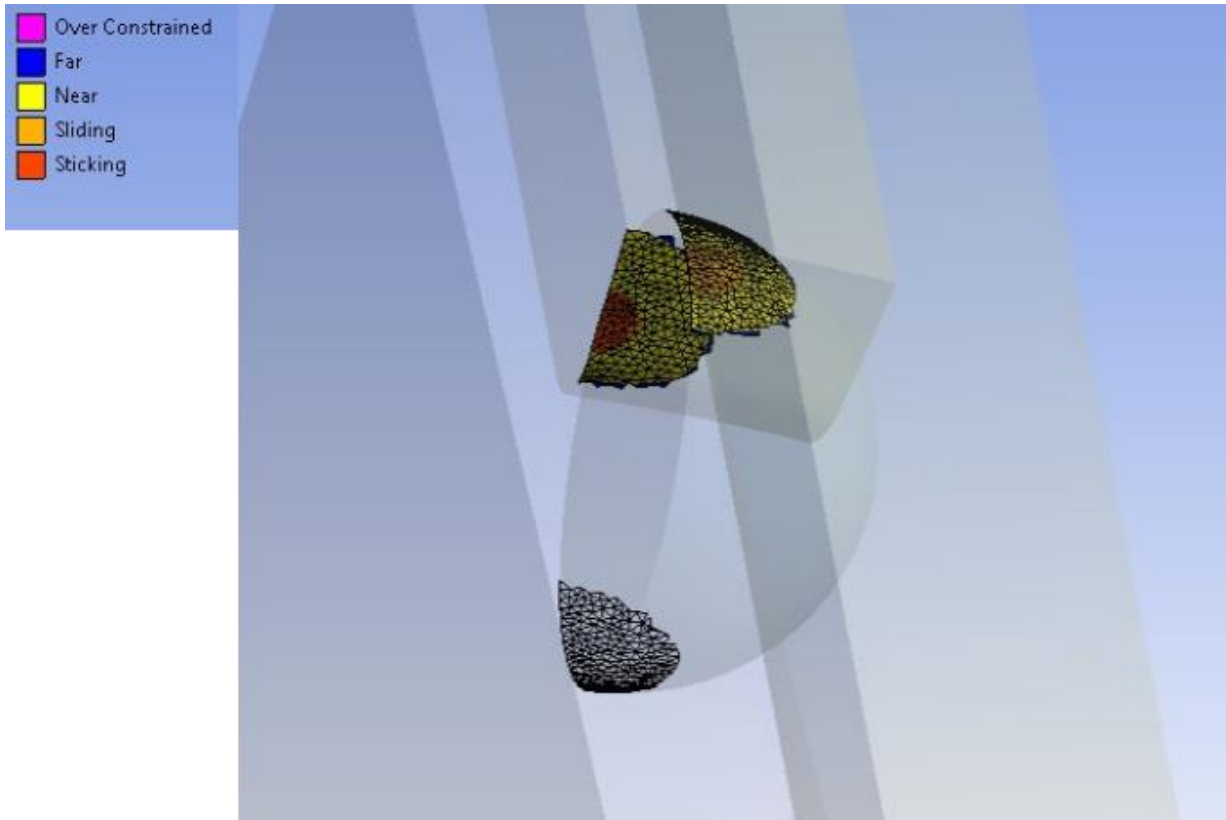


Figure 7:4: Overview of where the steel ball slides and sticks to the contact surfaces

## Bilinear material curve

For the elastic-plastic analysis, set-pipe and the pipeline were assigned bilinear curve. The bearing steel ball and the cone were assumed to be in the linear-elastic area and do not have any stress-strain curve. This was done because the empirical testing was mainly performed in the linear-elastic area of the cone and steel balls.

The material properties used in ANSYS, is given in pipeline material certificate presented in Appendix I and Table 7:1.

Table 4-3 Proposed non-linear properties for S355 steels (Engineering stress-strain)			
	S355		
Thickness [mm]	$t \leq 16$	$16 < t \leq 40$	$40 < t \leq 63$
E [MPa]	210000		
$\sigma_{prop}/\sigma_{yield}$	0.9		
$E_{p1}/E$	0.001		
$\sigma_{prop}$ [MPa]	319.5	310.5	301.5
$\sigma_{yield}$ [MPa]	355	345	335
$\sigma_{yield2}$ [MPa]	358.4	348.4	338.4
$\sigma_{ult}$ [MPa]	470	470	450
$\epsilon_{p y1}$	0.004		
$\epsilon_{p y2}$	0.02		
$\epsilon_{p ult}$	0.15		
$E_{p2}/E$	0.0041	0.0045	0.0041

Table 7:1: Non-linear material properties for S355 steels [39].

Table 7:1 was used to fill in missed material information about the pipeline. Moreover, the material property Table 7:1 is only an approximation, which was the best match with pipeline material certificate.

## Mesh Refinement Study

A tetrahedron dominated mesh was selected in the model, because of its advantages in meshing complex geometries. ANSYS workbench mesh metric tool was used to control the shape, size and number of elements/nodes. Strain and stress are solved from derivative of the displacement gradients; therefore, it is normally recommended to use finer mesh to obtain stress than for displacement [35, 47].

A mesh refinement study was performed with both linear-elastic and elastic-plastic model to determine the number of elements and nodes to describe stresses, forces and the deformations.

### 7.1. Elastic-Plastic mesh refinement study

In the mesh refinement study, the displacement was set to 2 mm and the friction coefficient was set to 0,2.

Due to the very complex simulation and small tangent modulus of the bilinear parts, it seems that the model will not converge properly when deformations are in the plastic area. Figure 7:5 illustrates the contact sizing element vs reaction force. Figure 7:6 illustrates the contact sizing element vs indentation in pipeline. Figure 7:7 illustrates the contact sizing vs maximum equivalent stress. These figures show the solution converges with a contact size element of 0,2. This gives 162960 elements and 236880 nodes.

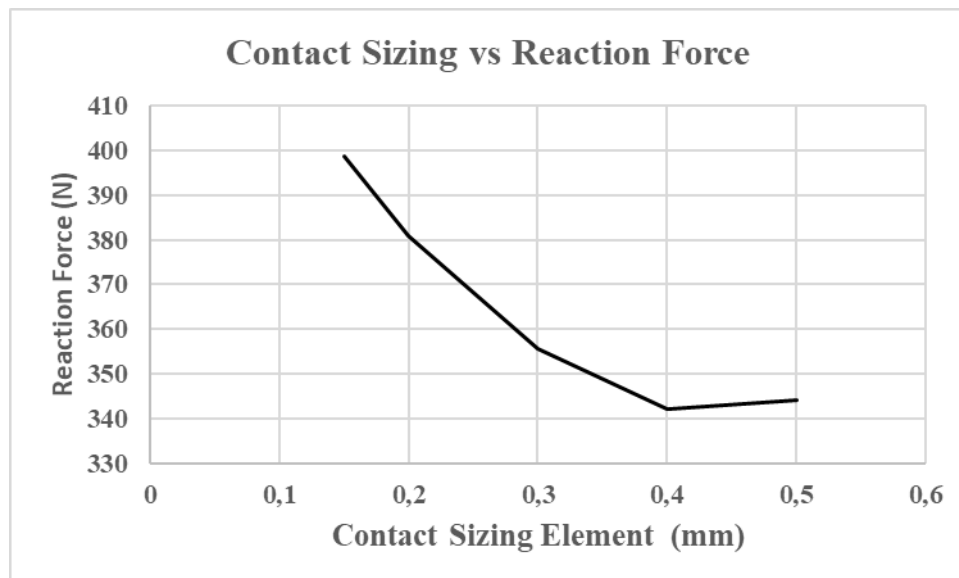


Figure 7:5: Reaction force vs Contact size element in elastic-plastic simulation

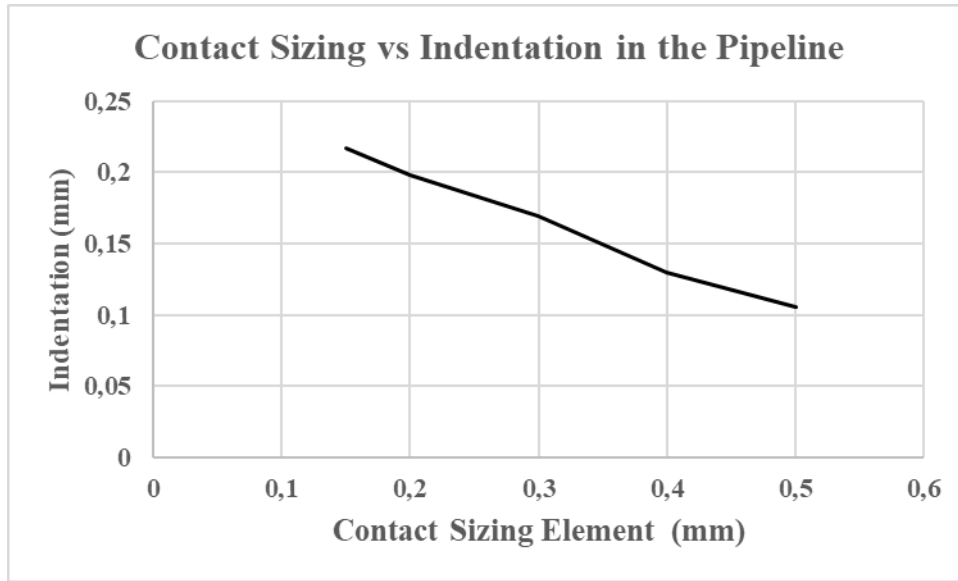


Figure 7:6: Indentation in pipeline wall vs Contact size element in elastic-plastic simulation

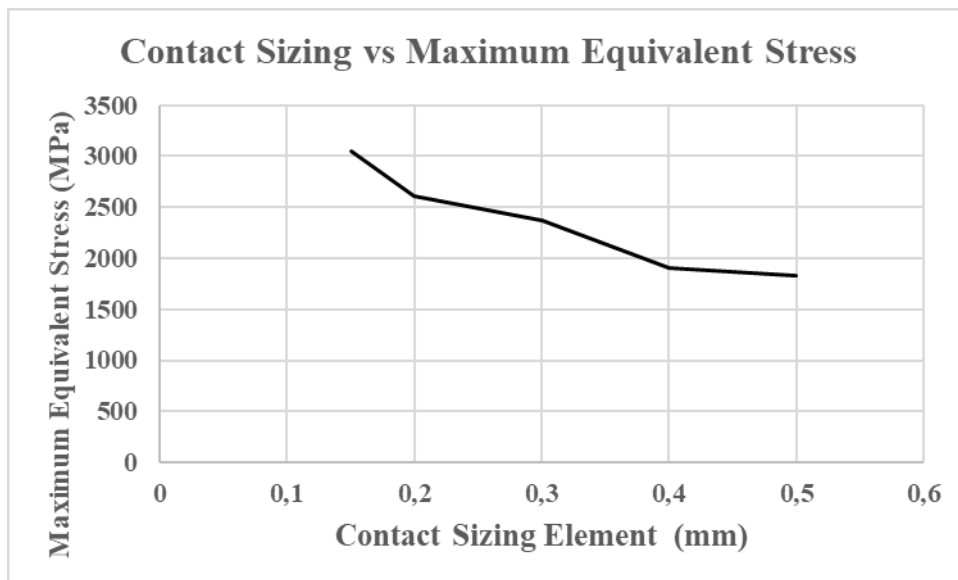


Figure 7:7: Maximum equivalent stress vs Contact size element in elastic-plastic simulation

Contact Size Element (mm)	Mesh Elements (-)	Mesh Nodes (-)
0,15	337523	478814
0,2	162960	236880
0,3	73873	112109
0,4	51437	79632
0,5	42879	67229

Table 7:2: Number of elements and Nodes with different contact size element in an Elastic-plastic model

## 7.2. Sensitivity Study on Elastic-Plastic

After the mesh size has been established, a sensitivity study on yield strength and tangent modulus has been performed on the elastic-plastic model. The following sensitivity studies was carried out with a friction coefficient of 0,2 and a steel ball displacement of 2 mm.

Figure 7:8 illustrates the yield stress vs pipeline indentation depth. Figure 7:9 illustrates the yield stress vs reaction force. Figure 7:10 illustrates the yield stress vs maximum equivalent stress.

Figure 7:11 illustrates the tangent modulus vs pipeline indentation depth. Figure 7:12 illustrates the tangent modulus vs reaction force. Figure 7:13 illustrates the tangent modulus and maximum equivalent stress.

The graphs presented below shows that the indentation depth in the pipeline, reaction force from the set-pipe and equivalent stress is approximately linear and varies a lot with different yield stresses.

### Sensitivity study of Yield Strength

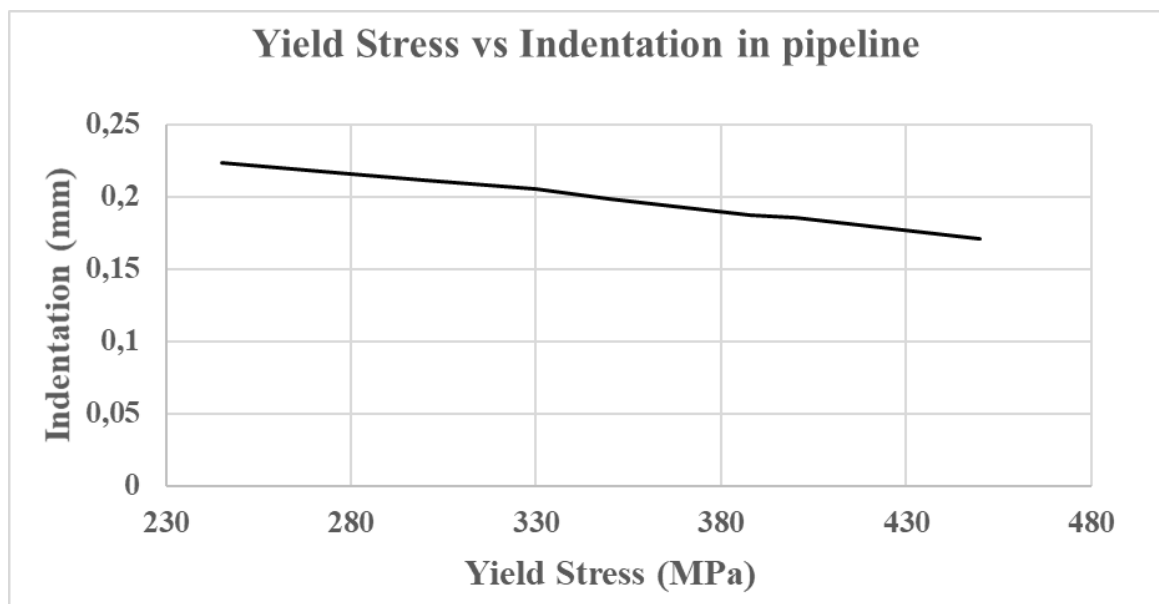


Figure 7:8: Yield stress vs Indentation in pipeline in elastic-plastic area.



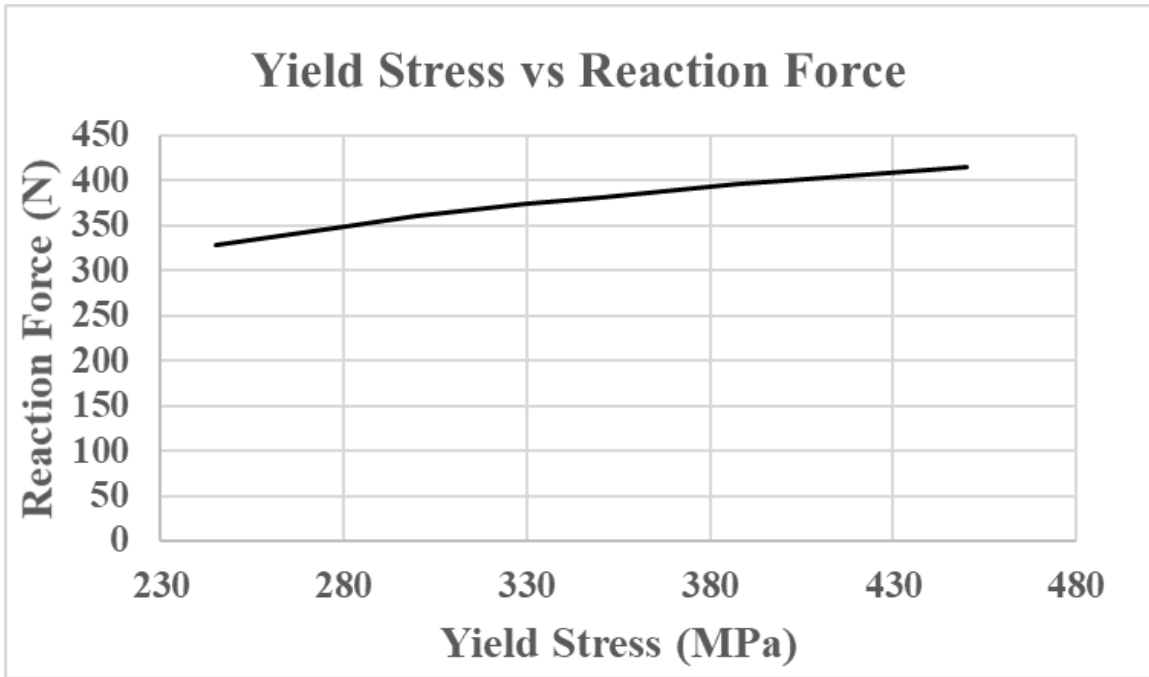


Figure 7:9: Yield stress vs Reaction force in pipeline in elastic-plastic area.

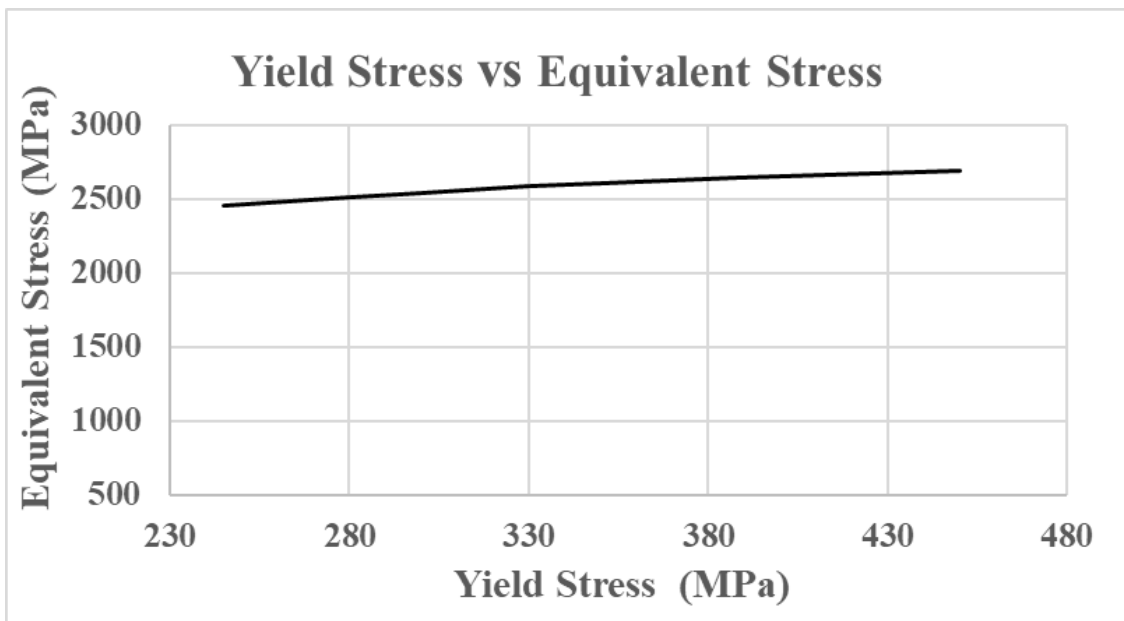


Figure 7:10: Yield stress vs Maximum equivalent stress in pipeline in elastic-plastic area.

## Sensitivity study of Tangent Modulus

The graphs presented below shows that the indentation depth in the pipeline, reaction force from the set-pipe and equivalent stress varies a lot with different tangent modulus. The magnitude of the tangent modulus has a large impact on the stress-strain curve. This modelled case involves plastic deformation and Figure 7:11 shows that with small tangent modulus, the indentation becomes much larger than with high tangent modulus.

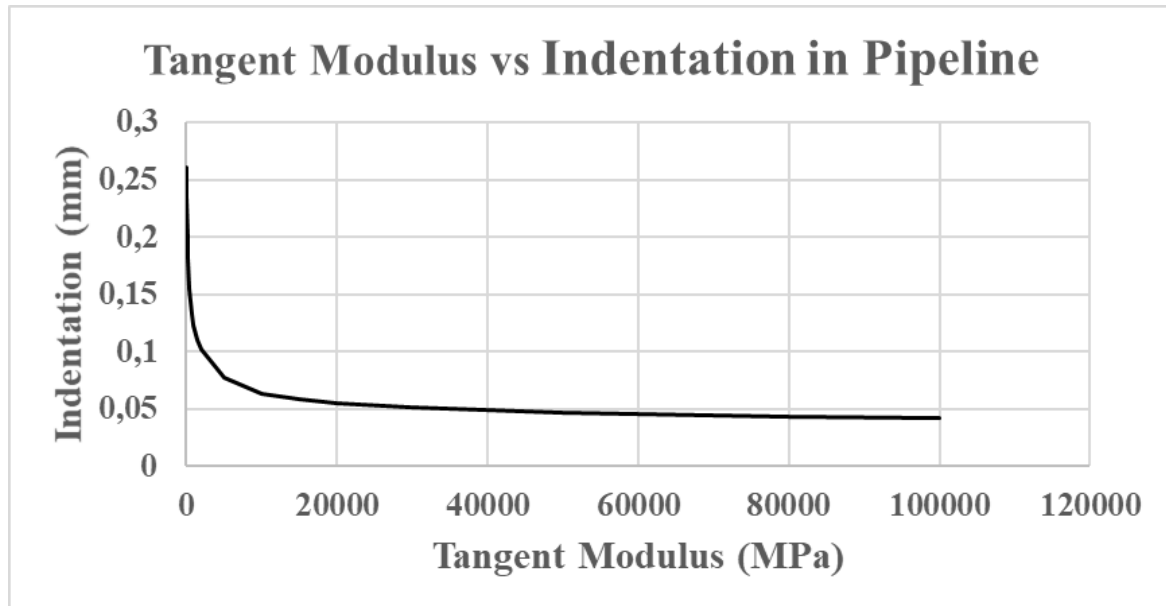


Figure 7:11: Tangent Modulus vs Indentation in pipeline in pipeline in elastic-plastic area.

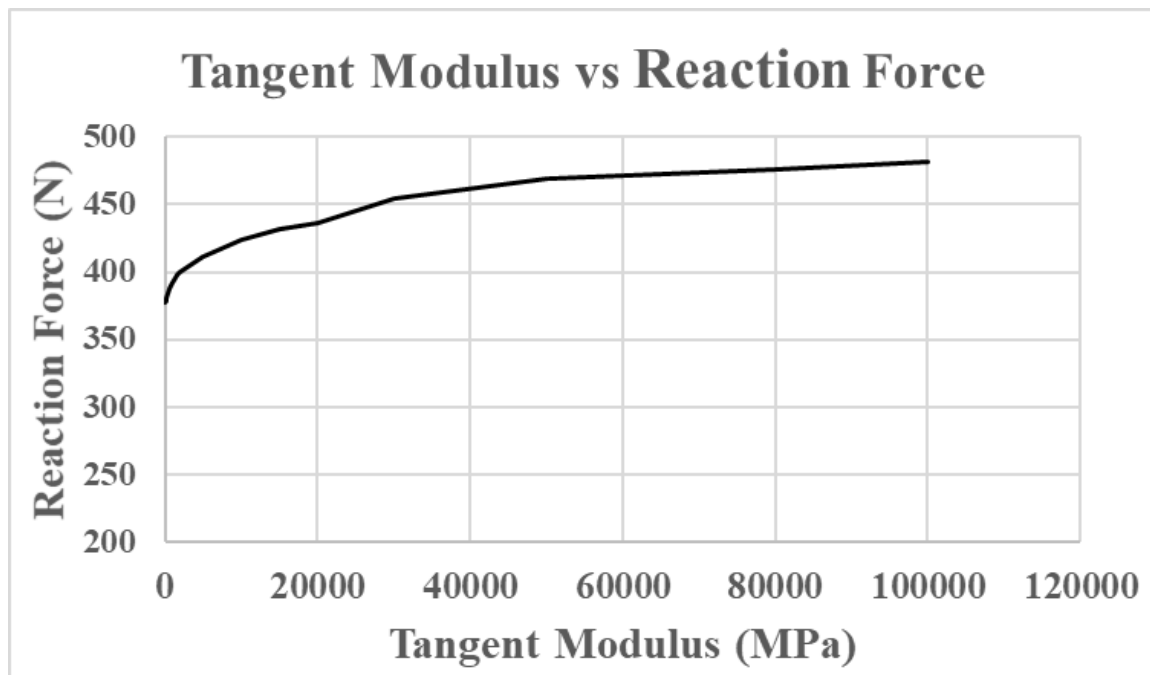


Figure 7:12: Tangent Modulus vs Reaction force in pipeline in elastic-plastic area.

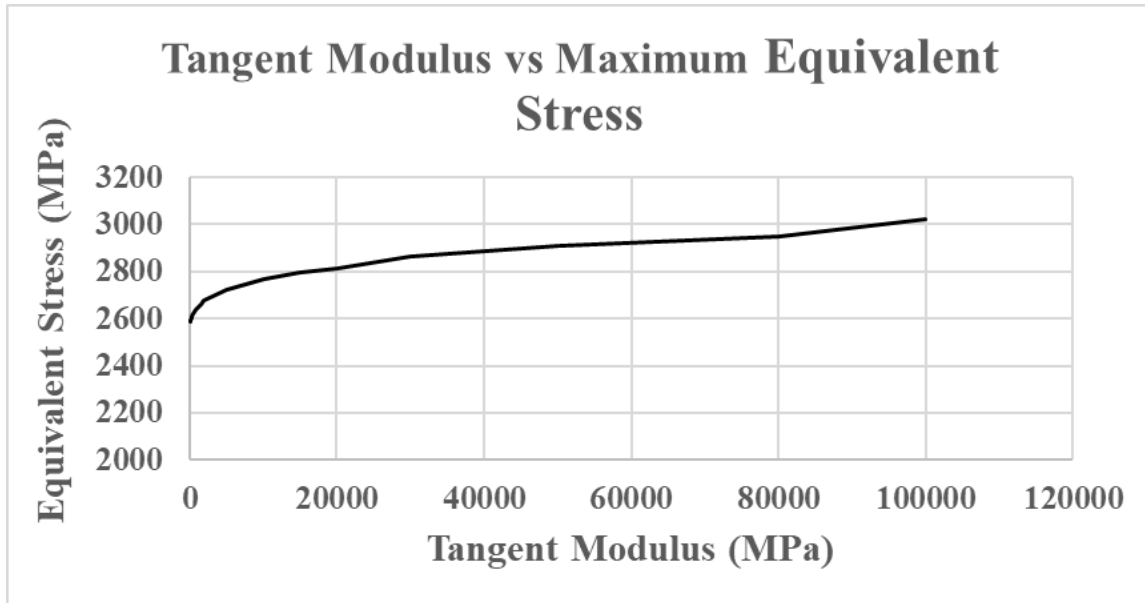


Figure 7:13: Tangent Modulus vs Maximum equivalent stress in elastic-plastic area.

### 7.3. Linear-Elastic mesh refinement study

In the mesh refinement study, the displacement was set to 2 mm and the friction coefficient was set to 0,2. A linear-elastic mesh refinement study was performed to validate and compare the results obtained in elastic-plastic mesh refinement study.

Figure 7:14 illustrates the contact sizing element vs reaction force. Figure 7:15 illustrates the contact sizing element vs indentation in pipeline. Figure 7:16 illustrates the contact sizing vs maximum equivalent stress. The number of elements and nodes are presented in Table 7:3. Figure 7:16 indicates a convergence trend at contact size element of 0,3 mm. Furthermore, the remaining graphs below shows an adequate convergence trend at contact element size of 0,2 mm. This results in 162960 elements and 236880 nodes.

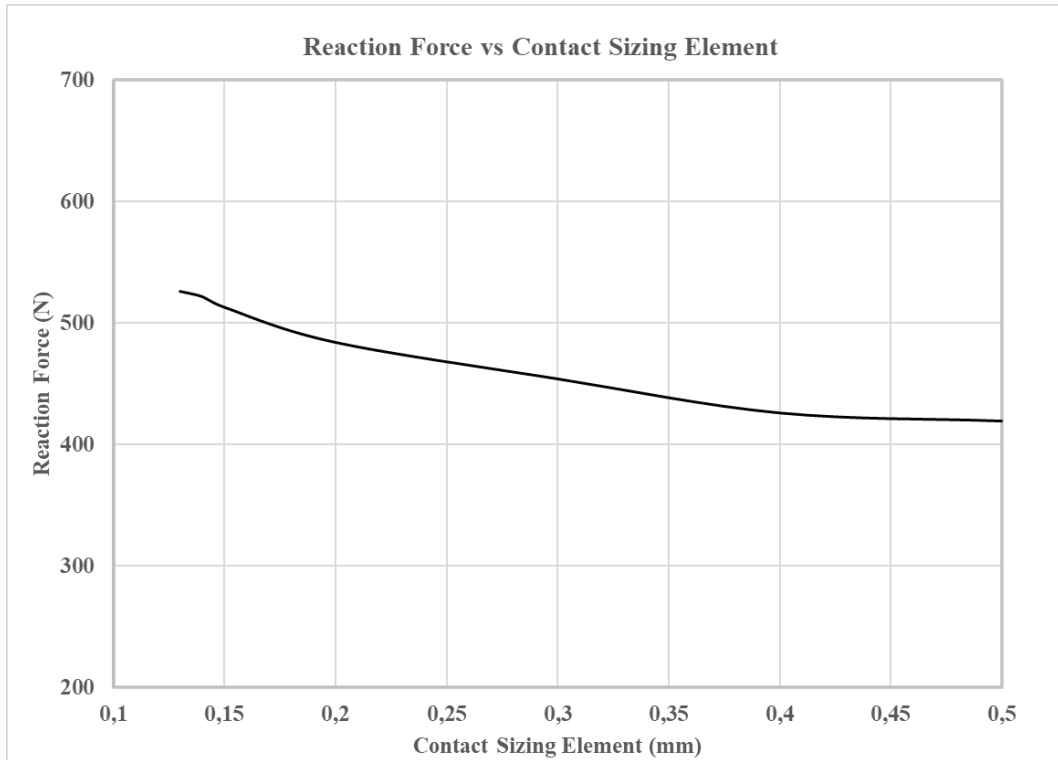


Figure 7:14: Reaction force vs Contac sizing element in a Linear-elastic model

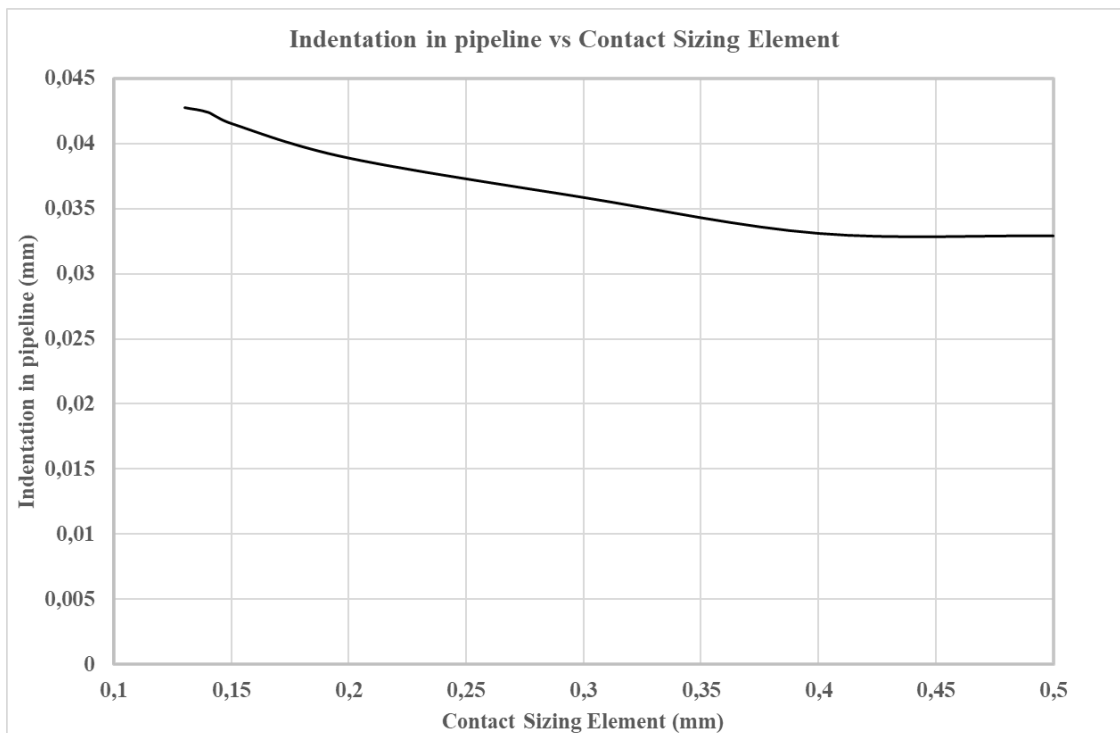


Figure 7:15: Indentation in pipeline vs Contac sizing element in a Linear-elastic model

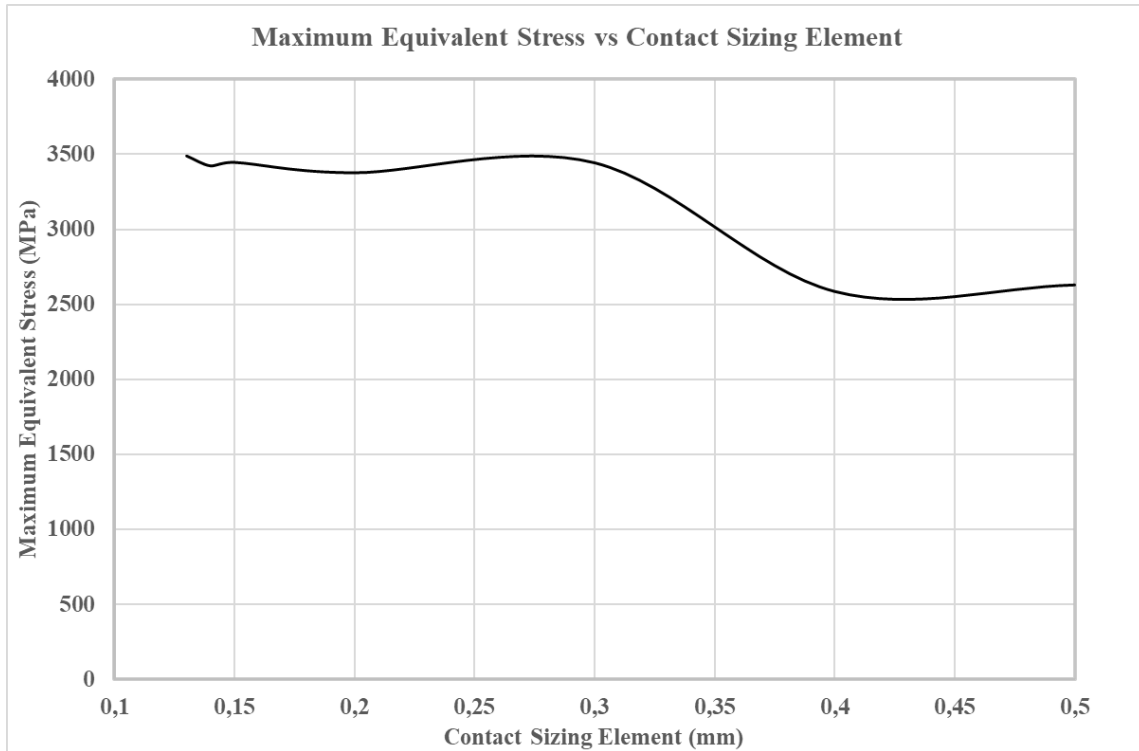


Figure 7:16: Maximum Equivalent stress vs Contac sizing element in a Linear-elastic model

Contact Size Element (mm)	Mesh Elements (-)	Mesh Nodes (-)
0,13	502451	706338
0,14	407883	576474
0,15	337523	478814
0,2	162960	236880
0,3	73873	112109
0,4	51437	79632
0,5	42879	67229

Table 7:3: Number of elements and Nodes with different contact size element in a Linear-Elastic model

## 8. Calculations, empirical results and FEA results

This chapter presents the analytical calculations performed to predict and describe the stresses and indentations that occur at the contact surface between the steel balls and pipeline and cone. A cone-angle of 3 degrees are mostly used in the calculations.

The empirical results are obtained from Calmax and 34CrNiMo6 alloyed cone.

FEA results are obtained from the ANSYS model presented in Chapter 7.

### 8.1. Analytical Calculations

#### Reaction force due to friction and static vectors

Table 8:1 presents the reaction force from the bearing steel ball on the pipeline and cone with respect to different angles as illustrated in Figure 5:2. This is obtained through basic vector calculation in a static situation as illustrated in Figure A-2.

Angle°	Reaction force on pipeline	Reaction force on cone
3	19,08*F	19,107*F
4	14,3*F	14,34*F
5	11,43*F	11,47*F
6	9,51*F	9,57*F
8	7,11*F	7,18*F
10	5,67*F	5,76*F

Table 8:1: Static reaction force from bearing steel ball on pipeline and cone illustrated in Figure A-3

The reaction forces including various friction coefficients are presented in Table 8:2. This is calculated through free body diagram illustrated in Figure A-1.

Angle °	Friction coefficient	Reaction force
3	0,1	6,527*F
3	0,2	3,92*F
3	0,3	2,8*F
3	0,4	2,16*F
3	0,5	1,763*F
3	0,6	1,485*F

Table 8:2: Friction coefficient and reaction force from bearing steel ball with an angle of 3 degrees.

The reaction force at the set-pipe is presented in Table 8:3. The area of the cylinder is shown in Figure A-3. Moreover, the pressure in the cylinder is logged and presented in Appendix F.

Set pressure (MPa)	Total reaction force (N)	Reaction force from each bearing steel ball (N)
5	15708	561
3,5	10995,6	392,7
3	9424,8	336,6
2,5	7854	280,5
1,75	5497,8	196,35
1,5	4712,4	168,3
1,25	3927	140,25
1	3141,6	112,2
0,75	2356,2	84,15
0,5	1570,8	56,1

Table 8:3: Cylinder set-pressure and reaction force from the bearing steel balls

### **Average stress Vs yield stress to find out the reaction force between each bearing steel ball and pipeline, with a cone that has an angle of 3 degrees**

Assuming that equation (3.34), the yield stress of the pipeline is 388 MPa and the empirical data from the test-rig are correct. The reaction force between the pipeline and bearing steel ball can be calculated using the following equation are used:

$$F * x = n * A * \sigma \quad (8.1)$$

Where:

F = total reaction force from set-pipe that is connected to the cylinder

x = is the unknown reaction constant between the bearing steel ball and pipeline

n = number of bearing steel balls

A = area from a spherical indenter from Chapter 3.4

$\sigma$  = Onset of plastic deformation from Chapter 3.8 “When the plastic deformation occurs”

The indentation depths are obtained from the empirical testing and presented in Table 8:14. Assuming that the real indentation depth is close to 0,3 mm for a set-pressure of 5 MPa. This results in a reaction constant x a value of 7,17. However, this applies only for the cone with an angle of 3 degrees. Figure 8:1 illustrates the indentation depth into the pipeline when the steel balls are applied 5 MPa pressure from the set-pipe. Below the line “onset of plastic deformation” in Figure 8:1, there is no plastic deformation. Moreover, the reaction force between the steel ball and the pipeline are calculated to be 7.17\*F.

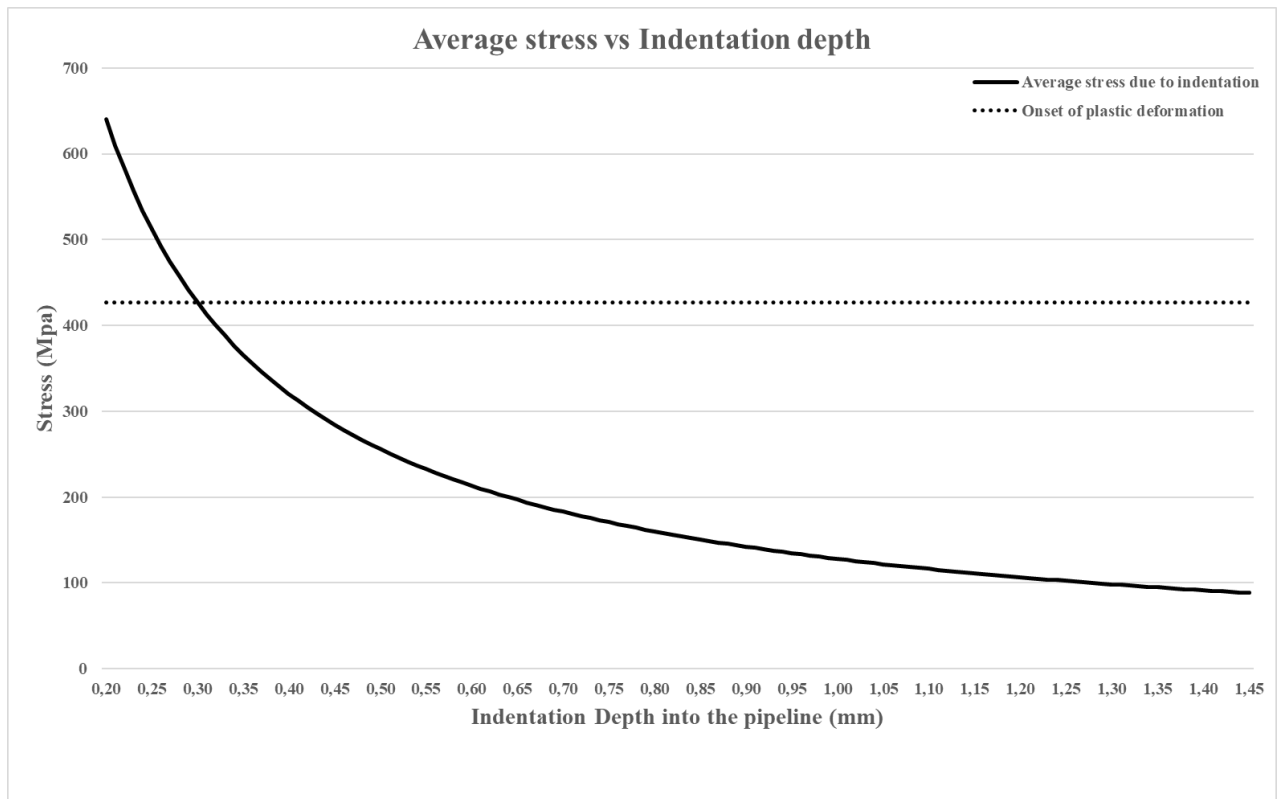


Figure 8:1: Indentation depth vs average stress with a reaction coefficient of 7,17 and a set-pressure of 5 MPa.

After obtaining the reaction force constant, equation (8.1) was used to calculate the indentation depth with other set-pressures on a cone with an angle of 3 degrees.

Using a reaction force constant  $x$  of 7.17, the following dent depth with different set-pressures from equation (8.1) are presented in Table 8:4.

Set pressure (MPa)	Reaction force for each steel ball (N)	Indentation depth (mm)
5	561	0,299991
3,5	392,7	0,209993
3	336,6	0,179994
2,5	280,5	0,149995
1,75	196,35	0,104997
1,5	168,3	0,089997
1,25	140,25	0,074998
1	112,2	0,059998
0,75	84,15	0,044999
0,5	56,1	0,029999

Table 8:4: Approximated indentation depth into the pipeline



## Onset of plastic deformation with Tresca and Huber-Mises criterion

The onset of plastic deformation occurs is presented in Table 8:5. Equation (3.34) are used to obtain the mean pressure at the onset of plastic deformation.

Yield (MPa)	Pm (MPa)
245	269,5
260	286
275	302,5
290	319
305	335,5
320	352
335	368,5
350	385
365	401,5
380	418
395	434,5

Table 8:5: Huber-Mises and Tresca criterion for when plastic deformation starts to occur with a spherical indenter with various yield stresses

## Mean pressure at onset of fully plastic deformation of an ideally plastic metal

Using equation (3.35), the mean pressure at when fully plastic deformation occur is calculated and presented in Table 8:6.

Yield (MPa)	Pm (MPa)
245	735
260	780
275	825
290	870
305	915
320	960
335	1005
350	1050
365	1095
380	1140
395	1185

Table 8:6: When fully plastic deformation occurs with various Yield stresses.

## Load for when plastic deformation occurs

Table 8:7 presents the load for when the plastic deformation starts to occur. Equation (3.36) is used to calculate the load at which the onset of plastic deformation occurs.

Yield (MPa)	W <sub>L</sub> (N)	Grams (g)
245	0,581446	59,27069
260	0,694914	70,83727
275	0,822259	83,81849
290	0,964284	98,29598
305	1,121787	114,3513
320	1,295569	132,0662
335	1,486433	151,5222
350	1,695176	172,8009
365	1,922602	195,9839
380	2,16951	221,1529
395	2,4367	248,3894

Table 8:7 : Loads for when plastic deformation occurs with a spherical indenter with a radius of 5mm with various yield stresses.

## Brinell Hardness Number

Figure 8:2 illustrates the Brinell hardness number with different values of set-pressure and indentation diameter. This graph is calculated with the forces in a static state, which is illustrated in Figure A-2. The reaction forces that are used are presented in Table 8:1. Moreover, the graphs in Figure 8:2 are obtained with the use of equation (3.24)

The friction force is not included in the Brinell graph. A conversion table is used to get out a Brinell number in the pipeline [48], it is assumed that the pipeline has a tensile strength of 450 MPa. The hardness Brinell number used in the analytical calculation is 127.

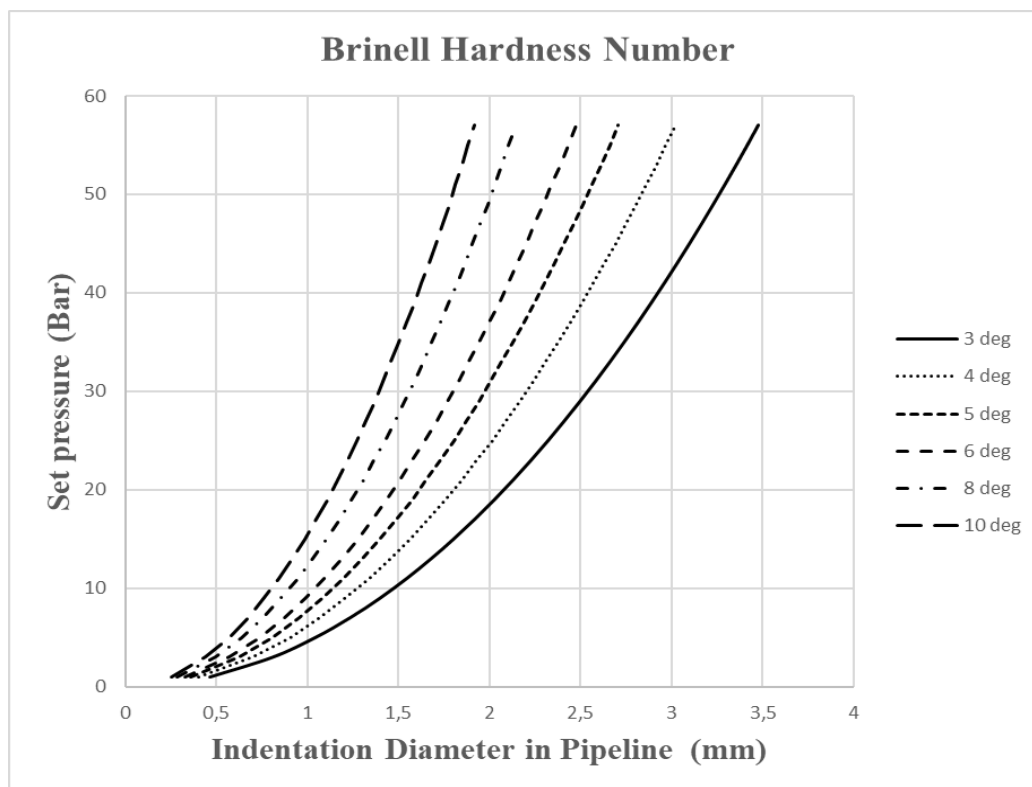


Figure 8:2: Brinell hardness number in terms of force applied on the steel balls and indentation diameter into the pipeline

## Contact stresses

Figure 8:3 illustrates the location of reaction forces that occurs between the steel ball and cone, pipeline and set-pipe. Reaction forces used to calculate the contact stresses are calculated to  $7.17 \cdot F$  found with equation (8.1). Youngs modulus of 210 GPa are assumed to be the same in all the interacting parts [39]. Moreover, Poisson number of 0,3 is assumed to be the same in all the interacting parts.

The analytic calculations are done in accordance with Chapter 3.2. Moreover, the cone-angle used when calculating the contact stresses are 3 degrees.

The constants in Table 8:8 are approximately the same in both test-rigs as presented in Chapter 5.

The difference between the test-rigs presented in Chapter 5 in magnitude of A and B from equation (3.2) and (3.3) are negligible. Moreover, this will result in the same constants on both of the test-rigs listed in Table 8:8.

The cone has the following magnitude of  $A \approx 0,1$  and  $B \approx 0,1122$  and pipeline has the following magnitude of  $A \approx 0,0905$  and  $B \approx 0,1$ .

Constants	Magnitude
$C_b$	0.88
$C_\delta$	2,2
K	0.95
$C_G$	0.2
$C_\tau$	0.22
$C_\sigma$	0.67
$C_{zs}$	0.49

Table 8:8: Contact stress constants.

The stresses that occur between each bearing steel ball and the cone for various set-pressure are presented in Table 8:9. Moreover, the stresses that occur between each bearing steel ball and the pipeline for various set-pressure are presented in Table 8:10.

Set-pressure (MPa)	Reaction force between each steel ball and cone (N) ( $F_c$ )	$b$ (mm)	$\Delta$ ( $\text{mm}^3/\text{N}$ )	$\sigma_{max}$ (MPa)	$\tau_{max}$ (MPa)	$\tau_{(oct(max))}$ (MPa)	$\delta$ (mm)	$z_s$ (mm)
5	4022,37	0,481954	0,00004084	-7906,68	2596,22 4	2360,20 4	0,05065	0,2362
3	2413,422	0,406495	0,00004084	-6668,75	2189,74	1990,67 3	0,03603	0,1992
1,5	1206,711	0,322636	0,00004084	-5292,99	1737,99 8	1579,99 8	0,0227	0,1581
1	804,474	0,281848	0,00004084	-4623,86	1518,28 1	1380,25 6	0,01732	0,1381
0,5	402,237	0,223703	0,00004084	-3669,96	1205,06 1	1095,51	0,01091	0,1096

Table 8:9: Analytical calculated stresses between each bearing steel ball and cone with an angle of 3 degrees

Set-pressure (MPa)	Reaction force between each steel ball and pipeline (N) ( $F_y$ )	$b$ (mm)	$\Delta$ (mm <sup>3</sup> /N)	$\sigma_{max}$ (MPa)	$\tau_{max}$ (MPa)	$\tau_{(oct(max))}$ (MPa)	$\delta$ (mm)	$z_s$ (mm)
5	4022,37	0,499628	0,0000455	- 7357,17	2415,786	2196,169	0,048867	0,244818
3	2413,422	0,421403	0,0000455	- 6205,27	2037,553	1852,321	0,034763	0,206487
1,5	1206,711	0,334468	0,0000455	- 4925,13	1617,207	1470,188	0,021899	0,163889
1	804,474	0,292184	0,0000455	-4302,5	1412,76	1284,327	0,016712	0,14317
0,5	402,237	0,231907	0,0000455	- 3414,89	1121,308	1019,371	0,010528	0,113634

Table 8:10: Analytical calculated stresses between each bearing steel ball and pipeline with a cone angle of 3 degrees

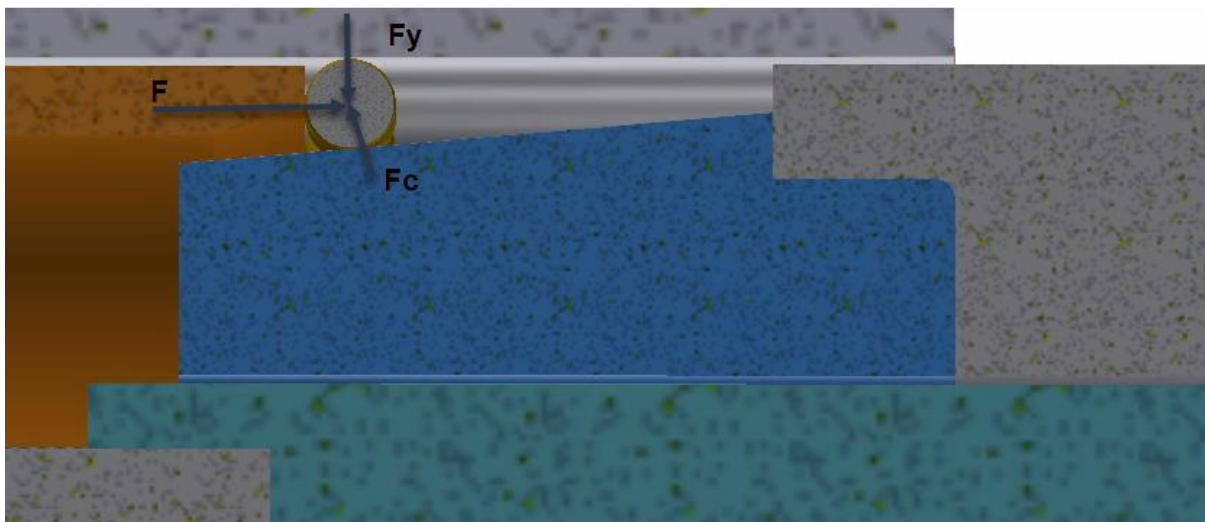


Figure 8:3: Reaction forces from the bearing steel ball

## Hertzian unimodal contact

The contact area and deflection between a 3-degree angle cone and bearing steel ball are presented in Table 8:11. The analytical calculations are done in compliance with Chapter 3.3.1 and the reaction force is obtained from equation (8.1).

Set-pressure (MPa)	Reaction force between each steel ball and pipeline (N) ( $F_y$ )	$a$ (mm)	$1/E$ ( $\text{mm}^2/\text{N}$ )	$\delta$ (mm)	$e$ (mm)
5	4022,37	0,5075	0,000008666667	0,05152	0,715923
3	2413,422	0,4281	0,000008666667	0,03665	0,604282
1,5	1206,711	0,33975	0,000008666667	0,0231	0,480069
1	804,474	0,2968	0,000008666667	0,01762	0,419392
0,5	402,237	0,235571	0,000008666667	0,0111	0,332982

Table 8:11: Contact area and deflection that occurs between the 3-degree cone and bearing steel ball

## 8.2. Empirical results:

### Results from a cone alloyed with 34CrNiMo6

As explained in Chapter 5.2, the cone angle used was 5 degrees and was loaded with 10 tons of pressure on the pipeline. The pipeline travel distance, bearing steel ball set-force and maximum applied load on the pipeline are presented in Table 8:12.

The final dent depth and dent diameter are presented in Table 8:13. The pressure in the cylinder was logged and is illustrated in Figure 8:4. The indentation and dent diameter are illustrated in Figure 8:5.

Total Set-Force on the steel balls	Travel distance for set-pipe	Travel distance for pipe	Max load on pipeline	Angle of cone	Steel ball size (radius)
14137,2	(-)	19mm	5 tons	5°	5 mm
14137,2	(-)	35mm	10 tons	5°	5 mm

Table 8:12 : Set-Force on steel balls, pipeline distance travelled and applied load on pipeline with a 34CrNiMo6 alloyed cone.

Part	Dent depth/ deformation (mm)	Dent Diameter (mm)
Cone	0.47	3.9
Pipe	0.56	4.9
Steel balls	No deformation	(-)

Table 8:13: 34CrNiMo6 alloyed cone test results with an angle of 5 degrees.

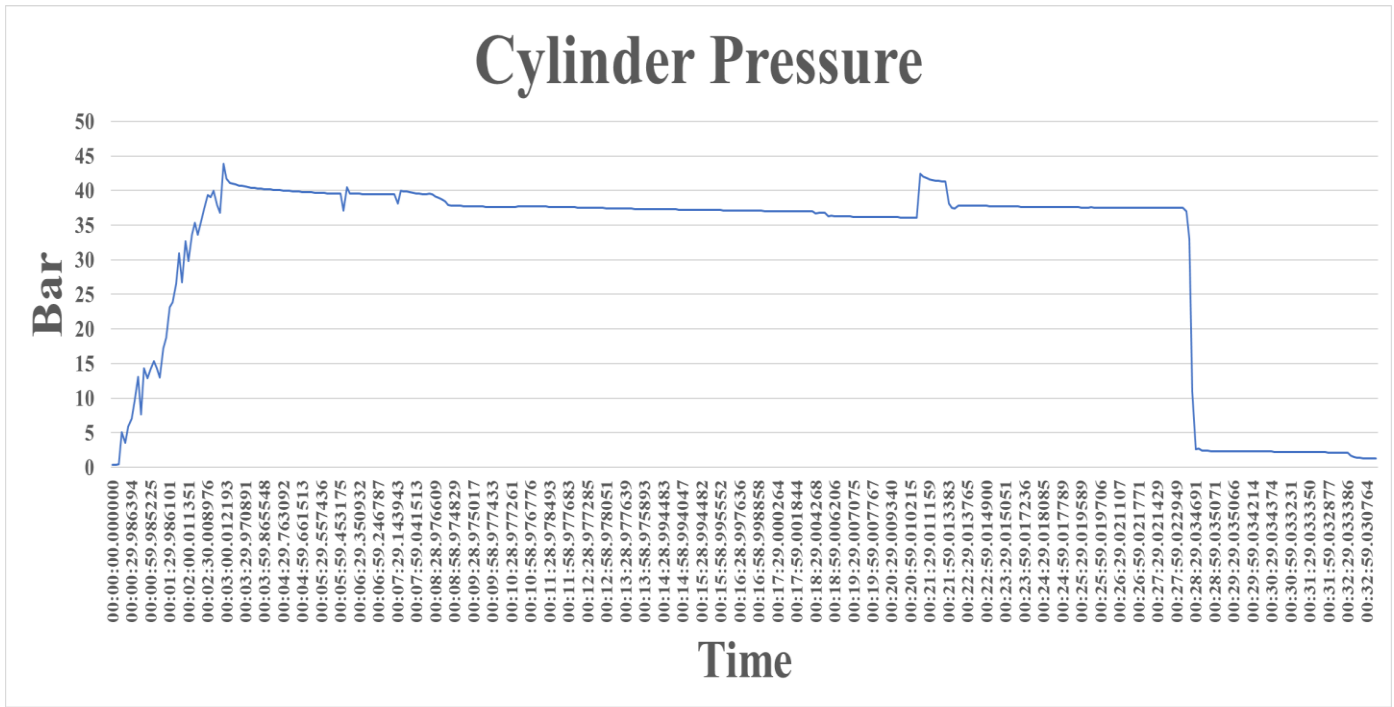


Figure 8:4: Cylinder pressure when testing 34CrNiMo6 alloyed cone

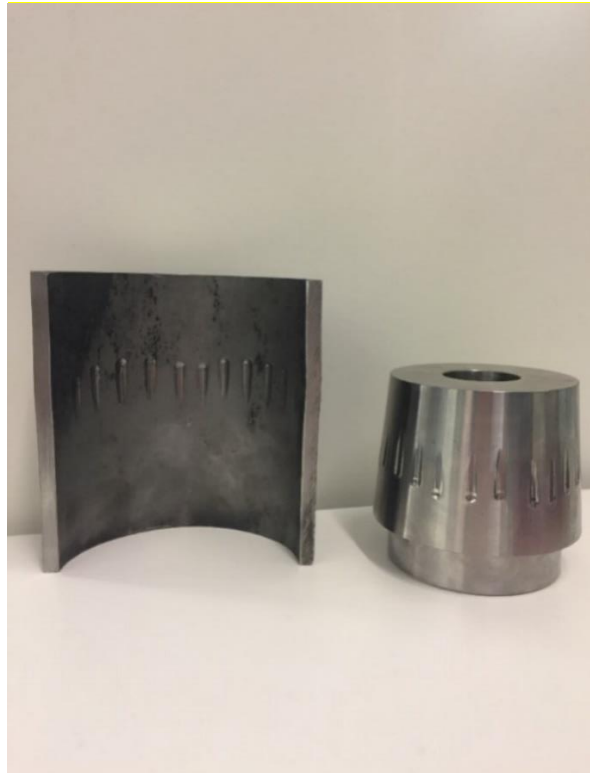


Figure 8:5: Deformation on the 34CrNiMo6 alloyed cone and inside of the pipe wall

## Results from cones alloyed with Calmax

Due to time limitations, the cone-angles that were empirically tested were 3,4 and 10 degrees. The set-pressure and results are presented in Table 8:14. Moreover, the results shown in Table 8:14 present the extreme points, i.e. the lower bound and upper bound. A graph of the mean indentation depths from the spherical indenter are illustrated in Figure 8:6. The following results shows the indentations from spherical steel balls with a diameter of 10 mm as described in Chapter 6.

The visible spherical indentations in the pipeline are presented with the following figures:

- Figure 8:7 illustrates the indentations with set-pressure of 15,30 and 50 bars when, with a 3-degree cone is used.
- Figure 8:8 illustrates the indentations with a set-pressure of 7,5, 10 and 12,5 bars when a 4-degree cone is used. Moreover, Figure 8:9 illustrates the spherical indentations when a 4-degree cone is loaded with 17,5 and 25 bars.
- Figure 8:10 illustrates the indentations with a set-pressure of 25 and 35 bars when, a 10-degree cone is used.

Some of the indentations illustrated in the figures described above shows the “tear”-shaped geometry.

Angle (°)	Set-pressure (bar)	Steel balls distance travelled on cone + indentation diameter (mm)	Dent diameter: cone (mm)	Dent diameter: steel pipeline (mm)	Steel balls distance travelled on pipeline + indentation diameter (mm)	Calculated dent depth into pipeline (mm)	Self-locking	Comments:
3	5	0	0	1,1 0,44	0	0,03042 0,004842	Yes	No visible dents on cone. Some visible dents on pipeline.
3	10	0	0	2 1,7 1,4 1,2	0	0,101021 0,07278 0,049242 0,036131	Yes	No visible dents on cone. Few, but clear dents on the pipeline.
3	15	2,8 2,3	0,7 0,5	2,222 1,8 1,7	3,9 3,2 3,5 4,3	0,124994 0,081667 0,07278	Yes	Few and vague dents on cone. Clear indentation on pipeline from few steel balls.
3	30	6 3,5	1,1 1	2,8 2,369 2,195	4,365 6,15 5,3	0,2 0,14233 0,121938	Yes	Clear indentation on cone. Most of the steel balls made indentation on the pipeline
3	50	14 6	1,8	3,8 2,465	6,3 0,5 6,955	0,375 0,325 0,1543	Yes	Clear indentation on cone. Most of the steel balls made indentation on the pipeline
4	7,5	0	0	0,9 0,8	0	0,020291 0,016026	Yes	No indentation on cone. Barely visible dents on the pipeline (few dents)
4	10	0	0	1,3 1	0	0,04243 0,025063	Yes	No indentation on cone. Barely visible dents on the pipeline (few dents)
4	12,5	2 3,4 1,5	0,6 1 0,3 0,7	2,7 1,6 1,2	0	0,185698 0,064415 0,036131	Yes	Few deformation marks on cone. Clear dents on the pipeline, but few of them.
4	17,5	5,5 3,8 2,3	1,2 1,4 1,145	2,9 2,4 1,7 1,4	0	0,214867 0,146136 0,07278 0,049242	Yes	Few deformation marks on cone. Clear dents on the pipeline, but not from all of them.
4	25	4,1 3,6	1,1 1,4 1,6	2,3 2,22 2,1 2,05	0	0,134047 0,124767 0,111493 0,10619	Yes	Few deformation marks on cone. Clear dents on the pipeline, but not from all of them.
10	15	0	0	0	0		Yes	No indentation on neither the cone or the pipeline.
10	25	0	0	2,6 1,6 1,5 1,4	0	0,171957 0,064415 0,05657 0,049242	Yes	Some deformation marks on the cone. Clear and many indentations on the pipeline.
10	35	3,155	0,52 1,48 0,96 1,145 1,035	2,965 2,38 2,02 1,75	0	0,224836 0,143674 0,103072 0,077158	Yes	Some deformation marks on the cone. Clear and many indentations on the pipeline.

Table 8:14: Empirical testing results with 3,4- and 10-degree cone-angle alloyed with Calmax.



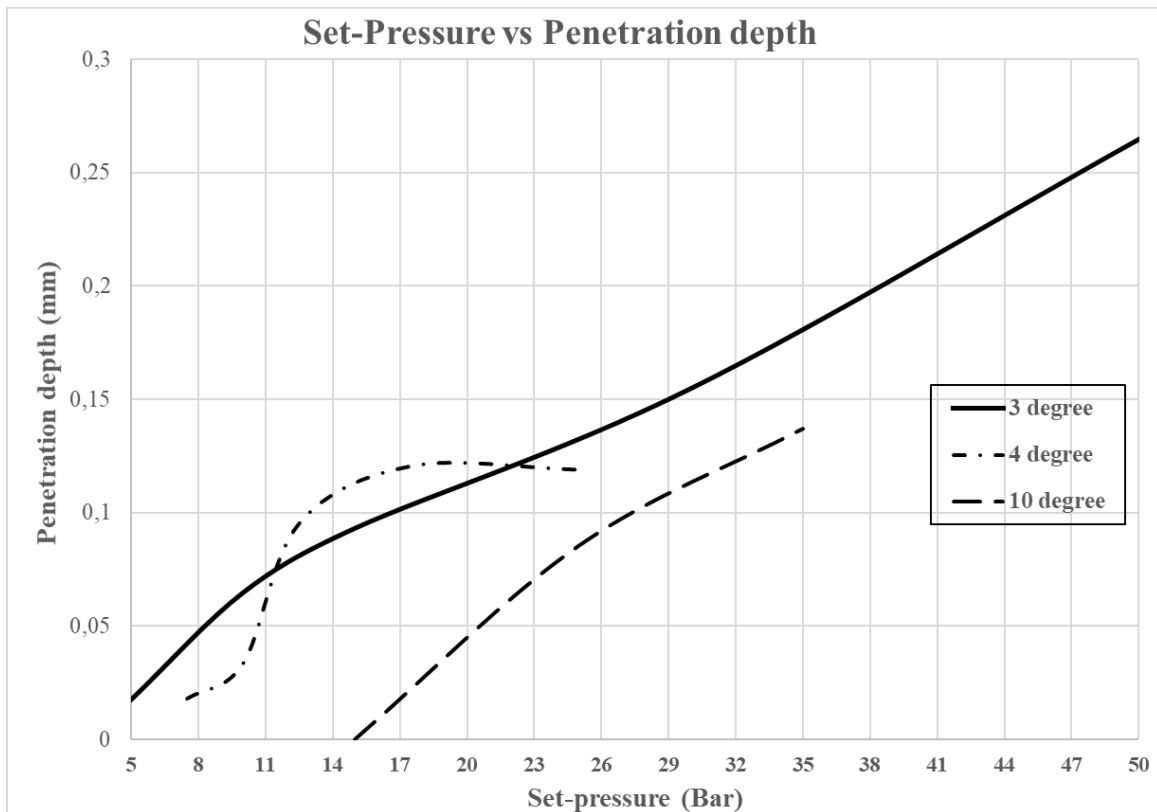


Figure 8:6 : Indentation depth vs Set-Pressure from empirical testing

### Pipeline indentations when used a cone angle of 3 degrees



Figure 8:7: Picture of spherical deformation on the pipeline wall with Set-Pressure of 15,30 and 50 bar when used a cone of 3-degree angle alloyed with Calmax.

## Pipeline indentations when used a cone angle of 4 degrees

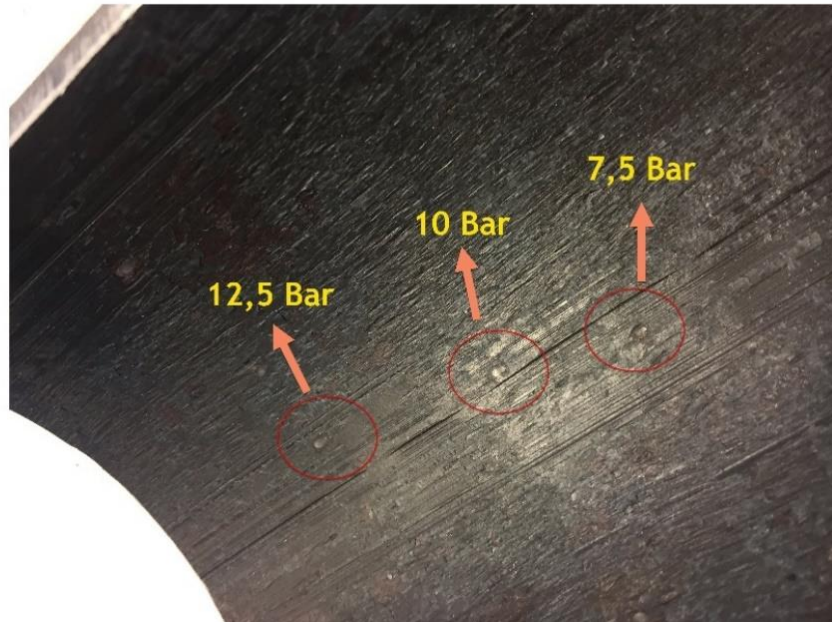


Figure 8:8: Picture of spherical deformation on the pipeline wall with Set-Pressure of 7,5 , 10 and 12,5 bar when used a cone of 4-degree angle alloyed with Calmax.



Figure 8:9: Picture of spherical deformation on the pipeline wall with Set-Pressure of 17,5 and 25 bar when used a cone of 4-degree angle alloyed with Calmax.

## Pipeline indentations when used a cone angle of 10 degrees

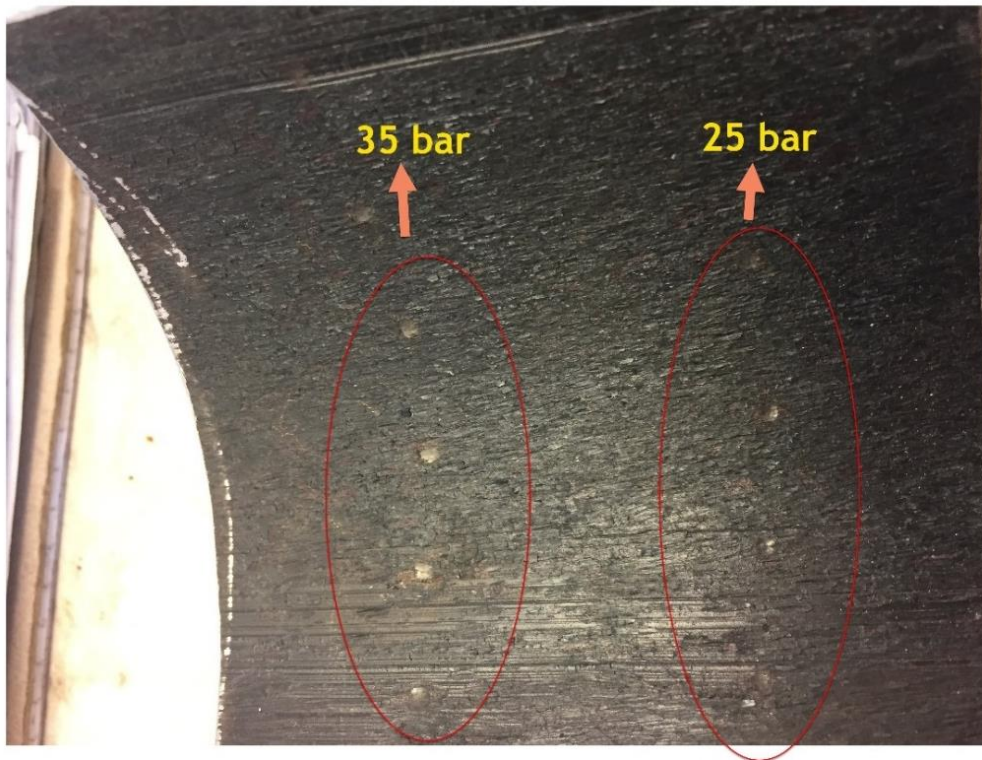


Figure 8:10: Picture of spherical deformation on the pipeline wall with Set-Pressure of 25 and 35 bar when used a cone of 10-degree angle alloyed with Calmax.

### 8.3. ANSYS Results

As mentioned in Chapter 7, the simulations are performed with a cone angle of 3 degrees. Moreover, all the simulations were done with a mesh contact size element of 0,2. This chapter presents results from both the elastic-plastic and linear-elastic models.

#### Elastic-plastic results

The bilinear material curve used in the elastic-plastic model are explained in Chapter 7.

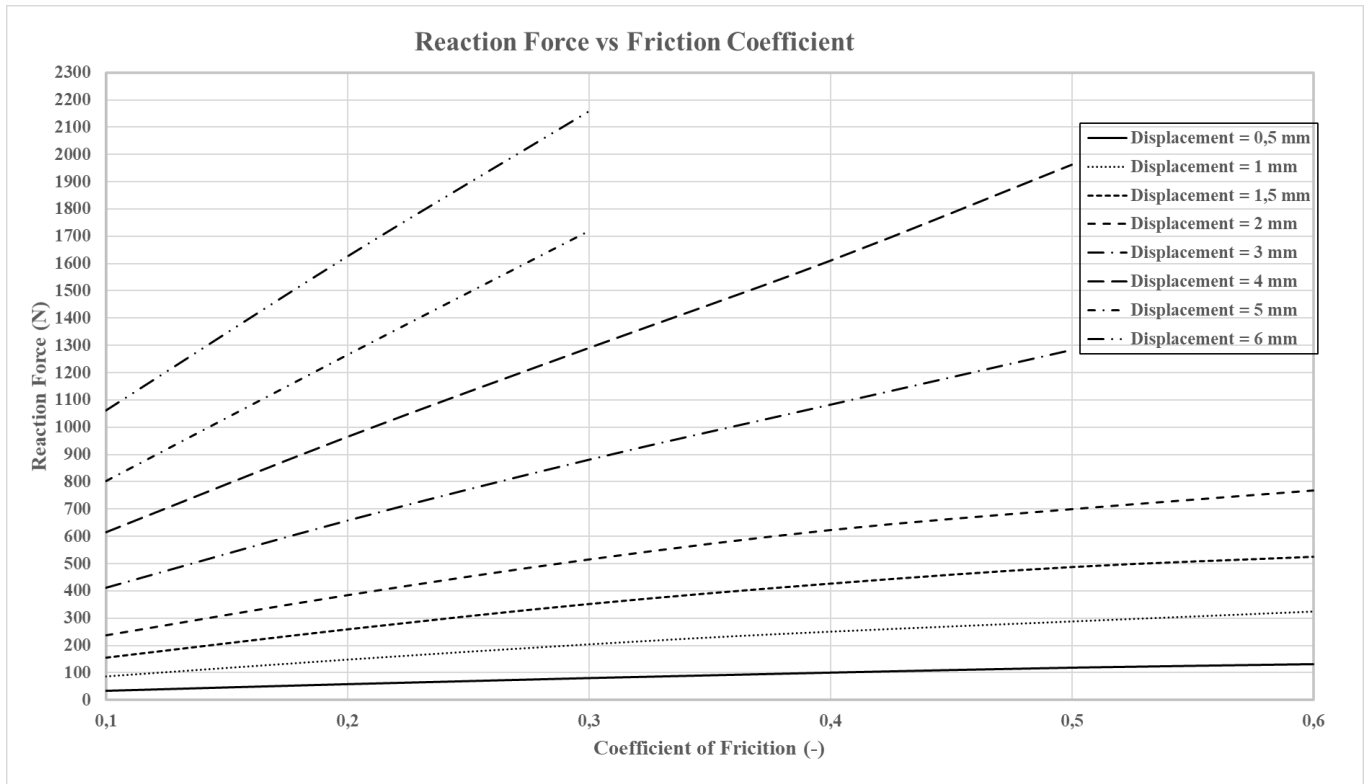


Figure 8:11 Reaction force vs friction coefficient results from ANSYS simulation of an Elastic-Plastic model

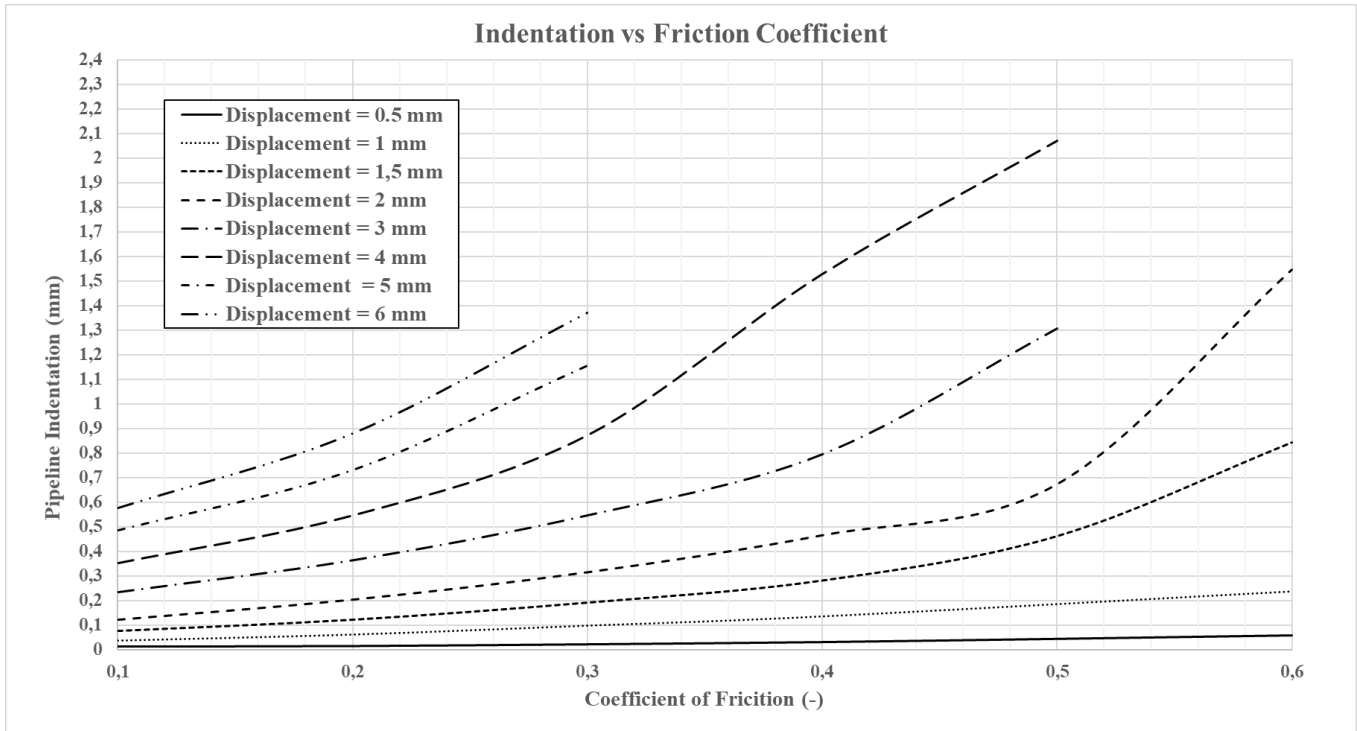


Figure 8:12: Indentation in pipeline vs friction coefficient results from ANSYS simulation of an Elastic-Plastic model

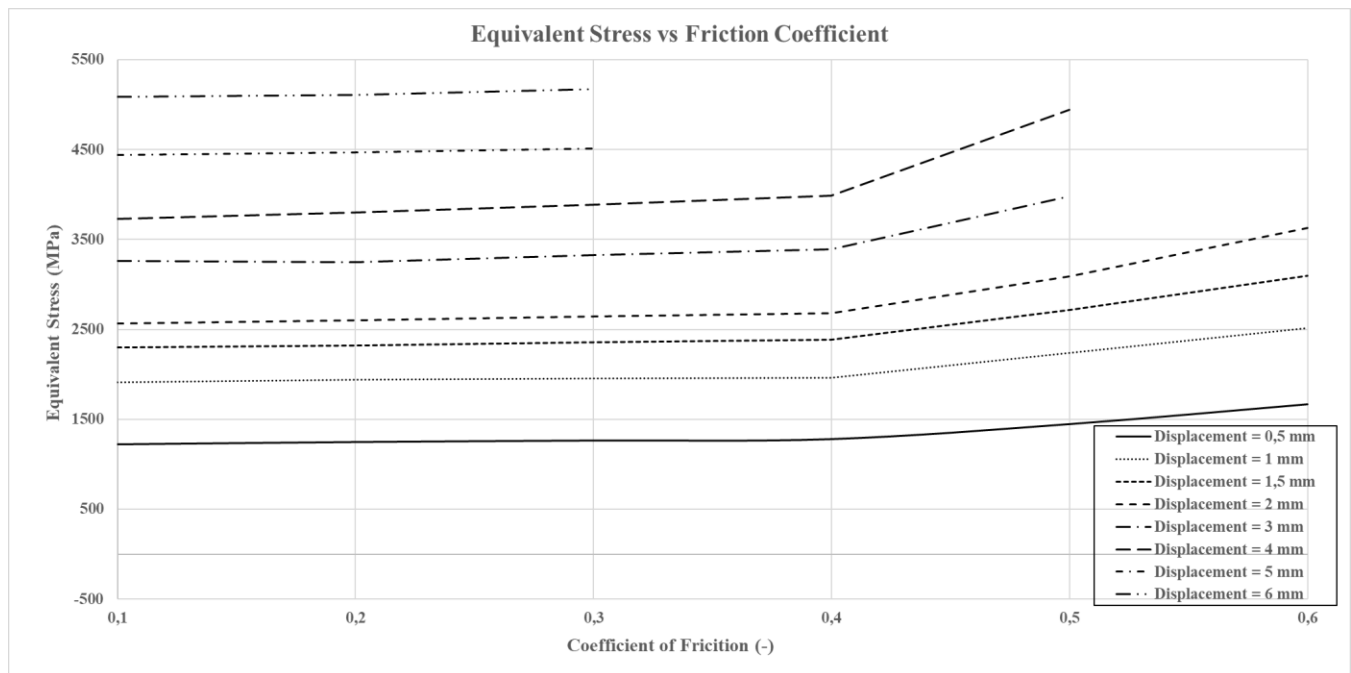


Figure 8:13: Maximum Equivalent stress vs friction coefficient results from ANSYS simulation of an Elastic-Plastic model

The evolution of the deformation pattern from the spherical steel ball with increasing steel ball displacement are presented in Figure 8:14, Figure 8:15, Figure 8:16 and Figure 8:17. The friction coefficient is chosen to be 0,2.

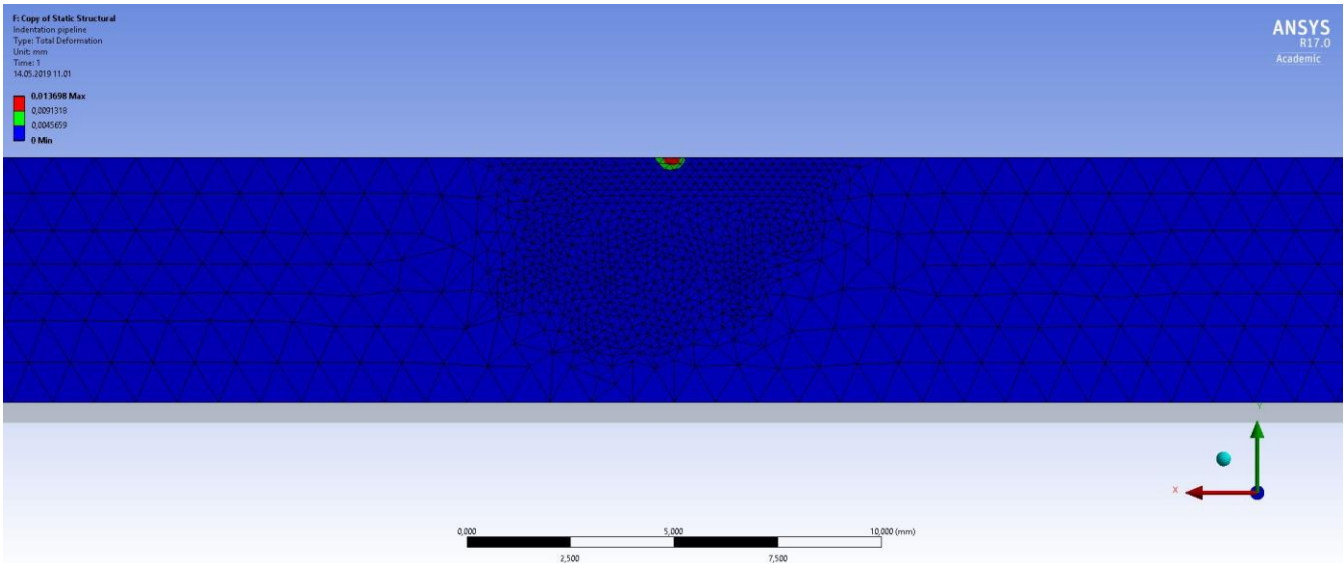


Figure 8:14: Pipeline indentation in ANSYS with a displacement of 0,5 mm and friction coefficient of 0,2.

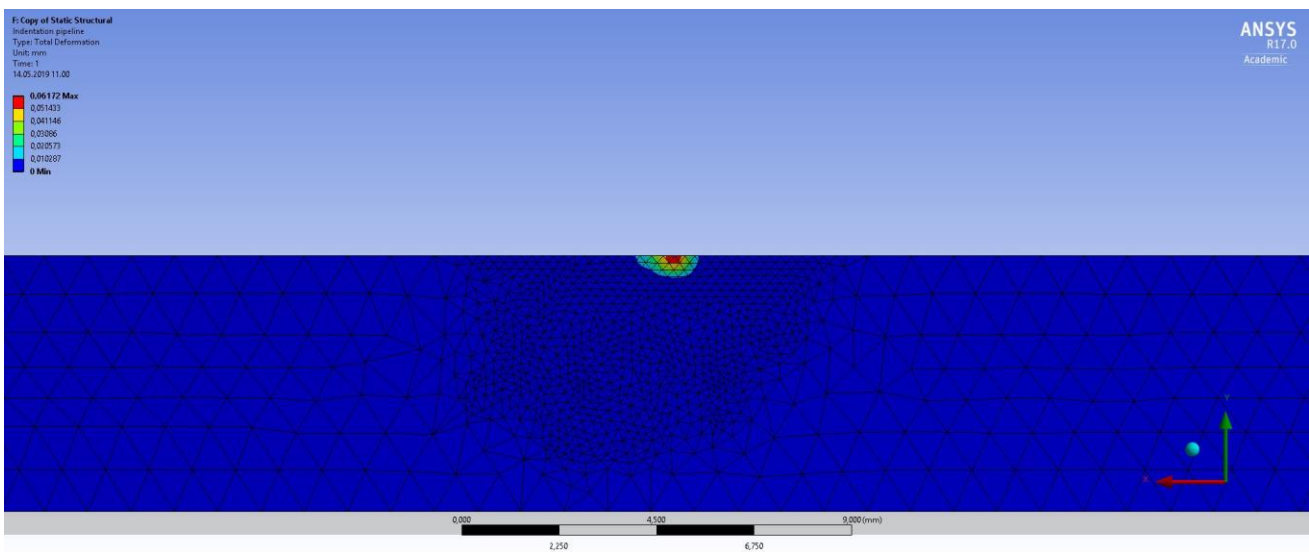


Figure 8:15: Pipeline indentation in ANSYS with a displacement of 1 mm and friction coefficient of 0,2.

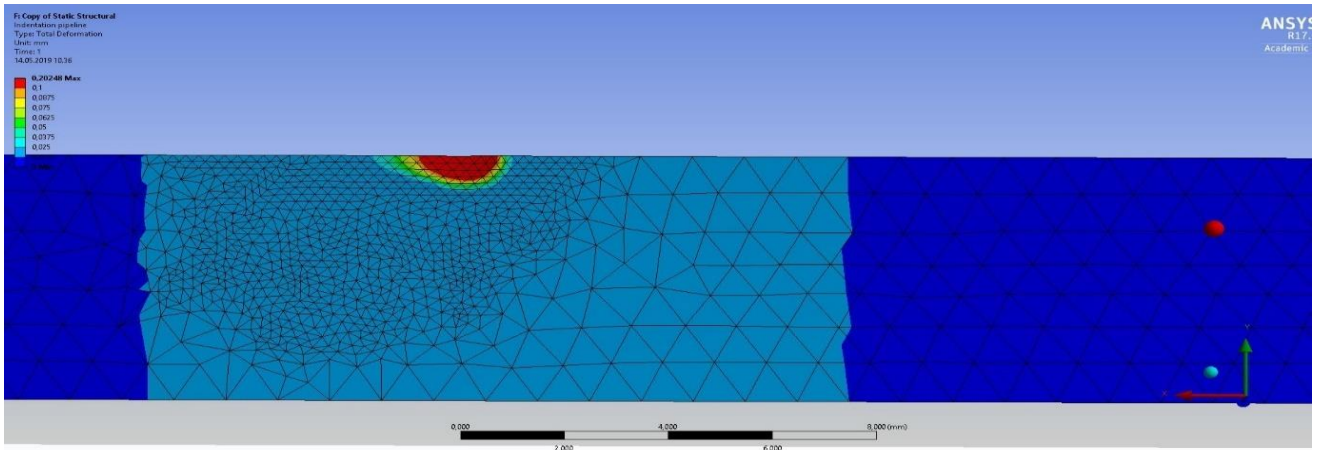


Figure 8:16: Pipeline indentation in ANSYS with a displacement of 2 mm and friction coefficient of 0,2.

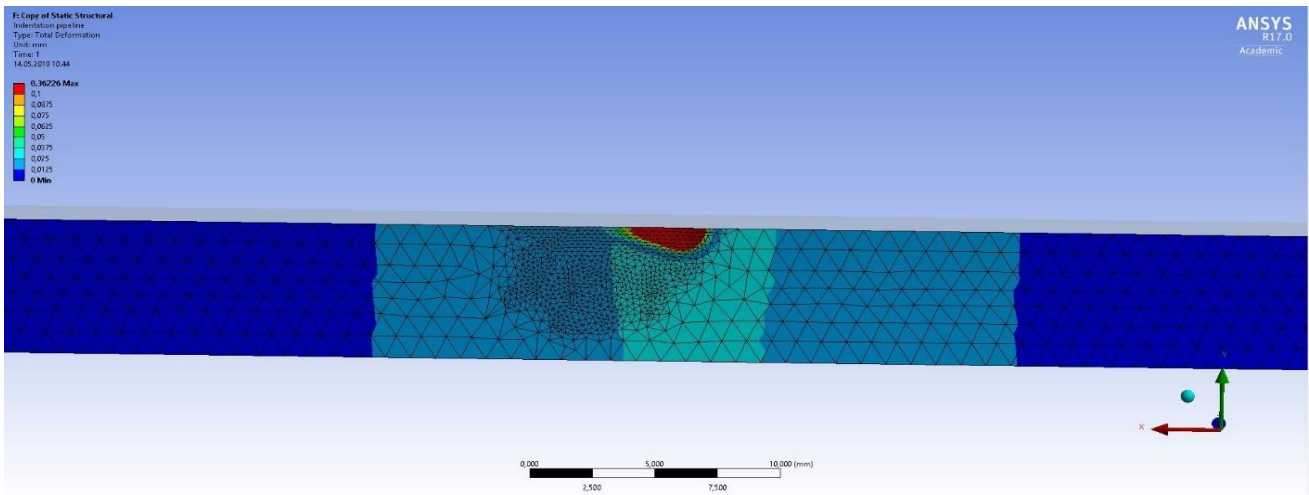


Figure 8:17: Pipeline indentation in ANSYS with a displacement of 3 mm and friction coefficient of 0,2.

## Linear-Elastic results

The following FEA results are carried out in the linear-elastic area of the interacting parts. In Figure 8:20, a numerical error has occurred when a friction coefficient of 0,2 was used.

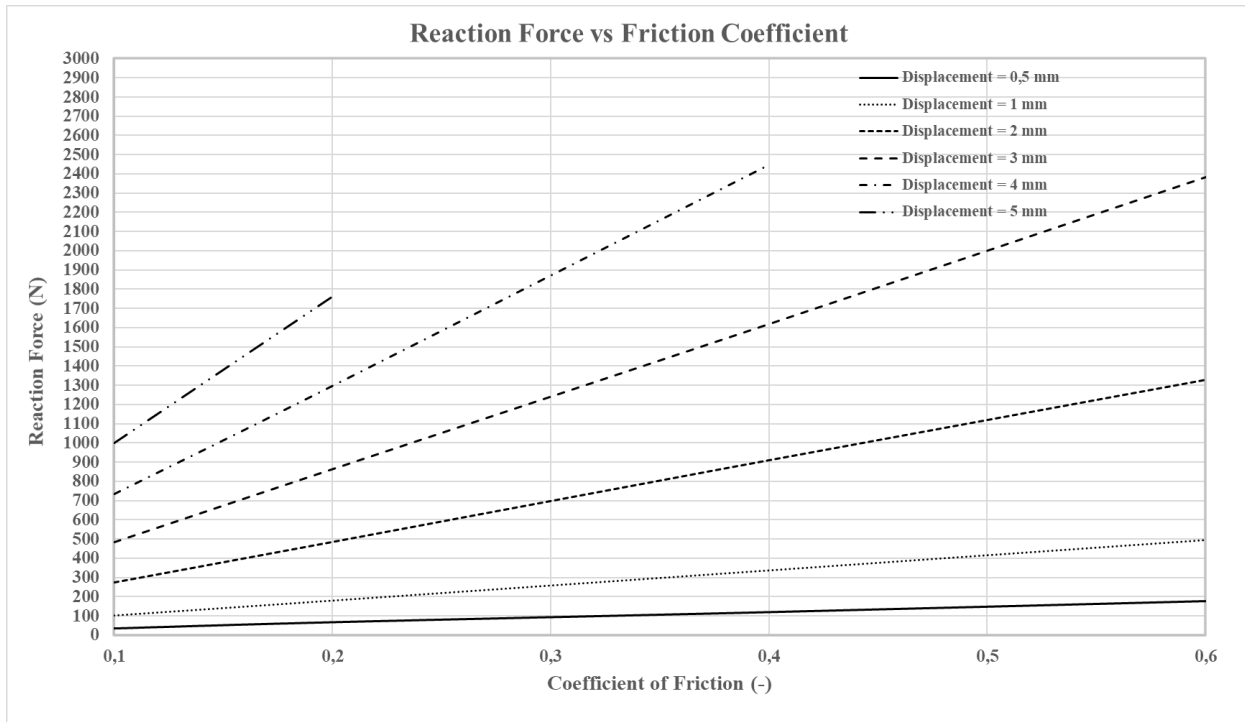


Figure 8:18: Reaction force vs friction coefficient results from ANSYS simulation of a Linear-Elastic model

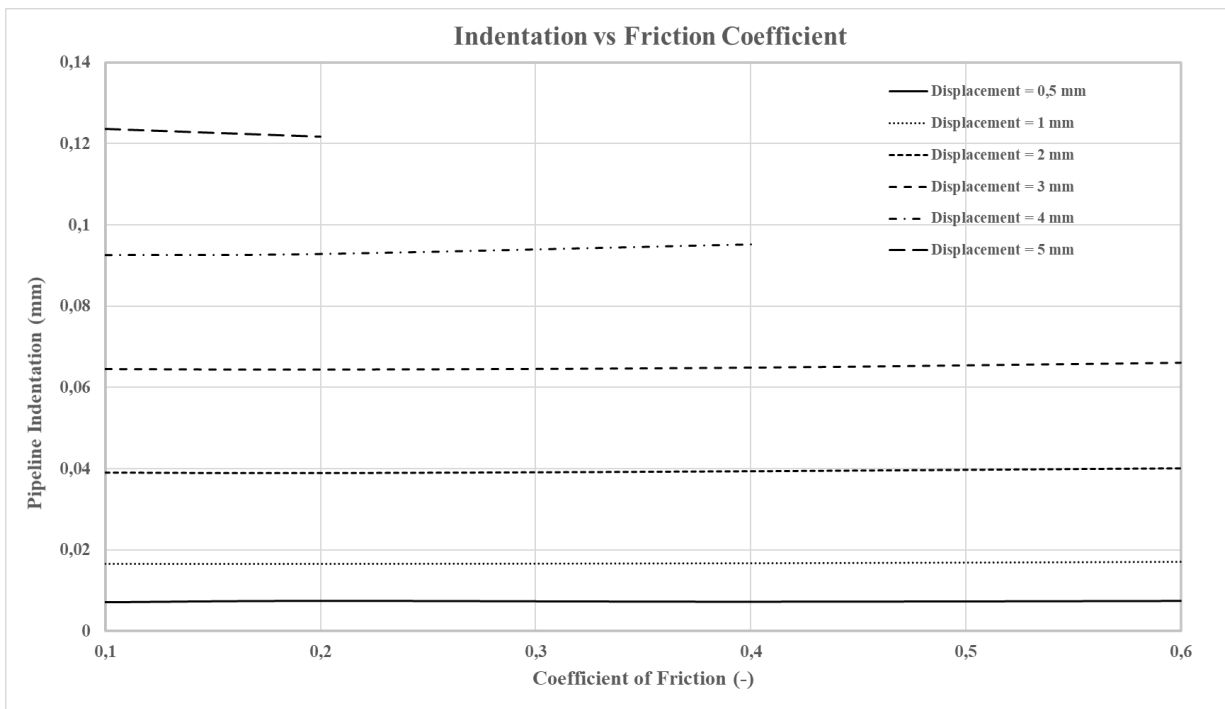


Figure 8:19: Indentation in pipeline vs friction coefficient results from ANSYS simulation of a Linear-Elastic model



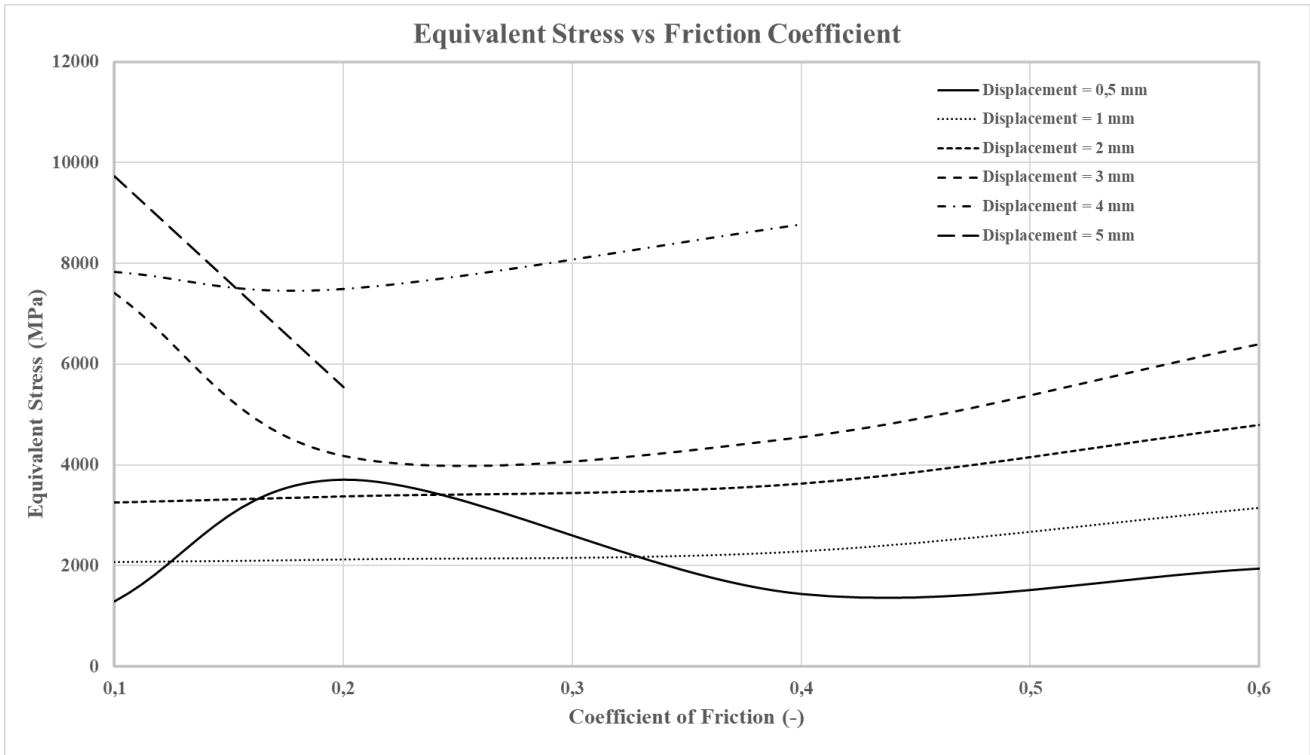


Figure 8:20: Maximum equivalent stress vs friction coefficient results from ANSYS simulation of a Linear-Elastic model

## 9. Discussion

The results from empirical testing, analytical calculations and ANSYS analysis did not match well in some cases, when compared with each other. However, it was possible to make analytical approximation using the testing results. The FEA model, showed correlating results compared to the test results. However, due to the large uncertainties in the friction coefficient, it can be difficult to predict the stress and deformation occurring between the steel ball and cone and pipeline accurately. Moreover, the results in the FEA model showed that the friction coefficient must lie between 0.1 to 0.4. This corresponds with the range of values found in technical tables of the friction coefficient for steel against steel interfaces.

Ideally the bearing steel ball should rotate when pre-set-force from the set-pipe acts on the steel balls along the surface of the cone. This is because of avoiding the friction force occurring when the steel balls are sliding [41]. As illustrated in Figure 7:4, the simulation in ANSYS shows that the steel balls slides along the surface of the cone and the pipeline. This results in that a friction force occurs when performing the empirical tests.

### Empirical results

The displacement of the steel balls caused by the applied force from the set-pipe causes the steel balls to deform both cone and steel pipe as shown in Figure 8:5 and Figure 8:7. As expected, the results from Table 8:14 show that there is a correlation between the angle of the cone, set-pressure and indentation. Figure 8:6 presents the set-pressure vs the average indentation, which shows that for every cone angle, the indentation has an approximately linear trend. However, the results with the cone-angle of 4 degrees does not have the same slope on the results as the other cone-angles, which implies that there are irregularities in these results. Moreover, this indicates that the test-rig is very sensitive to misalignment in components, which causes the steel balls to be misplaced relative to each other. Furthermore, this causes variations in the results. Table 8:14 also shows that there are significant variations in both cone and pipeline indentation diameter. Furthermore, small loads will result in bigger variance in indentation than with high loads, when the steel balls are not aligned with the same height in the test-rig. The misalignment of the steel balls around the cone will cause an uneven distribution of the set-force, which will cause high stresses and high reaction force on fewer steel balls than intended. Figure 8:5 and Figure 8:9 also show that the indentation starts at different heights. A possible explanation to this is human error: Machining errors and misalignment of the test-rig when assembled, will result in uneven distribution of the bearing steel balls.

The sensitivity on the test-rig due to misalignment is also bigger with smaller cone-angles, as with a displacement of 1 mm of the pipeline causes a bigger down-drop of the steel ball in a cone-angle of 3 degrees than for a cone-angle of 10 degrees.

There were also tear shaped marks and some signs of indentation along the cone. However, these marks were very difficult to spot, and the indentation was not measurable. The area of contact on the cone are presented in Table 8:14. However, it is not possible to determine if it was in linear-elastic area or in plastic area. This is because; First, the mark could come from the contact area when the parts are still in linear-elastic area as explained in Chapter 3.3. Second, the onset of deformation has occurred, and the marks are small indentations which are too small to measure with the available tool.

The results presented in Table 8:12 gives the pipeline travel distance with the loads of 5 and 10 tons. However, with a cone-angle of 5 degrees, alloyed with 34CrNiMo6 and 10 tons load are applied on the pipeline, the final indentation diameters are 3.9 mm into the cone and 4.9 mm into the pipeline. The set-pressure upon the steel balls presented in Figure 8:4, was initially to make sure that the steel balls had mechanically wedge-locked itself between the pipeline and the cone, before applying the load on the

pipeline from the press. Since the indentation into the cone was so severe, in term of a functional PRT, it did not satisfy the requirement of small to zero deformation on the cone. However, it shows that there are very high reaction forces between the bearing steel balls and its contact surfaces, and it has great capacity potential as a pipeline recovery tool.

## Analytical calculations

The analytical calculations from equation (8.1) gave good approximations of the indentation depth. The calculated indentation depth on the pipeline from Table 8:4 compares quite well with the empirical results from Table 8:14. The empirical results from a cone-angle of 3 degrees with a set-pressure of 50 bar, was used to calculate the reaction constant obtained from equation (8.1). However, this reaction constant fits quite well when calculating and comparing the indentation depth with the other set-pressures presented in Table 8:14 involving the 3-degree cone-angle. This implies that the mean pressure  $P_m$  does not vary significantly with indentation depth and that the material is isotropic and homogeneous. However, the results from the empirical testing varies a lot, which makes it difficult to determine the indentation depth with the corresponding set-force pressures presented in Table 8:14. It is assumed that the real value lies between the extreme points presented in Table 8:14 and a reasonable value is used to compare with the results in ANSYS and calculations.

There is a lot of empirical and analytical research on a spherical indentation which are presented in Chapter 3. However, this theory is limited to evaluate indentations in one direction. This study involves indentations in multi-axial directions. To minimize the deformation on the cone, it should be 2.5 times the hardness of the steel balls and the steel balls should be 2.5 times the hardness of the pipeline. Moreover, if the mean pressure is below around  $3*Y=5550$  MPa between the steel ball and the cone, where  $Y=1850$  MPa for the annealed cone presented in Chapter 6.3.1, it should not have any visual deformation. However, to avoid any onset of plastic deformation, the mean pressure should be below  $1.1*Y=2035$  MPa in this case. This gives that yield stress and the reaction forces between the cone and steel ball sets the limit for the PRT lifting capacity, if no deformation shall occur on the cone.

As presented in Table 8:5, Table 8:6 and Table 8:7, variations in the material properties, especially various yield stresses results in very different indentations with the same magnitude of reaction force. As the manufacturer sets the yield and tensile strength limits as shown in the material certificate in Appendix I, will have an impact on the indentations along the same pipeline.

From Chapter 3.8.3, it is stated that the mean pressure does not change with the size of the indentation. Furthermore, this means that the indentation area is expected to be the same with an increase or decrease in the steel ball diameter. Moreover, this gives an advantage in designing and predicting PRT capacity, when scaling up or down the bearing steel balls. However, it is also stated that the mean pressure could vary some with the indentation depth, but in Chapter 3.8.4 it is said to be so small that it is neglected.

With the use of hardness conversion table [48], it is found that the pipeline has a B.H.N of 127. Furthermore, Figure 8:2 gives an approximation that is close to the empirical results with a cone-angle of 3 degrees. However, it also shows the bigger the angle is, the more it differs from the empirical results. The reaction force used to calculate the indentation diameter from equation (3.24) are from static vector forces presented in Table 8:1. This is used to obtain the indentation diameter in one load direction, which the Brinell hardness is based on. Even though the reaction force is relatively high in Table 8:1, the indentation diameters shown in Figure 8:2 are in the lower area when compared with the empirical results in Table 8:14.

The theory of contact stresses is limited to the linear-elastic area of the interacting parts. The results presented in Table 8:9 and Table 8:10 gives an indication on the stress levels, shear stresses and deflections if there is no plastic deformation occurring. This gives a good indication on when to expect any indentation on either the cone or the pipeline. Which in this case implies that if the stresses are higher than  $1.1*Y = 426.8$  MPa, you can expect indentation into the pipeline. Furthermore, this gives that the results in Table 8:9 and Table 8:10 will not be correct as long as you get plastic deformation.

The Hertzian contact stress is presented in Table 8:11 and shows an approximation on the contact area with the reaction force obtained from equation (8.1). The Hertzian contact stress is also limited to linear-elastic area. Given that the reaction force is valid between the cone and the steel ball, it should give a good approximation of the contact area. The contact area obtained from Table 8:11 gives an indication that it could be an approximation when compared with the empirical results in Table 8:14. However, the Hertzian theory used is a special case for a spherical ball pressed against a flat surface. This is assumed comparable because the diameter of the cone is much bigger than the diameter of the spherical steel ball, which makes it approximately a flat surface relative to the steel ball.

## Finite element analysis

The results from the linear-elastic and elastic-plastic model shows that friction coefficient has a major impact on reaction force, equivalent stress and indentation depth. This can be seen in Figure 8:11, Figure 8:12 and Figure 8:13 for the elastic-plastic model, and Figure 8:18, Figure 8:19 and Figure 8:20 for the linear-elastic model. Naturally, the indentation does not vary in the linear-elastic model.

With a cylinder pressure of 50 bar, the reaction force in the set-pipe on each steel ball is 561 N presented in Table 8:3. From Figure 8:11 with a reaction force of 561 N, results in only the possibility of 3 mm or 2 mm displacement. Moreover, when consider the indentation depth of  $\pm 0.3$  mm and a displacement of 2 mm or 3 mm gives the friction coefficient of 0.1~0.4 according to Figure 8:12. Finally, from Figure 8:13, the maximum equivalent stress varies from 2650 MPa to 3300 MPa depending on displacement and friction coefficient. Moreover, the maximum equivalent stress occurs between the steel ball and the cone. Figure 8:13 also shows that the equivalent stress approximately constant when the friction coefficient is 0.1~0.4.

Using the cylinder pressure and indentation depth obtained from empirical testing with a cone-angle of 3 degrees, Figure 8:11, Figure 8:12 and Figure 8:13 gives:

Cylinder pressure (bar)	Indentation depth (mm)	Friction coefficient (-)	Displacement (mm)	Maximum equivalent stress on the cone (MPa)
30	0,18	0.15~0.3	1.5~2	2300~2600
15	0,085	0,1~0,4	1~1,5	2000~2300
10	0,06	0,15~0,4	0,5~1	1300~2000

Table 9:1: Friction coefficient, Displacement and stresses obtained from ANSYS results.

The results from ANSYS show the sensitivity of friction, and the fact that it has a huge impact on the result. Figure 8:11 shows that with big displacements it is desired to have a low friction coefficient, if the goal is keep the indentation at the lowest possible. Low friction can be reached if the steel balls are lubricated.

Another parameter that affects the result, is the yield stress of the interacting parts. Figure 7:8, Figure 7:9 and Figure 7:10 shows that the yield stress has a huge impact on the reaction force, indentation depth and equivalent stress. This is because for a given stress, the magnitude of yield stress will determine whether it acts in linear-elastic or in the plastic area. Moreover, tangent modulus also has a big impact on the results, shown in Figure 7:11, Figure 7:12 and Figure 7:13. This is because the tangent modulus sets the slope for the material in the stress-strain diagram. Which implies that with high tangent modulus and with an increase in stress will result in a smaller impact on the strain, than if the tangent modulus was lower. The tangent modulus slope is illustrated in Figure 3:26.

From Figure 8:17, it is evident that the “tear”-shape indentation enhances with the displacement of the bearing steel ball. This compare quite well with Figure 8:5 and Figure 8:7. This indicates that the model in ANSYS gives out valid results.

## Source of error: Material uncertainties

There are a lot of uncertainties when evaluating the analytical calculation, the test-rigs and the model in ANSYS.

Young's modulus do not vary much between different material specimen. Yield and tensile stress have variations as illustrated in Appendix I and this uncertainty influences the results greatly. As previously explained, especially the yield stress has a significant effect on the results. Moreover, Figure 9:1 illustrates how various yield stresses is crucial in terms of the result in strain. The tangent modulus is obtained from DNVGL-RP-C208 and used in the FEA simulations. This is a close estimate, but it is an uncertainty that should be considered when evaluating the final result. Human errors that occur when measuring the indentation is also an uncertainty factor.

Furthermore, it is not statistically significant to conclude with any of the measured results because of the lack of tests. Taken confidence intervals into account, when standard deviation is unknown. It is suggested to do at least 30 samples. To go through with 30 samples would be very time consuming and to make the tests the same would not be possible. Therefore, the number of tests will be reduced. One assumption will be that the standard deviation will be so low, that it is not necessary to do so many tests.

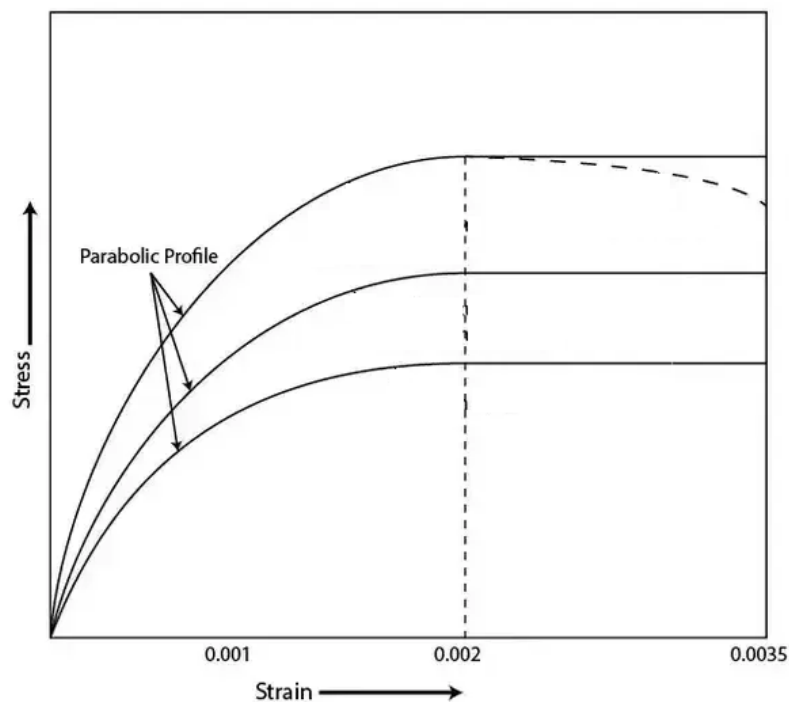


Figure 9:1: Strain-Stress variation of the same material

# 10. Conclusion and Recommendations for Future Work

## 10.1. Conclusion

In this thesis, the comparison between analytical, empirical and FEA results was carried out to make a good prediction about the properties and behaviour of the wedge-lock mechanism in a new PRT concept. The following conclusions are made:

1. The reaction force constant calculated using equation (8.1) is a good approximation as the calculations presented in Table 8:4 compares well with the empirical results presented in Table 8:14. However, this is only valid for this exact case with an unknown friction factor and a cone-angle of 3 degrees.
2. Uncertainties in the coefficient of friction and yield stress lead to significant variations in the results.
3. The model in ANSYS could give a good representation of the test-rig if the friction coefficient is known.
4. The results from the capacity test presented in Chapter 8.2 shows that the PRT can withstand 10 tons with a travel distance of 35 mm on the pipeline. This is considered to be a large capacity relative to the size. It is noted that this test was not performed to the failure point. This means the actual capacity of the RPT is higher large.
5. The size and simplicity of the designed PRT in Chapter 4 shows that maintenance and operation work could be efficient in both economical and practical sense.
6. If there is to be no deformation in the cone, the lifting capacity of the tool will be determined mainly by the yield stress of the cone, cone-angle and friction coefficient. Furthermore, a low friction coefficient ensures a minimum indentation depth. Low friction coefficients can be achieved by lubricating the steel balls.
7. The results show that an increase in the cone-angle will lead to a decrease in the indentation depth when the same magnitude of force is applied on the steel balls.
8. If self-locking and onset of plastic deformation are present between the steel balls and pipeline, the angle should be as large as possible to minimize the stresses occurring between the steel balls and the cone.

## 10.2. Recommendations for Future Work

The following recommendations for future work are made:

- 1. Obtain knowledge about the exact friction coefficient and yield stress.**  
It is essential to have knowledge of the actual coefficient of friction and yield stress in order to obtain accurate results from the ANSYS simulations and empirical tests. The onset of plastic deformation can also be better predicted when knowing the actual yield stress is known.
- 2. Design a more accurate test-rig or improve the existing test-rig.**  
The test-rig used in this study was sensitive to the alignment between every part to get out valid results. Tolerance stackup studies can be performed to improve the test rig design.
- 3. Perform more tests with different cone-angles.**  
Due to limited time, not all of the cone-angles were studied empirically and numerically. It is interesting to investigate how the cone-angle affects the sensitivity study with tangent modulus, yield stress, reaction force, equivalent stress and indentation in ANSYS.
- 4. Perform load capacity tests with the Calmax alloyed cone.**  
It is interesting to perform a full capacity test with the annealed cones. This is to evaluate how the cone-angles affects the lifting capacity for a PRT.
- 5. Investigate how sizing and a decrease of hardness of the steel ball affects the results.**  
Perform FEA and empirical tests with different steel ball diameter. Moreover, perform tests to study the optimum hardness relationship between the cone, pipeline and steel balls, to minimize the indentation into the cone.
- 6. Perform FEA and empirical tests with steel balls casted into polyurethane.**  
Finally, execute both FEA and empirical tests with steel balls casted into polyurethane to evaluate the sealing, locking and lifting capacity if implemented into a PRT.
- 7. Make a track for the steel balls**  
A track for the steel balls to slide in can be machined into the cone. This allows the balls to make a line contact instead of a point contact. This will result in a smaller indentation depth.

# References

- [1] Manoucherhri, S. (2017). "Subsea Pipelines And Flowlines Decommissioning - What We Should Know for a Rational Approach." ResearchGate.
- [2] Venas.A (2016), *DNV GL, Offshore Pipelines Outlook, Oil and gas*.
- [3] Improved Pipe recovery tool for 8 inch pipeline. Harald Egeli (2001), Hovedoppgave. Universitetet i Stavanger.
- [4] Subsea, F. (2018). "Pipeline Recovery Tool." : <http://www.firstsubsea.com/products/prt.html>
- [5] Internationals, P. (2018). "Offshore Pipeline Recovery Tool for Ichthys LNG Projects." : <https://www.pipelinesinternational.com/2014/06/18/offshore-pipeline-recovery-tool-for-ichthys-lng-project/>
- [6] 16 inch pipeline recovery tool Operating manual. 03.09.01. Industrikonsult
- [7] Industrikonsult, Calculation of 12 inch recovery tool
- [8] Industrikonsult, Design premise pipeline recovery tools
- [9] 16 inch PRT structural calculations, Industrikonsult
- [10] Pipeline recovery tool, IK-Norway, Subsea 7 copsas ekofisk vb, calculation report.
- [11] IPLT structural calculations and design criteria, Nippon Steel. Industrikonsult
- [12] Operating & maintenance manual, IPRT, Industrikonsult
- [13] William D. Callister, J. (2015). *Materials Science and Engineering*.s231. 2015
- [14] Materials, A. (2018). "Structural Steel - S235, S275, S355 Chemical Composition, Mechanical Properties and Common Applications."
- [15] Russell, J, the Statistics Tutor's Quick Guide to commonly Used Statistical Tests, University of Sheffield : <http://www.statstutor.ac.uk/resources/uploaded/tutorsquickguidetostatistics.pdf>
- [16] Arthur P.Boresi, R. J. S., Omar M. Sidebottom (1992). "Advanced Mechanics Of Materials." 801.
- [17] John A.Williams , R. S. D.-J. (2001). "Contact Between Solid Surfaces."
- [18] Lgia, C. B. (2014). "Contact stresses between two cylindrical bodies: cylinder and cylindrical cavity with parallel axes-Part1: Theory and FEA 3D modeling." ScienceDirect.
- [19] MathWorld, W. (2018). "Spherical Cap."
- [20] Qiu, M. (2017). "Bearing Tribology." National Defence Industry Press, Beijing and Springer.
- [21] roymech (2018). "Tribology - static and dynamic friction."
- [22] Toolbox, T. E. (2018). "Youngs Modulus of Elasticity for Metals and Alloys."
- [23] Tylor, B. (2016). "Tutorial - Hertz Contact Stress."
- [24] Wikipedia (2018). "Spherical Cap." [https://en.wikipedia.org/wiki/Spherical\\_cap](https://en.wikipedia.org/wiki/Spherical_cap) , (10.06.2019).
- [25] Zhang, J. (2011). Multi-functional nanocomposites for the mechanical actuation and magnetoelectric conversion.



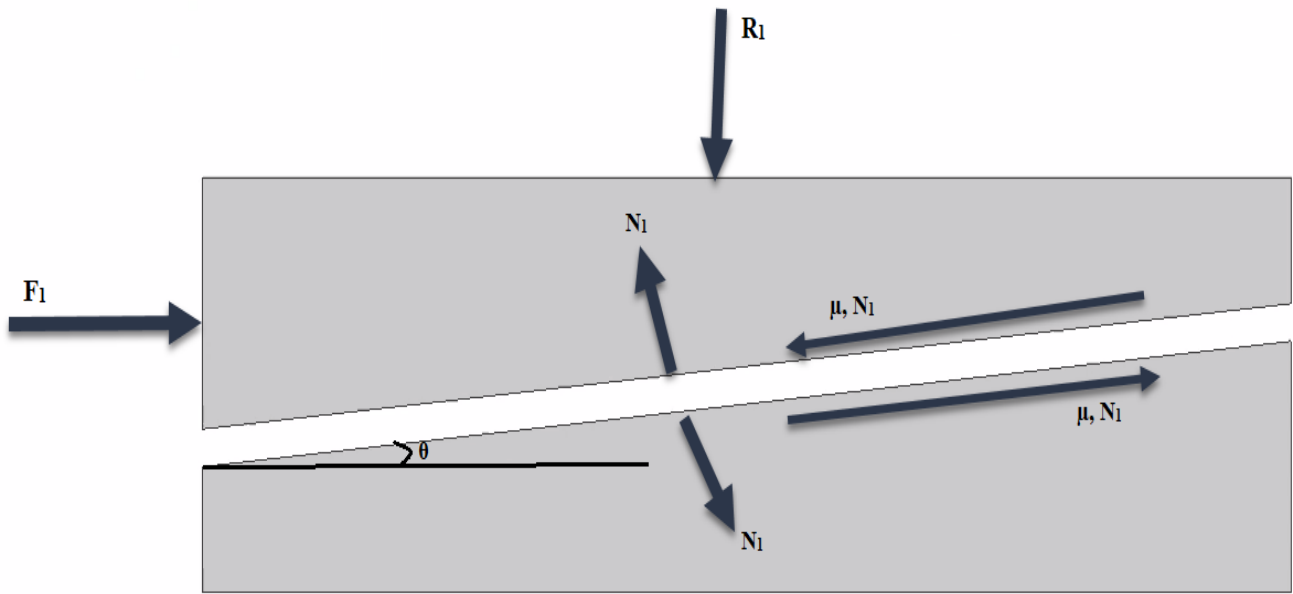
- [26] Grande E. Design of a 12" External Pipeline Recovery Tool, Master's Thesis.
- [27] Graham.S. (2009). Recent Pipeline repair tooling developments
- [28] bbShalmstad (2018). "Hardness Conversion Table - Tensile Strength, Vickers, Brinell and Rockwell." (DIN 50150)
- [29] Tabor, D. (1951). "The Hardness of Metals". Oxford at the clarendon press
- [30] Clemitson, I.R.(2015) "Castable Elastomers: Polyurethane". CRC Press.
- [31] Dishovasky, N. and Mihaylov, M. (2018) "Elastomer-Based Composite Materials: Mechanical, Dynamic, and Microwave properties and Engineering Applications" CRC Press, CPD certified, Apple Academic Press.
- [32] Hofsrud. H. K (2017) "Load Deflection Characteristics of Guide Vane End Seal". Master thesis from NTNU.
- [33] Ilseng, A. (2016) "Mechanical Behaviour of particle-filled elastomers at various temperatures". Doctoral thesis NTNU
- [34] Dariusz, M. B, Ryszard, K. Gennady, E.Z. (2015) "High Performance Elastomer Material: An engineering Approach". Apple academic press, CRC Press.
- [35] R. D. Cook, D. S. Malkus, M. E. Plesha, and R. J. Witt, (2002) "*Concepts and applications of finite element analysis*", 4th ed. ed. New York: Wiley,
- [36] ANSYS, "User's guide ", 17.0 Academic ed: ANSYS
- [37] R. C. Hibbeler, (2010) "*Mechanics of materials*", 8th ed. ed. Upper Saddle River, N.J: Pearson Prentice Hall
- [38] Element Types (04.06.2019)  
[http://osupdocs.forestry.oregonstate.edu/index.php/Element\\_Types](http://osupdocs.forestry.oregonstate.edu/index.php/Element_Types)
- [39] DNVGL-RP-C208. (2013) "Determination of Structural Capacity by Non-linear FE analysis Methods"
- [40] What-when-how. "FEM for 3D solids: Part 1" (04.06.2019)  
<http://what-when-how.com/the-finite-element-method/fem-for-3d-solids-finite-element-method-part-1/>
- [41] Sutyagin, O.V. (2013). "Friction of Spherical Indenter over Elastoplastic Coating" Tver State Technical University, nab. Afanasiya Nikitina 22, Tver, 170026 Russia
- [42] Simrit. (2005). "Simrit Catalogue". Edition 2005. Freudenberg Simrit KG.
- [43] Schaeffler steel balls. DIN 17 230, DIN 5 401/ISO 3 290. (04.06.2019)  
<https://medias.schaeffler.com/medias/en!hp.info/KUG>
- [44] Uddeholm, "Calmax", Assab. (04.06.2019)  
<http://www.assab-singapore.com/media/CALMAX-D20140711.pdf>
- [45] Bhadeshia, H.K.D.H, Honycombe, R.W.K. (2006). "Steels: Microstructure and Properties". Third Edition.
- [46] Theisen, W. Berns, H. (2008). "Ferrous Metals: Steel and Cast Iron"
- [47] D. L. Logan, K. K. Chaudhry, and P. Singh, *A first course in the finite element method*, 4th ed., SI ed. ed. Stamford, Conn: Cengage Learning, 2011
- [48] Steelexpress. "Steel Hardness Conversion Table". (04.06.2019)  
<https://www.steelexpress.co.uk/steel-hardness-conversion.html>

- [49] Jamari, J. Schipper, D.J. (2006) “Experimental Investigation of Fully Plastic Contact of a Sphere Against a Hard Flat” University of Twente, Surface Technology and Tribology. Tribology Division of ASME.
- [50] Brake, M.R. (2012) “An analytical elastic-perfectly plastic contact model”. International Journal of Solids and Structures.
- [51] “Offshore pipeline recovery tool for Ichthys LNG Project” (10.06.2019)  
<https://www.pipelinesinternational.com/2014/06/18/offshore-pipeline-recovery-tool-for-ichthys-lng-project/>
- [52] “First Subsea: Pipeline Recovery Tool”, Brochure (13.06.2019)  
<http://www.firstsubsea.com/doc/25.pdf>

# Appendices

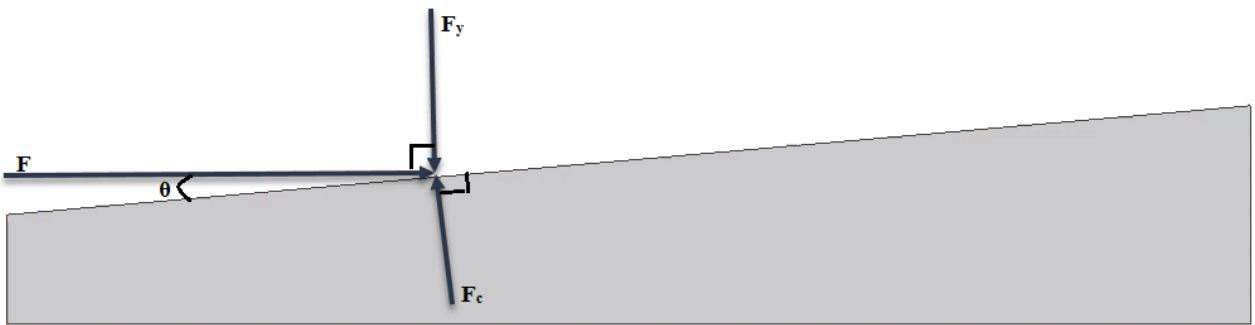
APPENDIX A	Reaction forces due to static force vectors and friction + Area of the cylinder
APPENDIX B	Technical drawings of test-rig with a cone alloyed with 34CrNiMo6
APPENDIX C	Technical drawings of the test-rig, with pressure test possibilities and cone alloyed with Calmax
APPENDIX D	Test rig procedure for spherical indentation and mechanical wedge lock force
APPENDIX E	Test rig procedure for testing the sealing properties of bearing steel balls casted in polyurethane.
APPENDIX F	Cylinder Set-Pressure graphs
APPENDIX G	Pictures of the first test-rig with a cone alloyed with 34CrNiMo6
APPENDIX H	Pictures of test rig with a cone alloyed with Calmax Uddeholm
APPENDIX I	Material Certificates

## **APPENDIX A – Reaction forces and cylinder area**



$$\begin{aligned}
 & \textcircled{1} \quad F_1 - \mu N_1 \cos(\theta) - N_1 \sin(\theta) = 0 \\
 & \textcircled{2} \quad R_1 + \mu N_1 \sin(\theta) - N_1 \cos(\theta) = 0
 \end{aligned}
 \quad \longrightarrow \quad
 R_1 = F_1 \cdot \frac{(\cos(\theta) - \mu \sin(\theta))}{(\mu \cos(\theta) + \sin(\theta))}$$

Figure A-1: Reaction force due to friction



$$\begin{aligned}
 -F_c &= 1/\tan(\theta) \\
 -F_y &= 1/\sin(\theta)
 \end{aligned}$$

Figure A-2: Reaction force due to static force vectors

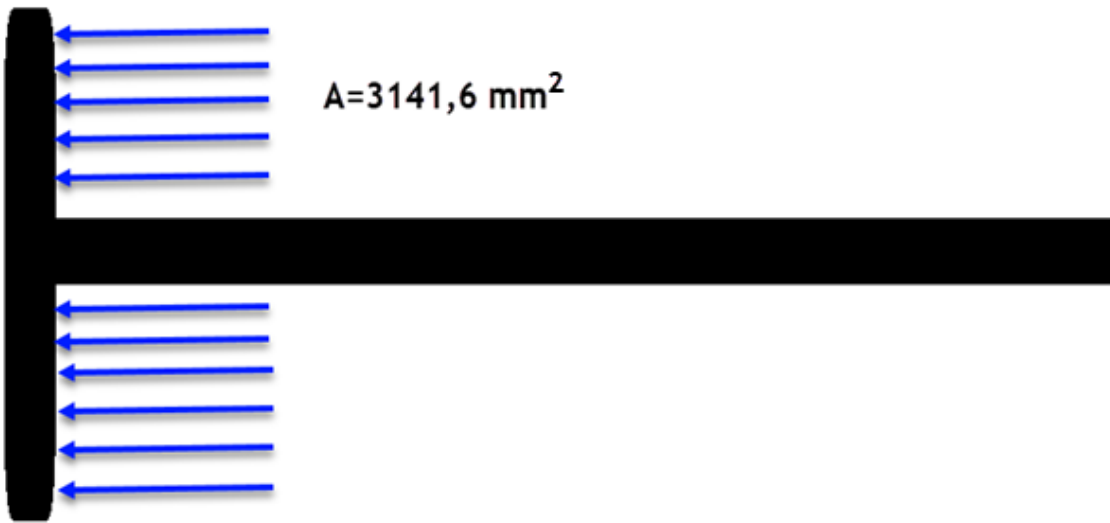
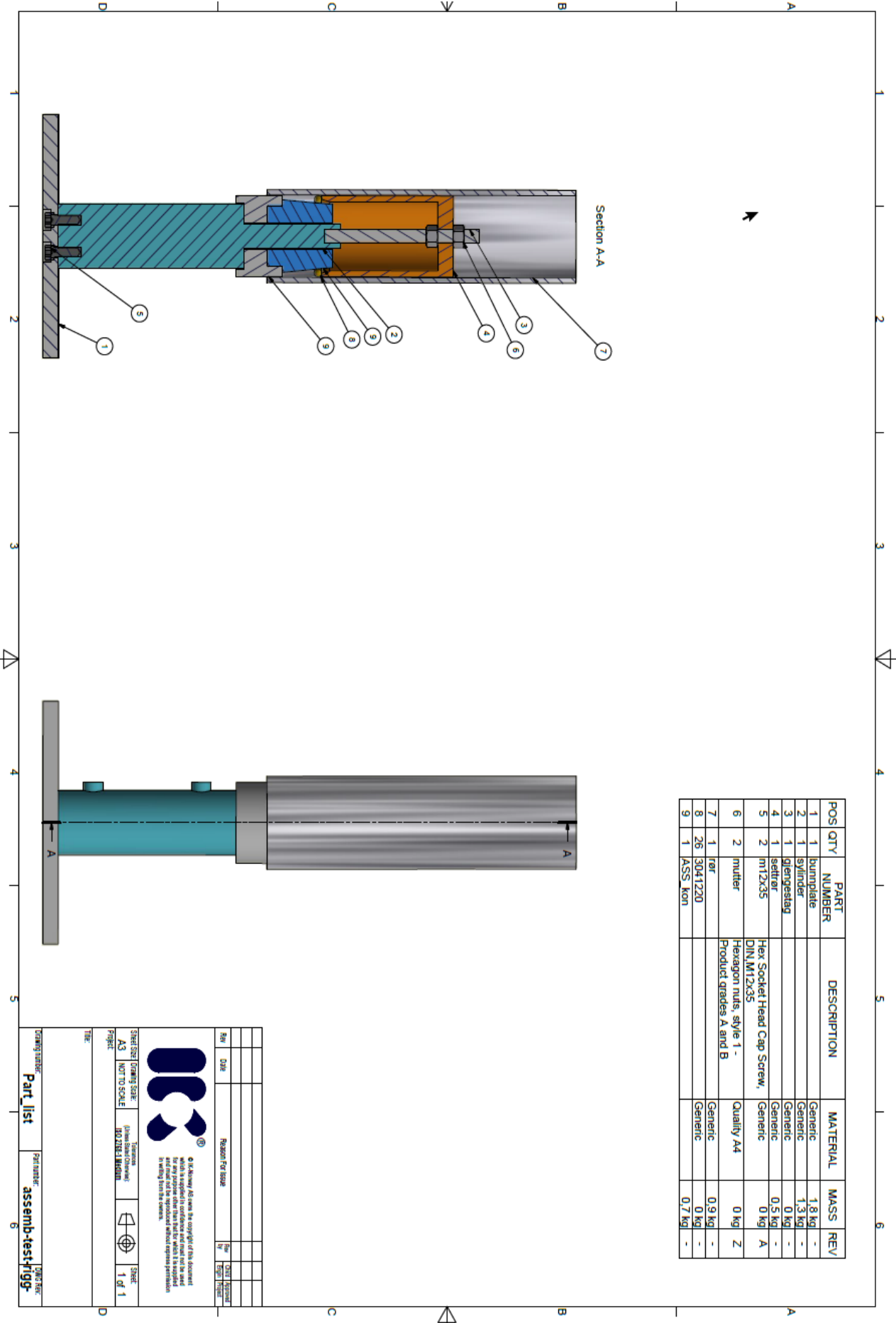


Figure A-3: Cylinder area

# **APPENDIX B - Technical drawings of test-rig with a cone alloyed with 34CrNiMo6**



POS	QTY	PART NUMBER	DESCRIPTION	MATERIAL	MASS	REV
1	1	burndplate		Generic	1.8 kg	-
2	1	syfnder		Generic	1.3 kg	-
3	1	qlergerstng		Generic	0 kg	-
4	1	setvrer		Generic	0.5 kg	-
5	2	m12x35	Hex Socket Head Cap Screw, DIN M12x35	Generic	0 kg	A
6	2	nutler	Hexagon nuts, style 1 - Product grades A and B	Quality A4	0 kg	Z
7	1	ror		Generic	0.9 kg	-
8	26	3041220		Generic	0 kg	-
9	1	ASS Kon		Generic	0.7 kg	-

**Reason For Issue**

Rev	Date	By	Checked

**Sheet Size / Drawing Scale:** A3 / NOT TO SCALE

**Project:** NO. 2181.1 INSDRM

**Sheet:** 1 of 1

**Drawing Number:** Part\_list

**Part number:** assemb-test-figg-

**Drawn By:** [Signature]

**Checked By:** [Signature]

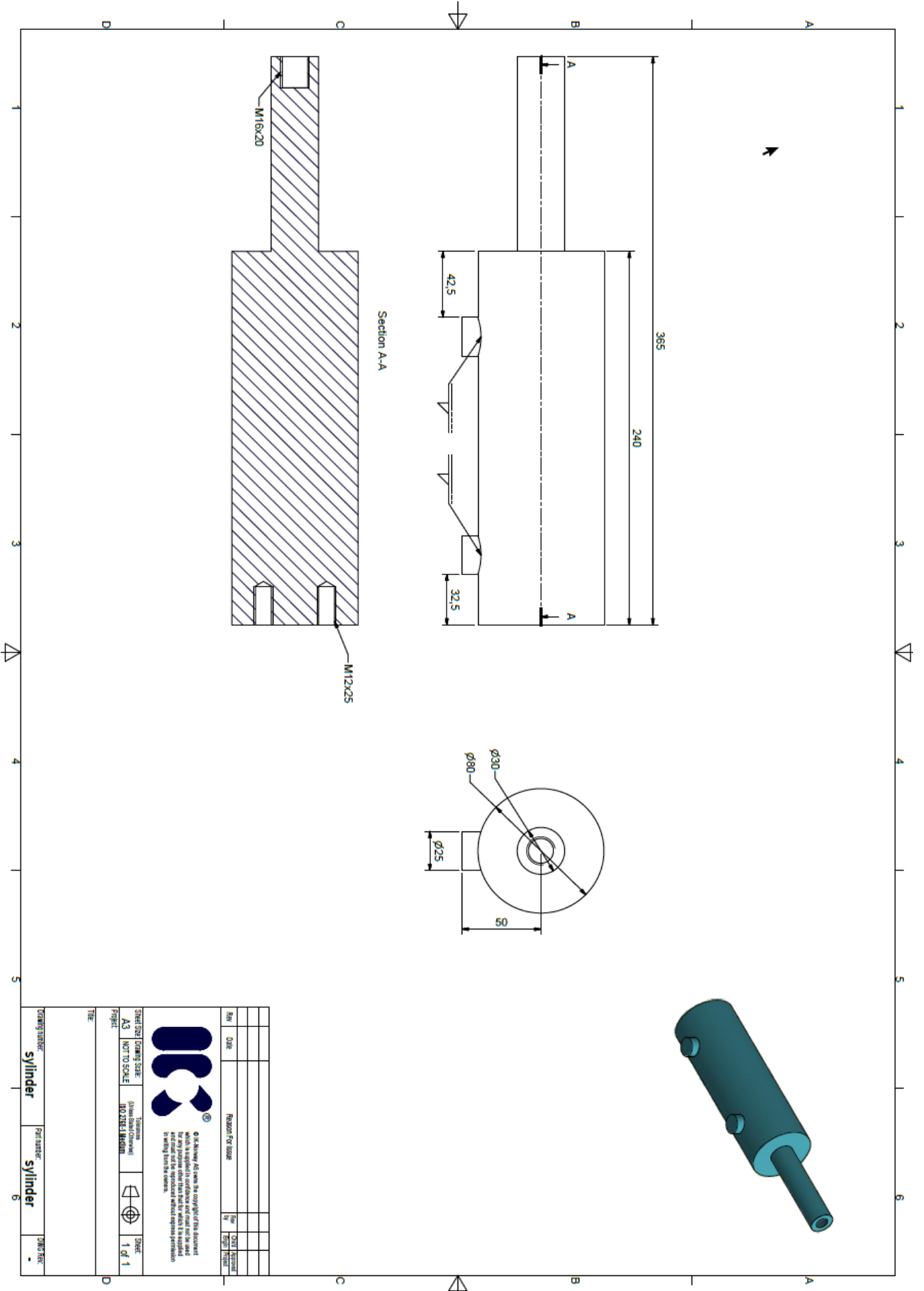
**Scale:** 1:1

**Material:** [Material]

**Notes:**

© All Rights Reserved. No part of this document may be reproduced, stored in a retrieval system, or transmitted, in any form or by any means, without the prior written permission of the copyright owner.





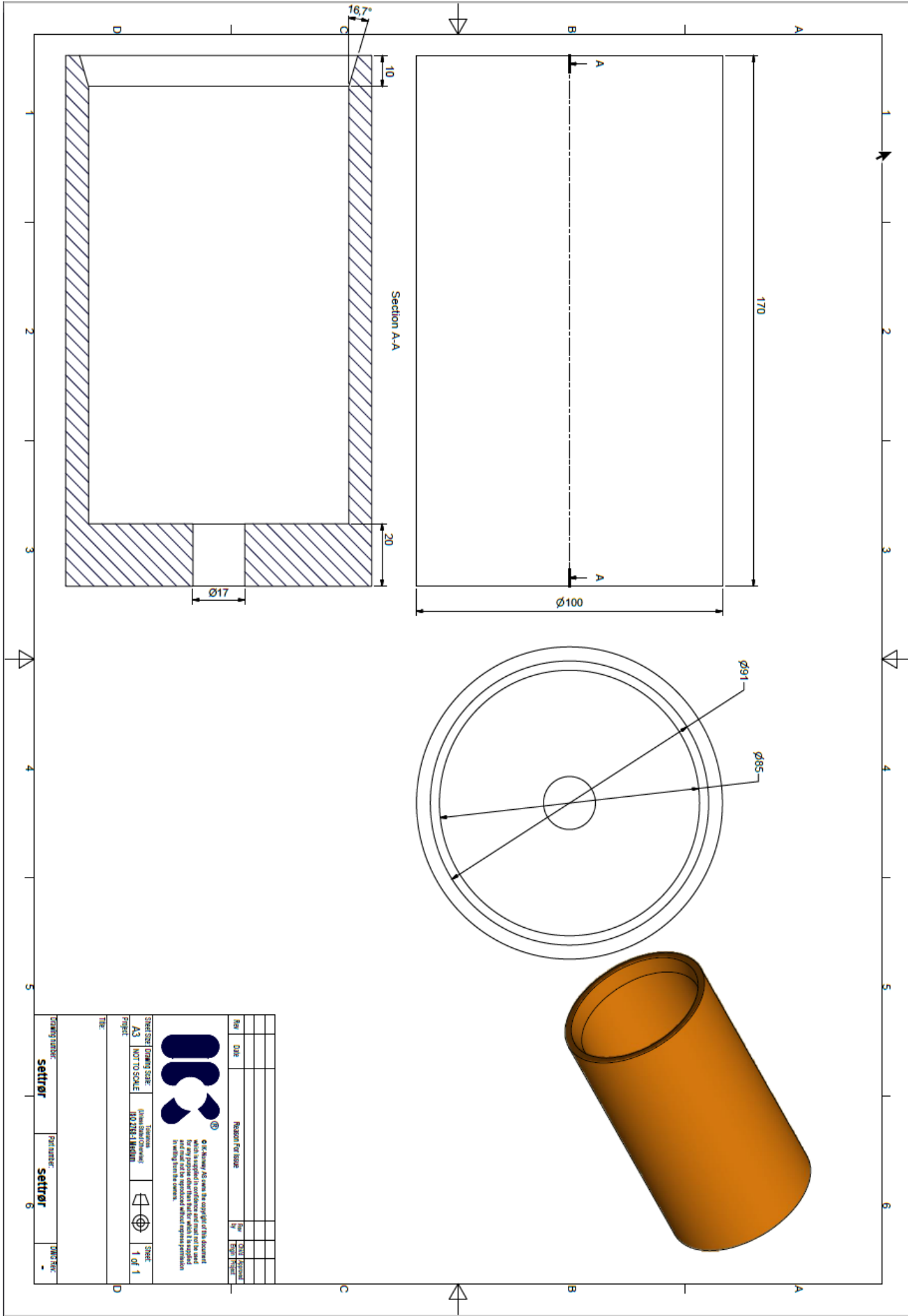
Section A-A



T.C. Milli Eğitim Bakanlığı  
 Millî Eğitim Bakanlığı  
 Millî Eğitim Bakanlığı  
 Millî Eğitim Bakanlığı

© All rights reserved. No part of this document may be reproduced, stored in a retrieval system, or transmitted in any form or by any means, electronic, mechanical, photocopying, recording, or by any information storage and retrieval system, without the prior written permission of the copyright owner.

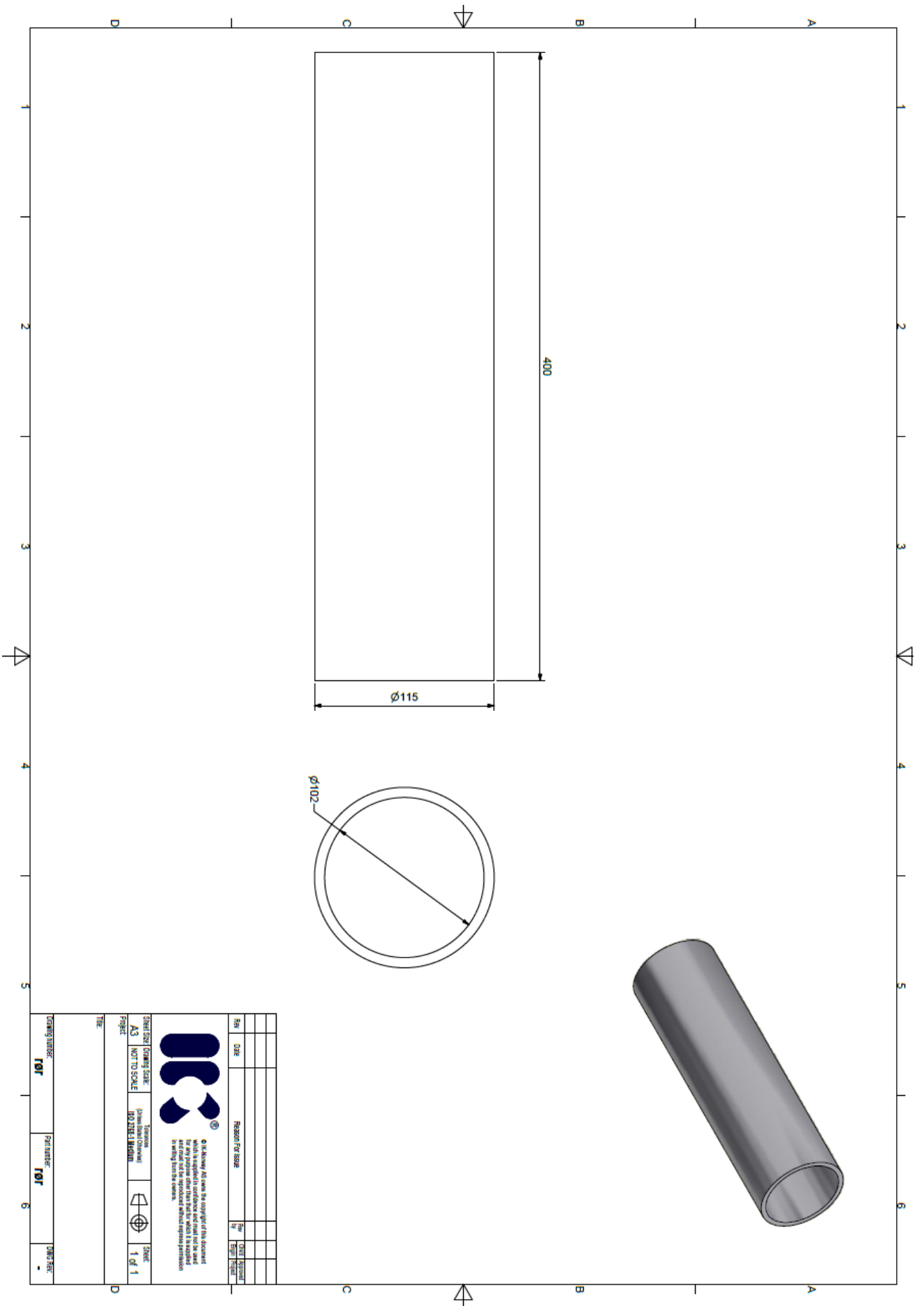
Sheet Size (Drawing Size)	A3	Scale	1/1
Project	MILLÎ EĞİTİM BAKANLIĞI		
Part Number	sylinder		
Part Name	sylinder		
Sheet No.	1		



Rev	Date	Reason for Issue	By	CHK	DATE

© 2016 Bentley All rights reserved. Bentley reserves the right to modify the contents of this document without notice. Bentley does not warrant the accuracy of the information contained herein for any purpose other than that for which it is supplied. In whole or in part, without express permission.

STANDARD DRAWING SCALE Project: A3 NOT TO SCALE TITLE:	DRAWING NUMBER: <b>settror</b>	SHEET NUMBER: 1 of 1	SHEET: 1 of 1
---	-----------------------------------	-------------------------	------------------

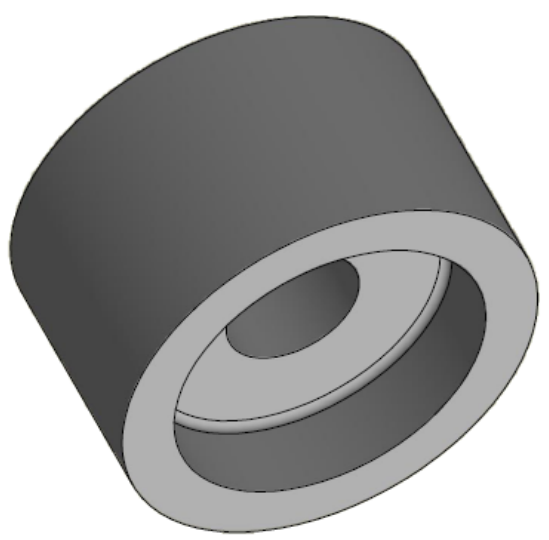
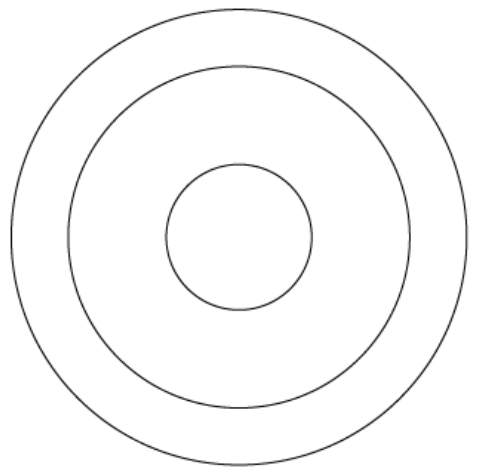
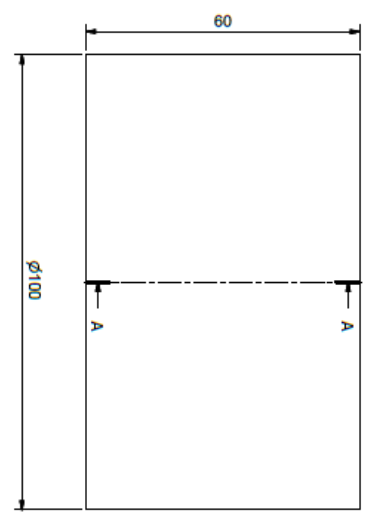
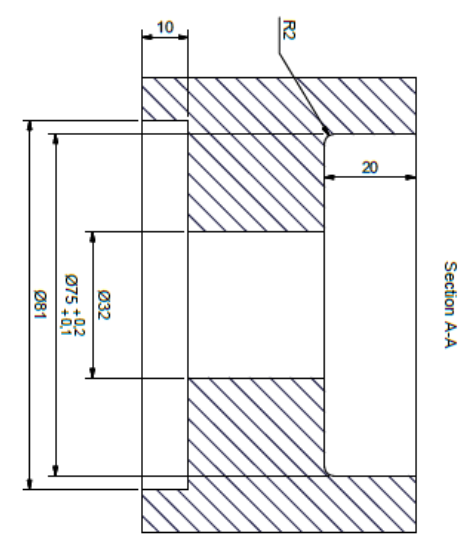


Rev	Date	Revised by	Checked by



© All Rights Reserved. The copyright of this document is reserved for the company. No part of this document may be reproduced, stored in a retrieval system, or transmitted in any form or by any means, electronic, mechanical, photocopying, recording, or by any information storage and retrieval system, without express permission in writing from the company.

SHEET SIZE	DRAWING SCALE	DATE	NO. OF SHEETS
A3	1:1	10/10/2023	1 of 1
PROJECT		TITLE	
101		101	

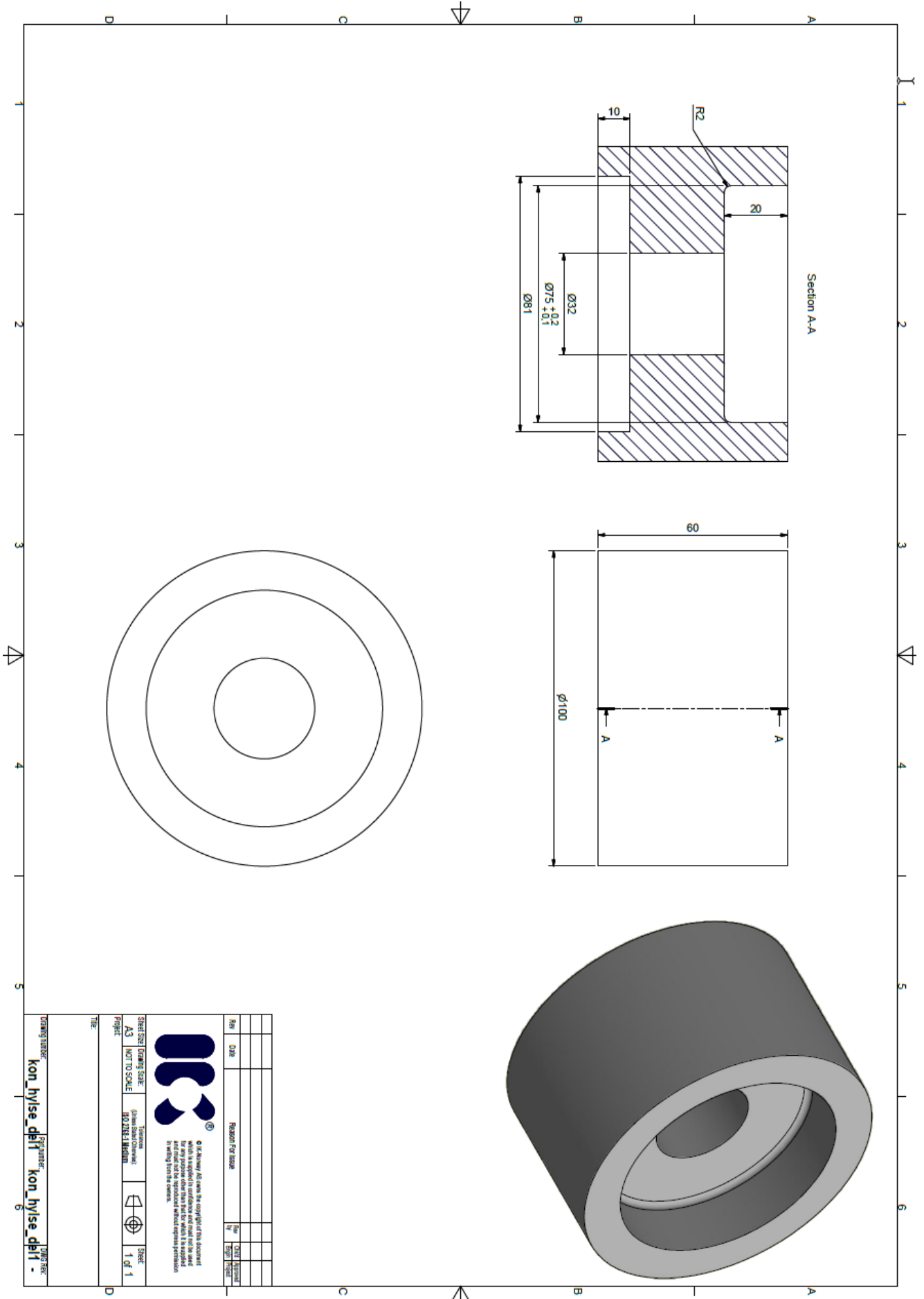


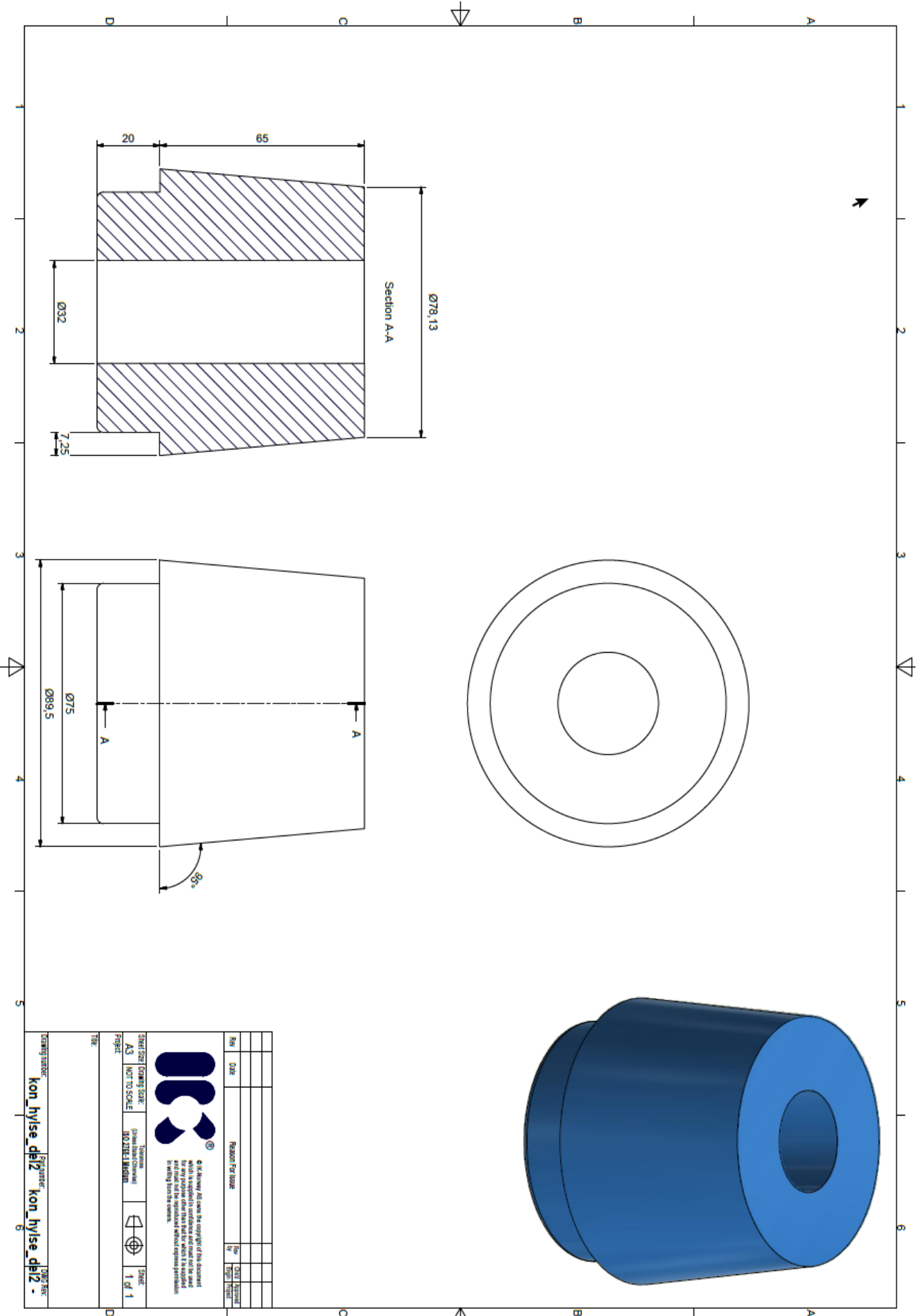
Rev	02B	Revision For Issue	By	DATE

© IBC Grouping. All rights reserved. This document is the property of IBC Grouping and shall not be used, reproduced, or transmitted in any form or by any means, electronic, mechanical, photocopying, recording, or by any information storage and retrieval system, without the prior written permission of IBC Grouping.

Sheet Size: Drawing Scale: A3 NOT TO SCALE  
 Project: KONIKAL BAHARI  
 Title:   
 Scale: 1 of 1

DRAWING NUMBER: kon\_lvise\_dpi1  
 DRAWING DATE: kon\_lvise\_dpi1





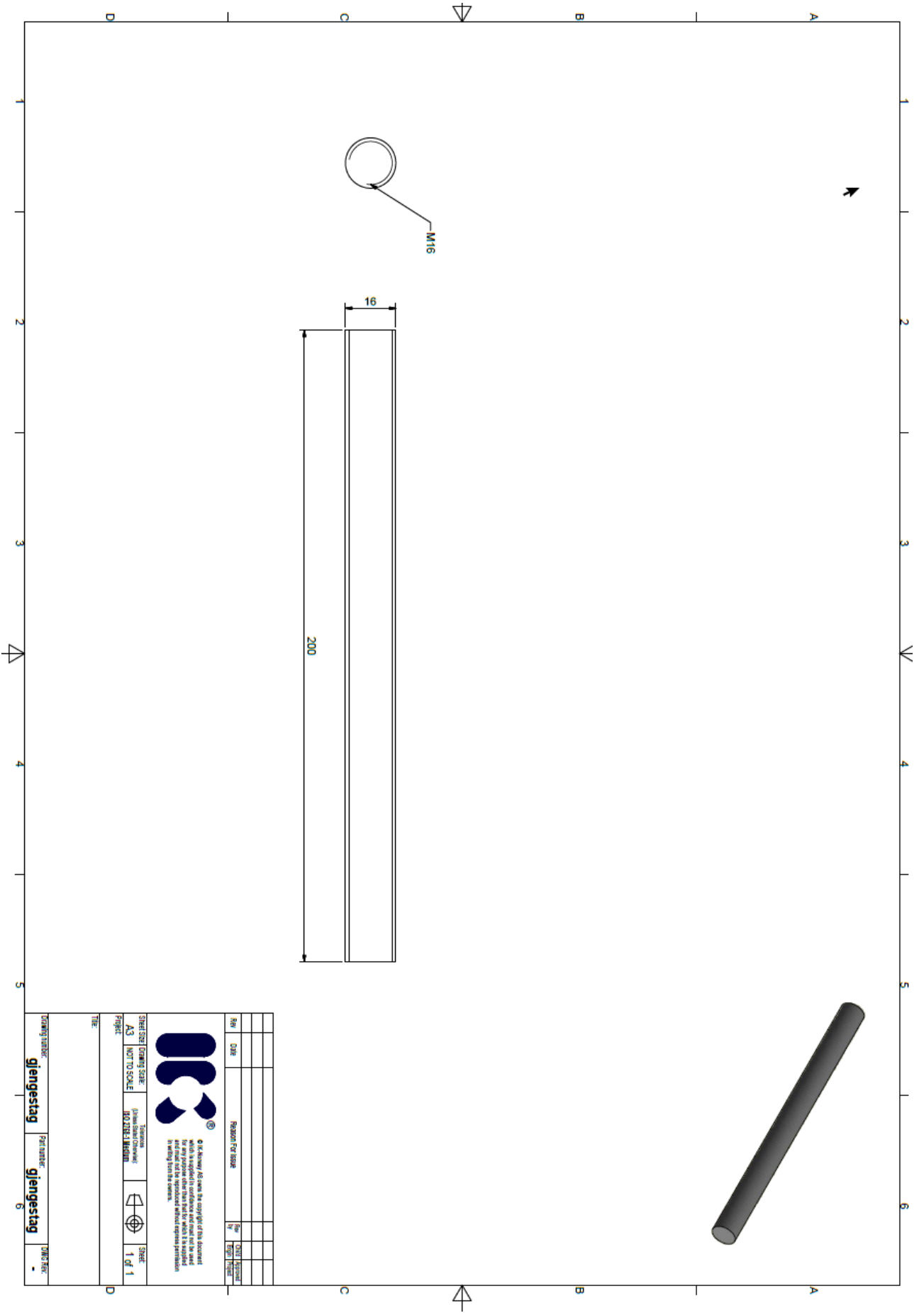
Rev	Date	Reason for Issue	Rev	Date	Reason for Issue



© 2014 Konyak. All rights reserved. The copyright of this document is reserved for Konyak. No part of this document may be reproduced, stored in a retrieval system, or transmitted in any form or by any means, electronic, mechanical, photocopying, recording, or by any information storage and retrieval system, without the prior written permission of Konyak. All trademarks are the property of their respective owners.

Sheet Size / Drawing Scale	Standard / Drawing Standard	Sheet
A3	ISO 2768 / ISO 2768	1 of 1
NOT TO SCALE	ISO 2768 / ISO 2768	1 of 1

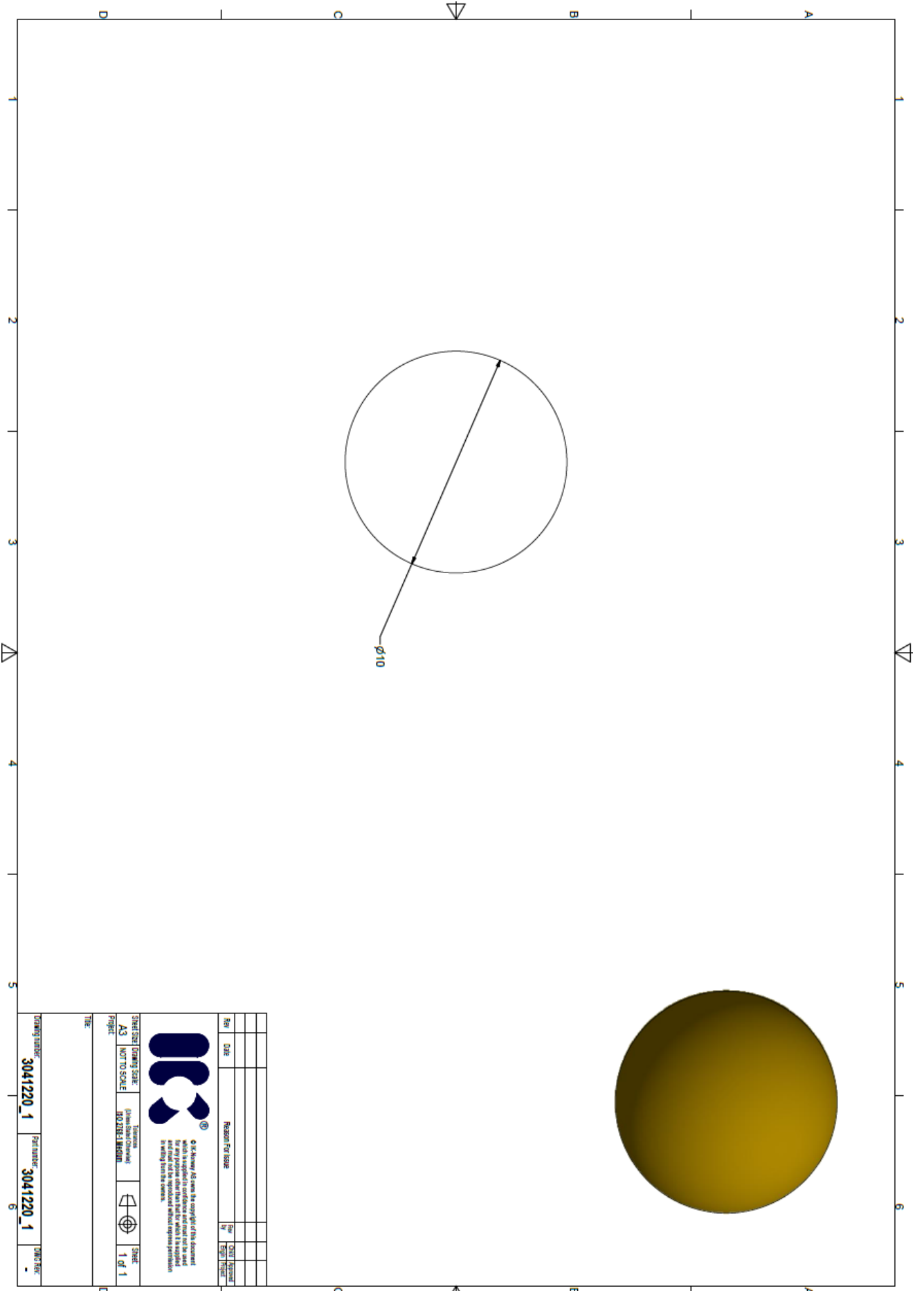
Drawing Number: **kon\_hylse\_dh12** / Part Number: **kon\_hylse\_dh12** - **01**



© McAlamy. All rights reserved. No part of this document may be reproduced, stored in a retrieval system, or transmitted in any form or by any means, electronic, mechanical, photocopying, recording, or by any information storage and retrieval system, without express permission in writing from the owner.

Rev	Date	Reason For Issue	By	Scale	Quantity

Sheet Size	Drawing Scale	Tolerance	Sheet
A3	NOT TO SCALE	METRIC/IMPERIAL	1 of 1
Project			
Title			
Drawing number	Part number	DWG REV	
glengestag	glengestag	-	



Rev	Date	Reason For Issue	Rev	DATE



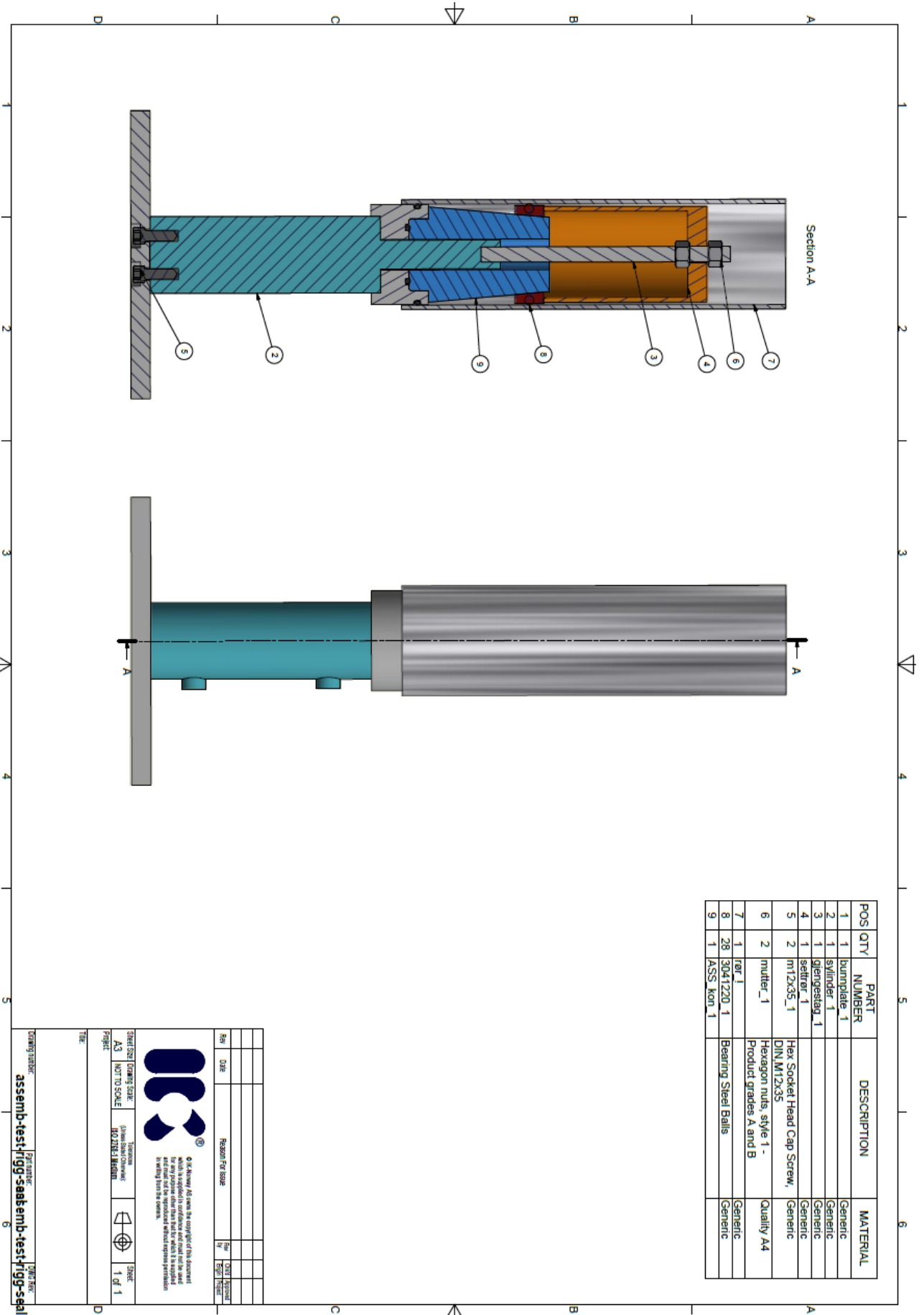
© All Material IS under the copyright of this document which is supplied in confidence and must not be used for any purpose other than that for which it is supplied without the express written permission of the company.

SHEET SIZE: DRAWING SCALE: A3 NOT TO SCALE  
 PROJECT: MOTORS IN ROOM  
 SHEET: 1 of 1

DRAWING NUMBER: 3041220\_1  
 PART NUMBER: 3041220\_1  
 DATE: -

## **APPENDIX C - Technical drawings of the test-rig, with pressure test possibilities and cone alloyed with Calmax**





POS	QTY	PART NUMBER	DESCRIPTION	MATERIAL
1	1	bunnpåte_1		Generic
2	1	svilinder_1		Generic
3	1	gljengestjäd_1		Generic
4	1	settrör_1		Generic
5	2	m12x35_1	Hex Socket Head Cap Screw, DIN M12x35	Generic
6	2	mutter_1	Hexagon nuts, style 1 - Product grades A and B	Quality A4
7	1	för_1		Generic
8	28	3041220_1	Bearing Steel Balls	Generic
9	1	ASSS_kon_1		Generic

REV	DATE	REASON FOR CHANGE	BY	DATE



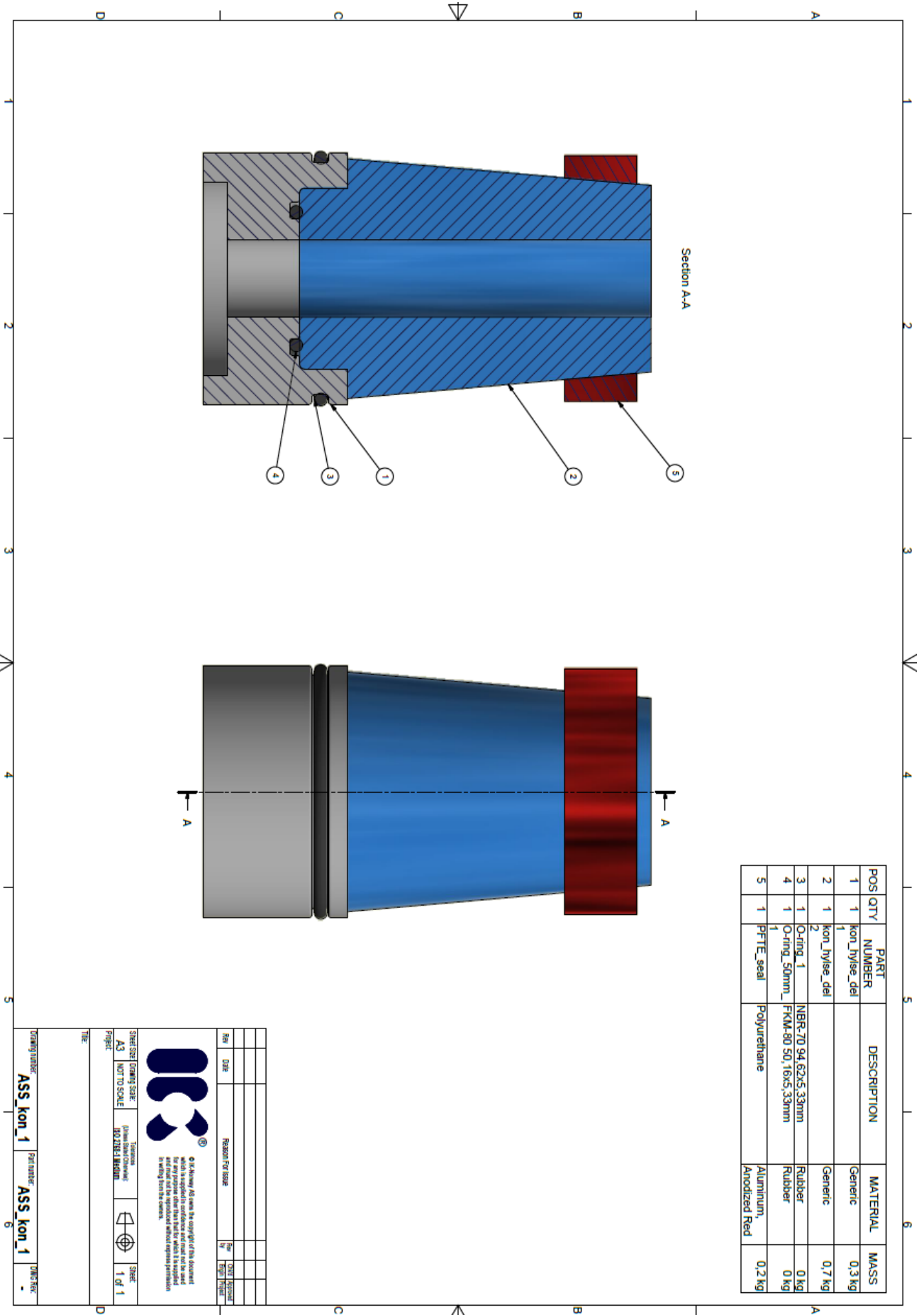
© De Kiewit Ag owns the copyright of this document which is supplied in confidence and shall not be used for any other purpose without the express written permission of De Kiewit Ag. All rights reserved.

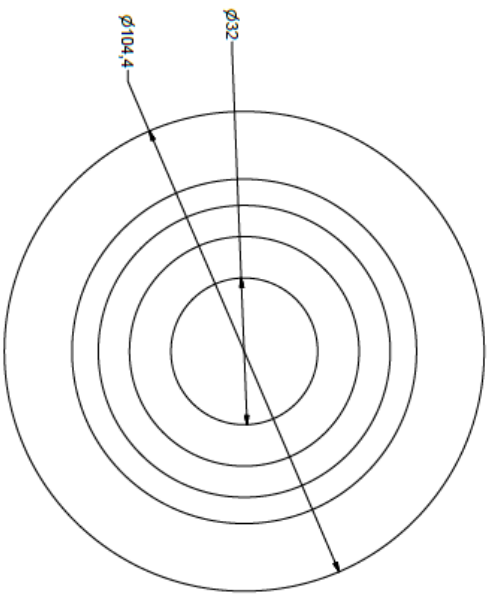
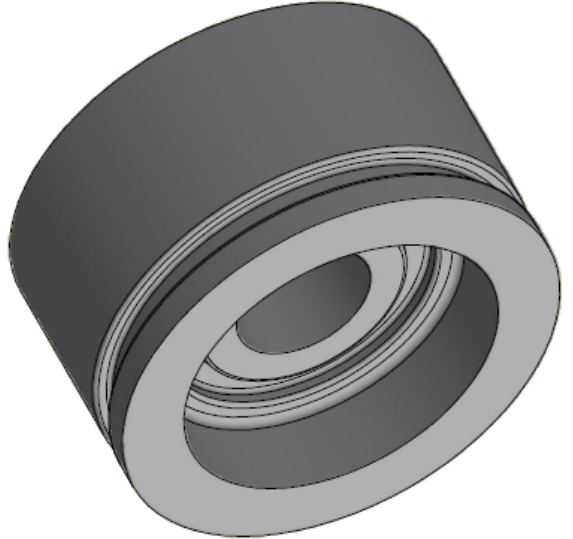
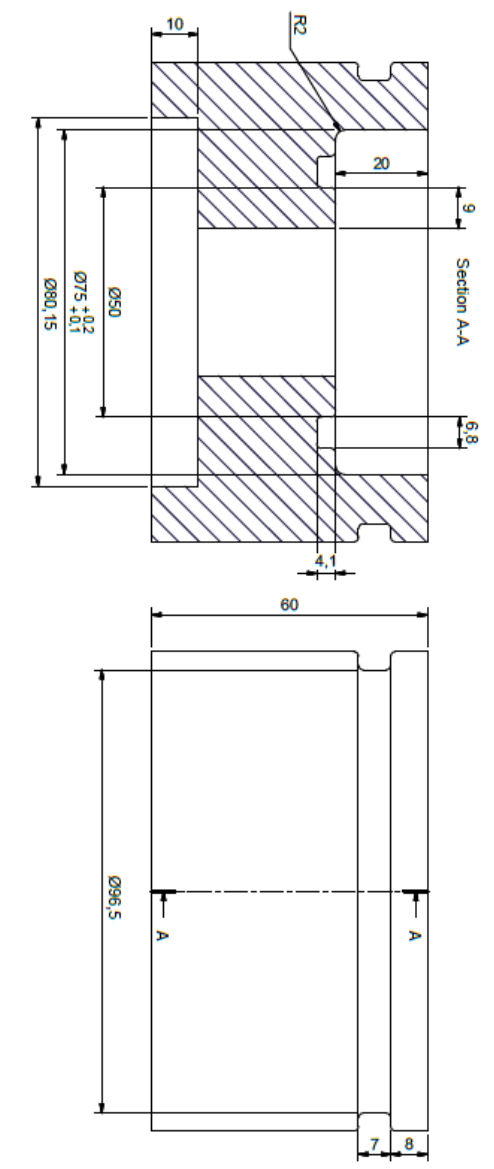
Sheet Size: Drawing Scale: A3 NOT TO SCALE

Project: **MOJIBEL/MSKOM**

Sheet: 1 of 1

Drawing number: **assemb-test-igg-saabbmb-test-igg-seal**





© IKC know AG owns the copyright of this document which is applied to confidence and must not be used for other projects without explicit approval in writing from the company.

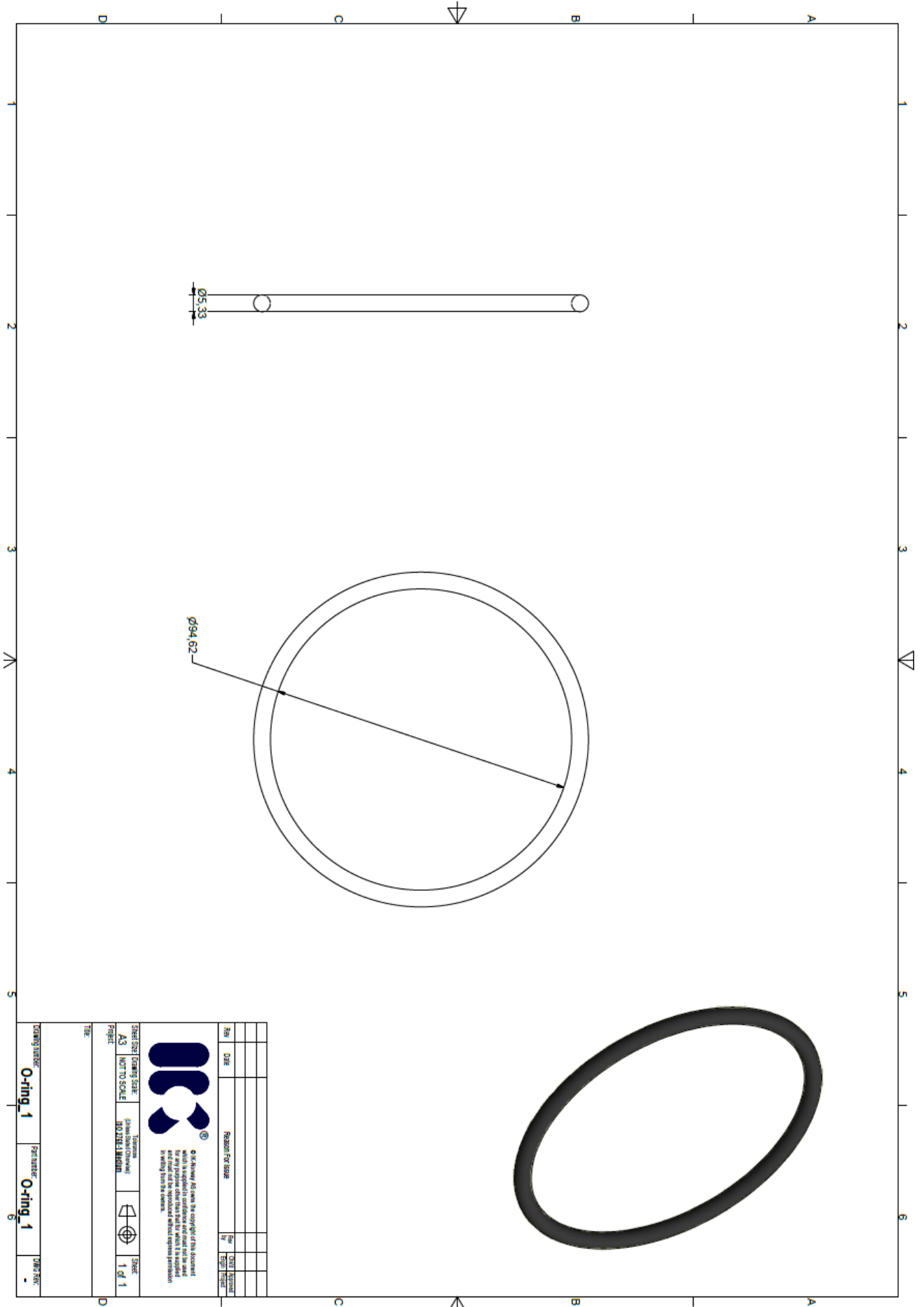
Rev	Date	Reason For Issue	Rev	DATE	REASON
			1		

Sheet Size	Drawing Scale	Technical Drawing Standard	Sheet
A3	1:1	ISO 22838-1:2004	1 of 1

Project	Task	Sheet
kon_hylse_dpl1	kon_hylse_dpl1	1 of 1



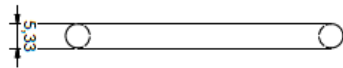
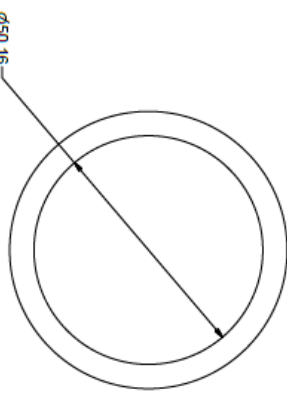
Rev	Date	Reason for change	Rev	Checked



© It is hereby declared the copyright of this document is reserved for the company. Any reproduction or use for any purpose other than that for which it is supplied is prohibited without express permission in writing from the company.

**Sheet Size:** Drawing Scale: A3  
**NOT TO SCALE**  
**Project:** IROZEM MARMER  
**Sheet:** 1 of 1  
**Drawing number:** O-ring\_1  
**Parameter:** O-ring\_1  
**DWG Rev:** -

1 2 3 4 5 6



1 2 3 4 5 6

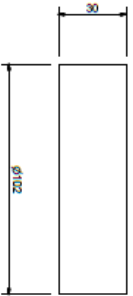
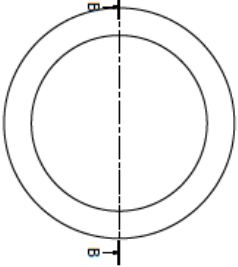
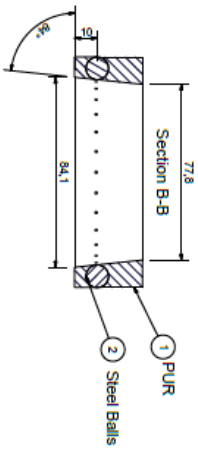
Rev	Date	Report For Issue	Rev	Chart Approval



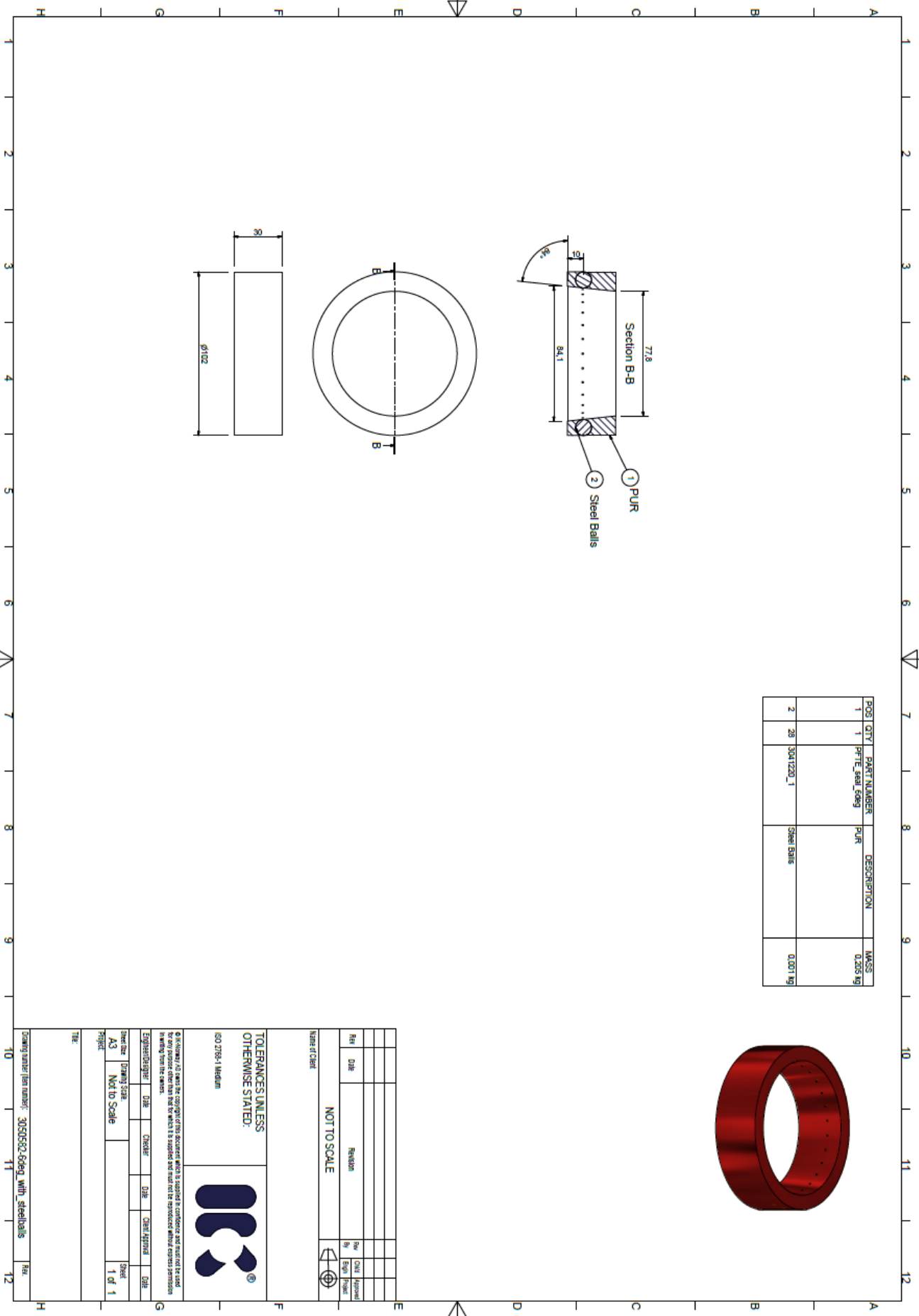
© 2016 by IK. All rights reserved. This document is the property of IK. It is not to be reproduced, stored in a retrieval system, or transmitted in any form or by any means, electronic, mechanical, photocopying, recording, or by any information storage and retrieval system, without express permission in writing from IK.

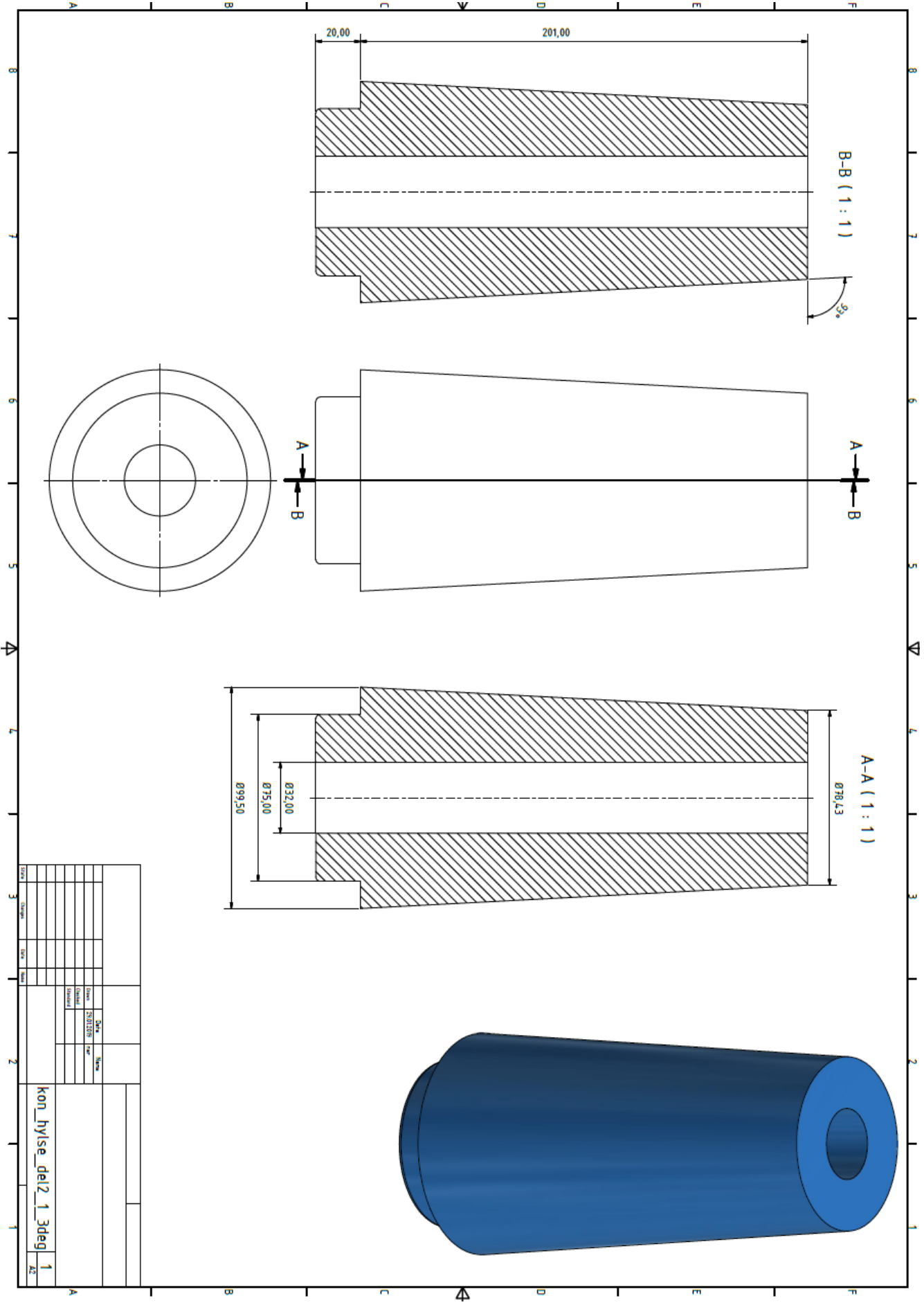
**STREET SIZE DRAWING SCALE**     **Technical Drawing**  
**A3**     **NOT TO SCALE**     **NO DIMENSIONS**     **SHEET 1 OF 1**  
 Project:     The:     Drawing number: **O-ring, 50mm, 1**     Part number: **O-ring, 50mm, 1 -**

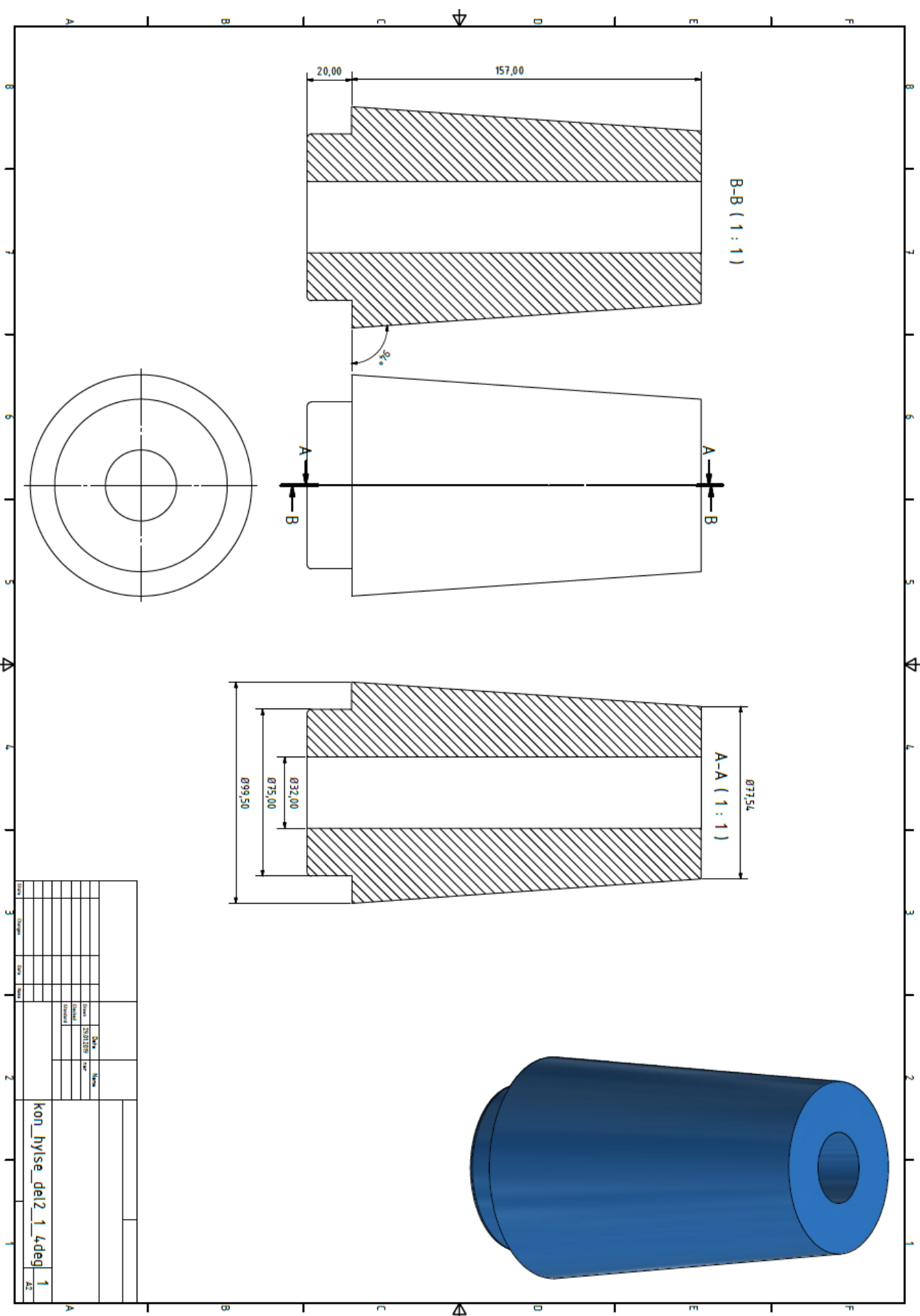
POST	QTY	PART NUMBER	DESCRIPTION	MASS
1	1	PURTE_skel_5069	PUR	0.205 kg
2	28	3041220_1	Steel Balls	0.207 kg



Rev	Date	Revision	Rev	Drawn	Checked	Approved
<b>NOT TO SCALE</b>						
Name (Code)						
<b>TOLERANCES UNLESS OTHERWISE STATED:</b>						
ISO 2768-1 Medium						
<small>© Issuance of any part of this document which is subject to conditions and that not be used in any other way than that for which it is supplied without the express permission in writing from the owner.</small>						
Engineer/Designer	Date	Checker	Date	Chief Approval	Date	
Standard	Drawing Issue					Sheet
Project	Not to Scale					1 of 1
Title						
Drawing number (Item number): 3050502-5069 with steelballs						
						Rev

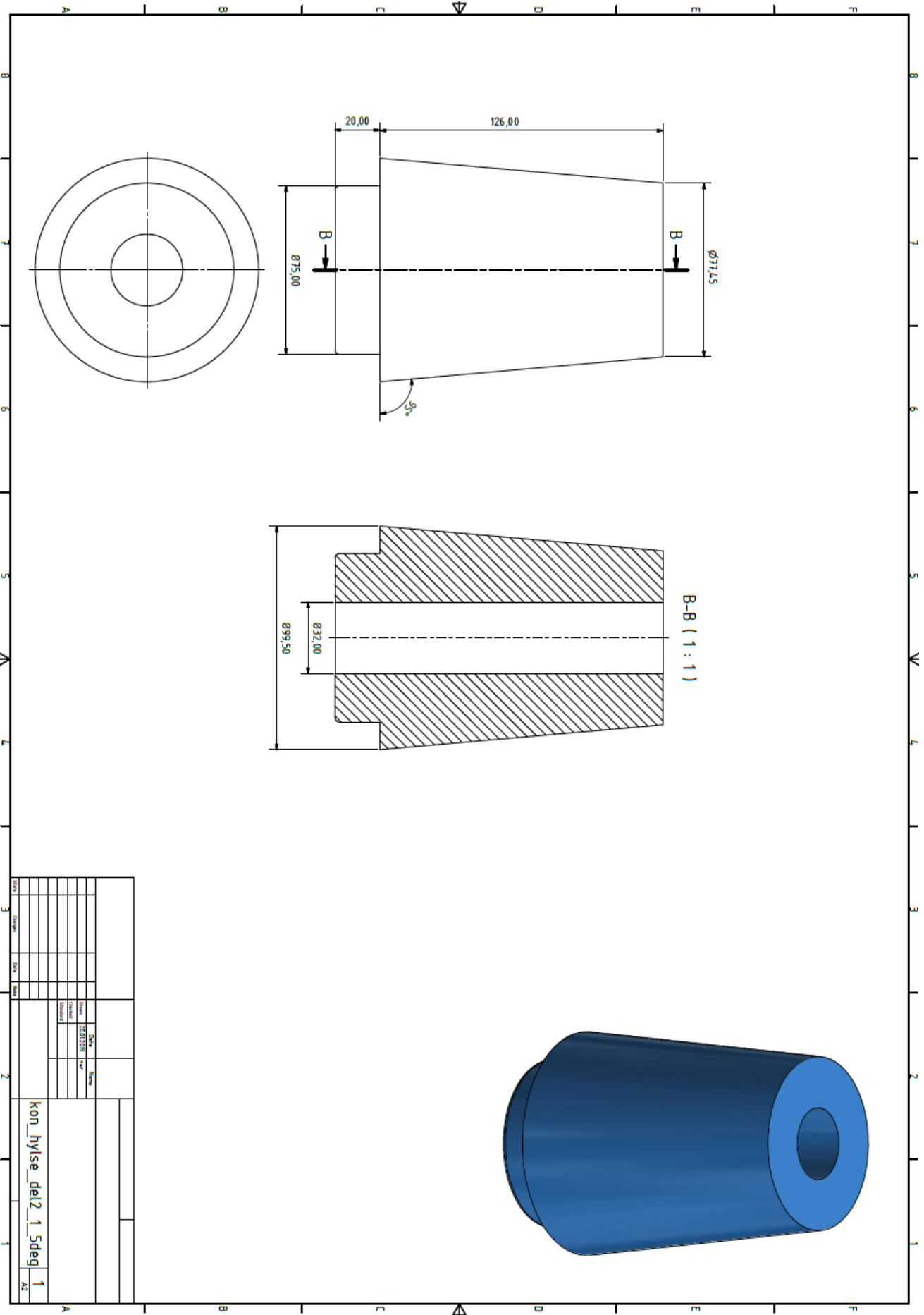




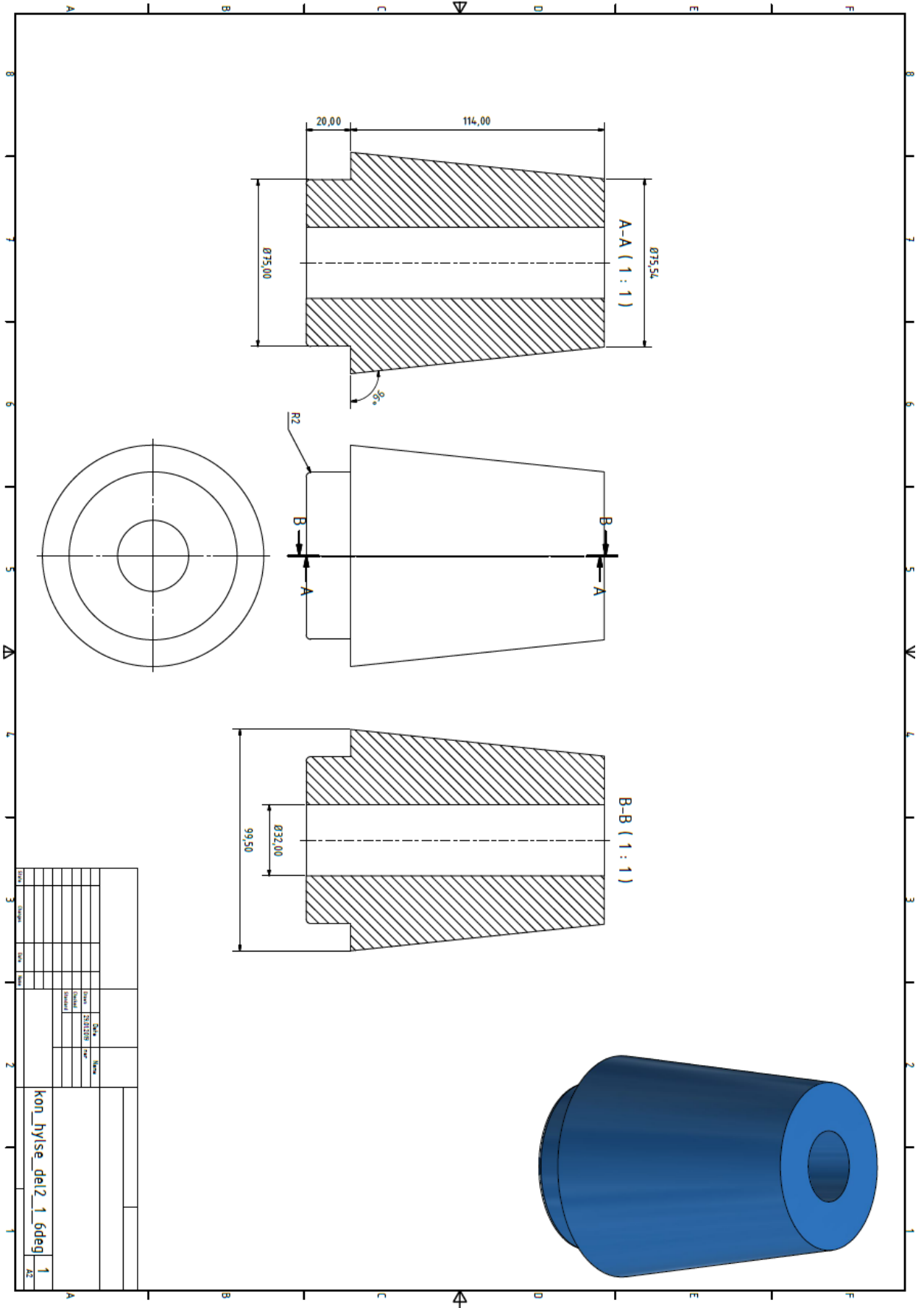


1	kon_hylse_del2_1_4deg	1
2		
3		
4		
5		
6		
7		
8		
9		
10		
11		
12		
13		
14		
15		
16		
17		
18		
19		
20		
21		
22		
23		
24		
25		
26		
27		
28		
29		
30		
31		
32		
33		
34		
35		
36		
37		
38		
39		
40		
41		
42		
43		
44		
45		
46		
47		
48		
49		
50		
51		
52		
53		
54		
55		
56		
57		
58		
59		
60		
61		
62		
63		
64		
65		
66		
67		
68		
69		
70		
71		
72		
73		
74		
75		
76		
77		
78		
79		
80		
81		
82		
83		
84		
85		
86		
87		
88		
89		
90		
91		
92		
93		
94		
95		
96		
97		
98		
99		
100		



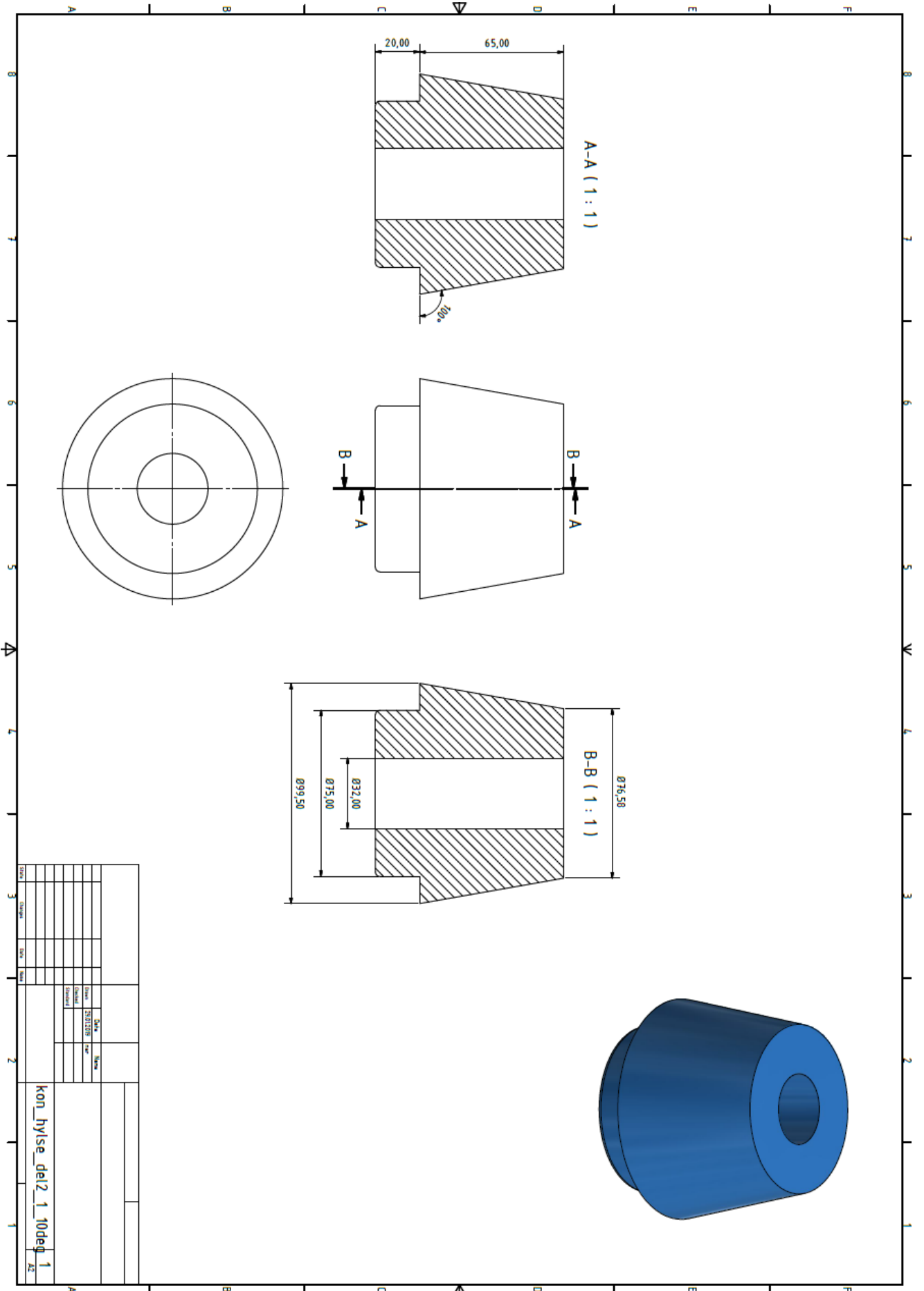


kon_hylse_diel2_1_Sdag		1																
1		42																
<table border="1"> <tr> <td>DATE</td> <td>DESIGNER</td> <td>DATE</td> <td>DATE</td> </tr> <tr> <td></td> <td></td> <td></td> <td></td> </tr> </table>			DATE	DESIGNER	DATE	DATE												
DATE	DESIGNER	DATE	DATE															
<table border="1"> <tr> <td>DATE</td> <td>DESIGNER</td> <td>DATE</td> <td>DATE</td> </tr> <tr> <td></td> <td></td> <td></td> <td></td> </tr> </table>		DATE	DESIGNER	DATE	DATE					<table border="1"> <tr> <td>DATE</td> <td>DESIGNER</td> <td>DATE</td> <td>DATE</td> </tr> <tr> <td></td> <td></td> <td></td> <td></td> </tr> </table>	DATE	DESIGNER	DATE	DATE				
DATE	DESIGNER	DATE	DATE															
DATE	DESIGNER	DATE	DATE															

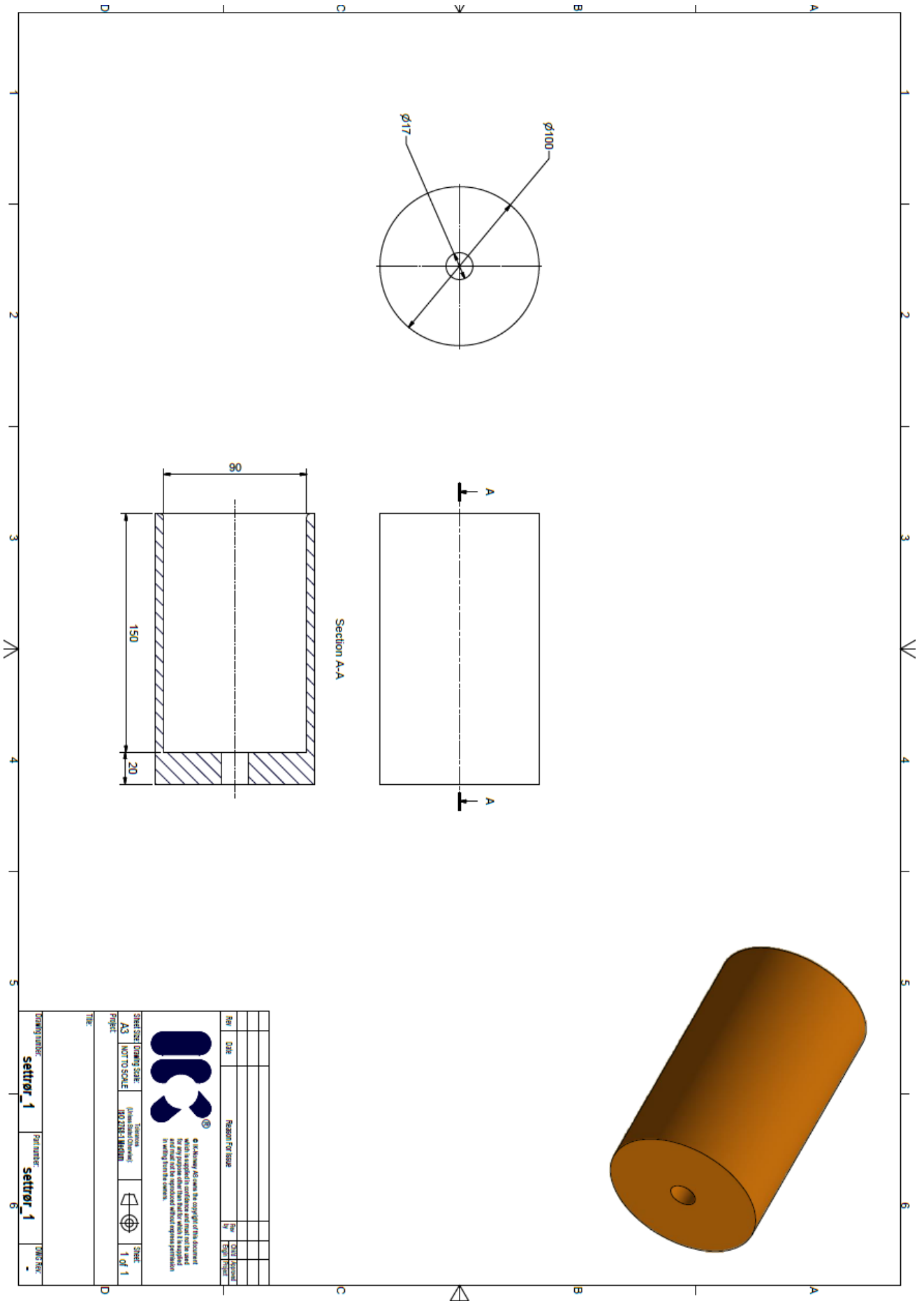


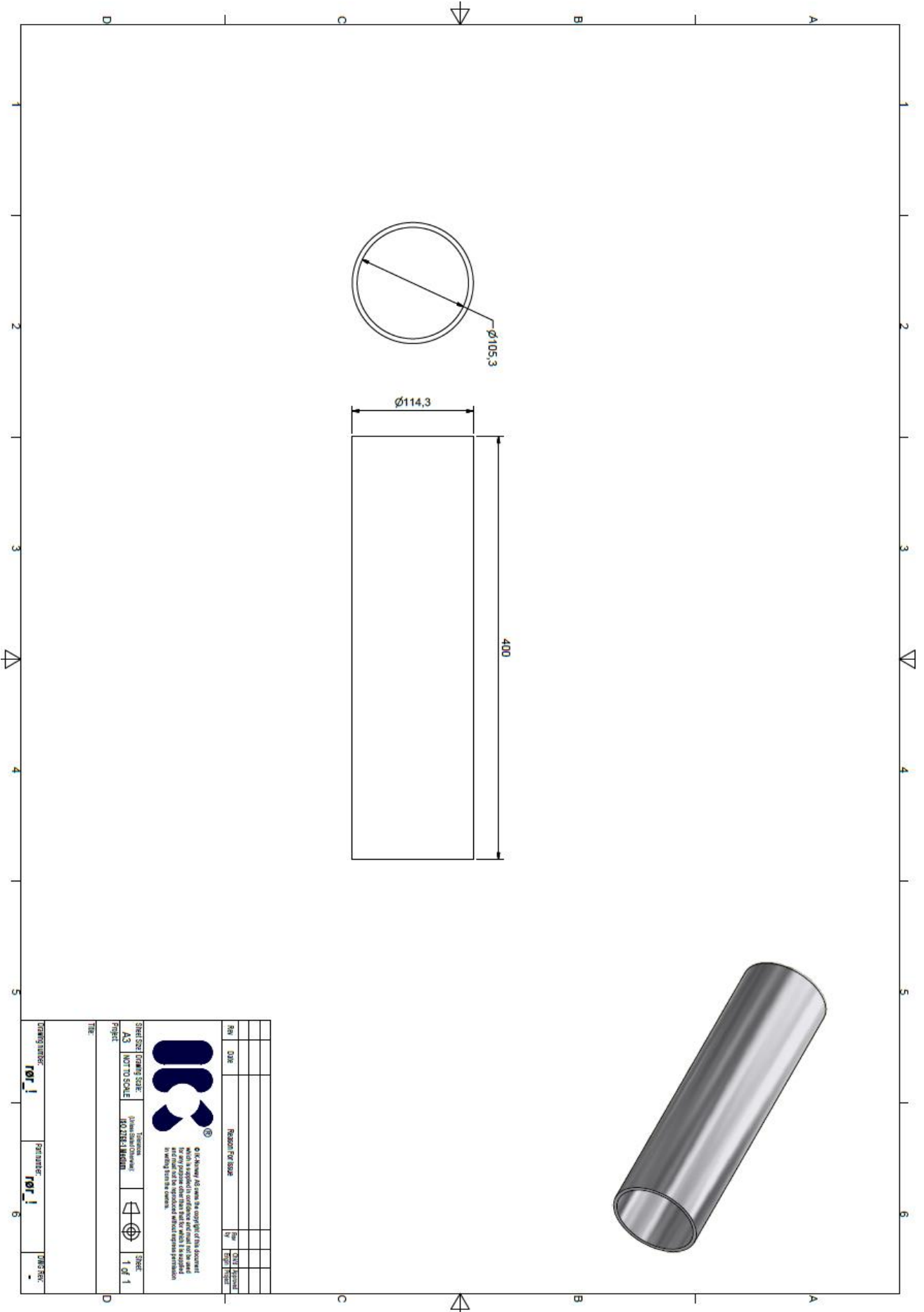
TITEL		MATERIALE		MATERIALE		MATERIALE		MATERIALE		MATERIALE		MATERIALE		MATERIALE		MATERIALE		MATERIALE		MATERIALE	
NOMENCLATURE		NOMENCLATURE		NOMENCLATURE		NOMENCLATURE		NOMENCLATURE		NOMENCLATURE		NOMENCLATURE		NOMENCLATURE		NOMENCLATURE		NOMENCLATURE		NOMENCLATURE	
DATE		DATE		DATE		DATE		DATE		DATE		DATE		DATE		DATE		DATE		DATE	
DESIGNER		DESIGNER		DESIGNER		DESIGNER		DESIGNER		DESIGNER		DESIGNER		DESIGNER		DESIGNER		DESIGNER		DESIGNER	
CHECKER		CHECKER		CHECKER		CHECKER		CHECKER		CHECKER		CHECKER		CHECKER		CHECKER		CHECKER		CHECKER	
DATE		DATE		DATE		DATE		DATE		DATE		DATE		DATE		DATE		DATE		DATE	
SCALE		SCALE		SCALE		SCALE		SCALE		SCALE		SCALE		SCALE		SCALE		SCALE		SCALE	
PROJECT		PROJECT		PROJECT		PROJECT		PROJECT		PROJECT		PROJECT		PROJECT		PROJECT		PROJECT		PROJECT	
DRAWING NO.		DRAWING NO.		DRAWING NO.		DRAWING NO.		DRAWING NO.		DRAWING NO.		DRAWING NO.		DRAWING NO.		DRAWING NO.		DRAWING NO.		DRAWING NO.	
REV.		REV.		REV.		REV.		REV.		REV.		REV.		REV.		REV.		REV.		REV.	
1		1		1		1		1		1		1		1		1		1		1	
kon_hyise_dai2_1_6deg		kon_hyise_dai2_1_6deg		kon_hyise_dai2_1_6deg		kon_hyise_dai2_1_6deg		kon_hyise_dai2_1_6deg		kon_hyise_dai2_1_6deg		kon_hyise_dai2_1_6deg		kon_hyise_dai2_1_6deg		kon_hyise_dai2_1_6deg		kon_hyise_dai2_1_6deg		kon_hyise_dai2_1_6deg	






Date		Name	
Drawn	Checked	Drawn	Checked
2023.12.15			
kon_hyise_del2_1_10deg_1			
A2			



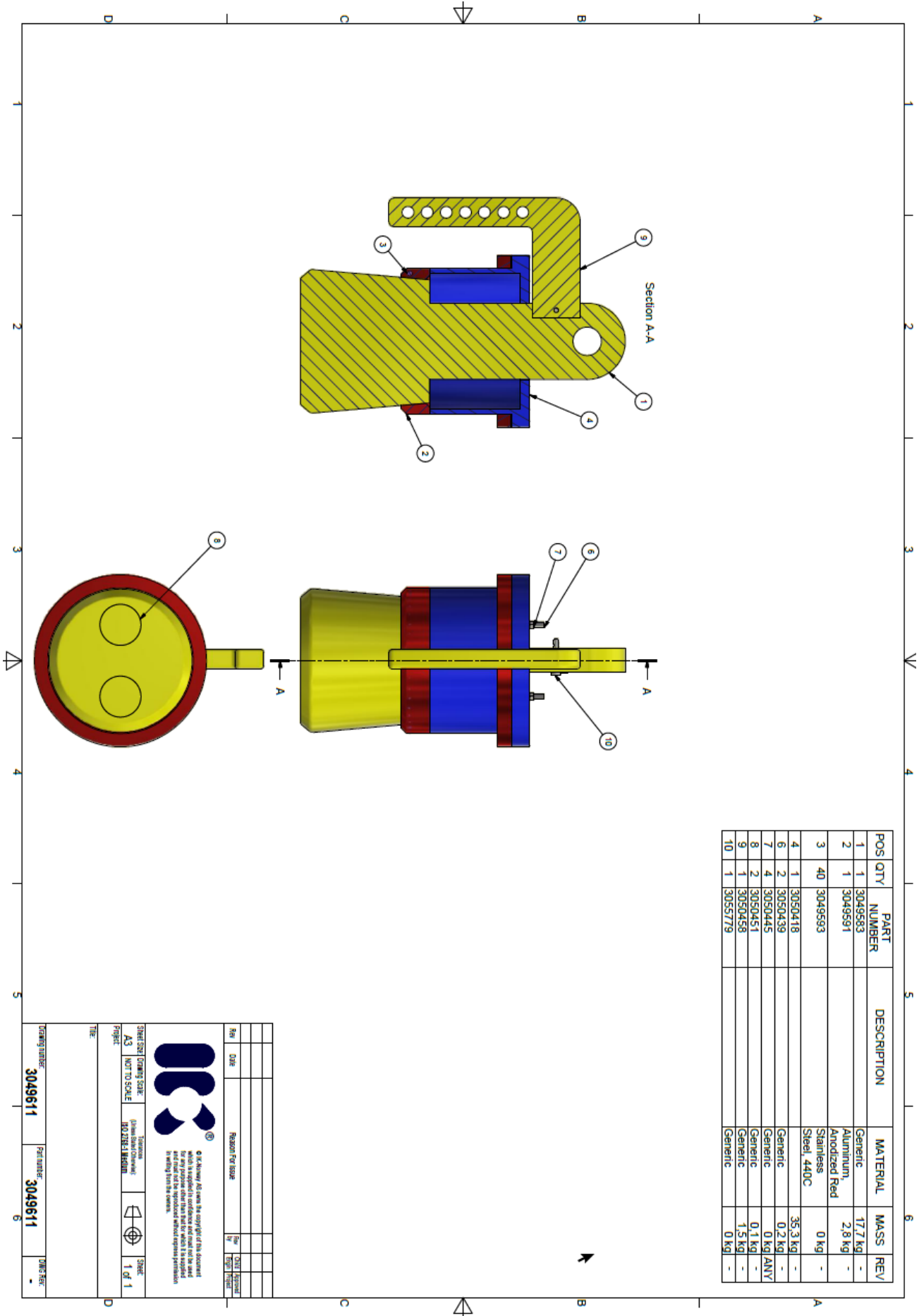


Rev	DATE	Reason for issue	By	DATE


 © IC-Technology AG. All rights reserved. This document is the property of IC-Technology AG. It is not to be used, copied, or reproduced in any form without the prior written permission of IC-Technology AG.

Sheet Size	Drawing Scale	Technical Drawing	Sheet
A3	1:1	ISO TECHNICAL DRAWING	1 of 1
Project			
Title			
Drawing Number	Part Number	Unit's Name	
101_1	101_1	-	

**APPENDIX C - Technical drawings of an ROV compatible PRT – 12-inch pipeline**



POS	QTY	PART NUMBER	DESCRIPTION	MATERIAL	MASS	REV
1	1	3049583	Generic	Aluminum	17.7 kg	-
2	1	3049591	Generic	Anodized Red	2.8 kg	-
3	40	3049593	Generic	Stainless Steel 440C	0 kg	-
4	1	3050418	Generic	Steel 440C	35.3 kg	-
6	2	3050439	Generic	Generic	0.2 kg	-
7	4	3050445	Generic	Generic	0 kg	ANY
8	2	3050451	Generic	Generic	0.1 kg	-
9	1	3050458	Generic	Generic	1.5 kg	-
10	1	3055779	Generic	Generic	0 kg	-

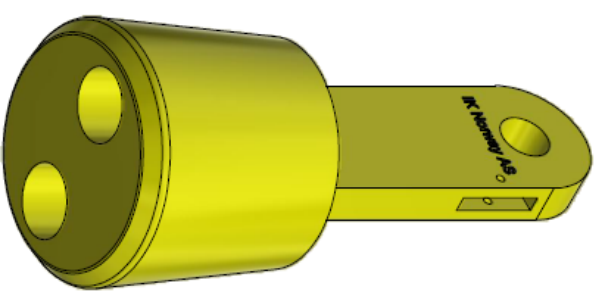
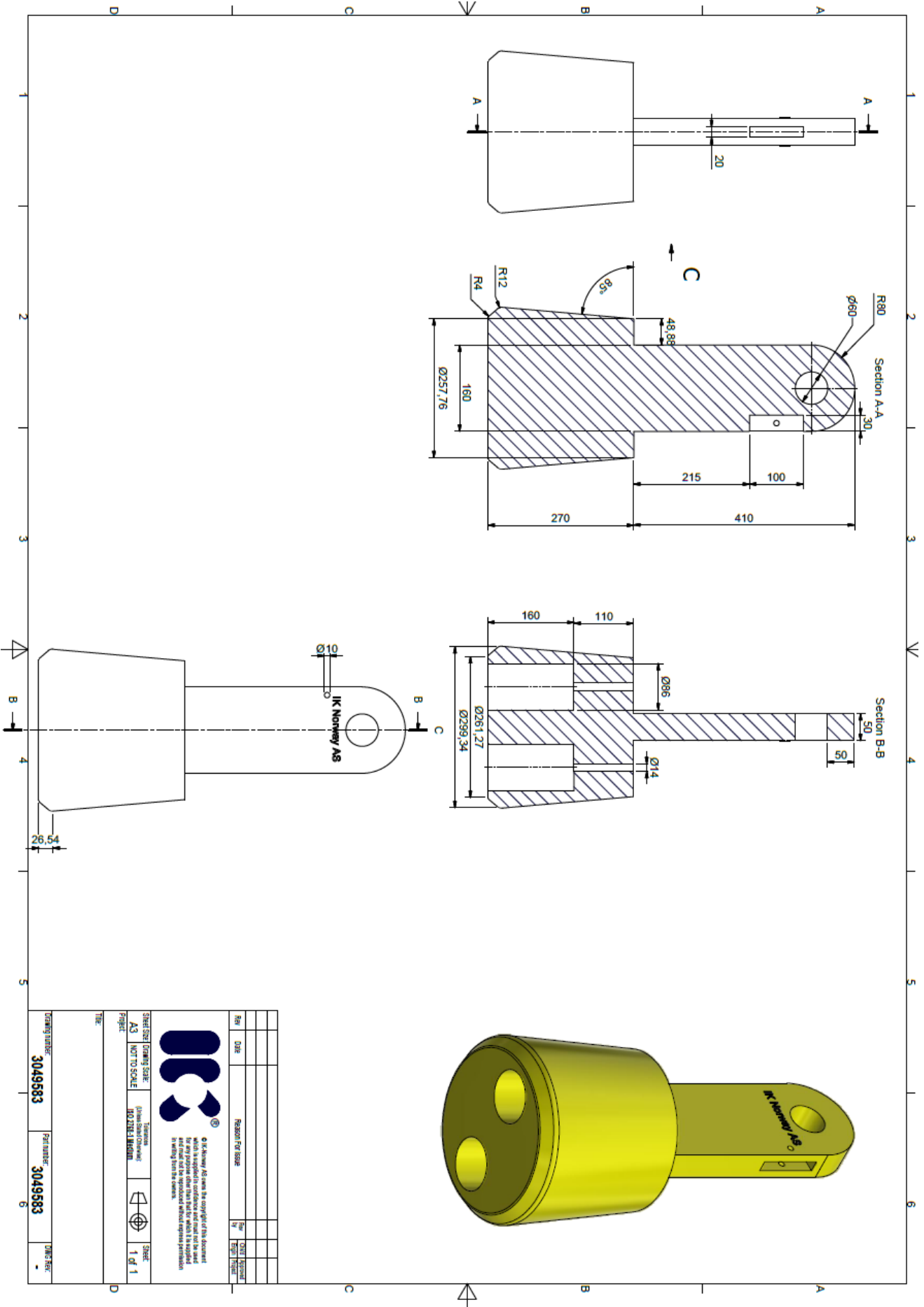
Rev	DATE	Reason For Issue	By	DATE



© C.A. Kiewit & Co. All rights reserved. This document is the property of C.A. Kiewit & Co. and is not to be reproduced, stored in a retrieval system, or transmitted in any form or by any means, electronic, mechanical, photocopying, recording, or by any information storage and retrieval system, without the prior written permission of C.A. Kiewit & Co.

Sheet Size	Drawing Scale	Form	Scale
A3	NOT TO SCALE	NO ZHESL INFORM	1 of 1
Project			
Title			
Drawing Number	3049611	Part Number	3049611
			DATE HERE





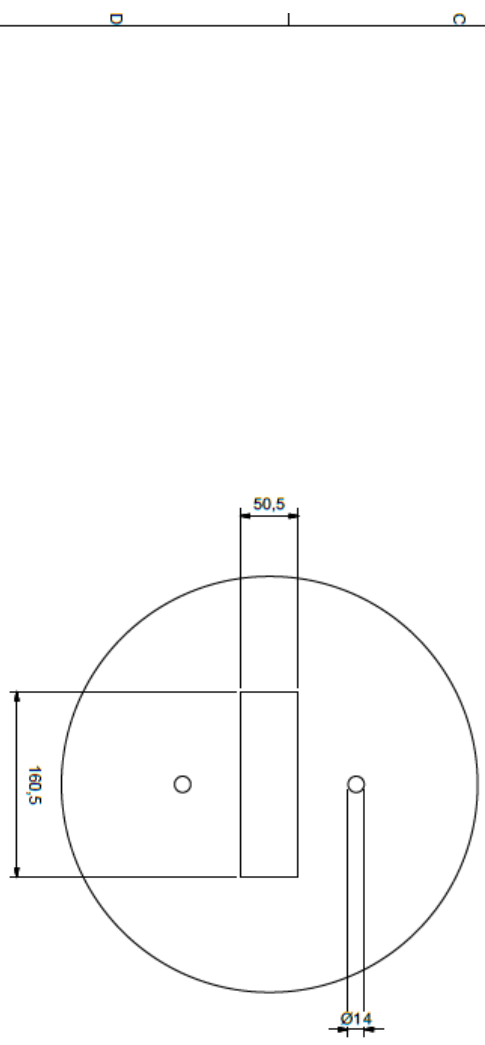
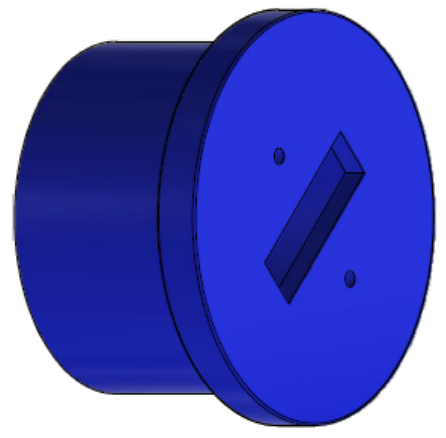
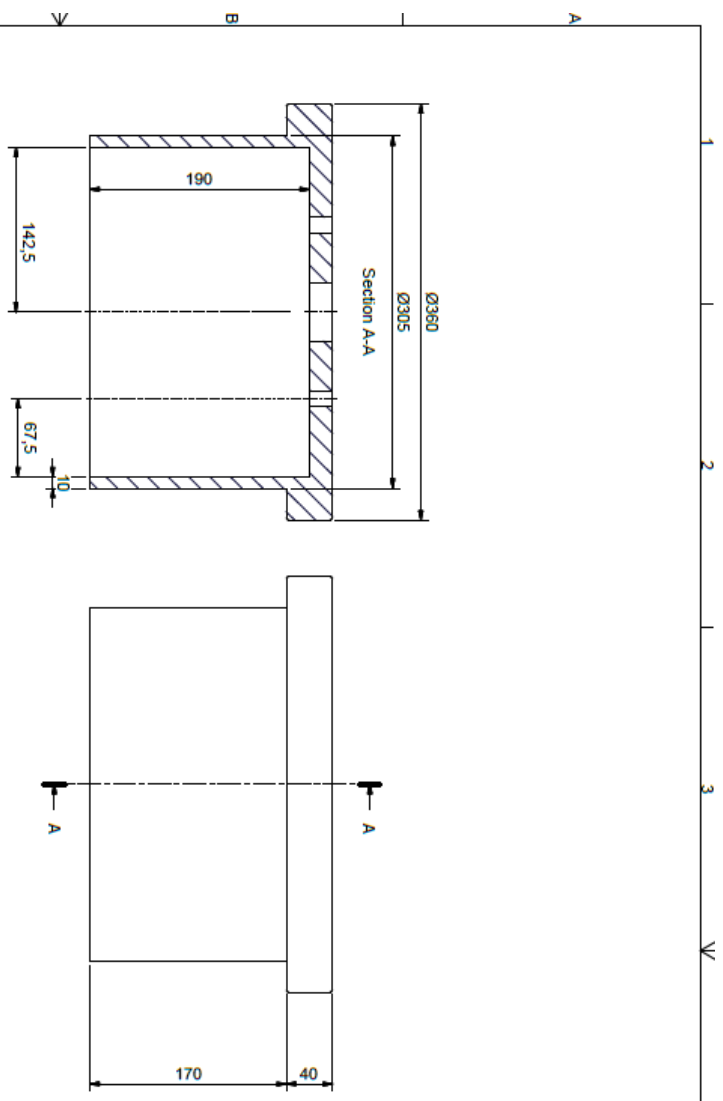
Rev	Date	Reason for issue	By	Checked/Reviewed

© IK Nonney AS. All rights reserved. This document is the property of IK Nonney AS. It is not to be reproduced, stored in a retrieval system, or transmitted in any form or by any means, electronic, mechanical, photocopying, recording, or by any information storage and retrieval system, without express permission in writing from the company.



Sheet Size: A3  
 Drawing Scale: 1:1  
 Part Number: 3049583  
 Sheet 1 of 1

Drawing Number: 3049583  
 Part Number: 3049583  
 Drawing Title: IK Nonney AS



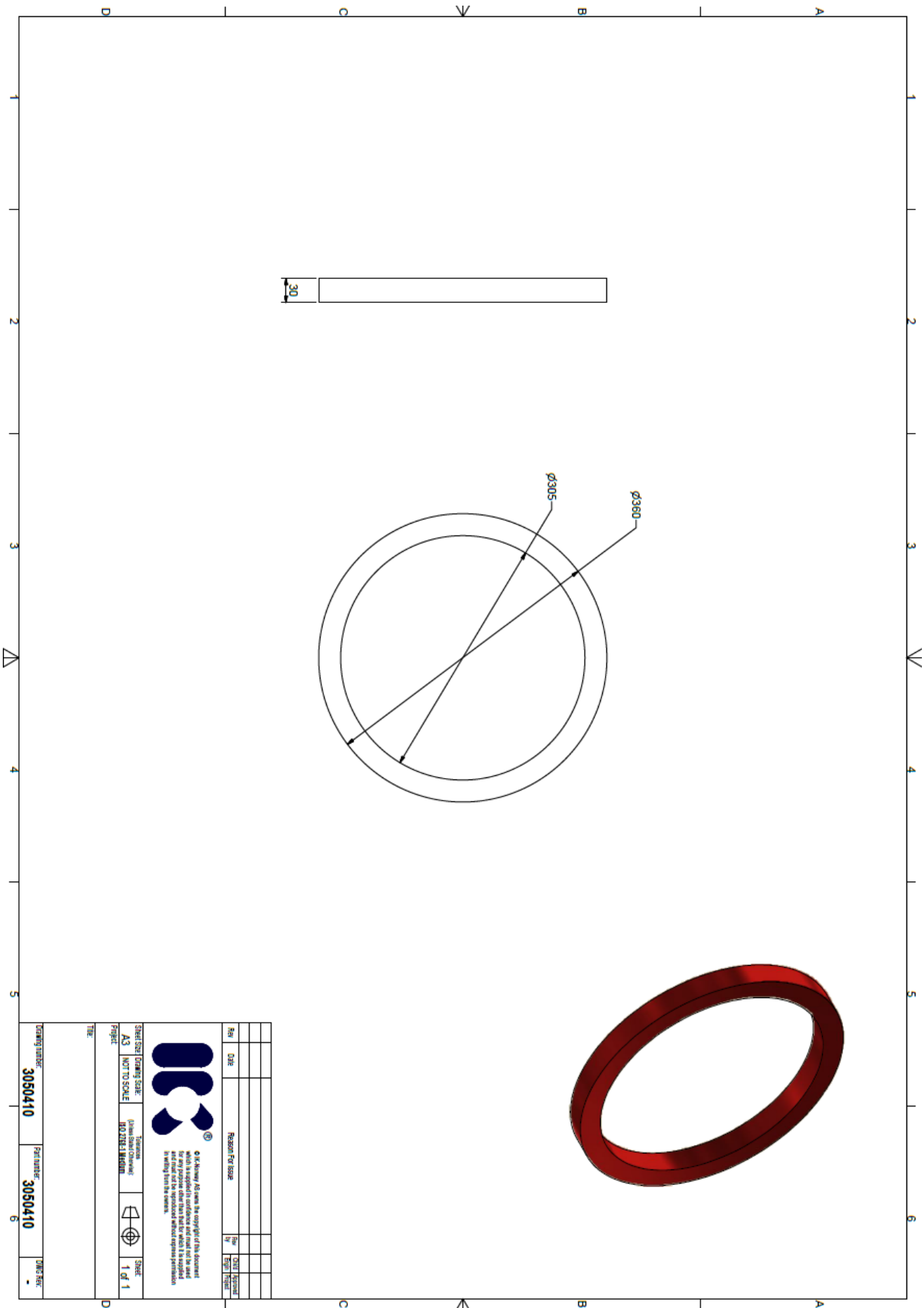
Rev	Date	Reason For Issue	Rev	OUT	APP



© M. Akbayrak. All rights reserved. No document which is supplied in electronic and print form to be used for any purpose other than that for which it is supplied in writing without the express permission of the Ministry of Environment, Urbanization and Climate Change.

SHEET SIZE | DRAWING SCALE: 1/1  
 A3 | NOT TO SCALE  
 PROJECT: MÜHÜRLEME  
 SHEET: 1 of 1

DRAWING NUMBER: 3050409  
 PART NUMBER: 3050409  
 DATE: -



Rev	Scale	Reason For Issue	Rev	DATE

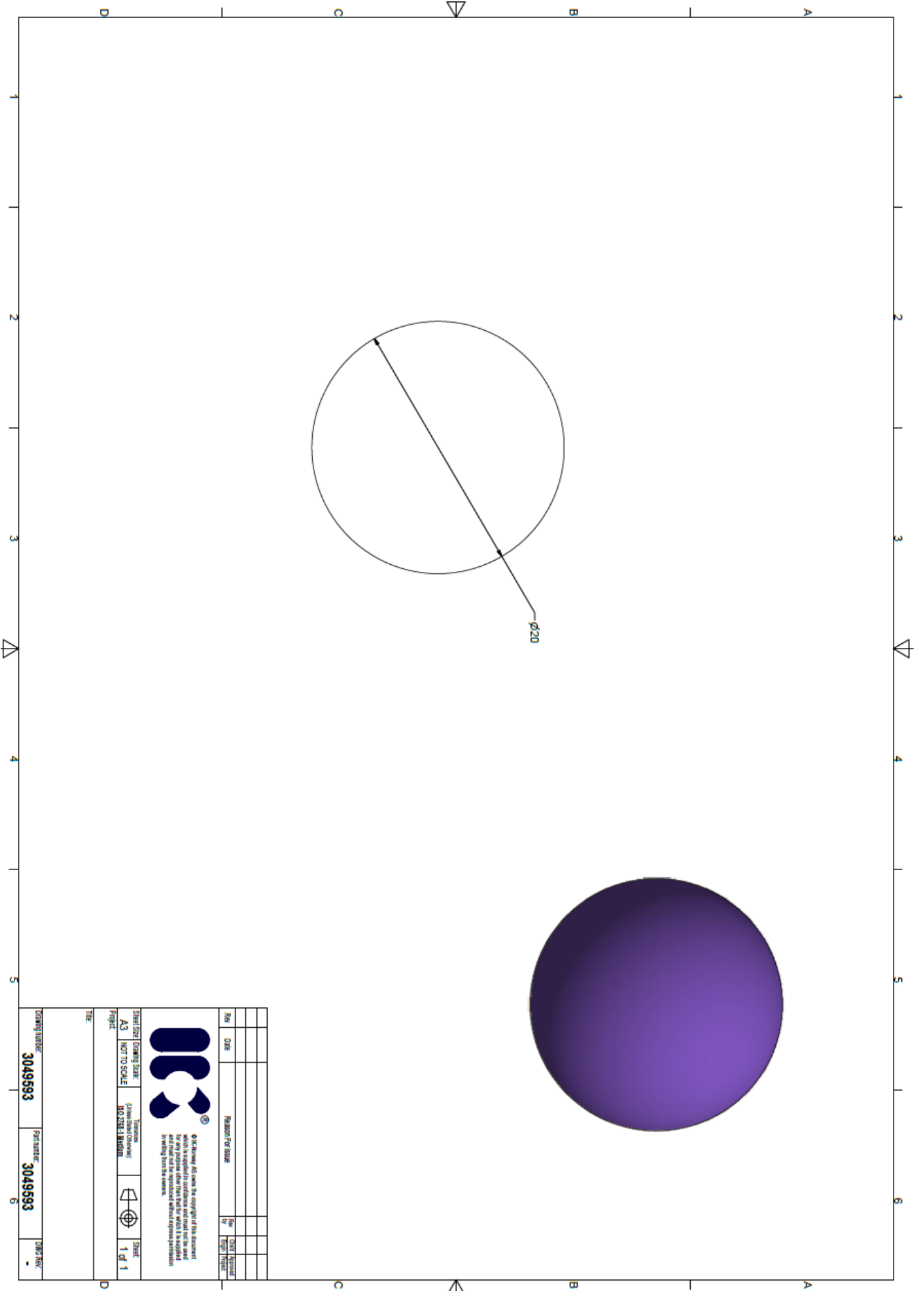


© All drawings are the copyright of this document. No part of this document may be reproduced, stored in a retrieval system, or transmitted in any form or by any means, electronic, mechanical, photocopying, recording, or by any information storage and retrieval system, without the prior written permission of the copyright owner.

SHEET SIZE / Drawing Scale:	A3 / NOT TO SCALE	Project:	MOJIBAH MASHRU'	Sheet:	1 of 1
Title:					

Drawing number:	3050410	Part number:	3050410	Drawn by:	
-----------------	---------	--------------	---------	-----------	--





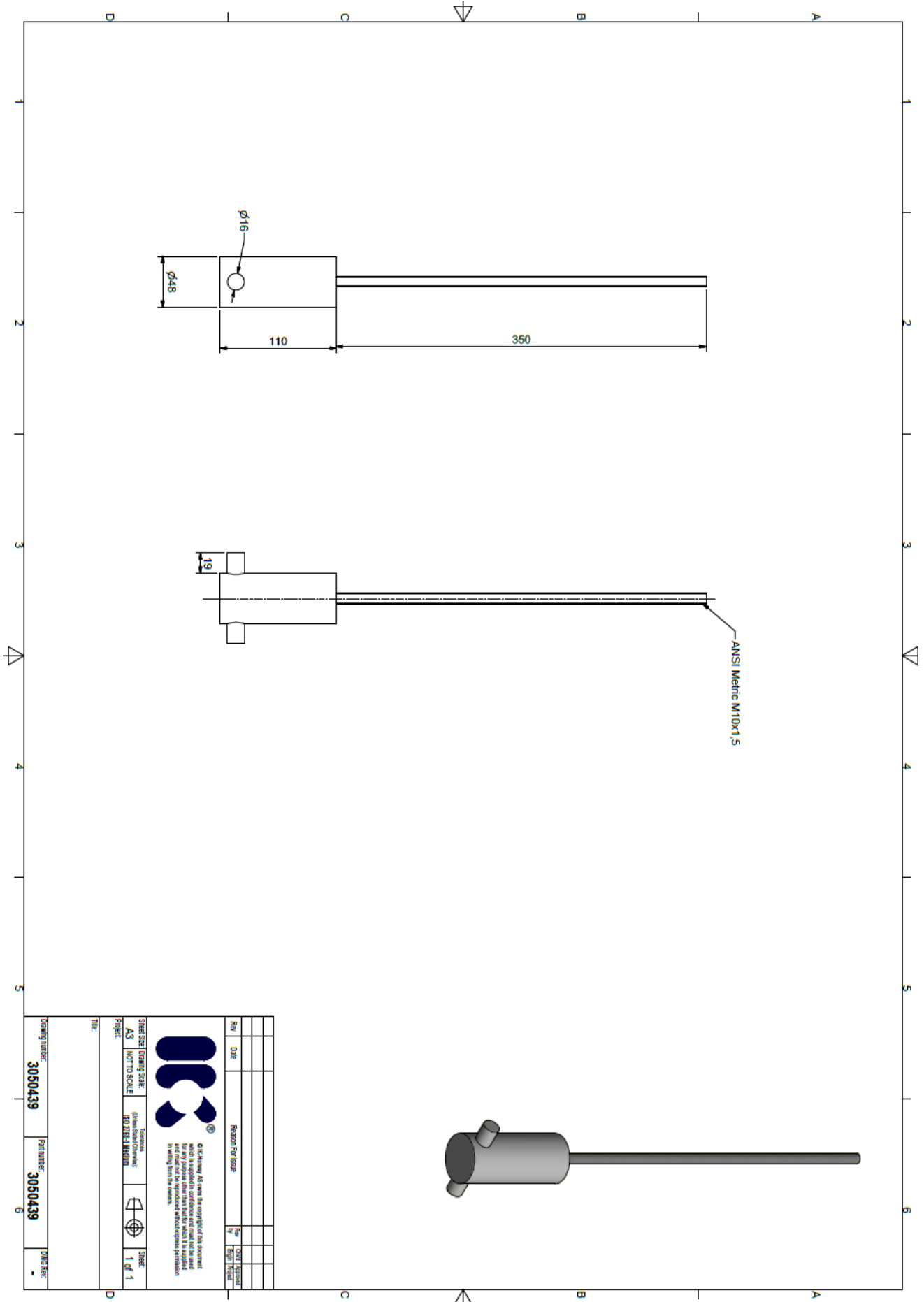
Rev	Date	Reason For Issue	Rev	Checked By



© D.C. Manning AS reserves the copyright of this document which is registered in accordance with the Copyright Act 1962. No part of this publication may be reproduced, stored in a retrieval system, or transmitted in any form or by any means, electronic, mechanical, photocopying, recording, or by any information storage and retrieval system, without express permission in writing from the owner.

**STREET SIZE DRAWING SCALE**  
 Project: **A3** NOT TO SCALE  
 Drawing Number: **3049593**  
 Title: **1 of 1**

Drawing number: **3049593** Part number: **3049593** Sheet: **1 of 1**



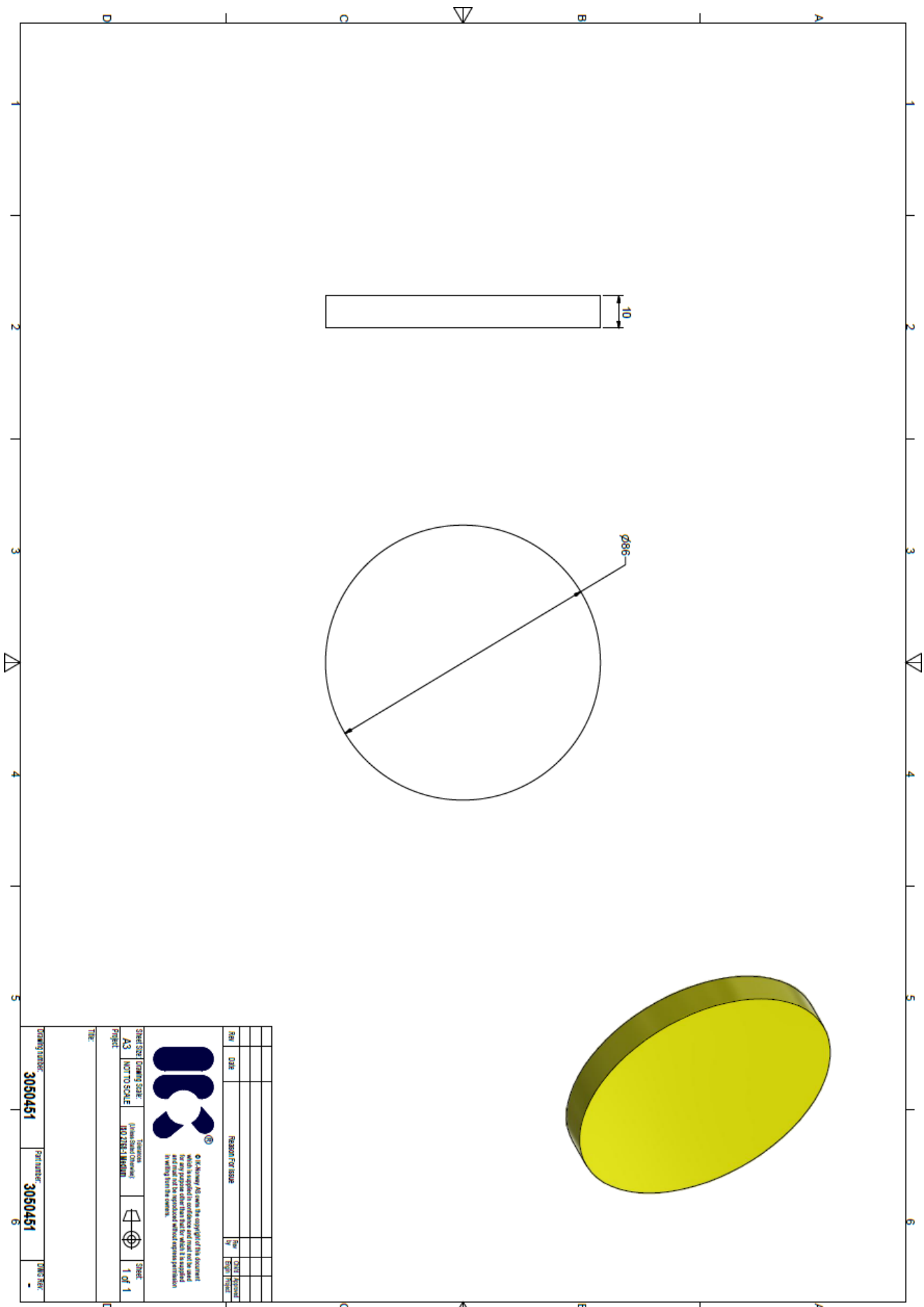
ANSI Metric M10x1.5



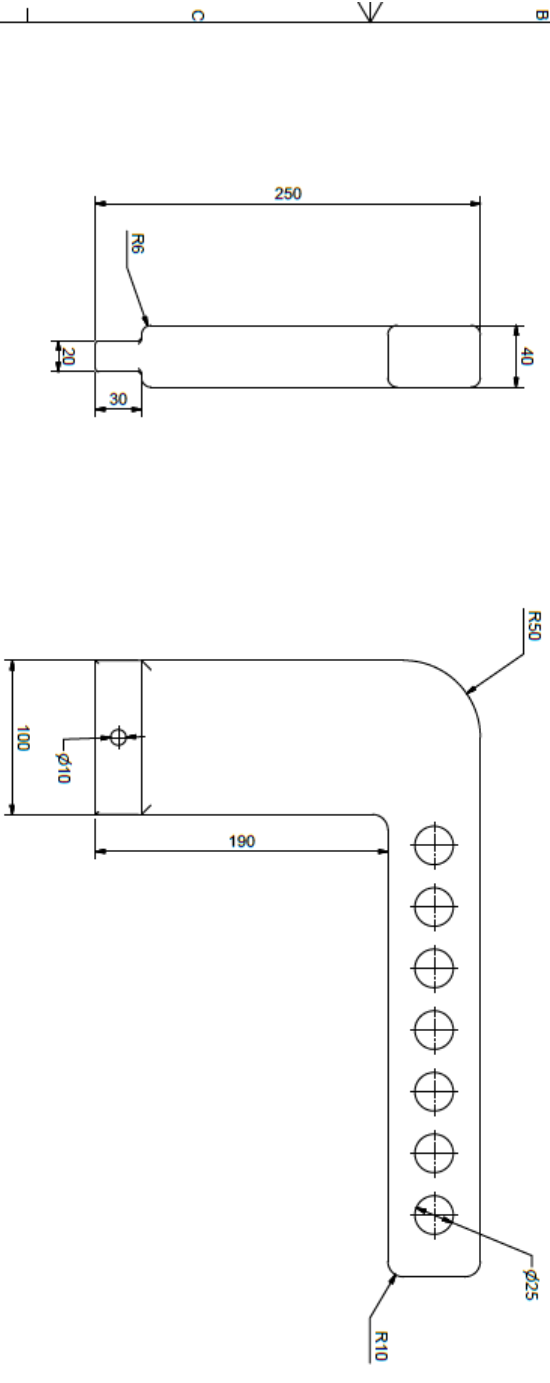
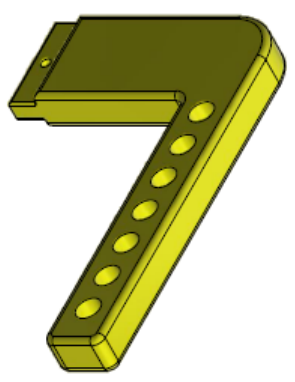
© Kichway AG owns the copyright of this document which is applied to confidence and must not be used or reproduced in any form without the written permission of Kichway AG. All rights reserved.

Rev	Date	Reason For Issue	By	CHK	APP

Standard	Forming State	Revision	Sheet
A3	NOT TO SCALE	NO ZONE I-MANUAL	1 of 1
Project		Title	
3050439		3050439	
Part number		Order Ref	
0		-	



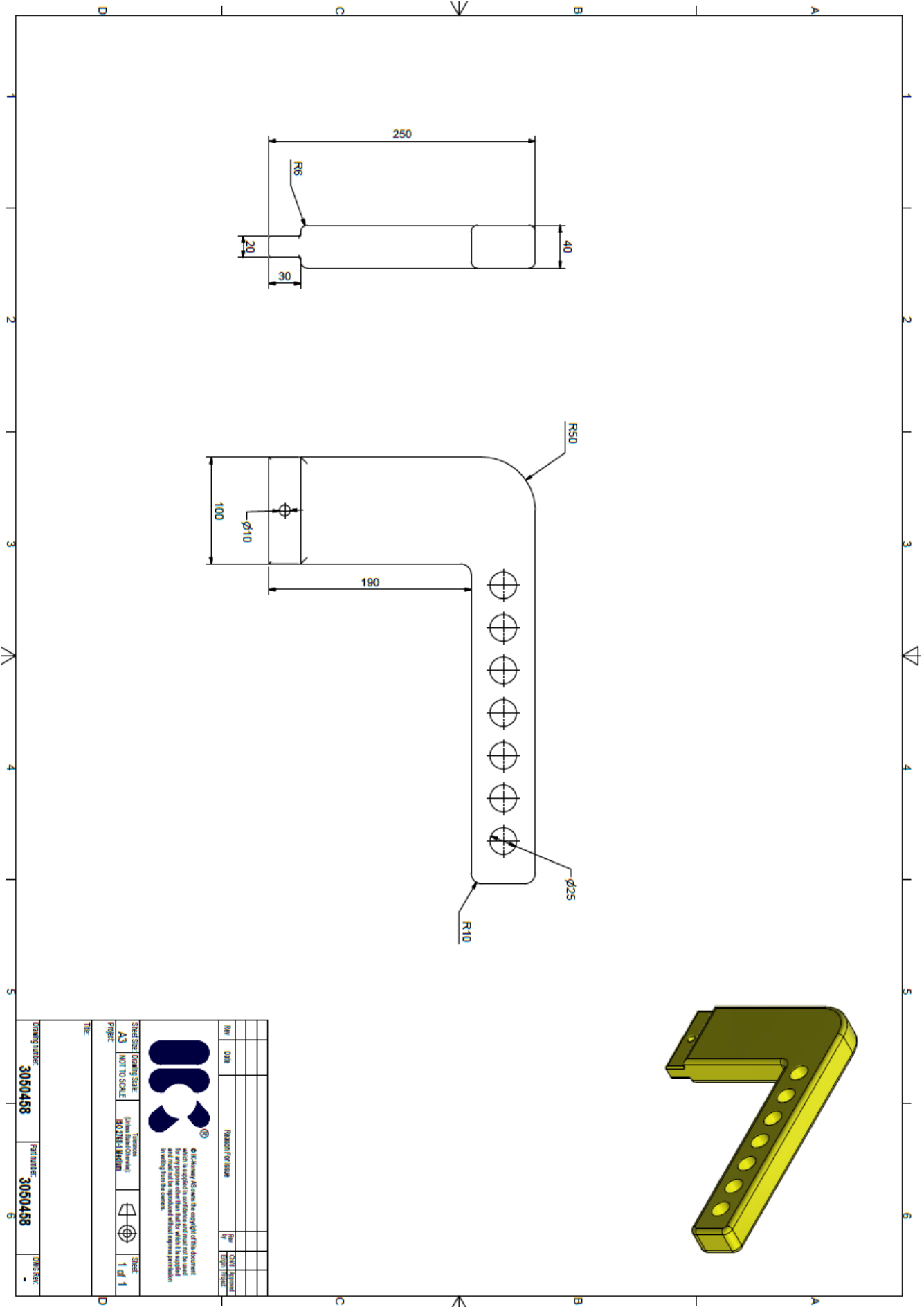
DRAWING NUMBER	3050451	REV NUMBER	3050451	DATE	-
<p><b>IK</b> ©</p> <p>As a company we own the copyright of this document which is issued in confidence and may not be used for any purpose other than that for which it is supplied without the express written and signed permission in writing from the company.</p>					
SHEET SIZE: Drawing Scale:		Drawing Standard:		SHEET	
A3 NOT TO SCALE		ISO/DIN/BSI/ASME		1 of 1	
<p>Project: _____</p> <p>Title: _____</p>					
Rev	DATE	Reason for issue	Rev	DATE	Reason for issue



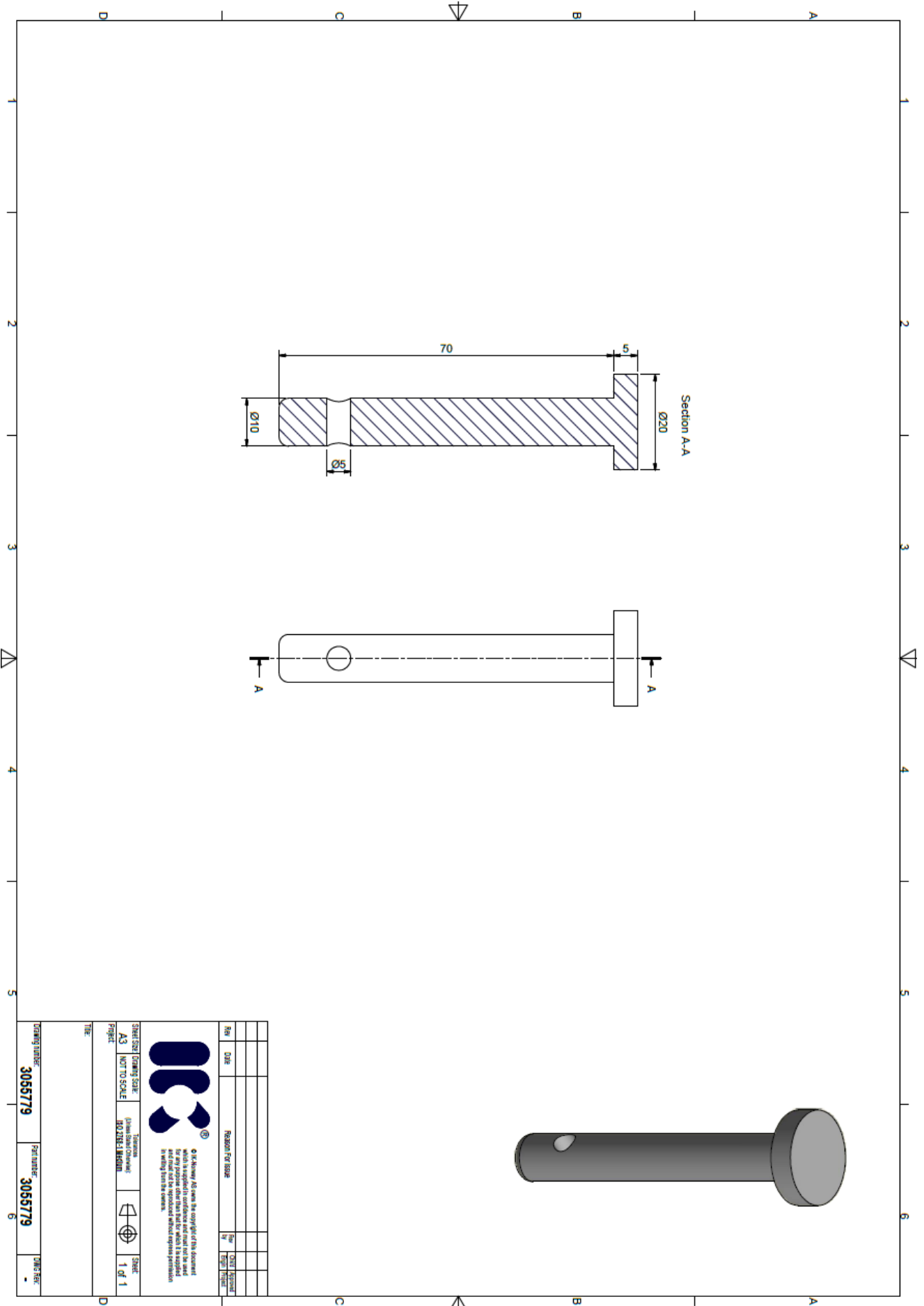
© De Aluwing AG aanvaardt de aansprakelijkheid van het document, welke is vervaardigd in overeenstemming met de specificaties, welke zijn opgegeven in de tekening en welke zijn toegepast in het vervaardigen van de afgebeelde onderdelen.

Sheet Size Drawing Scale	Dimensions	Sheet
A3	1:1	1 of 1
Project	HOOFDSTUK 10	
Title:		

Drawing Number	Part Number	Drawn Rev.
3050458	3050458	-







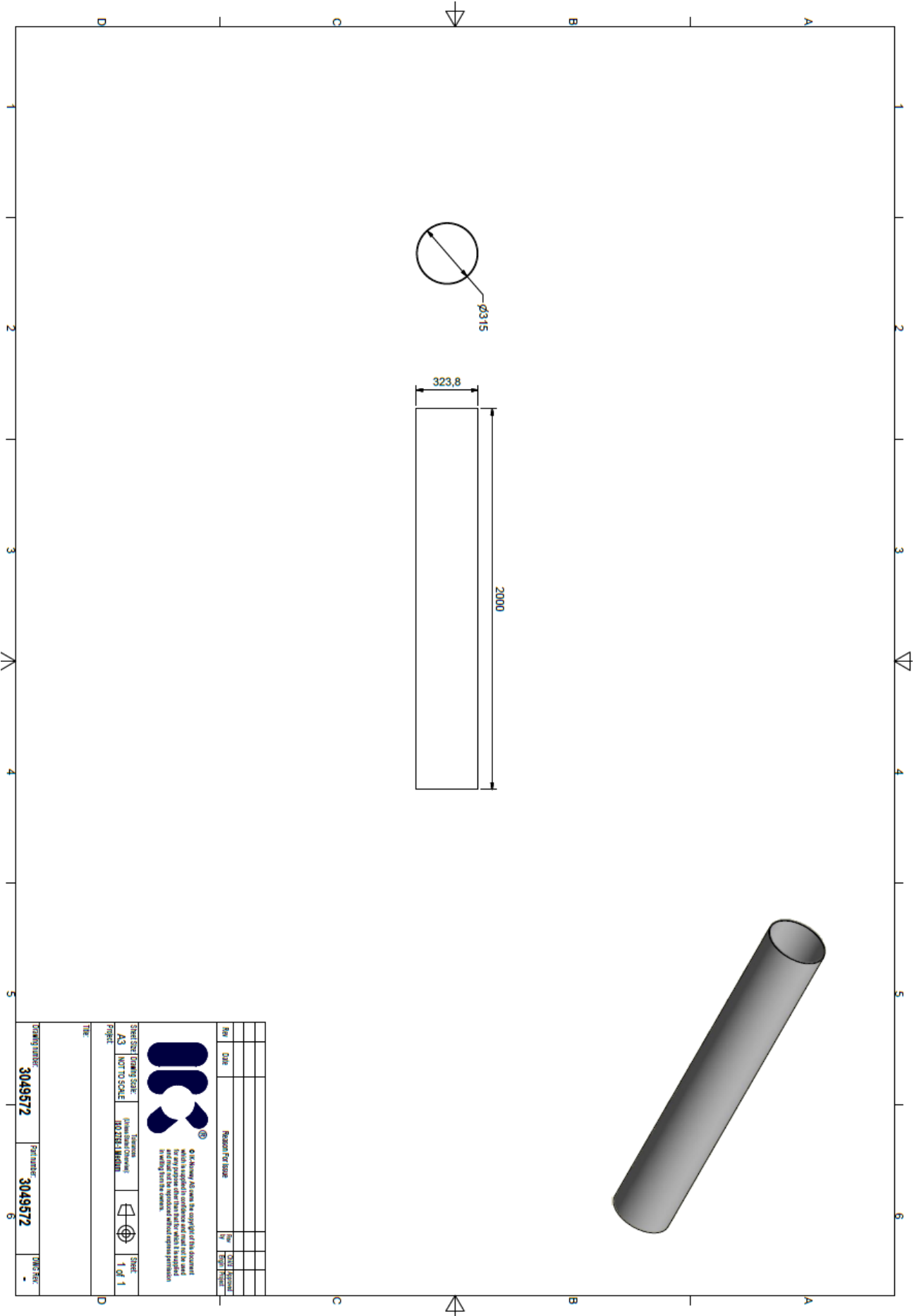
Rev	Date	Reason for Issue	By	Checked	Approved



© Mühürler, firmaya ait olup, diğer firmaların kullanması yasaktır. Herhangi bir amaçla kullanılmadan önce yazılı izin alınmalıdır. Herhangi bir amaçla kullanılmadan önce yazılı izin alınmalıdır.

SHEET/DRAWING SCALE:	1/1	SHEET
A3	NOT TO SCALE	1 OF 1
Project:	NOZEL SİLMENİ	
Title:		

DRAWING NUMBER:	3095779	Part number:	3095779	DATE:	-
-----------------	---------	--------------	---------	-------	---



REV	DATE	REASON FOR ISSUE	BY	CHKD



© All Rights Reserved. All rights reserved. This document is the property of the company and its contents are confidential. Any reproduction or distribution of this document without express permission is strictly prohibited.

Sheet Size	Drawing Scale	Revision	Sheet
A3	1:1	1	1 of 1
Project	NO. 3049572		
Title			

Drawing Number	3049572	Part Number	3049572	Unit's Name	-
----------------	---------	-------------	---------	-------------	---

## **APPENDIX D – Test-rig procedure for spherical indentation and mechanical wedge lock force**

## Executive summary:

This Appendix describes the installation and testing manual for the PRT test rig and equipment related to the testing. The document contains all the necessary steps and guidelines for installation and operation that involves the testing.

This Procedure includes the following steps with equipment to be installed/operate and maintain

- Pre-Start checklist
- Required Equipment/Parts
- Installation of Test-rig
- Operation of Test-rig
- Disassembly of Test-rig

## Required Equipment/Parts:

Item	Description	Qty.	Comments
1	Cylinder	1	
2	Pipe	1	
3	Steel balls	28/26	
4	Steel plate	1	
5	Set-pipe	1	
6	Cone Calmax	6	Six cones with an angle of: 3°,4°,5°,6°,8° and 10°
7	Cone 34CrNiMo6	1	Cone-angle of 5 degrees
8	Studbolt M16	1	
9	Hex nut M16	2	
10	M12 bolts	2	

For technical view, part list and description for the different parts, see Appendix B and C. Appendix G and H contains pictures of the different parts in the test rig.

Item	Description	Qty.	Comments
1	Press machine	1	
2	Manometer	2	
3	Hydraulic pump	1	
4	Computer	1	

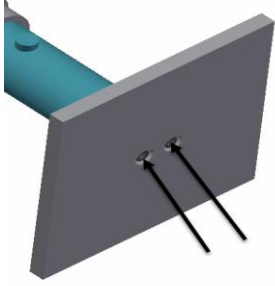
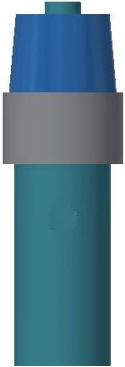
Item	Description	Qty.	Comments
5	Transmitter	1	
6	Manifold	1	
7	Digital measuring tool	1	

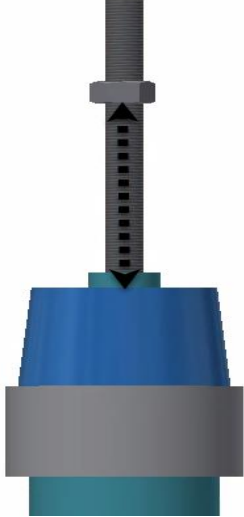

See Appendix B for pictures of the equipment used in relation with completion of the testing and measuring tools for dent depth.

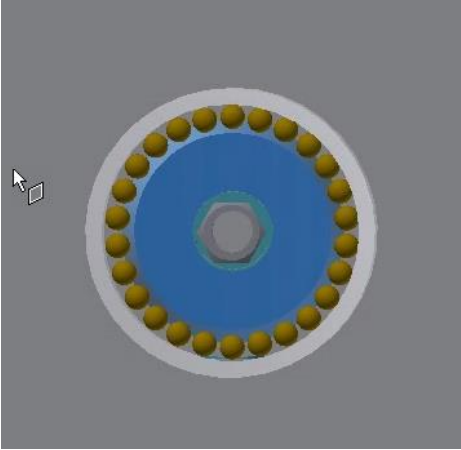
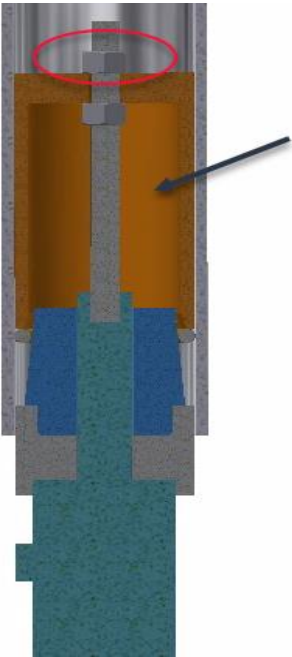

### Pre-start Checklist:

Activity	Description	Acceptance Criteria	Signature
<b>1</b>	<b><u>Perform a visual check of tool</u></b> a) Check for transport damages. b) Check hydraulic lines and fittings c) Etc. etc.	No damage	
<b>2</b>	Tool Box talk / SJA performed	Signature	
<b>3</b>	Check all documents	Procedure approved	
<b>4</b>	Define roles/contact persons		
<b>5</b>	Verify that operation area is prepared for operation		

Part 1 – Test-rig

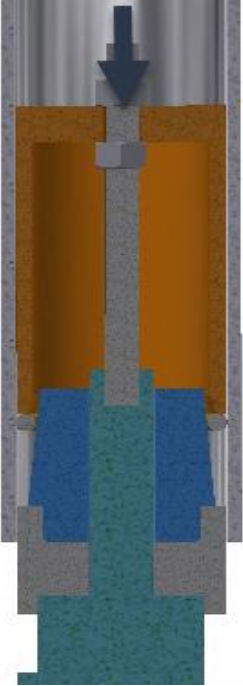

Step	Description/Pictures	Acceptance Criteria if Applicable	Comments
1	<p>Place the cylinder on top of the plate, and torque the M12 bolts to 20 Nm</p> 		
2	<p>Install the Cone on top of the cylinder</p> 		

Step	Description/Pictures	Acceptance Criteria if Applicable	Comments
3	<p>Insert the studbolt on the cylinder and screw a hex nut on top of the bolt. The distance shall be around 170 mm.</p> 		
4	<p>Place the pipe at the desired height, approximately 270 mm</p> 		

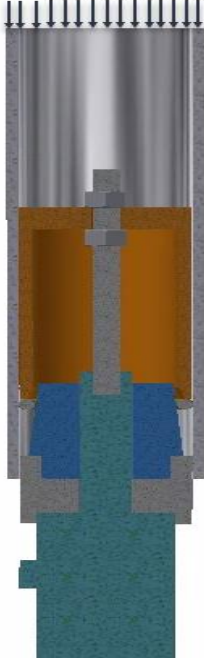
Step	Description/Pictures	Acceptance Criteria if Applicable	Comments
5	<p>Drop the steel ball in between the cone and the pipe.</p> 		
6	<p>Insert the set-pipe and screw a hex nut on top of the pipe.</p> 		
<p>7</p> 	<p>Make sure that all the parts are aligned and positioned. Make sure that the distance between the pipe and the hydraulic input port on the cylinder is satisfied.</p>		



Part 2 – Apply pressure on the set-pipe.

Step	Description/Pictures	Acceptance Criteria if Applicable	Comments
1	<p>Apply pressure into the cylinder which make a force on the set-pipe. The pressure shall be set to 4 MPa.</p> 		<p>Check that the pressure is stable. Note down the set-pressure.</p>
2	 <p>Verify that all the parts are still aligned. Check travel distance of the steel balls. Inspect the behaviour of the different parts.</p>		

Part 3 – Completion of test – Apply load on pipe



Step	Description/Pictures	Acceptance Criteria if Applicable	Comments
1	<p>Apply a pre-decided pressure on the pipe.</p> <p>Note down the pressure and the pipe travel distance.</p> 		<p>Follow up the pressure drop in the cylinder.</p> <p>(keep a steady set pressure)</p>
2	<p>Continue with step 1 until visible dents can be seen on the test-rig or that the pipe starts to slide/travel without any load increase.</p> <p>Measure the maximum reached pressure just before failure.</p>		

## Checklist in between each test

Write down all the critical parameters. This must be written down each time the test is performed.

- Set force
- Travel distance for set-pipe
- Travel distance for pipe
- Maximum load on pipeline
- Angle( $\alpha$ )
- Steel ball size and number
- Magnitude of force when deformation starts in pipeline

## Disassembly of Test rig

Step	Description/Pictures	Acceptance Criteria if Applicable	Comments
1	Set the hydraulic press in its initial position, so that the pipe has no applied force on it.		
2	Set the cylinder in its top position.  		
3	Check that nothing is pressurized or in tension.  		
4	Start disassembly all the parts.		

## Post Installation:

Activity	Description	Check/Comments
1	Inspect the tooling for any damage.	Especially the cone, inside of the pipe and the steel ball itself.
2	Clean all the parts and lubricate where applicable	

Table: Post Installation / Operation

**APPENDIX E - Test rig procedure for testing the sealing properties of bearing steel balls casted in polyurethane.**

## Executive summary:

This Appendix describes the installation and testing manual for the PRT test rig and equipment related to the testing. The document contains all the necessary steps and guidelines for installation and operation that involves the testing.

This Procedure includes the following steps with equipment to be installed/operate and maintain

- Pre-Start checklist
- Required Equipment/Parts
- Installation of Test-rig
- Operation of Test-rig
- Disassembly of Test-rig

## Required Equipment/Parts:

Item	Description	Qty.	Comments
1	Cylinder	1	
2	Pipe	1	
3	Bearing balls casted in PUR	1	Shore 90 A
4	Bearing balls casted in PUR	1	Shore 70 A
5	Steel plate	1	
6	Set-pipe	1	
7	Cone	1	Six cones with an angle of: 3°,4°,5°,6°,8° and 10°
8	Studbolt M16	1	
9	Hex nut M16	2	
10	M12 bolts	2	

For technical view, part list and description for the different parts, see Appendix C. Appendix H contains pictures of the different parts in the test rig.

Item	Description	Qty.	Comments
1	Press machine	1	
2	Manometer	2	
3	Hydraulic pump	1	
4	Computer	1	
5	Transmitter	1	
6	Manifold	1	
7	Digital measuring tool	1	

See Appendix H for pictures of the equipment used in relation with completion of the testing and measuring tools for dent depth.

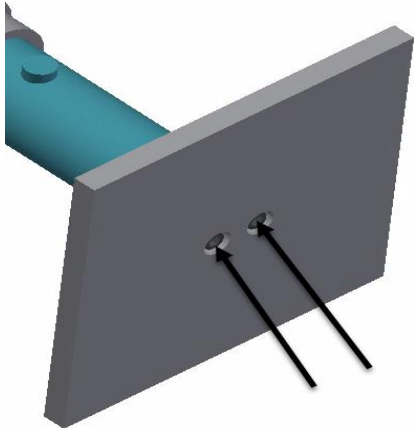
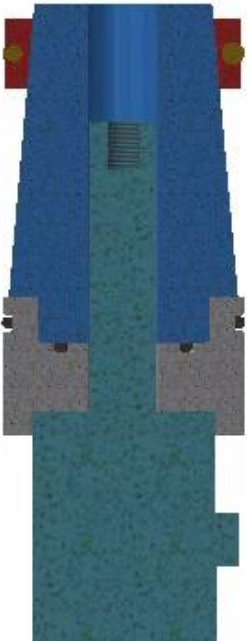
## Pre-start Checklist

Activity	Description	Acceptance Criteria	Signature
1	<p><b><u>Perform a visual check of tool</u></b></p> <ul style="list-style-type: none"> <li>d) Check for transport damages.</li> <li>e) Check hydraulic lines and fittings</li> <li>f) Etc. etc.</li> </ul>	No damage	
2	Tool Box talk / SJA performed	Signature	
3	Check all documents	Procedure approved	
4	Define roles/contact persons		
5	Verify that operation area is prepared for operation		

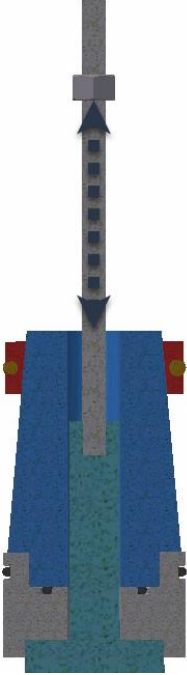
# Installation of Test-rig

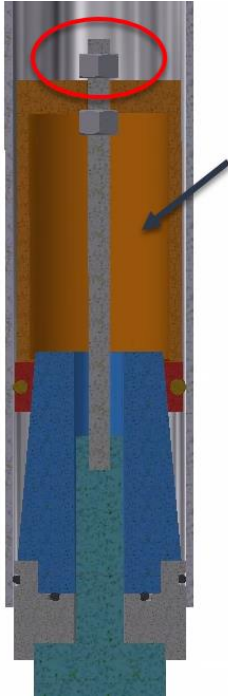

This procedure only relates to the tooling and equipment included in this Installation and Operation Manual.

## Part 1 – Test-rig

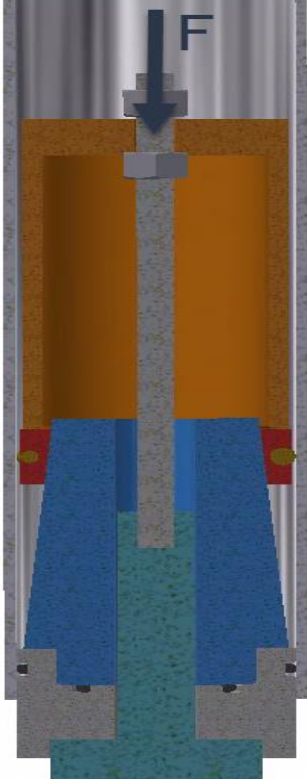

Step	Description/Pictures	Acceptance Criteria if Applicable	Comments
1	<p>Place the cylinder on top of the plate, and torque the M12 bolts to 20 Nm</p> 		
2	<p>Install the Cone on top of the cylinder including all the packers.</p> 		



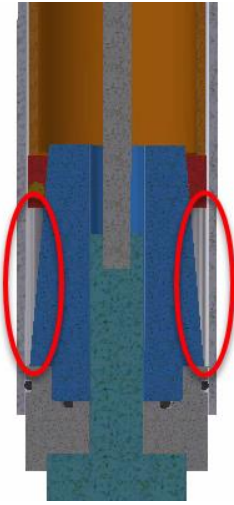
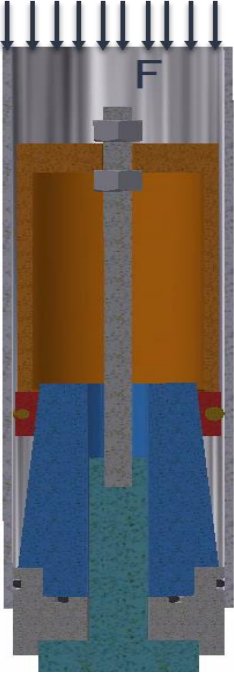
Step	Description/Pictures	Acceptance Criteria if Applicable	Comments
3	<p>Insert the studbolt on the cylinder and screw a hex nut on top of the bolt. The distance shall be around 170 mm.</p> 		
4	<p>Place the pipe at the desired height, approximately 270 mm</p> 		


Step	Description/Pictures	Acceptance Criteria if Applicable	Comments
5	<p>Insert the set-pipe and screw a hex nut on top of the pipe.</p> 		
<p>6</p> 	<p>Make sure that all the parts are aligned and positioned. Make sure that the distance between the pipe and the hydraulic input port on the cylinder is satisfied.</p>		

## Part 2 – Apply pressure on the set-pipe.

Step	Description/Pictures	Acceptance Criteria if Applicable	Comments
1	<p>Apply pressure into the cylinder which make a force on the set-pipe. The pressure shall be set to X MPa. Which is the indentation pressure.</p> 		<p>Check that the pressure is stable. Note down the set-pressure.</p>
2	 <p>Verify that all the parts are still aligned. Check travel distance of the steel balls. Inspect the behaviour of the different parts.</p>		

## Part 3 – Completion of test – Apply load on pipe

Step	Description/Pictures	Acceptance Criteria if Applicable	Comments
1	<p>Apply pressure in the marked area. The empty volume between the “kon_hylse_del 1 og 2” and “rør_!” shall be pressurized with water to xx bar.</p> 		Keep a steady pressure.
2	<p>Apply a pre-decided pressure on the pipe. Note down the pressure and the pipe travel distance.</p> 		<p>Follow up the pressure drop in the cylinder.  (keep a steady set pressure)</p>
2	<p>From the previous test, it is known what the mechanical properties are.</p>		

Step	Description/Pictures	Acceptance Criteria if Applicable	Comments
	<p>Repeat step 1 or step 2 until the packers don't hold the pressure inserted.</p> <p>Measure the maximum reached pressure just before failure.</p> <p>Note down each time you increase the pressure on the packer, the pipeline or the volume between the "kon_hylse_del 1 og 2" and "rør!".</p>		

## Checklist in between each test

There are six different cones with different angles that is going to be evaluated in this test. All the critical parameters shall be written down. This must be written down each time the test is performed.

- Set force
- Travel distance for set-pipe
- Travel distance for pipe
- Maximum load on pipeline
- Angle( $\alpha$ )
- Steel ball size and number
- Magnitude of force when deformation starts in pipeline
- Shore value or the packer
- Sealing properties of the packer, magnitude of pressure it can withstand.

## Post Installation:

Activity	Description	Check/Comments
3	Inspect the tooling for any damage.	Especially the cone, inside of the pipe, the steel ball itself and the polyurethane.
4	Clean all the parts and lubricate where applicable	

## **APPENDIX F - Cylinder Set-Pressure graphs**

# Cone with angle of 3 degrees – 5,10,15,30 and 50 bar



**CUSTOMER INFORMATION:**

Test certificate: 3deg\_5bar-7

Certificate date: 28.03.2019

Customer ref: 3deg\_5bar

Our ref: 3deg\_5bar

Test performed by:

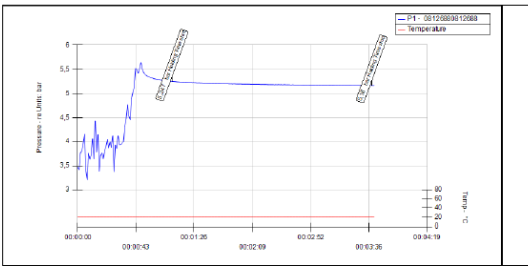
**OBJECT INFORMATION:**

Object description: Working pressure:

Serial number: Test pressure:

Test fluid: Max drop value:

Test name	Test start	Test stop	Drop	Test time	00:02:28	(28/03/2019 13:36:38)
Holding Time	Pressure: 5,247	5,16	0,09 (1,72 %)	Transmitter (Range)	P1 - 0812688 0812688 ( 400 Bar)	
	Temperature: 20,1	20,1	0 °C	Calibration date	22/05/2018 13:00:00	



Comments: \_\_\_\_\_

Signature: \_\_\_\_\_



**CUSTOMER INFORMATION:**

Test certificate: 3deg\_10bar-6

Certificate date: 28.03.2019

Customer ref: 3deg\_10bar

Our ref: 3deg\_10bar

Test performed by:

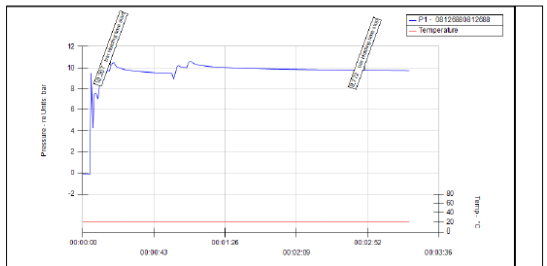
**OBJECT INFORMATION:**

Object description: Working pressure:

Serial number: Test pressure:

Test fluid: Max drop value:

Test name	Test start	Test stop	Drop	Test time	00:02:34	(28/03/2019 13:07:38)
Holding time	Pressure: 10,207	9,772	0,44 (4,31 %)	Transmitter (Range)	P1 - 0812688 0812688 ( 400 Bar)	
	Temperature: 19,9	19,9	0 °C	Calibration date	22/05/2018 13:00:00	



Comments: \_\_\_\_\_

Signature: \_\_\_\_\_



**CUSTOMER INFORMATION:**

Test certificate: 3deg\_15bar-5

Certificate date: 27.03.2019

Customer ref: 3deg\_15bar

Our ref: 3deg\_15bar

Test performed by:

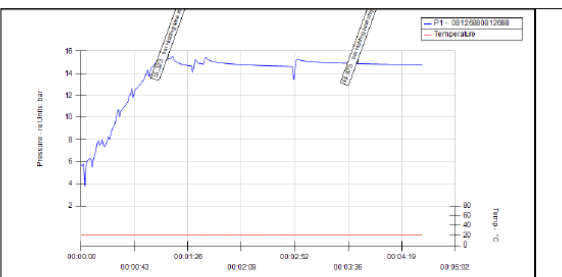
**OBJECT INFORMATION:**

Object description: Working pressure:

Serial number: Test pressure:

Test fluid: Max drop value:

Test name	Test start	Test stop	Drop	Test time	00:02:33	(27/03/2019 16:16:58)
Holding time	Pressure: 15,323	14,875	0,45 (2,94 %)	Transmitter (Range)	P1 - 0812688 0812688 ( 400 Bar)	
	Temperature: 20,3	20,3	0 °C	Calibration date	22/05/2018 13:00:00	



Comments: \_\_\_\_\_

Signature: \_\_\_\_\_



**CUSTOMER INFORMATION:**

Test certificate: 3deg\_30bar-4

Certificate date: 27.03.2019

Customer ref: 3deg\_30bar

Our ref: 3deg\_30bar

Test performed by:

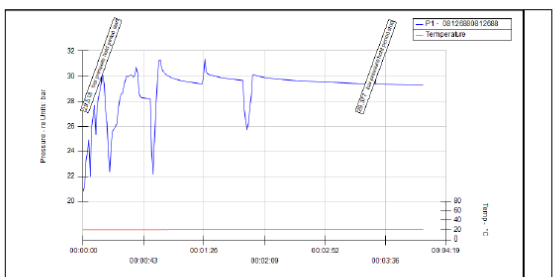
**OBJECT INFORMATION:**

Object description: Working pressure:

Serial number: Test pressure:

Test fluid: Max drop value:

Test name	Test start	Test stop	Drop	Test time	00:03:16	(27/03/2019 13:36:45)
pressure hold period	Pressure: 29,518	29,377	0,14 (0,47 %)	Transmitter (Range)	P1 - 0812688 0812688 ( 400 Bar)	
	Temperature: 19,6	19,7	-0,1 °C	Calibration date	22/05/2018 13:00:00	



Comments: \_\_\_\_\_

Signature: \_\_\_\_\_



CUSTOMER INFORMATION:

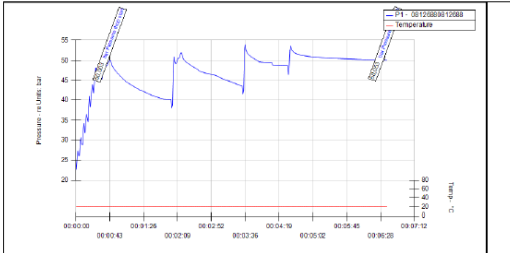
Empty box for customer information

Test certificate: 3deg\_50bar-3  
Certificate date: 26.03.2019  
Customer ref:  
Our ref: 3deg\_50bar  
Test performed by:

OBJECT INFORMATION:

Object description:  
Serial number:  
Test fluid:  
Working pressure:  
Test pressure:  
Max drop value:

Test name	Test start	Test stop	Drop	Test time	00:05:52	(26/03/2019 16:28:48)
Pressure drop	Pressure: 50,003	50,053	-0,05 (-0,1 %)	Transmitter (Range)	P1 - 0812688 0812688 ( 400 Bar)	
	Temperature: 20,4	20,4	0 °C	Calibration date	22/05/2018 13:00:00	



Comments:

Empty box for comments

Signature:

\_\_\_\_\_

# Cone with angle of 4 degrees – 7,5 , 10 , 12,5 , 17,5 and 25 bar



CUSTOMER INFORMATION:

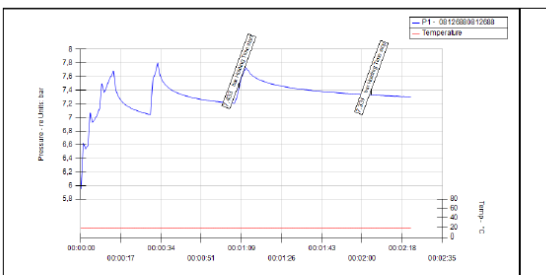
Empty box for customer information

Test certificate: 4deg\_7,5bar-9  
Certificate date: 01.04.2019  
Customer ref:  
Our ref: 4deg\_7,5bar  
Test performed by:

OBJECT INFORMATION:

Object description:  
Serial number:  
Test fluid:  
Working pressure:  
Test pressure:  
Max drop value:

Test name	Test start	Test stop	Drop	Test time	00:00:57	(01/04/2019 10:11:16)
Holding Time	Pressure: 7,433	7,331	0,1 (1,35 %)	Transmitter (Range)	P1 - 0812688 0812688 ( 400 Bar)	
	Temperature: 18,4	18,4	0 °C	Calibration date	22/05/2018 13:00:00	



Comments:

Empty box for comments

Signature:

\_\_\_\_\_



CUSTOMER INFORMATION:

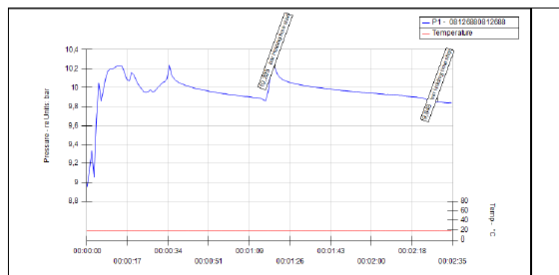
Empty box for customer information

Test certificate: 4deg\_10bar-10  
Certificate date: 01.04.2019  
Customer ref:  
Our ref: 4deg\_10bar  
Test performed by:

OBJECT INFORMATION:

Object description:  
Serial number:  
Test fluid:  
Working pressure:  
Test pressure:  
Max drop value:

Test name	Test start	Test stop	Drop	Test time	00:01:09	(01/04/2019 10:46:14)
Holding time	Pressure: 10,205	9,848	0,36 (3,53 %)	Transmitter (Range)	P1 - 0812688 0812688 ( 400 Bar)	
	Temperature: 18,6	18,6	0 °C	Calibration date	22/05/2018 13:00:00	



Comments:

Empty box for comments

Signature:

\_\_\_\_\_





CUSTOMER INFORMATION:

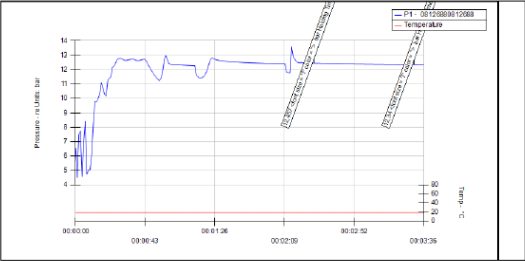
Empty box for customer information

Test certificate: 4deg\_12,5Bar-11

Certificate date: 01.04.2019  
Customer ref:  
Our ref: 4deg\_12,5Bar  
Test performed by:

OBJECT INFORMATION:

Object description:  
Serial number:  
Test fluid:  
Working pressure:  
Test pressure:  
Max drop value:



Comments:

Signature:



CUSTOMER INFORMATION:

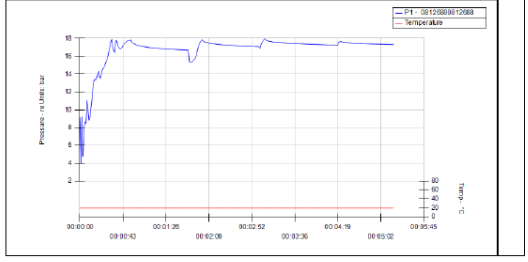
Empty box for customer information

Test certificate: 4deg\_17,5bar-12

Certificate date: 01.04.2019  
Customer ref:  
Our ref: 4deg\_17,5bar  
Test performed by:

OBJECT INFORMATION:

Object description:  
Serial number:  
Test fluid:  
Working pressure:  
Test pressure:  
Max drop value:



Comments:

Signature:



CUSTOMER INFORMATION:

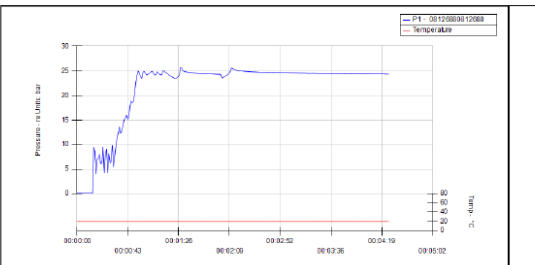
Empty box for customer information

Test certificate: 4deg\_25bar-13

Certificate date: 01.04.2019  
Customer ref:  
Our ref: 4deg\_25bar  
Test performed by:

OBJECT INFORMATION:

Object description:  
Serial number:  
Test fluid:  
Working pressure:  
Test pressure:  
Max drop value:



Comments:

Signature:

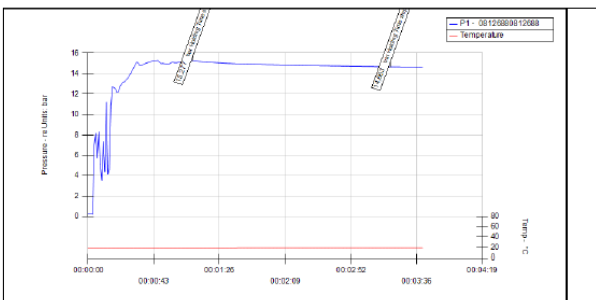
# Cone with angle of 10 degrees – 15, 25 and 35 bar



**CUSTOMER INFORMATION:**  
 Test certificate: 10deg\_15bar-14  
 Certificate date: 02.04.2019  
 Customer ref:  
 Our ref: 10deg\_15bar  
 Test performed by:

**OBJECT INFORMATION:**  
 Object description: Working pressure:  
 Serial number: Test pressure:  
 Test fluid: Max drop value:

Test name	Test start	Test stop	Drop	Test time	00:02:10	(02/04/2019 09:38:38)
Holding time 1	Pressure: 15,277	14,663	0,61 (3,99 %)	Transmitter (Range)	P1 - 0812688 0812688 ( 400 Bar)	P1 - 0812688 0812688 ( 400 Bar)
	Temperature: 18,7	18,8	-0,1 °C	Calibration date	22/05/2018 13:00:00	



Comments: Signature: \_\_\_\_\_

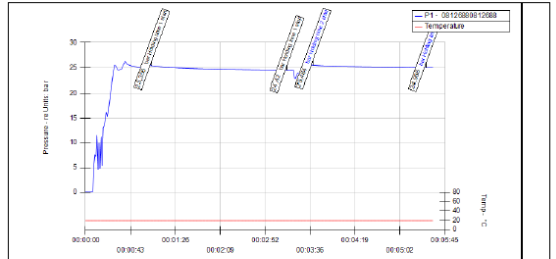


**CUSTOMER INFORMATION:**  
 Test certificate: 10deg\_25bar-15  
 Certificate date: 02.04.2019  
 Customer ref:  
 Our ref: 10deg\_25bar  
 Test performed by:

**OBJECT INFORMATION:**  
 Object description: Working pressure:  
 Serial number: Test pressure:  
 Test fluid: Max drop value:

Test name	Test start	Test stop	Drop	Test time	00:02:10	(02/04/2019 10:18:39)
Holding time 1	Pressure: 25,356	24,42	0,94 (3,71 %)	Transmitter (Range)	P1 - 0812688 0812688 ( 400 Bar)	P1 - 0812688 0812688 ( 400 Bar)
	Temperature: 19,2	19,2	0 °C	Calibration date	22/05/2018 13:00:00	

Test name	Test start	Test stop	Drop	Test time	00:01:49	(02/04/2019 10:18:39)
Holding time 2	Pressure: 25,454	24,956	0,51 (2 %)	Transmitter (Range)	P1 - 0812688 0812688 ( 400 Bar)	P1 - 0812688 0812688 ( 400 Bar)
	Temperature: 19,2	19,2	0 °C	Calibration date	22/05/2018 13:00:00	



Comments: Signature: \_\_\_\_\_

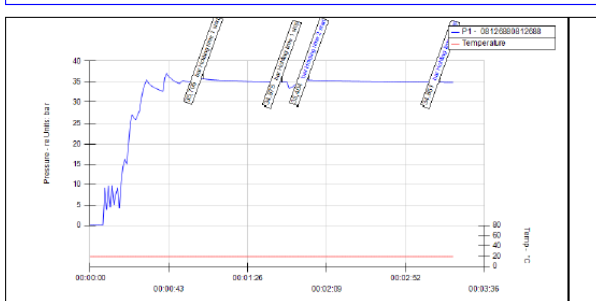


**CUSTOMER INFORMATION:**  
 Test certificate: 10deg\_35bar-16  
 Certificate date: 02.04.2019  
 Customer ref:  
 Our ref: 10deg\_35bar  
 Test performed by:

**OBJECT INFORMATION:**  
 Object description: Working pressure:  
 Serial number: Test pressure:  
 Test fluid: Max drop value:

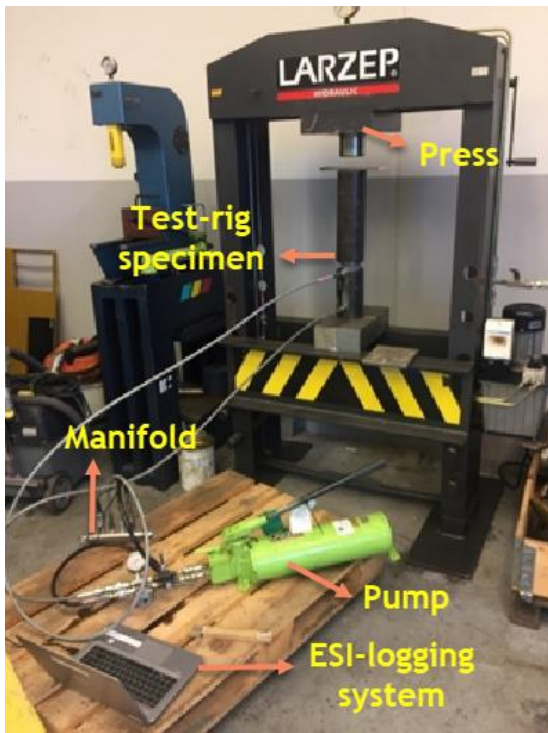
Test name	Test start	Test stop	Drop	Test time	00:00:43	(02/04/2019 10:36:24)
Holding time 1	Pressure: 35,705	34,875	0,83 (2,32 %)	Transmitter (Range)	P1 - 0812688 0812688 ( 400 Bar)	P1 - 0812688 0812688 ( 400 Bar)
	Temperature: 19,3	19,3	0 °C	Calibration date	22/05/2018 13:00:00	

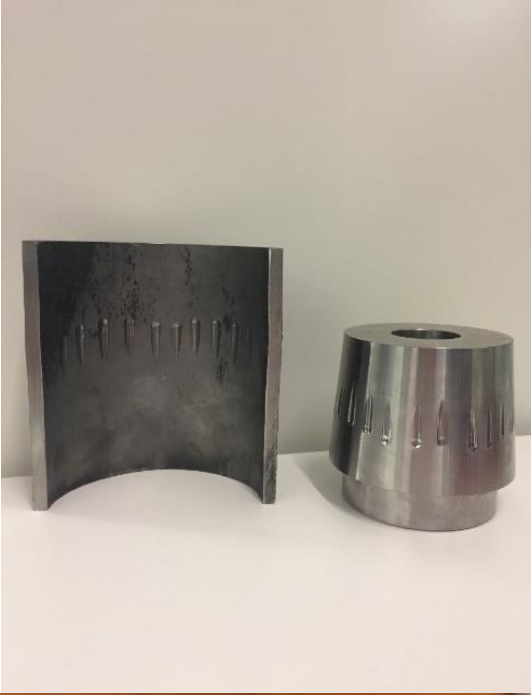
Test name	Test start	Test stop	Drop	Test time	00:01:12	(02/04/2019 10:36:24)
Holding time 2	Pressure: 35,404	34,851	0,55 (1,55 %)	Transmitter (Range)	P1 - 0812688 0812688 ( 400 Bar)	P1 - 0812688 0812688 ( 400 Bar)
	Temperature: 19,3	19,3	0 °C	Calibration date	22/05/2018 13:00:00	

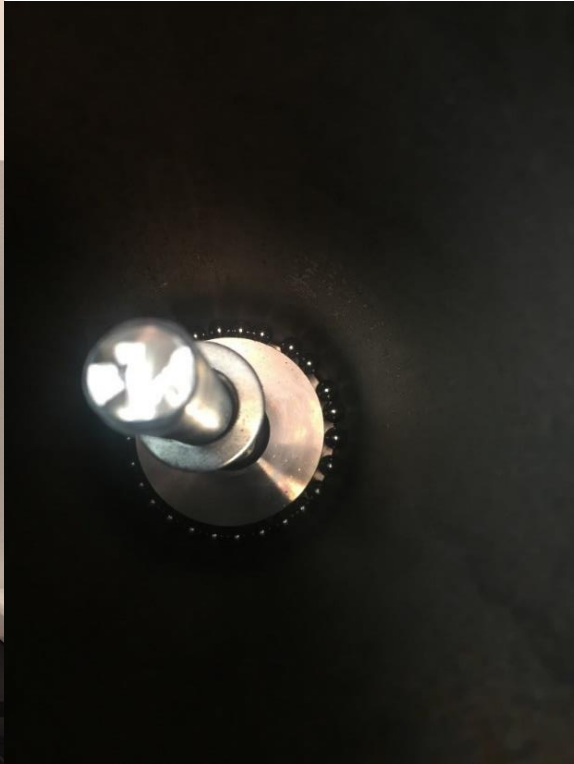


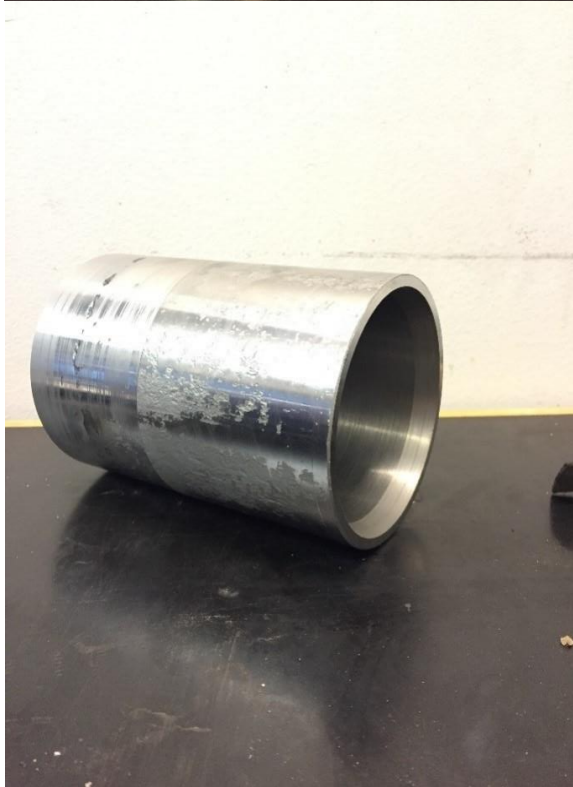
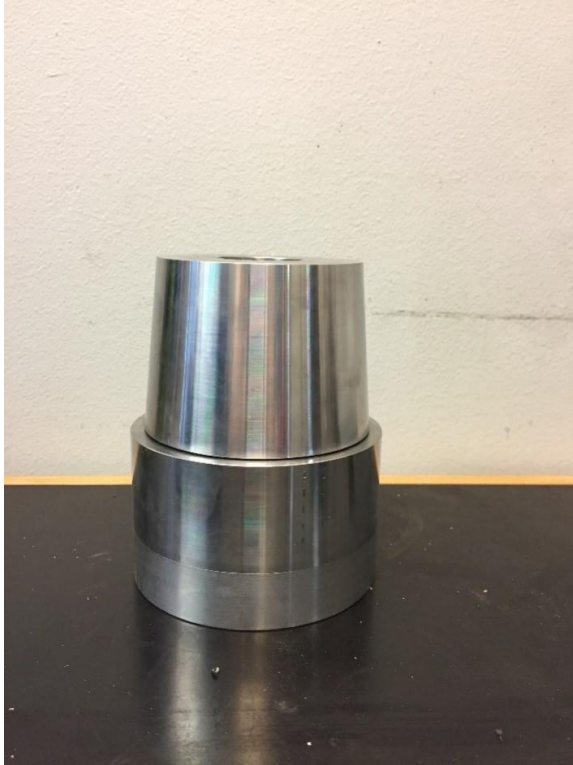
Comments: Signature: \_\_\_\_\_

## **APPENDIX G - Pictures of the first test-rig with a cone alloyed with 34CrNiMo6**





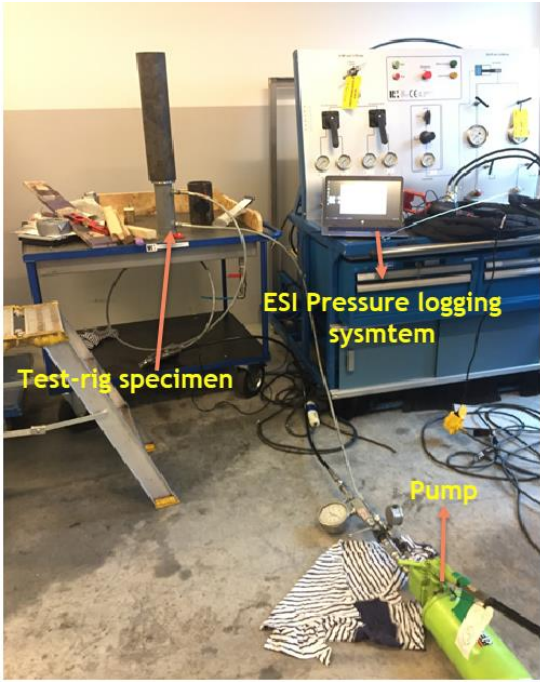


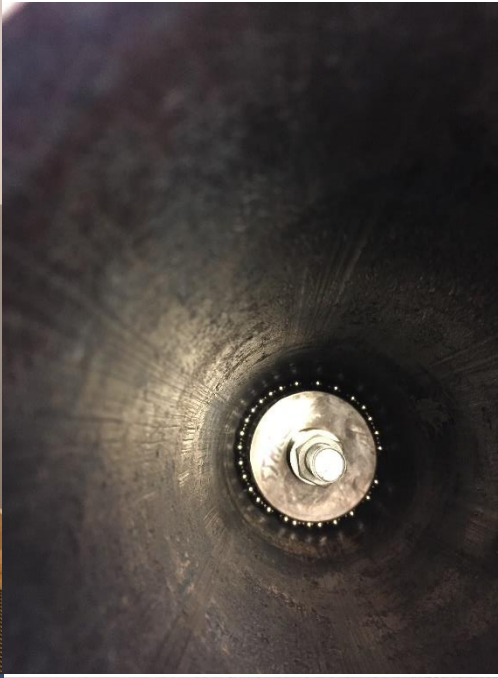


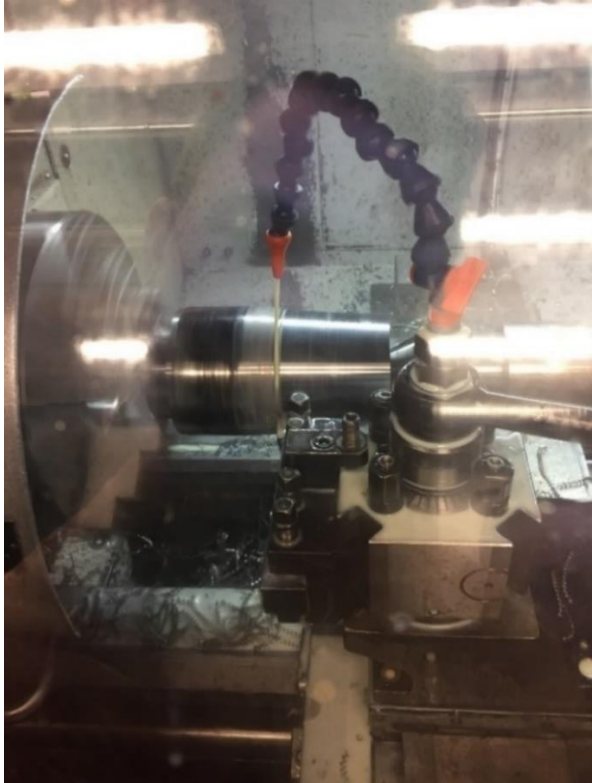




# **APPENDIX H - Test rig with a cone alloyed with Calmax Uddeholm**







# **APPENDIC I - Material Certificates**

Item #	Heat #	Code #	Item Text #1	Item Text #2
P-7	90799			



This document is electronically reproduced and is identical to the original. To be able to package this certificate, a digital signature had to be broken. Please contact your supplier if you need a copy with the signature intact.



**Inšpekčný certifikát**  
**Inspection certificate**  
**Abnahmeprüfzeugnis**  
**EN 10204:2004/3.1**

Číslo  
Number  
Number **10192/1/2019**

List č. - Sheet No. - Blatt Nr.: 1 / 3

Č. ext. obj. - External order No. - Externauftragsnummer:

**0M0187**

Číslo položky - Item number - Positionsnummer:

**7**

Identifikačné číslo - Ident. number - Ident. numer:

**1115009**

Č. obj. prij. - Consignee order No. - Auftrags Nr. des Empfängers:

**50058952**

Číslo zákazky výrobcu - Manufacturer's works order number  
- Werksauftragsnummer:

**VA 207609/1/1 2919021**

Číslo dopravného prostriedku - Transport No. - Waggon Nr.:

**TO092DX TO572YF**

Číslo ložného listu - Loading Bill No. - Ladebrief Nr.:

**38399**

Číslo aviza - Dispatch note - Lieferanzeige:

**3921170**

Výrobok - Product - Erzeugnis:

**Rúry oceľové bezožľavé, valcované za tepla - rúry pre tlakové účely**  
**Seamless hot finished steel tubes - Tubes for pressure purposes**  
**Nahtlose warmgewalzte Stahlrohre - Rohre für Druckbeanspruchungen**

Vonkajší priemer - Outside diameter  
- Aussendurchmesser: **114.300 mm**

Hrúbka steny - Wall thickness - Wanddicke: **4.500 mm**

Dĺžka - Length - Länge: **6000.000 mm [-0 +500] mm**

Počet kusov - Number of pieces - Stückzahl: **66**

Celková dĺžka - Total length - Gesamtlänge: **399.00 m**

Celková hmotnosť - Total mass  
- Gesamtmasse: **4918.00 kg**

Značka výrobcu - Symbol of the  
manufacturer's work - Herstellerzeichen



Pečiatka závodného zmalca - Works inspector's  
stamp - Stempel des Werks Sachverständigen



Material - Material - Material:

**L245 PSL1 EN ISO 3183 :2012, P235GH+N TC1 EN 10216-2 :2013**

Stav dodania - Products as delivered condition - Lieferzustand:

**Normalizačné tvárnenie - Normalizing forming - Normalisierendes Umformen**

Technické predpisy - Technical requirements/Demand - Prüfgrundlagen/Anforderungen:

**AD 2000-Merkblatt W4, EN 10216-2 :2013, EN ISO 3183 :2012, EN 10220 :2002, PED 2014/68/EU**

Číslo tváby Cast number Schmelz Nr.	Počet kusov Number of pieces Stückzahl	Dĺžka Length Länge [m]	Hmotnosť Mass Masse [kg]	Druh tavenia Steelmaking process Erschmelzungsart
<b>90799</b>	<b>66</b>	<b>399</b>	<b>4918</b>	<b>E</b>

E = elektrická oblúčková pec - electric arc furnace - elektrolichtbogenofen

Miesto v Podbrezovej  
Location Ort

Dátum 21.02.2019  
Date Datum

Závodný zmalca  
Works Inspector  
Der Werks Sachverständige

Ing. Čížmárik Miroslav

Železiarne Podbrezová a.s., Kolčinská 35, 976 81 Podbrezová, Slovak Republic  
Phone: +421 48 645 3031, Fax: +421 48 645 3032, www.znafraba.sk  
CIN: 31 562 141, VAT No: SK2020458704  
Bank account: Slovenská sporiteľňa, a.s., IIBAN: SK69 0900 0000 0000 7990 0006, SWIFT (BIC): GIBASKHX  
Registered in Register of Business Names in the District Court Bratislava District, Section 5a, Entry No. 69/5



*Čížmárik*

Druh ocele - Steel grade - Stahlsorte:

**úplne ukľudnená oceľ - fully killed steel - vollberuhigter Stahl**

Úprava povrchu - Surface protection - Oberflächenschutz:

**Bez úpravy povrchu (neolejované) - Without surface treatment (without oil) - Ohne Oberflächenbehandlung (ungeölt)**

Chemické zloženie - Chemical composition - Chemische Zusammensetzung:

Číslo tváby Cast number Schmelze Nr.		C	Mn	Si	P	S	Cu	Cr	Ni	Al	Mo	Ti	V	Nb	
		[%]	[%]	[%]	[%]	[%]	[%]	[%]	[%]	[%]	[%]	[%]	[%]	[%]	
		Predpis - Requirements - Vorschrift													
	min.	0.16	1.20	0.35	0.025	0.010	0.30	0.30	0.30	0.020	0.08	0.040	0.020	0.020	
	max.	0.16	1.20	0.35	0.025	0.010	0.30	0.30	0.30	0.020	0.08	0.040	0.020	0.020	
<b>90799</b>		<b>0.15</b>	<b>0.53</b>	<b>0.22</b>	<b>0.012</b>	<b>0.008</b>	<b>0.16</b>	<b>0.07</b>	<b>0.07</b>	<b>0.025</b>	<b>0.03</b>	<b>0.001</b>	<b>0.006</b>	<b>0.001</b>	

P-7

Výrobová analýza - Product analysis - Stäckanalyse:

Číslo tváby Cast number Schmelze Nr.		C	Mn	Si	P	S	Cu	Cr	Ni	Al	Mo	Ti	V	Nb
		[%]	[%]	[%]	[%]	[%]	[%]	[%]	[%]	[%]	[%]	[%]	[%]	[%]
<b>90799</b>	<b>1</b>	<b>0.16</b>	<b>0.53</b>	<b>0.23</b>	<b>0.012</b>	<b>0.009</b>	<b>0.16</b>	<b>0.07</b>	<b>0.07</b>	<b>0.025</b>	<b>0.03</b>	<b>0.002</b>	<b>0.007</b>	<b>0.001</b>
<b>90799</b>	<b>2</b>	<b>0.16</b>	<b>0.53</b>	<b>0.23</b>	<b>0.012</b>	<b>0.008</b>	<b>0.16</b>	<b>0.07</b>	<b>0.07</b>	<b>0.025</b>	<b>0.03</b>	<b>0.002</b>	<b>0.006</b>	<b>0.001</b>

Skúška ťahom - Tensile test - Zugversuch : 20 °C

C. Nr	Číslo tváby Cast number Schmelze Nr.	Vzorka č. Test No. Probe Nr.	Rozmery Dimensions Masse [mm]	Směr odberu vzorky Direction of the test piece Probenrichtung	Medza klm Yield point - Proof stress Streck - Dehngrenze	Pevnosť v ťah Tensile strength Zugfestigkeit	Ťažnosť Elongation Bruchdehnung	
					Rt0,5 [MPa]	Rm [MPa]	A5,65 [%]	2" [%]
					min. max.	245 500	25.0 ---	* ---
					Predpis - Requirements - Vorschrift:			
<b>1</b>	<b>90799</b>	<b>A008743/19</b>	<b>12.42x4.64</b>	<b>L</b>	<b>388</b>	<b>450</b>	<b>30.9</b>	<b>28.8</b>

\* Ťažnosť - Elongation - Bruchdehnung : min. (1940\*So\*\*0.2)/(Rm\*\*0.9)

Skúška stlačením vyhovela.

Flattening test without objections.

Falversuch ohne Beanstandung.

Skúška rozširovaním vyhovela.

Flaring test without objections.

Aufweitversuch ohne Beanstandung.

Skúška vodným tlakom vyhovela.

Hydraulic pressure test without objections.

**11.60 MPa 5 sec 100%**

Wasserinnendruckversuch ohne Beanstandung.

Skúška vírivými prúdmi vyhovela

Eddy current test without objections

**EN ISO 10893-1 100 %**

Wirbelstromprüfung ohne Beanstandung

Miesto v Podbrezovej

 Location  
Taz  
Ort

Dátum 21.02.2019

 Date  
Datum

Závodný znalec

Works Inspector

Der Werks Sachverständige

Ing. Čížmárik Miroslav

Železiarne Podbrezová a.s., Kollárovi 35, 976 81 Podbrezová, Slovenská Republika

Phone: +421 48 645 3031, Fax: +421 48 645 3032, www.steelhub.sk

CIN: 31 562 141, VAT No: SK2020458704

Bank account: Slovenská sporiteľňa, a.s., IBAN: SK69 0900 0000 0000 7990 0086, SWIFT (BIC): OIBASKHX

Registered in Register of Business Names in the District Court Banská Bystrica, Section Sa, Entry No. 698



CO #	Item #	Del #	Heat	Lot	Your art #	Qty	Description
B39554	100	RP4640 84	23409			1	RUNDT SEIGH.34CrNiMo6 90 MM X Ø X 6 M



This document is electronically reproduced and is identical to the original.



Inspection certificate

EN 10204 3.1

1 / 2

1.7.2015

388021

Customer's order number 0046002939		Manufacturer's order number 120140 2	
Customer/consignee Tibnor Ab Abramsons väg 1 63510 Eskilstuna Sweden		Buyer Tibnor Ab Box 600 16926 Solna Sweden	
Customer reference number 0046002939/45918			
Product Round bar Quenched and tempered Hot rolled, reeled		Steel grade SS 2541-03 M Specification SS 2541 MTIBNOR 30.12.09	
Charge 23409	Abbreviation C4C	Diameter/dimensions 90 mm	Reduction ratio 18,04 :1

100

CAST ANALYSIS

	C	SI	MN	P	S	CR	NI	MO
Min	0,32	0,10	0,50	0,019	0,020	1,30	1,30	0,15
Result	0,35	0,28	0,70	0,019	0,034	1,38	1,40	0,17
Max	0,39	0,40	0,80	0,035	0,035	1,70	1,70	0,30

ALS

Min	0,011
Result	0,011
Max	

CHARPY V2/-20 C

	KV1	KV2	KV3	KV	AVER
Min	J	J	J	J	27
Result	66	79	141	95	
Max					

TENSILE TEST

	REH	Rp0.2	Rm	A 5	Z
Min	MPa	MPa	MPa	%	%
Result		700	900	12,0	
Max		810	941	16,4	56
			1050		

HARDNESS (HBW 10/3000)

	HARDNESS HBW
Min	270
Result	287
Max	325

The products supplied are in compliance with the requirements of the order

Ovako Imatra Oy Ab  
Quality control  
FI-55100 Imatra  
Tel. +358 (0)5 68021  
Fax. +358 (0)5 6802 211

Ovako Imatra Oy Ab  
Teollisuuskaja 1  
FI-14200 Turenki  
Tel. +358 (0)5 68021  
Fax. +358 (0)3 6334032

Certified Quality System to  
ISO/TS 16949 by DNV  
Business ID 2067276-0  
Domicile Imatra





## CERTIFICATE OF CONFORMITY

**Customer:** IK-Norway AS  
**Customer Ref No:** B40262  
**IK-UK Order No:** IKSO-19-02-168

Item	Qty	Description
1	4	PU Packer manufactured to Drg: 3050582 2 pcs – Colour: Blue – Shore 70°A 2 pcs – Colour: Red – Shore 90°A

This is to certify that the products covered by this certificate have been manufactured, inspected and tested in accordance with the quality management system requirements of BS EN ISO 9001:2018, and that they conform to the requirements of the specifications and drawings referred to in the purchase order.

*Without Prejudice*

Signed on behalf of **IK-UK Limited**

Date: 08.03.2019

**Health and Safety at Work Act 1974 (HASAW)**

*These products and associated equipment are supplied with safety features included so that as far as is reasonably practical, they do not present a risk to health and safety when used properly and safely for the purpose for which they are intended. Since IK-UK has no control over the method of operation, the responsibility for ensuring that the equipment is not used or operated in a manner that is unsafe or dangerous, rests entirely with the user.*

IK-UK the right to alter specifications and/or designs without notice.

QS-SF-10.03 Rev 1

**IK-UK Limited**

1 Grindon Way  
Heighington Business Park  
Newton Aycliffe. Co. Durham  
DL5 6SH. United Kingdom

Phone : +44 (0) 1325 307508  
Fax : +44 (0) 1325 316748  
Web : [www.ik-worldwide.com](http://www.ik-worldwide.com)  
E-mail : [sales@ik-worldwide.com](mailto:sales@ik-worldwide.com)

Company Registered in England  
Reg. No : 07448597  
VAT No : GB103739039  
Bank : DnB Bank London EC4